DISSERTATION | DOCTORAL THESIS

Titel | Title

Use of embryonic and extra-embryonic stem cells to infer the signalling interactions directing differentiation and morphogenesis during implantation stages

verfasst von | submitted by

Viktoria Holzmann B.Sc. MSc

angestrebter akademischer Grad | in partial fulfilment of the requirements for the degree of

Doctor of Philosophy (PhD)

Wien | Vienna, 2024

Studienkennzahl lt. Studienblatt | Degree programme code as it appears on the student record sheet:	UA 794 620 490
Dissertationsgebiet lt. Studienblatt | Field of study as it appears on the student record sheet:	Molekulare Biologie
Betreut von | Supervisor:	Nicolas Rivron PhD

Acknowledgements

As I reach the end of my PhD journey, I am truly grateful for the transformative experience the past four and a half years have been. They have helped me grow as a scientist but also as a person. For this, I want to first and foremost thank Nicolas Rivron. I am genuinely grateful that he gave me the opportunity to join his group right from its start at IMBA. I deeply appreciate his continuous trust in me, his support of my decisions, and his encouragement throughout the years. His imperturbable positivity during challenging times is truly admirable. I also extend a massive thank you to all the current and former members of the Rivron lab. You are an incredible group of intelligent, hard-working individuals and it has been a pleasure to work alongside you and to learn from each of you. I have especially benefitted from my discussions with Harunobu Kagawa, who challenged me with tough questions, but would also provide invaluable guidance whenever I faced difficulties. A big thank you goes to Elena Bartoli, who actively worked alongside me as part of her Master thesis, while together we "learnt by fucking up". Thank you also to my fellow PhD students in the lab, Theresa Sommer, Giovanni Sestini, and Marlene Müller for their support whenever things felt "desperation-driven". Finally, I want to express my appreciation to Yvonne Scholte op Reimer, who kept an impeccable lab environment that was fun to work in, and always made sure to provide delicious home-made cakes and cookies. I will surely miss the cake-breaks with all of you.

I also want to thank Jolien Jacobs in Derk ten Berge's lab at Erasmus MC, with whom I continue to work closely for more than a year now. A significant part of the work presented in this thesis is the product of our ongoing, productive discussions. I am sincerely grateful to both Jolien and Derk for their valuable insights.

During my time on campus, I was privileged to receive the outstanding support provided by the facilities at the VBC campus, particularly the biooptics, stem cell, and bioinformatics facilities. Specifically, I want to highlight Gerald Schmauss, Marietta Weninger, Alberto Moreno Cencerrado, Pawel Pasierbek, and Maria Novatchkova for their exceptional help on numerous occasions. I am grateful to Christa Bücker and Bon-Kyoung Koo for their valuable advice as part of my thesis advisory committee, and especially for Christa's support over the last year of my PhD. Additionally, I want to thank Stephanie Ellis and Sally Lowell for reviewing this thesis.

Beyond the scientific journey, I am extremely grateful for the wonderful group of friends I have made during my time at the VBC. My favourite "naïve PhD students of the blue floor" Issy, Esther, and Joonsun – I consider myself incredibly lucky to have you. Thank you so much for all our lunchies and coffee breaks, travel experiences, party nights, and encouraging words in times when nothing seemed to work. Big shoutout also to Gustav, Sabrina, Saku, and Ameya for a lot of fun memories outside the lab.

Lastly, I want to wholeheartedly thank my family and friends for their never-ending support. I deeply appreciate them being so understanding and accommodating of the somewhat crazy working hours that come with stem cell research. Anna, your continuous

confidence in me and your pride in my achievements mean the world to me. Sean, I am incredibly thankful for your love and unwavering support. Your belief in me has been a driving force in achieving this, and I am immensely grateful for that.

Abstract

The development of a complex multicellular organism from a single fertilised cell necessitates differentiation and morphogenesis. Both processes are guided by a variety of signalling cues, often arising from interactions between developing tissues. During uterine implantation in mammals, such interactions occur between the embryonic epiblast as well as the extra-embryonic primitive endoderm and trophectoderm. However, our understanding of the specific signals exchanged between these tissues that drive their transition from pre- to post-implantation stages remains incomplete. This is also due to the inherent challenges associated with studying mammalian embryos, as they are concealed within the uterus during development.

Alternatively, stem cells derived from both embryonic and extra-embryonic lineages of the conceptus have become invaluable tools for investigating the signalling pathways involved in lineage differentiation. Over the past decade, there has been increasing use of these cells to generate embryoids, which are stem cell-based models replicating aspects of differentiation and morphogenesis *in vitro*. Embryoids can be formed by combining embryonic and extra-embryonic stem cells, thereby offering valuable insights into the interactions between them. Nevertheless, current stem cell culture conditions and embryoid protocols require further refinement to accurately mimic the embryo at defined developmental stages. Arguably, identifying the signals exchanged between embryonic and extra-embryonic lineages directing their developmental progression can inform us about the signalling requirements of their *in vitro* equivalents. Enhancing the fidelity of stem cells to their *in vivo* counterparts should then again improve current embryoid models, ensuring greater reliability in the results obtained from them.

In this PhD thesis, embryonic and extra-embryonic stem cell lines were utilised across three projects, each with its own objectives related to understanding the developmental progression of embryonic and extra-embryonic lineages during implantation. The results of these projects will be discussed focusing on two overarching themes. Firstly, the contribution to advancing integrated embryoid models that mimic embryonic and extra-embryonic tissues during implantation stages. Secondly, the progress made in understanding the culture requirements of extra-embryonic stem cells. Specifically, the work presented here contributed to refining trophoblast stem cell culture conditions, which could enhance blastoid models. Additionally, novel stem cell-based models of primitive endoderm and epiblast co-development were established. Finally, I used publicly available resources to predict signalling interactions between epiblast, primitive endoderm, and trophectoderm at the onset of implantation *in silico*. Subsequent investigation of predicted signalling interactions revealed a previously undescribed role of Wnt signalling in maintaining stem cells of the extra-embryonic primitive endoderm in an undifferentiated state. Collectively, this work expands our toolkit of embryoid models for studying development during implantation and makes advancements in the culture conditions of extra-embryonic stem cells.

Zusammenfassung

Die Entwicklung eines komplexen multizellulären Organismus aus einer einzigen befruchteten Zelle erfordert Differenzierung und Morphogenese. Beide Prozesse werden durch eine Vielzahl von Signalen gesteuert, die häufig aus Interaktionen zwischen den sich entwickelnden Geweben hervorgehen. Während der Einnistung in die Gebärmutter von Säugetieren kommt es zu solchen Interaktionen zwischen dem embryonalen Epiblast sowie dem extraembryonalen primitiven Endoderm und Trophektoderm. Unsere Kenntnisse über die spezifischen Signale, die zwischen diesen Geweben ausgetauscht werden und den Übergang von der Prä- zur Postimplantationsphase steuern, sind jedoch noch unvollständig. Dies liegt auch an den Schwierigkeiten, die mit der Untersuchung von Säugetierembryonen verbunden sind, da diese während ihrer Entwicklung in der Gebärmutter unzugänglich sind.

Alternativ dazu sind Stammzellen, die sowohl aus embryonalen als auch extraembryonalen Linien des Konzeptus stammen, zu wertvollen Instrumenten für die Untersuchung der Signalwege geworden, die an der Differenzierung der Linien beteiligt sind. In den letzten zehn Jahren wurden diese Zellen zunehmend zur Erzeugung von Embryoiden verwendet, d. h. von stammzellbasierten Modellen, die Aspekte der Differenzierung und Morphogenese in vitro nachbilden. „Embryoids“ können durch die Kombination von embryonalen und extraembryonalen Stammzellen gebildet werden und bieten so wertvolle Einblicke in die Interaktionen zwischen ihnen. Dennoch müssen die derzeitigen Kulturbedingungen für Stammzellen und die Protokolle für Embryoids weiter verfeinert werden, um den Embryo in bestimmten Entwicklungsstadien genau nachzubilden. Die Identifizierung der Signale, die zwischen embryonalen und extraembryonalen Zelllinien ausgetauscht werden, um deren Entwicklungsfortschritt zu steuern, kann uns Aufschluss über die Signalanforderungen ihrer in vitro Gegenstücke geben. Die Verbesserung der Übereinstimmung von Stammzellen mit ihren in vivo Pendants sollte dann wiederum derzeitige Embryomodelle verbessern und eine größere Zuverlässigkeit der mit ihnen erzielten Ergebnisse gewährleisten.

In dieser Doktorarbeit wurden embryonale und extraembryonale Stammzelllinien in drei Projekten verwendet, wobei jedes Projekt eigene Schwerpunkte in Bezug auf das Verständnis des Entwicklungsverlaufs embryonaler und extraembryonaler Linien während der Implantation setzte. Die Ergebnisse dieser Projekte werden mit Blick auf zwei übergreifende Themen diskutiert. Erstens, den Beitrag zur Weiterentwicklung integrierter embryonaler Modelle, die embryonale und extraembryonale Gewebe während der Implantationsstadien nachbilden. Zweitens, die Fortschritte im Verständnis der Kulturanforderungen von extraembryonalen Stammzellen. Insbesondere trugen die hier vorgestellten Arbeiten dazu bei, die Kulturbedingungen für Trophoblasten-Stammzellen zu verfeinern, was Blastoidmodelle verbessern konnte. Darüber hinaus wurden neue stammzellbasierte Modelle für die gleichzeitige Entwicklung von primitivem Endoderm und Epiblast erstellt. Schließlich nutzte ich öffentlich zugängliche Ressourcen, um Signalinteraktionen zwischen Epiblast, primitivem Endoderm und Trophektoderm zu Beginn der Implantation in silico vorherzusagen. Die

anschließende Untersuchung der vorhergesagten Signalinteraktionen ergab eine bisher unbeschriebene Rolle des Wnt-Signalwegs für die Erhaltung der Stammzellen des extraembryonalen primitiven Endoderms in einem undifferenzierten Zustand. Insgesamt erweitert diese Arbeit unser Repertoire an Embroymodellen zur Untersuchung der Entwicklung während der Implantation und bringt Fortschritte hinsichtlich der Kulturbedingungen für extraembryonale Stammzellen.

Table of Contents

CHAPTER 1:
Introduction

To form a complex multicellular organism from a single cell zygote, cells must self-organise into emerging tissue structures (morphogenesis) and simultaneously give rise to increasingly specialised cells of the definite tissues (differentiation). Which signals guide morphogenesis and differentiation, how signals are generated at the correct time and place, and how they are interpreted are some of the fundamental questions in developmental biology.

Uterine implantation marks a time of significant morphogenetic and cell fate changes in the embryo. At the onset of implantation, the blastocyst stage conceptus is a fairly simple structure consisting of only three distinct lineages: the epiblast, the trophectoderm, and the primitive endoderm (PrE)(Rossant & Tam, 2009). Only cells of the epiblast will later form the foetus, while the trophectoderm and PrE are the precursors for vital extra-embryonic tissues, specifically the placenta and the yolk sac (Artus & Hadjantonakis, 2012). Irrespective of their embryonic or extra-embryonic fate, all three lineages undergo multiple differentiation events during implantation, which coincide with a drastic increase in the structural complexity of the conceptus (Figure A)(Rossant & Tam, 2009; Artus & Hadjantonakis, 2012; Takaoka & Hamada, 2012; Rossant, 2018). Coordination of these developmental changes requires the communication between embryonic and extra-embryonic lineages through signalling molecules and other morphogenetic cues. However, studying the interactions between embryonic and extra-embryonic cells and their role in directing differentiation and morphogenesis in the mammalian embryo is technically challenging.

Importantly, stem cell cultures resembling the epiblast, trophectoderm, or PrE, at pre- and post-implantation stages have been established. These cells serve as invaluable *in vitro* tools for revealing the genetic basis and signalling requirements underlying lineage commitment and differentiation. Given the ethical and practical constraints associated with the use of embryos for research, there has been a growing utilisation of these cells to generate embryoids – stem cell-based structures which mimic aspects of differentiation and morphogenesis *in vitro*. Embryoids can integrate cells of embryonic and extra-embryonic lineages, thereby offering valuable insights into the interactions between them. However, current culture conditions, particularly for extra-embryonic stem cells, largely struggle to precisely capture cells in defined developmental states. This limitation inevitably translates to embryoid models, likely hindering their accuracy in mimicking the embryo. Arguably, gaining a deeper understanding of the signals exchanged between embryonic and extra-embryonic lineages at specific stages in development could help refine current culture conditions for their *in vitro* equivalents. Enhancing the fidelity with which stem cells replicate their *in vivo* counterparts, should ultimately improve the dependability of stem cell cultures and embryoids as tools for studying embryo development.

In the following, this chapter provides an overview of the late pre- to early post-implantation stages and the signalling cues known to control cell fate decisions and

morphogenesis during this time in development. It specially highlights signalling interactions between embryonic and extra-embryonic lineages that direct developmental progression during implantation. Additionally, this chapter summarises how embryonic and extra-embryonic lineages as well as their interactions and co-development have been modelled *in vitro*.

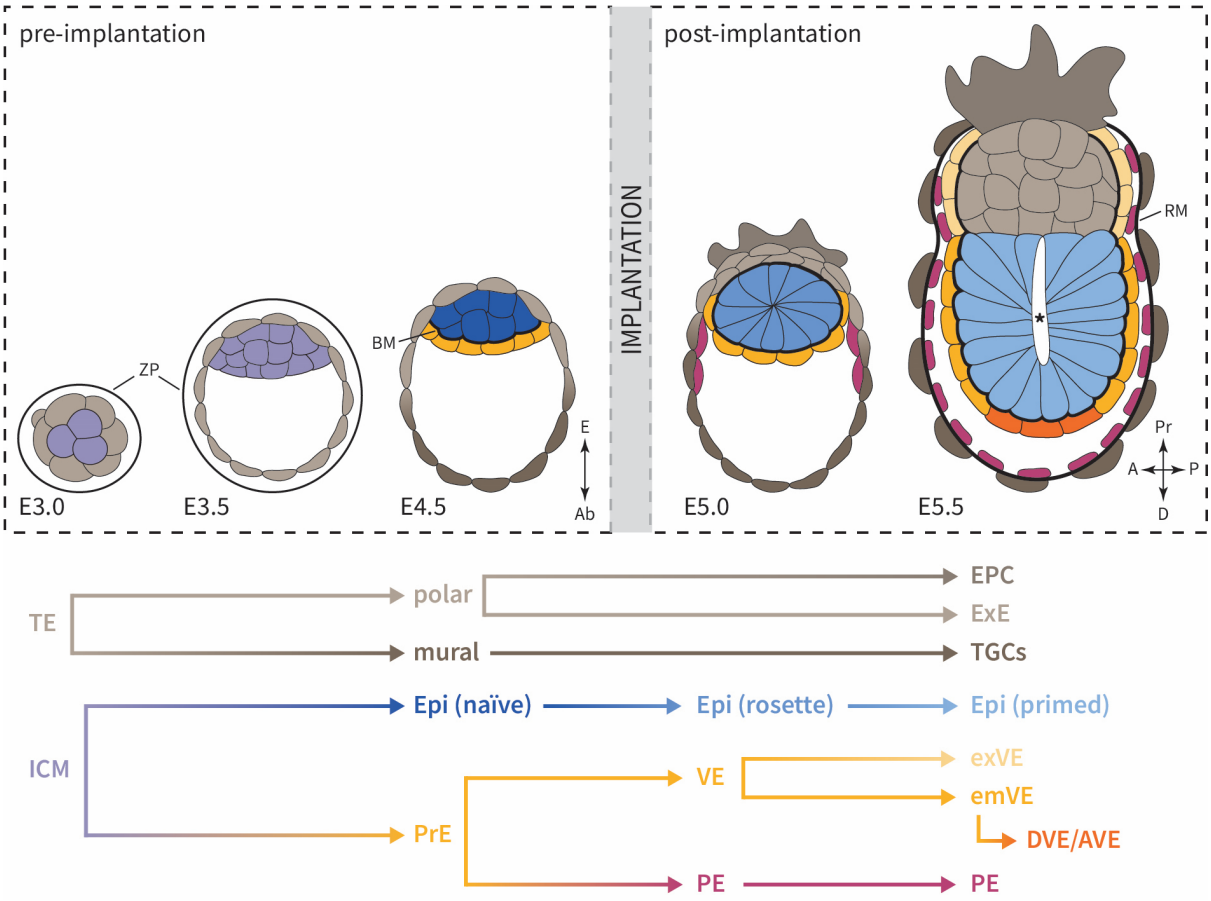

Figure A. Pre- to post-implantation development in mouse.

The corresponding embryonic day (E) is indicated at the bottom left of the respective developmental stage. Refer to the main text for details. Abbreviations: A: anterior, Ab: abembryonic, BM: basement membrane, D: distal, DVE/AVE: distal VE/anterior VE, E: embryonic, emVE: embryonic VE, EPC: ectoplacental cone, Epi: epiblast, ExE: extra-embryonic ectoderm, exVE: extra-embryonic VE, ICM: inner cell mass, P: posterior, PE: parietal endoderm, Pr: proximal, PrE: primitive endoderm, RM: Reichert's membrane, TE: trophectoderm, TGCs: trophoblast giant cells, VE: visceral endoderm, ZP: zona pellucida, *: pro-amniotic cavity

Note that while certain aspects are conserved, early post-implantation development is species specific. However, the mouse has been extensively used to study uterine implantation and is also the model organism for the following empirical work. Therefore, this chapter summarises our knowledge in mouse unless indicated otherwise.

1.1. Specification of blastocyst lineages pre-implantation

1.1.1. Trophectoderm and inner cell mass

Compaction and initial fate acquisition

Compaction of the blastomeres at the 8-cell stage into a tight ball-like structure precedes the initial cell fate decision, which specifies the trophectoderm as the first extra-embryonic lineage. Compaction coincides with polarisation of all cells, marked by the apical expression of polarity markers such as atypical protein kinase C (aPKC) and the partitioning defective (PAR) proteins PAR3 and PARD6B (Plusa *et al*, 2005; Vinot *et al*, 2005). Two consecutive rounds of cleavage then create a 16-cell and further a 32-cell morula with distinct inner and outer cells. Apical-basal polarity is retained in the outer cells, while the inner cells become apolar (Johnson & Ziomek, 1983). This difference in polarity is directly coupled to trophectoderm fate specification through differences in Hippo pathway activity. Here, Angiomotin (AMOT) has a central role in translating cell polarity information into Hippo signalling activity (Cockburn *et al*, 2013; Hirate *et al*, 2013). Hippo signalling is active in the inner cells which prevents the translocation of Yes-associated protein (YAP) to the nucleus. Conversely, in outer cells, Hippo signalling is repressed, leading to nuclear accumulation of YAP. In the nucleus YAP functions together with TEA domain family transcription factor 4 (TEAD4) to activate trophectoderm specific genes such as caudal-related homeobox 2 (*Cdx2*) and GATA binding protein 3 (*Gata3*) (Nishioka *et al*, 2008, 2009; Ralston *et al*, 2010). At the same time, YAP represses the expression of Sex determining region Y-box 2 (*Sox2*) in the outer cells, thereby restricting the expression of this first pluripotency factor to the inner cells (Frum *et al*, 2018).

Lumenogenesis, formation of embryonic-abembryonic axis, and fate restriction

Concurrent with the onset of trophectoderm specification, a fluid-filled lumen, the blastocoel, forms at the interface between the trophectoderm and the inner cells. The formation of the lumen is driven by the fusion of microlumens that emerge between cell contacts, resulting in the development of a single dominant lumen (Dumortier *et al*, 2019). Further expansion of the lumen also involves the activity of Na+/K+ ATPases and aquaporins in the trophectoderm cells to facilitate osmosis-based fluid transport across the trophectoderm (Manejwala *et al*, 1989; Barcroft *et al*, 2003). This process of lumenogenesis ultimately leads to the formation of the blastocyst, characterised by a single layer of trophectoderm cells enveloping the inner cell mass (ICM), which is positioned on one side of the trophectoderm. The positioning of the ICM establishes the primary axis during development, known as the embryonic-abembryonic axis (Rossant & Tam, 2009; Takaoka & Hamada, 2012). At the blastocyst stage, ICM and trophectoderm fate are further confined. Reliant on CDX2, expression of the ICM specific core pluripotency factors Octamer binding transcription factor 4 (OCT4) and NANOG are repressed in trophectoderm cells (Ralston & Rossant, 2008). Conversely, the repression of trophectoderm target genes by OCT4, SOX2 and NANOG retains ICM identity (Loh *et al*, 2006).

1.1.2. Primitive endoderm (PrE) and Epiblast

FGF4 signalling as a regulator of fate specification

Immediately after blastocyst formation, the ICM gives rise to the embryonic epiblast and the second extra-embryonic lineage, the PrE. Lumen expansion during blastocyst formation seems to directly affect successful lineage specification, possibly through luminally deposited Fibroblast growth factor 4 (FGF4)(Ryan *et al*, 2019). FGF/extracellular signal-regulated kinase (ERK) signalling has been identified as a key determinant in specifying PrE versus epiblast fate (Lanner & Rossant, 2010; Yamanaka *et al*, 2010). Genetically deleting *Fgf4*, FGF receptor 2 (*Fgfr2*), or Growth factor receptor-bound protein 2 (*Grb2*) completely prevents PrE formation (Feldman *et al*, 1995; Arman *et al*, 1998; Cheng *et al*, 1998; Goldin & Papaioannou, 2003; Chazaud *et al*, 2006). Moreover, culture of blastocysts with FGF4 strongly promotes PrE commitment (Yamanaka *et al*, 2010), while in the presence of FGF/ERK inhibitors cells of the ICM acquire epiblast fate at the expense of PrE (Nichols *et al*, 2009). Hence unsurprisingly, the amount of FGF4 is crucial for attaining the right balance of PrE and epiblast cells in the blastocyst (Krawchuk *et al*, 2013).

Fgf4 is the first gene to exhibit bimodal expression in ICM cells as early as E3.25 (Ohnishi *et al*, 2014). These expression differences likely stem from stochastic gene expression variation among otherwise identical ICM cells. From E3.5 onward, a reciprocal expression pattern emerges where *Fgf4* is expressed in epiblast-biased and *Fgfr2* in PrE-biased cells (Guo *et al*, 2010; Ohnishi *et al*, 2014), thereby generating a bias towards FGF4 secreting and FGF4 receiving cells. Interestingly, FGF4 primarily acts through FGFR1, expressed by all ICM cells, for PrE specification, implying that PrE-specific FGFR2-mediated signalling may play an additional role beyond lineage specification (Kang *et al*, 2017; Molotkov *et al*, 2017)(refer also to section 1.3.1. for more details).

Transcriptional regulators of PrE and epiblast fate

Acquisition of PrE fate relies on the transcription factor GATA6, while the transcription factor NANOG mediates epiblast commitment (Chazaud *et al*, 2006). Both are initially co-expressed (Guo *et al*, 2010), suggesting that the final cell fate is determined by downregulation of one of the factors. Mutual repression of the two transcription factors has been proposed as a mechanism through which either PrE or epiblast fate are restricted (Chickarmane & Peterson, 2008), and *in vitro* models indicate direct regulatory interactions between GATA6 and NANOG (Singh *et al*, 2007; Wamaitha *et al*, 2015). However, autonomous GATA6/NANOG circuits must be coupled to FGF/MEK signalling to reliably complete lineage restriction at appropriate PrE/epiblast ratios (Bessonnard *et al*, 2014; Schröter *et al*, 2015). NANOG is needed for *Fgf4* expression and in turn FGF/ERK signalling represses *Nanog* (Frankenberg *et al*, 2011). Conversely, FGF/ERK signalling maintains *Gata6* expression (Kang *et al*, 2013), likely indirectly through alleviation of NANOG mediated repression of the *Gata6* promotor (Frankenberg *et al*, 2011).

Lineage segregation, polarisation, and epithelialisation

GATA6+ and NANOG+ cells specify in a salt and pepper manner in the ICM (Chazaud *et al*, 2006). Subsequently, PrE cells physically segregate from epiblast cells and align at the cavity-facing surface (Bassalert *et al*, 2018). Therefore, unlike trophectoderm and ICM fate, which is determined by cell position (outer vs. inner cells), epiblast and PrE fate precede their position in the conceptus. How PrE and epiblast cells sort into distinct compartments has long been unclear. Differential adhesion (Foty & Steinberg, 2004), differences in surface tension (Lecuit & Lenne, 2007), or differential cell-cell affinity between the two lineages (Amack & Manning, 2012; Maître *et al*, 2012) have been proposed as underlying mechanisms. However, recent work by Yanagida *et al*. demonstrates that none of the proposed mechanisms can sufficiently explain robust lineage sorting (Yanagida *et al*, 2022). Rather than static physical parameters, they show that it is enhanced surface fluctuations, or blebbing, of PrE cells that facilitate their sorting.

As PrE cells reach the blastocoel interface they polarise and epithelialize (Gerbe *et al*, 2008). This is accompanied by the asymmetric localisation of aPKC to the apical cell surface of PrE cells (Saiz *et al*, 2013), and the subsequent formation of a basement membrane by the polarised PrE (Gerbe *et al*, 2008). Interestingly, both aPKC and basement membrane components like laminin and collagen are already expressed in unsorted PrE precursors (Saiz *et al*, 2013; Ohnishi *et al*, 2014; Moghe *et al*, 2023) and have also been implicated in lineage sorting. For instance, inhibiting aPKC right after epiblast and PrE specification prevents PrE sorting (Saiz *et al*, 2013; Moghe *et al*, 2023). Additionally, a recent preprint proposes that the formation of an increasing laminin gradient within the ICM towards the blastocoel surface directs active PrE migration, potentially driven by aPKC mediated cell polarisation (Moghe *et al*, 2023). This is in line with findings that integrin β1 and laminin γ1 are essential for correct PrE segregation (Kim *et al*, 2022a). Hence, it might require the combination of PrE-specific surface properties (Yanagida *et al*, 2022) and PrE maturation factors, such as aPKC or laminin, to accomplish lineage sorting. Completion of consecutive PrE polarisation, epithelialisation, and basement membrane formation defines the late blastocyst stage at which the conceptus will initiate implantation.

1.2. Early post-implantation development

1.2.1. Trophectoderm and its derivatives during implantation

Trophectoderm patterning and attachment

Prior to implantation, the blastocyst must hatch from the zona pellucida, a glycoprotein matrix that encapsulates the conceptus during blastocyst formation (Wassarman *et al*, 2004). This process is facilitated by proteolytic enzymes which are secreted by the trophectoderm (Perona & Wassarman, 1986). After hatching, the trophectoderm mediates blastocyst attachment to the uterine epithelium. The mouse blastocyst specifically attaches from the abembryonic side (Molè *et al*, 2020), indicating that there are functional differences between the trophectoderm along the embryonic-abembryonic axis. Indeed, the trophectoderm diverges into the polar trophectoderm at the embryonic and the mural trophectoderm at the abembryonic pole (Rossant & Tam, 2009). Distinction of the trophectoderm into polar and mural regions is marked by differential expression levels of CDX2, which are higher in the polar region (Donnison *et al*, 2005; Strumpf *et al*, 2005; Christodoulou *et al*, 2019; Suzuki *et al*, 2022a). Additionally, cortical tension is lower in the polar trophectoderm (Chan *et al*, 2019). Cells of the polar side have been described as more proliferative (Copp, 1978; Gardner, 2000) and generate a proliferation flow that helps expand the mural population of the blastocyst (Copp, 1978; Gardner, 2000; Christodoulou *et al*, 2019). Later, a tissue boundary is established between the polar and mural trophectoderm, characterised by a high actomyosin contractility between trophectoderm cells expressing CDX2 at high and low levels (Christodoulou *et al*, 2019).

Trophectoderm derivatives and invasion

After enabling attachment, cells of the mural trophectoderm are the first to terminally differentiate and give rise to trophoblast giant cells (Cross, 2000; Sutherland, 2003). These cells undergo an epithelial to mesenchymal-like transition to acquire an invasive phenotype that is necessary for the conceptus to invade into the uterus (Mobley *et al*, 2017). Consistent with the reported downregulation of CDX2 in the mural trophectoderm, *Cdx2* overexpression counteracts differentiation into trophoblast giant cells and represses adhesion- and migratory-related genes such as Integrin β3 (*Itgb3*)(Suzuki *et al*, 2022b). On the other hand, cells of the polar trophectoderm, which express CDX2 at high levels, morphologically transform into columnar cells (Christodoulou *et al*, 2019) and give rise to the extra-embryonic ectoderm (ExE) and the ectoplacental cone. Cells of the ExE maintain *Cdx2* and Eomesodermin (*Eomes*) expression, making them a pool of self-renewing precursors for placenta formation (Simmons & Cross, 2005; Bedzhov *et al*, 2014a).The ectoplacental cone also contains subpopulations of proliferating cells which are a continuous supply of “secondary” trophoblast giant cells (Cross, 2000).

1.2.2. Epiblast cup formation

Epithelialisation and formation of the pro-amniotic cavity

As the blastocyst implants, the epiblast with the overlying PrE invaginates into the blastocoel towards the mural trophectoderm. This coincides with the epiblast transitioning from an amorphous ball of cells into a cup-shaped, polarised epithelium that surrounds the pro-amniotic cavity (Bedzhov *et al*, 2014a). Restructuring of the epiblast into a single-cell-layer epithelium is necessary to later ensure its robust patterning, for example during anterior-posterior axis formation (Girgin *et al*, 2021). Epiblast morphogenesis was originally proposed to be accomplished by the interplay of two signals: one that induces apoptosis of inner epiblast cells, and another rescue signal that allows cells in contact with the basement membrane to survive (Coucouvanis & Martin, 1995; He *et al*, 2010). Thereby, cavitation would occur through regulated cell death, resulting in a remaining single layer of epiblast cells adjacent to the basement membrane. However, it was later shown that apoptosis-mediated cavitation is not the mechanism underlying epiblast morphogenesis. Instead, the pro-amniotic cavity is a result of hollowing lumenogenesis (Bedzhov & Zernicka-Goetz, 2014). Induced by the formation of a basement membrane, cells of the epiblast polarise and reorganise into a rosette-like structure where all apical domains face towards the centre of the rosette. Lumen formation is subsequently initiated at the rosette centre, likely caused by membrane separation through charge repulsion due to the apical expression of proteins with high negative charges, such as Podocalyxin (Orlando *et al*, 2001; Meder *et al*, 2005; Bedzhov & Zernicka-Goetz, 2014). Further lumen expansion eventually gives rise to the epiblast cup around E5.5.

Transition of epiblast pluripotency

The morphological transition of the epiblast from an unpolarised cell cluster in the blastocyst to a polarised epithelium at E5.5 coincides with changes in epiblast cell state. Although epiblast cells are pluripotent throughout this period (*i.e.* capable of generating every cell in a mature organism), the early pre-implantation epiblast differs from the late post-implantation epiblast both transcriptionally and epigenetically. Right after its specification at the blastocyst stage, the epiblast is considered to be in a developmental ground state or “naïve” (Nichols & Smith, 2009). Naïve pluripotency is marked by the expression of the transcription factor Krüppel-like factor 4 (KLF4), alongside the general pluripotency factors NANOG, OCT4, and SOX2 (Morgani *et al*, 2017; Nichols & Smith, 2009). On the contrary, after epithelialisation, the early post-implantation epiblast becomes "primed". KLF4 is no longer expressed, levels of NANOG expression decrease, and instead cells upregulate markers of primed pluripotency such as Orthodenticle Homeobox 2 (OTX2) and OCT6 (Neagu *et al*, 2020). Moreover, in female embryos, one of the X chromosomes is inactivated in the primed epiblast, while both X chromosomes are active in the naïve epiblast (Nichols & Smith, 2009).

In addition, other states of intermediate pluripotency have been suggested as part of a developmental continuum. For example, “formative” pluripotency has been proposed as a transitionary state between naïve and primed (Smith, 2017; Kinoshita *et al*, 2021). Further, a

"rosette" state of pluripotency has been described, characterised by the expression of both naïve (KLF4) and primed (OTX2) markers during epiblast polarisation and rosette formation (Neagu *et al*, 2020). While these pluripotency states are transient in the embryo, the different nuances of pluripotency can be captured *in vitro* (see also section 1.3.2)(Morgani et al, 2017; Neagu et al, 2020; Kinoshita et al, 2021). Stem cells can be maintained in culture in distinct pluripotency states by diverse molecular mechanisms, offering valuable insights into the signalling requirements for sustaining specific pluripotency states and facilitating transitions between them (Wang & Wu, 2022). Nevertheless, if and how the transitions in pluripotency are mechanistically coupled to epiblast morphogenesis in the embryo is still unknown. A recent study, however, suggests that the small GTPase Ras Associated Protein 1 (Rap1) can coordinate epiblast morphology in sync with pluripotency state (Kim *et al*, 2022b).

1.2.3. Visceral and parietal endoderm formation

Formation of the parietal endoderm

Once the PrE epithelial layer is established, PrE cells at the interface with the trophectoderm adopt an elongated morphology that is characteristic of migratory cells (Enders *et al*, 1978). These cells start migrating along the luminal side of the trophectoderm towards the abembryonic pole of the blastocyst and form the parietal endoderm (PE)(Enders *et al*, 1978; Rossant, 1987; Filimonow & de la Fuente, 2022). Epithelial-to-mesenchymal transition is believed to facilitate the acquisition of a migratory phenotype, and proposed as an essential step for PrE-to-PE specification (Veltmaat *et al*, 2000; Filimonow *et al*, 2019). Following migration, these cells secrete large amounts of extracellular matrix components. Thereby they contribute alongside the trophectoderm to the formation of the Reichert's membrane, a thick basement membrane between the PE and the trophectoderm (Leivo *et al*, 1980; Hogan *et al*, 1980; Smith & Strickland, 1981).

Formation of the visceral endoderm and posterior/anterior visceral endoderm

PrE cells that remain in contact with the epiblast during early post-implantation development mature into the visceral endoderm (VE). Differentiation of PrE into VE strongly relies on the transcription factor Hepatocyte nuclear factor 4 (HNF4A), expression of which is regulated by GATA6 (Duncan *et al*, 1997; Morrisey *et al*, 1998). VE cells have microvilli and contain lots of phagocytic and pinocytotic vesicles, features related to their efficient processing of maternal nutrients (Kadokawa *et al*, 1987; Bielinska *et al*, 1999). Additionally, the VE secretes apolipoproteins as transport molecules and overall functions in nutrient uptake and transport (Bielinska *et al*, 1999). As the polar trophectoderm expands into the ExE, the visceral endoderm also aligns this extra-embryonic region of the egg cylinder. This results in the separation of the VE into an extra-embryonic VE (exVE) associated with the ExE, and an embryonic VE (emVE) that overlies the epiblast (Enders *et al*, 1978; Perea-Gomez *et al*, 2007).

A subgroup of cells located at the distal tip of the embryonic VE undergo specialisation into the distal visceral endoderm (DVE), which is distinct from the remaining VE in its gene expression (Zhu *et al*, 2023). Morphologically this becomes apparent as a localised thickening of the VE epithelium (Rivera-Pérez *et al*, 2003). Initially the prevailing view was that DVE cells migrate proximally, towards the prospective anterior side of the embryonic VE, thereby forming the anterior visceral endoderm (AVE)(Rivera-Pérez *et al*, 2003; Srinivas *et al*, 2004; Rossant & Tam, 2009). The AVE subsequently serves as a crucial signalling centre that determines anterior-posterior polarity in the embryo (see also section 1.3.1.). However, accumulating evidence now suggests that DVE and AVE arise independently despite sharing similar markers (Takaoka *et al*, 2011; Hoshino *et al*, 2015; Zhu *et al*, 2023).

1.3. Interactions between embryonic and extra-embryonic tissues during implantation

So far, the differentiation and morphogenetic events that occur during the pre- to post-implantation transition have primarily been laid out descriptively. This section highlights known interactions between embryonic and extra-embryonic lineages that regulate development during these stages *in vivo*. It also summarises current stem cell models that recapitulate pre- and post-implantation development *in vitro*, thus providing excellent study systems to further dissect the signalling interplay between embryonic and extra-embryonic lineages.

1.3.1. Embryonic and extra-embryonic tissue interactions *in vivo*

Epiblast signalling for PrE specification and survival during pre-implantation stages

Signalling interactions between the epiblast and the PrE at the blastocyst stage regulate PrE specification, survival, and proliferation. As discussed in section 1.1.2., FGF4 is the key signal driving PrE specification (Feldman *et al*, 1995; Goldin & Papaioannou, 2003; Chazaud *et al*, 2006). Specifically, the interaction between FGF4, secreted by epiblast precursors, and FGFR1, expressed by all cells of the ICM, induces PrE fate commitment (Kang *et al*, 2017; Molotkov *et al*, 2017). Additional signalling of FGF4 through PrE-specific FGFR2, is believed to have only a secondary role in PrE fate commitment (Kang *et al*, 2017; Molotkov *et al*, 2017). Instead, FGF4 – FGFR2 signalling promotes PrE survival and proliferation after specification (Molotkov *et al*, 2017; Molotkov & Soriano, 2018; Goissis *et al*, 2023). Interestingly, PrE-specific expression of FGFR2 is enhanced by BMP4 (Goissis *et al*, 2023), a signal which *in vivo* likely also originates from the epiblast, as the expression of *Bmp4* is specific to the epiblast at the early blastocyst stage (Guo *et al*, 2010).

While FGF4 – FGFR1 signalling is understood to mediate PrE specification via the MEK/ERK pathway (Yamanaka *et al*, 2010; Molotkov & Soriano, 2018), FGF4 – FGFR2 signalling for PrE survival relies on downstream activation of Phosphoinositide 3-kinase (PI3K) (Molotkov &

Soriano, 2018). Another receptor acting through PI3K for PrE survival and proliferation is platelet-derived growth factor receptor alpha (PDGFRA)(Artus *et al*, 2010, 2013; Molotkov & Soriano, 2018; Bessonnard *et al*, 2019). The corresponding ligand, platelet derived growth factor subunit A (PDGFA), is expressed by the epiblast (Ohnishi *et al*, 2014). Loss of PDGFRA leads to increased PrE apoptosis and a reduction in the number of PrE cells (Artus *et al*, 2013). However, this decrease in PrE cell number does not coincide with a compensatory increase in the number of epiblast cells as observed in *Fgf4*$^{-/-}$ or *Fgfr1*$^{-/-}$ embryos, or embryos treated with a MEK inhibitor (Kang *et al*, 2013, 2017; Nichols *et al*, 2009). This suggests PDGFRA-mediated signalling for PrE survival while emphasising the role of FGF4 acting through FGFR1 as the signal for PrE specification. Overall, FGF4 produced by epiblast precursors serves as a signal for both PrE specification and later PrE maintenance downstream of FGFR2 activation. Survival before lineage segregation is also facilitated through PDGFRA, with the interacting ligand likely provided by the epiblast.

Epiblast signalling for ExE expansion and proliferation during implantation stages

Just like the PrE, both the pre-implantation trophectoderm and the post-implantation ExE express FGFR2 (Ciruna & Rossant, 1999; Haffner-Krausz *et al*, 1999; Molotkov *et al*, 2017). Deletion of *Fgfr2* is embryonically lethal, proposed as a result of impaired expansion of the polar trophectoderm into the ExE (Arman *et al*, 1998; Kunath *et al*, 2004). FGF4, secreted by the epiblast, acts on the adjacent polar trophectoderm to maintain it in an undifferentiated, proliferative state, ultimately driving its expansion into ExE (Tanaka *et al*, 1998; Kunath *et al*, 2004; Christodoulou *et al*, 2019). Accordingly, undifferentiated, self-renewing stem cell lines can be derived from the trophectoderm and ExE using FGF4 (Tanaka *et al*, 1998)(see also section 1.3.2.). FGF4 stimulation of FGFR2 activates the ERK cascade and promotes the expression of CDX2, an essential transcription factor for maintaining multipotent progenitors in both trophectoderm and ExE (Murohashi *et al*, 2010; Bedzhov *et al*, 2014a).

Additional factors besides FGF4 were suggested to mediate the expression of ExE-specific genes including *Cdx2* and *Eomes* (Tanaka *et al*, 1998). Later, Nodal was identified as another epiblast-derived signal that maintains the niche of undifferentiated cells in the ExE (Guzman-Ayala *et al*, 2004). Specifically, the epiblast secrets Nodal propeptides which are activated extracellularly through cleavage by Furin (*Spc1*) and PACE4 (*Spc4*), proteases expressed by the ExE (Beck *et al*, 2002; Guzman-Ayala *et al*, 2004). Nodal signalling sustains an undifferentiated niche in the ExE, and in addition maintains FGF4 expression in the epiblast (Guzman-Ayala *et al*, 2004). Therefore, Nodal also indirectly promotes the maintenance of multipotent ExE progenitors by sustaining FGF4 – FGFR2 signalling. Collectively, FGF4 and Nodal, originating from the epiblast, promote the expression of *Cdx2* and *Eomes*, thereby maintaining an undifferentiated, proliferative population of cells first in the polar trophectoderm and subsequently in the ExE.

Epiblast remodelling through trophectoderm and PrE

Following implantation, the expansion and invagination of the polar trophectoderm pushes the epiblast into the blastocoelic cavity (Christodoulou *et al*, 2019; Weberling & Zernicka-Goetz, 2021). As previously mentioned (section 1.2.2.), this coincides with further remodelling of the epiblast into a polarised rosette. The key cue for polarisation is the formation of a basement membrane, assembled by the PrE between itself and the epiblast (Wallingford *et al*, 2013; Bedzhov & Zernicka-Goetz, 2014). Deletion of the laminin γ1 subunit impairs establishment of the basement membrane and results in embryonic lethality at early post-implantation stages, underscoring the significance of basement membrane formation at this developmental stage (Smyth *et al*, 1999).

Interactions of cells with a basement membrane and subsequent cell polarisation are facilitated by integrins and have been extensively described in various epithelial models (Aumailley *et al*, 2000; Yu *et al*, 2004; Akhtar & Streuli, 2013). Consistent with this, deletion of integrin β1 leads to failure of rosette formation in the epiblast, segregation and detachment of the PrE from the epiblast, and ultimately peri-implantation lethality (Fässler & Meyer, 1995; Stephens *et al*, 1995; Moore *et al*, 2014; Molè *et al*, 2021). Notably, apical-basal polarity can initially be established in *Itgb*$^{-/-}$ cells, but integrin β1 appears crucial for maintaining this polarity based on *in vitro* models of epiblast morphogenesis (Molè *et al*, 2021). The same study found that by the action of integrin β1 at the basolateral domain, actomyosin becomes apically confined, which is needed for epiblast maturation and lumen formation.

Further transition of the epithelialized epiblast into a cup shape is speculated to be guided by the Reichert's membrane, which could constrict horizontal epiblast growth and instead directs vertical expansion into a cup morphology (Weberling & Zernicka-Goetz, 2021). In summary, this illustrates how the formation of basement membranes by extra-embryonic lineages drives epiblast morphogenesis during implantation and is indispensable for embryogenesis to advance beyond early implantation stages.

DVE fate restriction through epiblast and ExE

Nodal, originating from the epiblast, is a crucial signal for driving the specification of DVE fate in the VE through Mothers against decapentaplegic homolog 2 (SMAD2)-mediated transcriptional activation, as evidenced by a failure of DVE formation in *Nodal*$^{-/-}$ and *Smad*$^{-/-}$ embryos (Waldrip *et al*, 1998; Brennan *et al*, 2001). Interestingly, *Nodal* expression by the VE itself is necessary to maintain normal levels of *Nodal* in the epiblast (Kumar *et al*, 2015). Downstream of Nodal-SMAD2 signalling, the transcription factors LIM homeobox protein 1 (LHX1), Forkhead box (FOX)A2, and FOXH1, promote the expression of DVE specific markers Left-Right Determination Factor 1 (*Lefty1*) and Cerberus 1 (*Cer1*)(Perea-Gómez *et al*, 1999; Takaoka *et al*, 2006). Early expression of *Lefty1* and *Cer1* can be detected in some PrE cells of the blastocyst, indicating that DVE specification already commences at pre-implantation stages (Takaoka *et al*, 2006; Torres-Padilla *et al*, 2007). At least the expression of *Lefty1* has also been shown to depend on Nodal-responsive FOXH1 at this earlier developmental stage (Takaoka *et al*, 2006).

The spatial confinement of the DVE to the distal tip of the embryonic VE at E5.5 is thought to be the result of an inhibitory BMP gradient emanating distally from the ExE (Rodriguez *et al*, 2005; Yamamoto *et al*, 2009). The ExE expresses BMP ligands, including *Bmp4* (Coucouvanis & Martin, 1999), expression of which is again induced by FGF4 signalling from the epiblast (Gotoh *et al*, 2005; Murohashi *et al*, 2010). The significance of the ExE in restricting DVE differentiation was demonstrated by physically removing it at E5.5, resulting in the expansion of DVE markers throughout the VE (Rodriguez *et al*, 2005; Mesnard *et al*, 2006). This phenotype could be rescued by culturing explants lacking the ExE in the presence of BMP4 (Yamamoto *et al*, 2009). When cultured with BMP4 from E5.2 to E5.5, embryos with an intact ExE showed a loss of *Cer1* and *Lefty1* expression (Yamamoto *et al*, 2009). Conversely, culture with Noggin, a BMP inhibitor, led to an expansion of the *Cer1* and *Lefty1* positive region in E5.5 embryos. Taken together, these data support a model where Nodal signalling from the epiblast induces DVE fate, while BMP4 from the ExE opposes DVE fate, resulting in the formation of a confined *Cer1*, *Lefty1* positive population of DVE cells around E5.5 (Figure B, left).

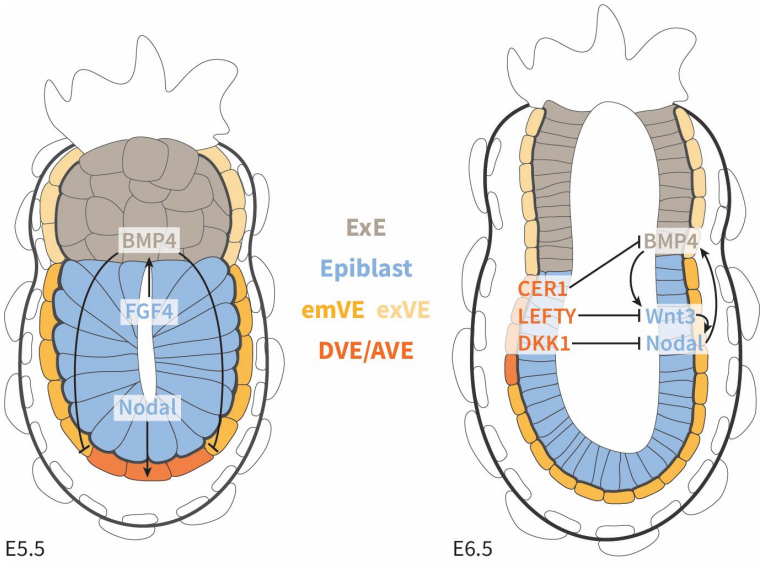

Figure B. DVE specification and anterior-posterior patterning.

Refer to the main text for details. Abbreviations: DVE/AVE: distal visceral endoderm/anterior visceral endoderm, E: embryonic day, emVE: embryonic visceral endoderm, ExE: extra-embryonic ectoderm, exVE: extra-embryonic visceral endoderm

Anterior-posterior patterning of the epiblast through signalling of AVE and ExE

Around E6.5, a distinct population of AVE cells emerges at the epiblast-ExE boundary on one side of the embryo, marking its future anterior side. Despite sharing a similar gene expression profile, proximally migrating DVE cells are not direct precursors of the AVE (Takaoka *et al*, 2011; Takaoka & Hamada, 2012; Zhu *et al*, 2023). Instead, cells acquire AVE fate *de novo*, with the DVE suggested to guide asymmetric migration of the emerging AVE (Takaoka & Hamada, 2012). The AVE is characterised by the expression of *Hex* and *Hesx1*. Observations that the anterior side of the embryo consistently arises in proximity to the *Hex*-positive AVE led to the initial proposal that extra-embryonic tissues may instruct embryonic tissue patterning (Thomas & Beddington, 1996; Thomas *et al*, 1998). Later, it became clear that the AVE establishes anterior identity in the epiblast by shielding it from the posteriorizing signals Nodal, Wnt, and BMP (Rossant & Tam,

2009; Arnold & Robertson, 2009; Takaoka & Hamada, 2012; Molè *et al*, 2020). Nodal is secreted by the epiblast and enhances BMP4 signalling from the ExE, leading to the upregulation of *Wnt3* in the epiblast, which, in turn, positively regulates *Nodal* transcription (Figure B, right)(Arnold & Robertson, 2009; Robertson, 2014). Unilateral expression of the signalling antagonists *Lefty1* (Nodal antagonist), *Cer1* (Nodal and BMP antagonist), *Dkk1*, and *Sfrp1* (Wnt antagonists) by the AVE establishes BMP, Nodal, and Wnt signalling gradients throughout the epiblast, thereby driving its anterior-posterior regionalisation (Belo *et al*, 1997; Perea-Gomez *et al*, 2002; Yamamoto *et al*, 2004; Kemp *et al*, 2005). In conclusion, breaking symmetry and establishing an anterior-posterior axis during early post-implantation development requires coordinated signalling interactions between the epiblast, AVE, and ExE, eventually providing the basis for the posterior initiation of gastrulation.

1.3.2. Modelling embryonic and extra-embryonic co-development *in vitro*

Self-renewing stem cell lines resembling the epiblast, trophectoderm, or PrE, at pre-and post-implantation stages have been established *in vitro*. These lines have proven essential in revealing the genetic basis and signalling requirements that underlie lineage commitment, maintenance, and differentiation. Although stem cell cultures can capture certain characteristics of embryonic and extra-embryonic lineages *in vitro*, these systems lack the structural complexity inherent to embryos. Consequently, developmental processes that require a structural context and/or depend on the interactions with other lineages, such as tissue patterning or regionalised differentiation events, cannot be studied using conventional culture methods. In response, various stem cell-based embryo models (“embryoids”) have been developed, which recapitulate specific aspects of embryonic development and allow to address questions that need the consideration of a 3D tissue architecture (Matthews *et al*, 2021). These models are of particular interest for studying human development, given the ethical and legal constraints associated with research involving human embryos. Embryoids can consist entirely of stem cells from a single lineage (non-integrated models), but have also been generated by combining embryonic and extra-embryonic stem cells (integrated models)(Rossant & Tam, 2021). Formation of embryoids leverages the ability of stem cells to self-organise into complex structures, representing a valuable bottom-up approach to decipher the cell-cell interactions that underlie the emergence of complexity during development. In the following section I will first discuss the stem cell equivalents of the three blastocyst lineages and then provide examples of how these cells have been combined to create embryoids. For the latter, I will specifically concentrate on embryoids that can offer insights into embryonic and extra-embryonic lineage interactions.

In vitro equivalents of the epiblast from pre- to post-implantation stages

Embryonic stem cells (ESCs) are regarded the *in vitro* counterpart of the embryonic pre-implantation epiblast. These cells could be derived from the blastocyst and were initially cultured on a feeder layer of mitotically inactivated fibroblasts in a medium containing foetal

bovine serum (Evans & Kaufman, 1981; Martin, 1981). Under these culture conditions, ESCs retained their pluripotency, as demonstrated by their ability to contribute to chimeric mice (Bradley *et al*, 1984). The need for feeder cells was later replaced by using Leukaemia inhibitory factor (LIF)(Williams *et al*, 1988). However, due to the use of serum, the culture conditions remained largely undefined and permitted heterogeneity within ESC cultures (Marks *et al*, 2012). Eventually, the combination of LIF with an inhibitor of glycogen synthase kinase-3 (GSK3)(*i.e*. canonical Wnt activator) and a MEK inhibitor efficiently promoted self-renewal and facilitated the establishment of homogenous cultures (Ying *et al*, 2008; Wray *et al*, 2011; ten Berge *et al*, 2011). These conditions, often referred to as 2i (2 inhibitors) maintain a state of naïve pluripotency, resembling the developmental ground state of the pre-implantation epiblast (Ying *et al*, 2008; Nichols & Smith, 2009).
In contrast, the establishment of primed pluripotent stem cell lines requires entirely different signalling cues. Unlike for naïve ESCs, MEK signalling must be activated through FGF, and in combination with active Activin/Nodal signalling allows for the derivation of primed epiblast stem cells (EpiSCs) from the post-implantation epiblast (Brons *et al*, 2007; Tesar *et al*, 2007). Consistent with the developmental trajectory *in vivo*, naïve ESCs can transition into primed EpiSCs in response to modified signalling cues. However, EpiSCs cannot revert to an ESC state unless forced by transgenic expression of the naïve-specific transcription factor KLF4 (Guo *et al*, 2009). Activin is also used to capture cells of formative pluripotency *in vitro*, but unlike EpiSCs these cells do not rely on FGF signalling and require Wnt inhibition (Kinoshita *et al*, 2021). Again, formative stem cells fail to revert to a naïve state when exposed to 2i culture conditions. This stands in contrast to cells of another intermediate pluripotency state, referred to as rosette stem cells. Despite also being cultured in Wnt-off and MEK-off conditions, these cells can be converted back into an ESC state by reactivating Wnt through GSK3 inhibition (Neagu *et al*, 2020).

Both, ESCs and EpiSCs correspond to the *in vivo* epiblast and thus only give rise to embryonic lineages in chimaeras (Bradley *et al*, 1984; Nagy *et al*, 1993; Huang *et al*, 2012; Wang & Wu, 2022). However, there have been efforts to culture pluripotent cells which maintain the capacity to differentiate into embryonic as well as extra-embryonic lineages. This includes extended pluripotent stem cells (EPSCs) (Yang *et al*, 2017b) and expanded pluripotent stem cells (Yang *et al*, 2017a).

Trophoblast stem cells from pre- and post-implantation stage embryos
Extra-embryonic trophoblast stem cell (TSC) lines can be directly derived from the embryo. In line with the role of FGF4 for polar trophectoderm and ExE expansion (Tanaka *et al*, 1998; Kunath *et al*, 2004; Christodoulou *et al*, 2019), the derivation of TSCs was first achieved by supplementing medium with FGF4 and Heparin alongside foetal bovine serum and feeder cell conditioned medium (Tanaka *et al*, 1998). TSCs retain the ability to differentiate into trophectoderm derivatives and, upon injection into a blastocyst, chimerise the placental portion of the conceptus (Tanaka *et al*, 1998). TGFβ and Activin were identified as additional key

factors that maintain TSC proliferation (Erlebacher *et al*, 2004), possibly mimicking the role of Nodal for maintaining the undifferentiated cells of the ExE *in vivo* (Guzman-Ayala *et al*, 2004). The use of TGFβ and Activin could replace feeder cell conditioned medium, resulting in a more chemically defined TSC culture medium (Erlebacher *et al*, 2004). However, culture of TSCs still relied on serum, an undefined component with high batch-to-batch variability. Eventually, a defined, serum free, feeder free protocol was developed, which also employed TGFβ1 and FGF4 (Kubaczka *et al*, 2014). Shortly after, another chemically defined protocol was published that in addition to FGF2 and Activin A included a canonical Wnt inhibitor and an inhibitor of the Rho-associated protein kinase p160ROCK (Ohinata & Tsukiyama, 2014).

Each of these protocols enables the derivation of TSCs from both pre-implantation trophectoderm as well as post-implantation ExE. Accordingly, TSCs express markers common to both trophectoderm and ExE, including CDX2, EOMES, and ELF5, albeit with considerable heterogeneity (Kubaczka *et al*, 2014; Kuales *et al*, 2015; Motomura *et al*, 2016). This heterogeneity has been suggested to reflect a range of differentiation states among TSCs (Motomura *et al*, 2016), however, it remains unclear which specific developmental stage TSCs represent *in vitro*.

PrE and its derivatives *in vitro*

Extra-embryonic stem cell lines, originating not only from the trophectoderm but also from the PrE, have been successfully established. Initially, extra-embryonic endoderm (XEN) stem cells were derived from mouse blastocysts on feeder cells in a serum-containing medium, with or without FGF4 supplementation (Kunath *et al*, 2005). XEN cells display characteristics of the PrE, PE, and VE, suggesting that they constitute a mixed population of different pre- and post-implantation states (Brown *et al*, 2010). When incorporated into chimaeras, XEN cells preferentially contribute to the PE, indicating a bias of XEN cells towards PE fate specification (Kunath *et al*, 2005). However, culture of XEN cells with Nodal or BMP4 leads them to adopt a phenotype more resembling the VE (Julio *et al*, 2011; Artus *et al*, 2012), in accordance with the role of these signalling molecules for VE differentiation *in vivo* (Mesnard *et al*, 2006; Yamamoto *et al*, 2009).

Extra-embryonic endoderm stem cells have also been generated through differentiation of ESCs. This can be achieved either chemically using Wnt signalling agonists and Activin (Anderson *et al*, 2017), or by overexpressing transcription factors crucial for PrE fate commitment, such as *Gata4* or *Gata6* (Mulvey *et al*, 2015; Wamaitha *et al*, 2015).

In an effort to establish cell lines that more accurately resemble the pre-implantation PrE, so called primitive XEN (pXEN) cells were derived from the embryo by reducing serum concentrations and adding LIF and PDGF to the medium (Zhong *et al*, 2018). More recently, another protocol was published that utilised a combination of FGF4, Heparin, PDGF, and a GSK3 inhibitor to generate stable PrE stem cell (PrESC) lines (Yasuhide *et al*, 2022). These cells transcriptionally resemble the pre-implantation PrE and show contribution to the PE as well as

the VE in chimaeras. While the importance of FGF4 and PDGF for PrE lineage commitment and maintenance *in vivo* has been well-described (discussed in section 1.3.1.), the role of Wnt activation through GSK3 inhibition in maintaining PrESCs with pre-implantation characteristics remains unclear.

Blastocyst-like structures generated from stem cells

Efforts to reconstruct the pre-implantation conceptus using only stem cells resulted in the creation of blastoids. In a first approach, TSCs were seeded on top of ESC aggregates inside agarose microwells, prompting cells to self-organise into structures that closely resemble the pre-implantation blastocyst (Rivron *et al*, 2018). Remarkably, co-culturing TSCs and ESCs in a blastocyst-like morphology altered their transcriptome to more closely resemble that of their *in vivo* counterparts, emphasising the significance of tissue architecture and lineage interactions in guiding proper lineage behaviour. Specifically, the model revealed that signals originating from the epiblast, including BMP4 and Nodal, can instruct trophectoderm proliferation and contribute to trophectoderm epithelial morphogenesis (Rivron *et al*, 2018). However, due to the limited capacity of ESCs to differentiate into extra-embryonic lineages, PrE-like cells were largely underrepresented in the inner cell compartment of blastoids (Rivron *et al*, 2018; Zhang *et al*, 2023). In an attempt to increase the number of PrE-like cells, TSCs were combined with aggregates of EPSCs instead of ESCs, resulting in the formation of EPS-blastoids (Sozen *et al*, 2019). Attributed to the extra-embryonic potential of EPSCs, PrE-like cells were specified more efficiently in EPS-blastoids. The authors reported that EPS-blastoids, unlike those generated with ESCs, could morphologically transition into early post-implantation-like structures (Sozen *et al*, 2019). This underscores the importance of interactions among all three blastocyst lineages for successful developmental progression beyond pre-implantation stages.

Several alternative blastoid models have emerged that do not require the use of TSCs. Instead, these models rely on cells that have been capacitated through different methods to generate both embryonic and extra-embryonic blastoid lineages (Kime *et al*, 2019; Li *et al*, 2019; Xu *et al*, 2022; Zhang *et al*, 2023). These blastoids thus form from only a single starting cell type, potentially offering *in vitro* tools suitable to explore the cell-cell interactions underlying earlier differentiation and morphogenetic events during blastocyst formation. In this vein, formation of blastoids with all three lineages from only a single cell type could serve as a useful assay to evaluate the enhanced potential of cell lines established in the ongoing pursuit of capturing totipotency *in vitro* (Malik & Wang, 2022).

To ensure the accuracy and reliability of findings obtained from blastoids, it is crucial to assess their fidelity in replicating the blastocyst embryo and its progression to post-implantation stages. While several studies have demonstrated that blastoids can elicit an implantation response when transferred back into the uterus, their developmental potential beyond implantation remains constrained (Rivron *et al*, 2018; Sozen *et al*, 2019; Kime *et al*, 2019; Li *et al*, 2019). Structures recovered from blastoid-induced deciduae are widely unorganised, ultimately leading to their resorption and inability to develop into *bona fide*

embryos. Furthermore, despite morphological similarities, generating blastoids with cell types accurately resembling all three blastocyst lineages, as well as achieving their appropriate ratios, has proven to be challenging. Comparative analysis of single-cell transcriptomic data from blastoids across different protocols and actual embryos revealed the presence of cell populations in blastoids with transcriptional profiles that do not correspond to any relevant *in vivo* lineage (Posfai *et al*, 2021; Zhang *et al*, 2023)(except for Kime *et al*, 2019, which did not generate single-cell transcriptomic data). Thus, further refinement of blastoid models to reliably mimic *in vivo* development will be necessary.

Nevertheless, the development of mouse blastoids, along with advances in human stem cell culture, has paved the way for the generation of blastoids also from human stem cells (Fan *et al*, 2021; Liu *et al*, 2021; Yanagida *et al*, 2021; Yu *et al*, 2021; Kagawa *et al*, 2022). Particularly when combined with uterine models, human blastoids now present an unprecedented opportunity to gain insights into human specific aspects of implantation.

Recapitulating interactions between epiblast and extra-embryonic endoderm using stem cells

While blastoids aim to recapitulate the full pre-implantation conceptus, partial models of only the inner epiblast and PrE lineage have also been established. When aggregated into embryoid bodies, ESCs on the outside of the aggregate would spontaneously differentiate into PrE-like cells, providing a first primitive model to study the signals supporting PrE specification and maturation (Shen & Leder, 1992; Murray & Edgar, 2001; Hamazaki *et al*, 2004). However, PrE-like cells can be generated from ESCs more efficiently through induced transient overexpression of the PrE-specific factors *Gata4* or *Gata6* prior to their aggregation (Mathew *et al*, 2019). The resulting "ICM organoids" present a robust model of epiblast and PrE co-development, spanning the period from lineage specification to early post-implantation stages (Mathew *et al*, 2019). Initially, ICM organoids comprised NANOG+ and GATA6+ cells in a salt-and-pepper distribution, reminiscent of the inner cells at an early blastocyst stage. However, after 2 days, GATA6+ cells had sorted to the outside of the aggregates and subsequently established a basal membrane between themselves and the inner ESCs. This coincided with the maturation of the inner cells, as reflected by the downregulation of NANOG (Mathew *et al*, 2019).

A similar model of human epiblast and hypoblast co-development has recently been published, combining wild type ESCs with cells that were genetically or chemically differentiated into hypoblast before aggregation (Okubo *et al*, 2024). Again, the hypoblast-like cells sorted to the outside of the aggregates, where they acquired a visceral endoderm-like fate. Remarkably, these cells then also specified AVE-like cells, capable of inducing anterior-posterior patterning of the underlying epiblast-like cells (Okubo *et al*, 2024).

AVE-like cells also specified in another recently established model which again relied on transient *Gata4* overexpression in mouse ESCs to specify a layer of VE-like cells surrounding an epithelialized layer of undifferentiated ESCs (BELAs)(Schumacher *et al*, 2023). Strikingly, the

subpopulation of AVE-like cells was spatially confined, contrary to expectations based on knowledge from the embryo where AVE restriction is believed to rely on signalling from the ExE (Rodriguez *et al*, 2005; Mesnard *et al*, 2006; Yamamoto *et al*, 2009). Instead, the observations in BELAs now support an alternative model where the AVE can be spatially restricted independently of the ExE. The study further suggests Wnt signalling as another pathway influencing DVE fate commitment, with active Wnt signalling countering DVE differentiation (Schumacher *et al*, 2023). This idea is supported by the expression of Wnt antagonists like *Dkk1*, *Sfrp1*, and *Sfrp5* in the DVE. This system therefore challenges current models of embryonic tissue patterning in mouse, emphasising the power of stem cell-based models to help dissect the minimum requirements of developmental events.

Embryoids recapitulating post-implantation embryonic and extra-embryonic lineages

A partial model of the early post-implantation embryo was developed by combining single ESCs with clumps of TSCs in Matrigel (Harrison *et al*, 2017). Cells self-organised into structures termed ETS embryos, which recapitulate the developmental steps from approximately E5.5 to E6.5. In these structures, ESCs formed a polarised epithelium surrounding a central lumen, while TSCs sat on top this epithelium and eventually polarised, creating their own lumen that connected with that of the ESCs (Harrison *et al*, 2017). Formation of ETS embryos highlighted the crucial role of epiblast-derived Nodal signals in ExE lumenogenesis. Expanding on the approach of ETS embryos, EpiTS embryoids were created by combining pre-formed aggregates of ESCs and TSCs (Girgin *et al*, 2021). By combining either epithelialized or non-epithelialized ESC aggregates with aggregates of TSCs, the authors demonstrated that epithelialisation is a major determinant for proper anterior posterior patterning.

However, these models lack cells from the extra-embryonic endoderm lineage. This was subsequently addressed by incorporating XEN cells in ETS embryos, leading to the development of ETX-embryos (Sozen *et al*, 2018; Zhang *et al*, 2019). XEN cells were able to engulf the epiblast and ExE- like compartments, resembling the VE *in vivo*. The inclusion of XEN cells replaced the need for Matrigel, as XEN cells could provide a laminin-containing basement membrane which induced lumenogenesis in the ESC and TSC compartments.

With the addition of XEN cells, ETX embryos exhibited features of gastrulation more efficiently compared to ETS embryos (Sozen *et al*, 2018). However, their ability to fully recapitulate gastrulation remained limited. Recognising the inherent bias of XEN cells towards PE rather than the required VE, an alternative approach was introduced (Amadei *et al*, 2020). In this protocol, XEN cells were replaced by ESCs differentiated into PrE-like cells by transiently overexpressing *Gata4*, resulting in the formation of ETiX embryos. ETiX embryos have significantly enhanced developmental potential, as they robustly establish an AVE-like signalling centre, which allows these embryoids to gastrulate (Amadei *et al*, 2020). Remarkably, by employing novel *ex utero* culture systems, the developmental capabilities of ETiX embryos could recently be significantly extended (Amadei *et al*, 2022).

Structures similar to ETiX embryos have been generated exclusively from ESCs. In this process, not only the extra-embryonic endoderm but also the trophectoderm lineage is derived through transient overexpression of lineage specific transcription factors (Langkabel *et al*, 2021; Lau *et al*, 2022; Tarazi *et al*, 2022). These embryoids have also demonstrated an extended developmental potential when cultured in *ex utero* culture devices (Lau *et al*, 2022; Tarazi *et al*, 2022).

1.4. Outline and objectives of the presented PhD research

This thesis combines three projects with my partial or full contribution. Although each project pursued its specific objectives related to understanding the developmental progression of embryonic and extra-embryonic lineages during implantation, they collectively relied on the use of embryonic and extra-embryonic stem cells.

Specifically, Chapter 2 comprises a published project aimed at refining the culture conditions for trophoblast stem cells by considering the *in vivo* interactions between epiblast and trophectoderm. The work underscores the pivotal role of the epiblast in patterning the trophectoderm, leading to the generation of polar and mural regions with distinct functions during implantation.

Chapter 3 presents another published project, aimed at developing an integrated stem cell-based model that recapitulates the co-development of the epiblast and PrE from pre- to post- implantation stages. Additionally, it outlines an approach to enhance the incorporation of PrE-like cells in blastoids which promotes the transition of blastoids towards post-implantation-like stages. Overall, this work highlights the reciprocal interactions that drive epiblast and PrE co-development during the pre- to post-implantation transition.

Chapter 4 summarises my own, unpublished work. I first aimed to identify interactions between all three blastocyst tissues more comprehensively using single cell sequencing data. Following up on predicted interactions between the two extra-embryonic tissues, the PrE and trophectoderm, defines a role of Wnt signalling in blocking differentiation of PrE-like cells *in vitro*. Moreover, we found that Wnt signalling also prevents PrE-like cells from establishing a basal membrane in a model of epiblast/PrE co-development – a crucial morphogenetic cue for developmental progression.

Given the significance of stem cells and embryoids as indispensable tools to study embryonic development, the concluding chapter will integrate the findings of the presented projects, focusing on two main aspects: (1) the progress made in integrated embryoid models of embryonic and extra-embryonic lineages during implantation stages, and (2) the advancements in our understanding of the culture requirements of extra-embryonic stem cells.

CHAPTER 2:
Epiblast inducers capture mouse trophectoderm stem cells *in vitro* and pattern blastoids for implantation *in utero*

Part of the work performed during my PhD was published in Cell Stem Cell 29 (7), 1102–1118, July 7, 2022 (https://doi.org/10.1016/j.stem.2022.06.002), and this publication is included as the following chapter. A summary of my exact contributions is provided at the end of this page.

2.1. Authors

Jinwoo Seong[1,7], Javier Frias-Aldeguer[2,3,7], Viktoria Holzmann[1,7], Harunobu Kagawa[1], Giovanni Sestini[1], Heidar Heidari Khoei[1,4], Yvonne Scholte Op Reimer[1], Maarten Kip[2], Saurabh J. Pradhan[1], Lucas Verwegen[5], Judith Vivié[2], Linfeng Li[3], Anna Alemany[2], Jeroen Korving[2], Frank Darmis[2], Alexander van Oudenaarden[2], Derk ten Berge[5], Niels Geijsen[2,6], and Nicolas C. Rivron[1,2,3,8,9]

2.2. Affiliations

1 Institute of Molecular Biotechnology of the Austrian Academy of Sciences, Vienna Biocenter, Vienna, Austria
2 Hubrecht Institute for Developmental Biology and Stem Cell Research, Utrecht, the Netherlands
3 Maastricht University, Maastricht, the Netherlands
4 Department of Stem Cells and Developmental Biology, Cell Science Research Center, Royan Institute for Stem Cell Biology and Technology, ACECR, Tehran, Iran
5 Department of Cell Biology, Erasmus MC, University Medical Center Rotterdam, Rotterdam, the Netherlands
6 Department of Anatomy and Embryology, LUMC, Leiden University, Leiden, the Netherlands
7 These authors contributed equally
8 Lead contact
9 Correspondence: nicolas.rivron@imba.oeaw.ac.at

2.3. Contributions

In this study, my contributions included conducting blastoid experiments, as depicted in Figure 5I and 5J as well as Figure S5M and S5N. Additionally, I performed experiments to demonstrate the re-establishment of CDX2 heterogeneity in TSC cultures, as illustrated in Figure S2I-K. Furthermore, I conducted experiments to optimise the Dox concentration for the *Cdx2* inducible cell line, as shown in Figure S6A. Lastly, I generated *Wnt7b*$^{-/-}$ and *Wnt6*$^{-/-}$ TSC lines (Figure S7D), which were utilised for subsequent experiments shown in Figure 7 and Figure S7.

Cell Stem Cell

Article

Epiblast inducers capture mouse trophectoderm stem cells *in vitro* and pattern blastoids for implantation *in utero*

Graphical abstract

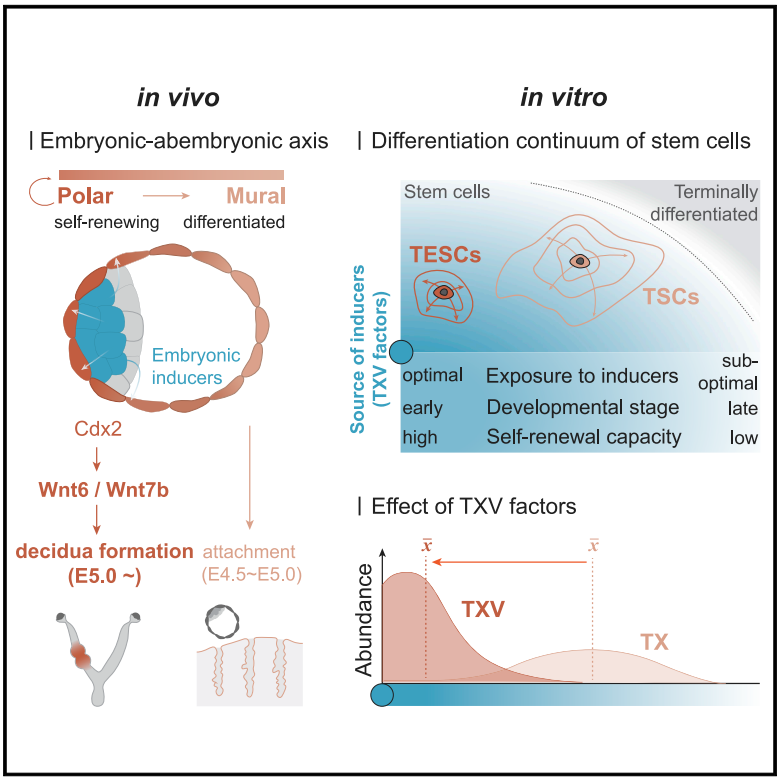

Highlights

- TSCs' heterogeneity reflects plastic transitions occurring during implantation
- Suboptimal inductions favor TSCs' heterogeneity and escape from self-renewal
- Optimal inducers capture TESCs reflecting blastocyst stage
- TESCs form more blastoids that better decidualize the uterus due to WNT6/7B secretion

Authors

Jinwoo Seong, Javier Frias-Aldeguer, Viktoria Holzmann, ..., Derk ten Berge, Niels Geijsen, Nicolas C. Rivron

Correspondence

nicolas.rivron@imba.oeaw.ac.at

In brief

Here, Seong et al. identify an optimal set of epiblast inducers that captures mouse trophectoderm stem cells (TESCs) as a stable and highly self-renewing state reflecting the blastocyst stage. TESCs have enhanced capacity to form blastoids that induce deciduae formation more efficiently *in utero* due to WNT6/7B secretion.

Seong et al., 2022, Cell Stem Cell *29*, 1102–1118
July 7, 2022
https://doi.org/10.1016/j.stem.2022.06.002

CellPress

CellPress
OPEN ACCESS

Cell Stem Cell

Article

Epiblast inducers capture mouse trophectoderm stem cells *in vitro* and pattern blastoids for implantation *in utero*

Jinwoo Seong,[1,7] Javier Frias-Aldeguer,[2,3,7] Viktoria Holzmann,[1,7] Harunobu Kagawa,[1] Giovanni Sestini,[1] Heidar Heidari Khoei,[1,4] Yvonne Scholte Op Reimer,[1] Maarten Kip,[2] Saurabh J. Pradhan,[1] Lucas Verwegen,[5] Judith Vivié,[2] Linfeng Li,[3] Anna Alemany,[2] Jeroen Korving,[2] Frank Darmis,[2] Alexander van Oudenaarden,[2] Derk ten Berge,[5] Niels Geijsen,[2,6] and Nicolas C. Rivron[1,2,3,8,*]

[1]Institute of Molecular Biotechnology of the Austrian Academy of Sciences, Vienna Biocenter, Vienna, Austria
[2]Hubrecht Institute for Developmental Biology and Stem Cell Research, Utrecht, the Netherlands
[3]Maastricht University, Maastricht, the Netherlands
[4]Department of Stem Cells and Developmental Biology, Cell Science Research Center, Royan Institute for Stem Cell Biology and Technology, ACECR, Tehran, Iran
[5]Department of Cell Biology, Erasmus MC, University Medical Center Rotterdam, Rotterdam, the Netherlands
[6]Department of Anatomy and Embryology, LUMC, Leiden University, Leiden, the Netherlands
[7]These authors contributed equally
[8]Lead contact
*Correspondence: nicolas.rivron@imba.oeaw.ac.at
https://doi.org/10.1016/j.stem.2022.06.002

SUMMARY

The embryo instructs the allocation of cell states to spatially regulate functions. In the blastocyst, patterning of trophoblast (TR) cells ensures successful implantation and placental development. Here, we defined an optimal set of molecules secreted by the epiblast (inducers) that captures *in vitro* stable, highly self-renewing mouse trophectoderm stem cells (TESCs) resembling the blastocyst stage. When exposed to suboptimal inducers, these stem cells fluctuate to form interconvertible subpopulations with reduced self-renewal and facilitated differentiation, resembling peri-implantation cells, known as TR stem cells (TSCs). TESCs have enhanced capacity to form blastoids that implant more efficiently *in utero* due to inducers maintaining not only local TR proliferation and self-renewal, but also WNT6/7B secretion that stimulates uterine decidualization. Overall, the epiblast maintains sustained growth and decidualization potential of abutting TR cells, while, as known, distancing imposed by the blastocyst cavity differentiates TR cells for uterus adhesion, thus patterning the essential functions of implantation.

INTRODUCTION

To implant into the uterus, mammals form a blastocyst comprising an inner epiblast (EPI) that later forms the body, surrounded by a fluid-filled, epithelial cyst called trophectoderm (TE) composed of trophoblasts (TRs) that will form the placenta. The EPI is placed asymmetrically in the TE cyst, a positioning that defines the first developmental axis (polar-mural, a.k.a. embryonic-abembryonic). Along this axis, the TE abutting the EPI (polar TE) proliferates and self-renews to progressively build the placenta into a composite organ that fulfills crucial functions (e.g., gas exchange, excretion of waste products, and functions that are immunological). The separation from the EPI, on the other hand, is associated with TE differentiation, decreased proliferation, and the capacity to attach to the uterus (Copp, 1978; Das et al., 1994; Gardner, 2000; Klaffky et al., 2001). Thus, one function of the blastocyst cavity is to separate the pools of TRs that will form the placenta or mediate the initial uterus attachment. In response to blastocyst implantation, uterine cells proliferate and undergo functional changes to create the decidua, a cocoon required for a successful pregnancy. Faulty decidualization is associated with infertility and miscarriages (Cha et al., 2012).

The TR lineage develops in a different way as compared to the EPI lineage: while the EPI lineage progress through pluripotency via a sequence of irreversible and epigenetically engraved lock steps with different signaling requirements (Nichols and Smith, 2012), TR progenitors self-renew *in vivo* thanks to a niche environment generated at the EPI/TR interface. This environment is currently defined by a number of soluble (Guzman-Ayala et al., 2004) and extracellular matrix (Kiyozumi et al., 2020) molecules that promote proliferation while inhibiting precocious differentiation, thus maintaining self-renewal. FGF4 is a niche factor produced by the EPI starting in mid-stage blastocysts (E3.25; Guo et al., 2010; Ohnishi et al., 2014) whose importance is evidenced by *Oct4*$^{-/-}$ mutant blastocysts that fail to express FGF4 but respond to exogenous FGF4 by increasing TR proliferation (Nichols et al., 1998). FGF4 induces the phosphorylation of ERK in some of the polar TE cells (E3.25–4.5) (Azami et al., 2019), which promotes proliferation and prevents differentiation and apoptosis (E4.5–5.0) through FGF receptors (Chai et al., 1998), FRS2 (Gotoh

et al., 2005), SHP2 (Yang et al., 2006), and the signaling effector kinase ERK2 (Hatano et al., 2003; Saba-El-Leil et al., 2003). During implantation, a tissue descending from the polar TE, the extraembryonic ectoderm (ExE), maintains the TR progenitors and has a continuous requirement for ERK signals between at least E4 and E8 (Corson et al., 2003; Azami et al., 2019). TGFβ superfamily members also contribute to the post-implantation maintenance of TR progenitors through activity of the Nodal receptor ACVR1B (Gu et al., 1998), the Nodal pro-protein convertases PCSK6 (PACE4) (Constam and Robertson, 2000) and Furin (Roebroek et al., 1998), and the effectors SMAD1 (Aubin et al., 2004) and SMAD2 (Weinstein et al., 1998). Finally, the Hippo and Notch pathways are important regulators of the initial TE specification (Nishioka et al., 2009; Rayon et al., 2014), and IGF2 is expressed at high levels in the polar TE (Nakamura et al., 2015), ExE, ectoplacental cone (EPC), allantois, and chorion (Lee et al., 1990) and contributes to TR proliferation (Gardner et al., 1999; Constância et al., 2002; Zechner et al., 2002).

The EPI/TR interface is a dynamic and regulative environment: the EPI sustains FGF4 production that stimulates BMP4 secretion from the ExE (Lawson et al., 1999; Murohashi et al., 2010) that might act as a direct niche factor (; Graham et al., 2014; Rivron et al., 2018) but also indirectly induces the EPI to express Nodal and Wnts (E6) (Ben-Haim et al., 2006; Miura et al., 2010). Nodal and Wnt ligands act in autocrine ways on the EPI but also feed back onto the TR progenitors to maintain self-renewal in part by regulating FGF4 expression (Guzman-Ayala et al., 2004; Ben-Haim et al., 2006). Altogether, this interface is a hotspot of regulative interactions maintaining the TR progenitors that are thought to persist until the mid-gestation placenta (Guzman-Ayala et al., 2004; Ueno et al., 2013; Natale et al., 2017).

In the presence of FGF4, TR progenitors isolated either from the blastocyst (E4.5) or ExE (E6.5) can proliferate and self-renew *in vitro* as TR stem cells (TSCs) (Tanaka et al., 1998). This shows that these progenitors possess an intrinsic, long-term self-renewal potential maintained by an EPI inducer. Here, we show that TSCs, which are notoriously heterogeneous (Sebastiano et al., 2010; Wu et al., 2011; Ohinata and Tsukiyama, 2014; Kuales et al., 2015; Motomura et al., 2016; Perez-Garcia et al., 2021), comprise fluctuating, interconvertible subpopulations resembling peri-implantation TRs. However, an optimal set of EPI inducers captures stable, highly self-renewing TRs resembling the blastocyst TE. We term these lines trophectoderm stem cells (TESCs). We show that TESCs not only maintain a high self-renewing capacity while inhibiting precocious differentiation but also secrete Wnt ligands that contribute to the decidual reaction *in utero*. Observing the behavior of TESCs and TSCs, we argue that optimal exposure to inducers sustains high self-renewal after implantation, while suboptimal exposure enables the concomitance of interconvertible subpopulations facilitating the exit from self-renewal and differentiation.

RESULTS

The transcriptome of pre- and post-implantation trophoblast cell types

In late mouse blastocysts, the transcription factor (TF) Caudal Type Homeobox 2 (CDX2) (Donnison et al., 2005; Strumpf et al., 2005) marks the polar TE. We confirmed that CDX2 expression decreases in the mural TE of E4.5 blastocysts, while KRT18 increases (mRNA and protein levels, Figures 1A and S1A). We first analyzed the transcriptomes of peri-implantation TRs to identify hallmarks for these states and candidate signaling pathways regulating them. Unsupervised clustering of E4.5 TE cells (late blastocyst stage) using an existing single-cell mRNA sequencing (scRNA-seq) dataset (Nakamura et al., 2015) confirmed a transcriptomic distinction between polar and mural TE (Figure 1B). We identified 2,107 differentially expressed genes (DE-Gs) (average LogFC ±0.25, $p < 0.05$, Figure S1B and Table S1A). Polar TE had increased expression of TFs regulating TR self-renewal (*Cdx2*, *Esrrb*, and *Elf5*) (Donnison et al., 2005; Strumpf et al., 2005; Gao et al., 2018), Wnt ligands *Wnt7b* and *BMP1/4/8b*, and the receptor *Il6st* (Figure 1D). Consistent with the established role of the MAPK pathway in regulating TR proliferation (Nichols et al., 1998; Tanaka et al., 1998), we found a pathway enrichment (*Fgfr1*, *Mapk1*, *Map2k1*, *Grb2*, and *Spry2*) and an upregulation of the proliferation machinery (*Cdk1*, *Ccnb1-2*, *Ccnd1*, *Mki67*, and *Pcna*) (Figures 1C and 1D). Polar cells also more abundantly expressed effectors of the SMAD signaling pathway (*E2f4*, *Smad3*, *Smad4*, and *Smad7*) (Nakao et al., 1997; Ishisaki et al., 1999) and *Pcsk6*, a secreted pro-convertase that cleaves the TGFβ family member pre-Nodal to locally enhance its potency. This supports an earlier role for SMAD signaling than previously reported (Tsuji et al., 2003; Guzman-Ayala et al., 2004; Mesnard et al., 2011). Similarly, Hippo pathway members (*Amot*, *Lats2*, *Ywhab*, and *Wwc1*) and targets (*Max*, *Myc*, and *Ccnd1*) that regulate *Cdx2* were also more abundant in the polar TE (Figures 1C, 1D, and S1C). We confirmed the presence of FGF4, BMP4, Nodal, and IL11 transcripts in the blastocyst EPI by single-molecule FISH (smFISH) (IL11 is also detected in the TE, Figure S1D). Finally, ERK, SMAD1/5/8, and STAT are phosphorylated in the TE, although ERK is restricted to few TRs (Figure S1D). We concluded that, beyond FGF signaling, the STAT, SMAD, and Hippo pathways are enhanced in the polar TE. We also extracted markers of the polar region (*Ly6a, Gsto1*, and *Ddah1*, Figure 1D and Table S1A) for their high expression. Mural TE had increased expression of integrins (*Itga5/6/7/v*), laminins (*Lama1/b1/b2*), galectins (*Lgals1* and *Lgalsl*), *Hb-egf*, and ephrins (*Efna1/b1/b2*), consistent with an adhesive and repulsive/invading phenotype initiating implantation (Klaffky et al., 2001; Sutherland, 2003; Barrientos et al., 2014) (Figure S1C). The mural TE was additionally characterized by molecules associated with the formation of intermediate filaments (*Krt8/18*) and tight junctions (*Ocln*, *Pard3*, and *Pard6b/g*) and by TFs *Gata2*, *Klf4/5/9*, *Tfap2a*, and *Tcf7l2* (Figure 1D).

High CDX2 expression also marks the post-implantation ExE (E6.5), while KRT18 is strongly expressed in surrounding cells (Figure 1E). When we compared the transcriptome of TE and ExE TRs using another published metadata set (Posfai et al., 2021) (Figures 1F and S1E–S1H), we identified 2,971 DE-Gs (average LogFC ±0.25, $p < 0.05$, Figure S1E and Table S1B), inferring differences in cell-cycle regulation and cell-cell adhesion (Figure S1I). Developmental progression was reflected by increased expression of *Elf5*, *Tead2*, *Id1*, *Cited2*, *Ascl2*, *Eomesodermin* (*Eomes*), *Hand1*, and *Sox2* and decreased expression of *Cdx2*, *Klf5*, *Tead4*, *Gata2/3*, *Ly6a*, and *Spry2* TFs (Figure S1J). Expression of the secreted ligands *Bmp4* and *Igf2* increased, whereas genes associated with insulin signaling decreased.

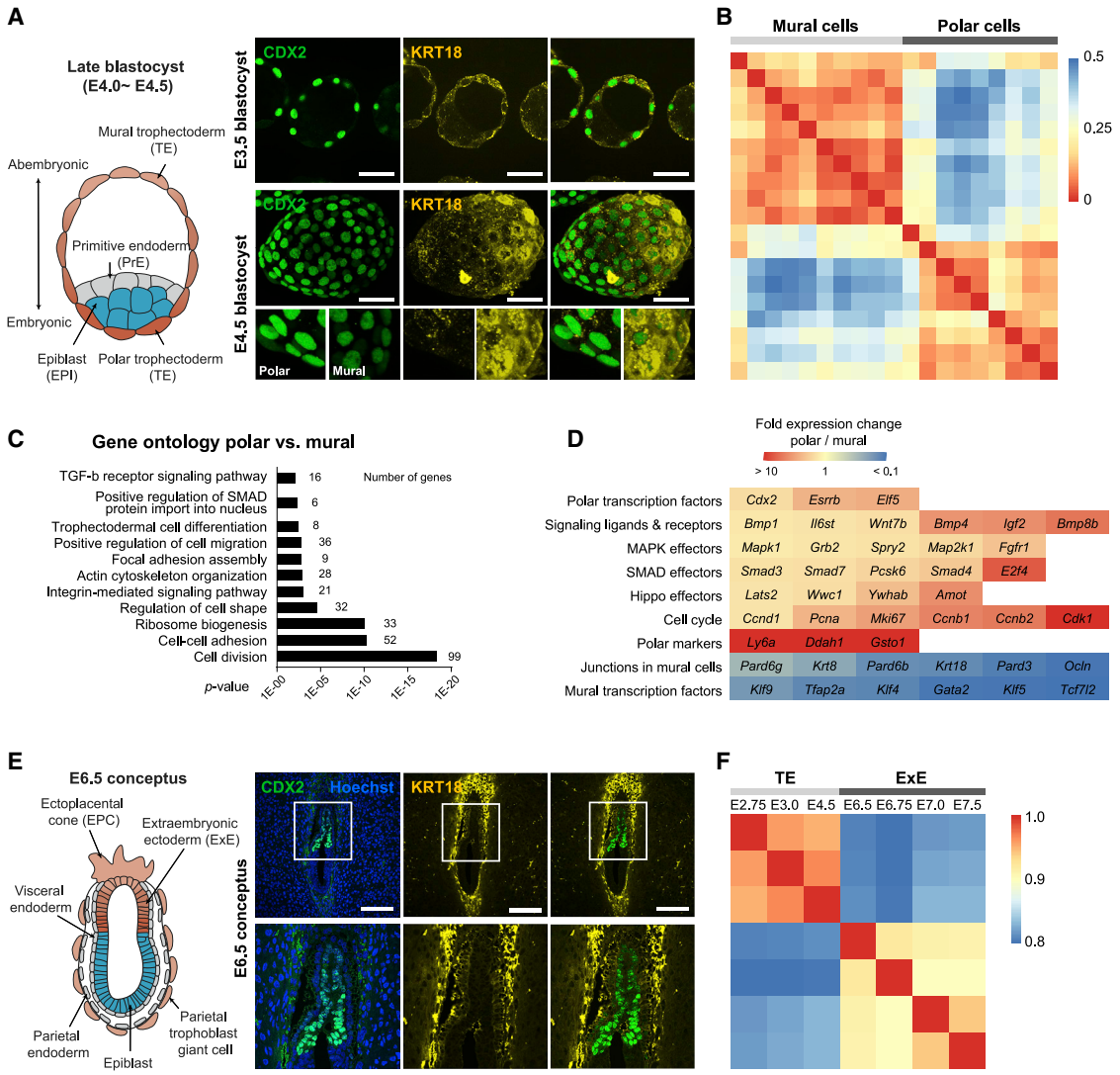

Figure 1. The transcriptomic transitions of pre- and post-implantation TRs

(A) Immunostaining for CDX2 and KRT18 showing uniform protein distribution at E3.5 but polar or mural bias in E4.5 blastocysts. Higher CDX2 expression in the polar region was detected in 65% of late blastocysts (11/17). Scale bar, 40 μm.

(B) Unsupervised clustering analysis (distance map from RaceID pipelines) of E4.5 TE single cells confirms the presence of two subpopulations: polar and mural. Each column and row represent a single cell from each group.

(C) Gene ontology analysis based on differentially expressed genes between polar and mural TE.

(D) Heatmap showing fold expression changes of indicated genes in the polar TE compared to the mural TE (see also Table S1).

(E) In an E6.5 (post-implantation) conceptus, CDX2 expression is restricted to the ExE and does not correlate with KRT18 localization. Scale bar, 150 μm.

(F) Spearman correlation analysis of TE and ExE at various developmental stages shows transcriptomic differences between TE and ExE.

See also Figure S1.

Altogether, this analysis highlights specific EPI inducers, TRs signaling pathway activities, and markers that define TR progression around implantation time.

Trophoblast stem cells encompass multiple subpopulations reflecting the trophectoderm, extraembryonic ectoderm, and differentiated trophoblasts

TSCs' intercellular heterogeneity has been visualized by CDX2 and EOMES immunofluorescence (Figure 2A) (Kuales et al., 2015; Motomura et al., 2016). To resolve transcriptional profiles of subpopulations, we performed bulk RNA-seq of 1,000 CDX2^{high} and CDX2^{low} TSCs derived from a CDX2-eGFP reporter mouse line (McDole and Zheng, 2012) (Figure 2B) and cultured in chemically defined medium complemented with FGF4/TGFβ1 (TX medium; Kubaczka et al., 2014), which are the minimal molecules necessary for maintaining *in vitro* TR proliferation and self-renewal. We identified 1,941 DE-Gs (FC > 1.5, p < 0.01, Table S2). CDX2^{high} TSCs were enriched for TFs regulating self-renewal (*Esrrb*, *Eomes*, and *Elf5*),

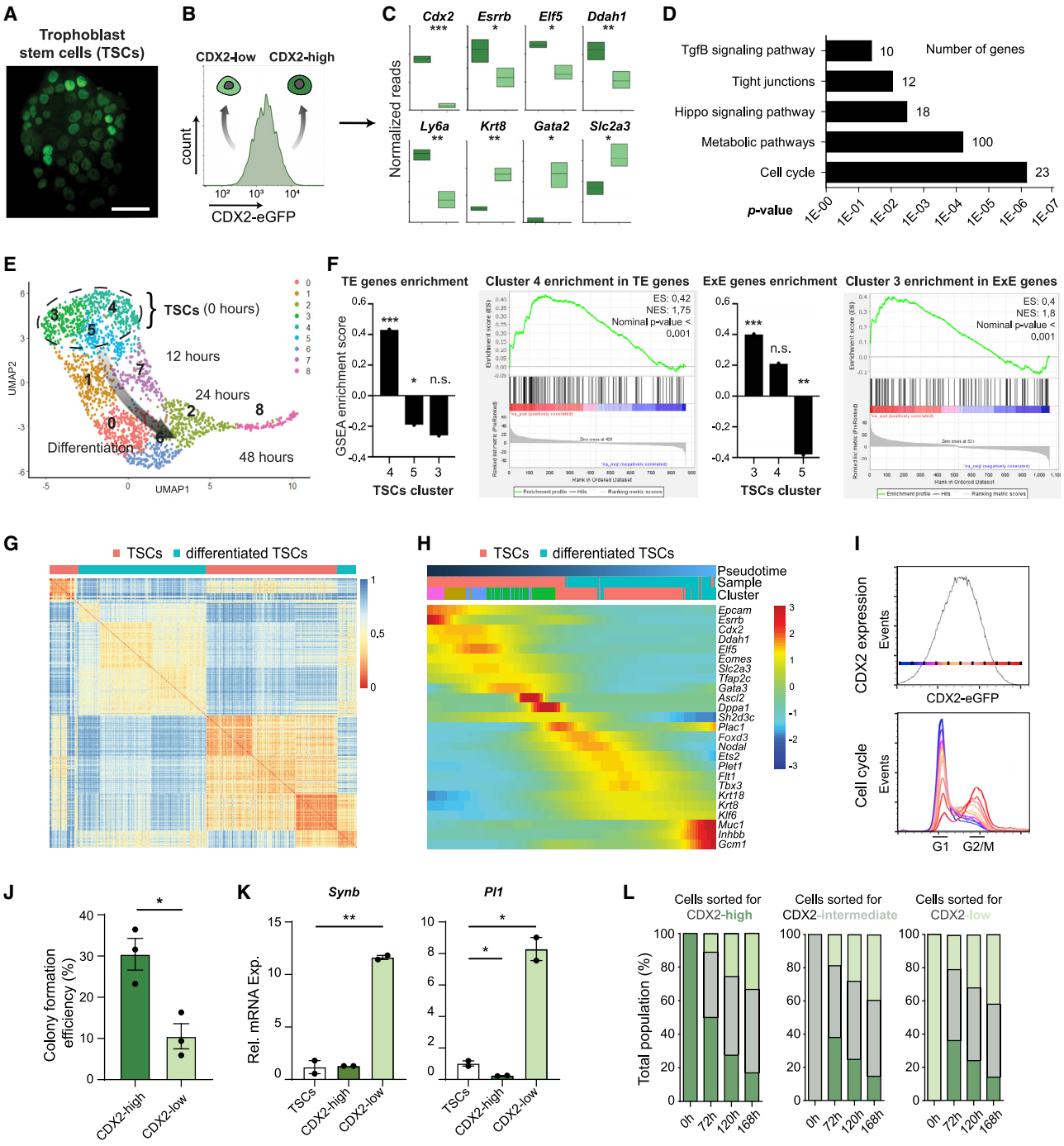

Figure 2. TSCs comprise heterogeneous and interconvertible states reflecting peri-implantation stages

(A) Naive GFP signal of CDX2-eGFP TSCs. Scale bar, 40 μm.

(B) CDX2^{high} and CDX2^{low} TSCs were sorted out with flow cytometry for RNA-seq.

(C) mRNA expression of self-renewal, polar, and differentiated marker genes in CDX2^{high} and CDX2^{low} TSCs (based on three independent bulk RNA-seq results). Dark and light green represent CDX2^{high} and CDX2^{low} TSCs, respectively.

(D) Gene ontology analysis based on differentially expressed genes enriched in CDX2^{high} compared to CDX2^{low} TSCs.

(E) Single-cell transcriptome analysis upon removal of minimal inducers.

(F) Gene set enrichment analysis (GSEA) for TE and ExE genes. Clusters 3, 4, and 5 are considered to be TSCs and show different gene enrichment, indicating heterogeneity of TSCs. Data were analyzed by Wilcox likelihood-ratio test.

(G) Unsupervised cell clustering analysis (distance map) of TSCs and 6-day-differentiated TSCs.

(legend continued on next page)

cell-cycle components, the Hippo pathway, and some polar markers (*Ly6a* and *Ddah1*). In contrast, the CDX2^{low} TSCs showed higher expression of differentiation markers *Krt8* and *Gata2* (Figures 2C and 2D).

Next, we delineated TSCs' heterogeneity through scRNA-seq analysis (Figures 2E and S2A). Three subpopulations (cluster 3, 4, and 5) were present (Figure 2E). One of these clusters (cluster 4) was enriched for TE-associated genes (GSEA, Normalized Enrichment Score [NES]: 1.75; e.g., *Gata3* and *Ly6a*), including genes associated with epithelia (*Cldn4/6*, *Krt18*, *Epcam*, *Ctnna1*, *Lgals9, Krt8/18*, and *Itga6*) (Table S3A). Another cluster (cluster 3) was enriched for ExE genes (GSEA, NES: 1.8; e.g., *Eomes*, *Elf5*, *Hand1*, *Tead2*, *Id1*, *Cited2*, and *Bmp4*) (Figures 2F and S2B and Table S3B). The third one (cluster 5) was significantly depleted in both TE and ExE genes (Figure S2C) and reflected more differentiated TRs. Upon removal of FGF4/TGFβ1, cells differentiated as indicated with a decrease in self-renewal and TE-related transcripts and an increase in differentiation-associated transcripts (Figure S2D).

By analyzing single TSCs and 6-day-differentiated TSCs, we obtained a different resolution of the heterogeneity profile. Unsupervised clustering analysis separated TSCs into four subpopulations and 6-day-differentiated TSCs into two subpopulations (Figure 2G). Cells aligned along a Monocle-predicted pseudotime trajectory (Figures 2H and S2E) (Trapnell et al., 2014) in which low pseudotime values corresponded to a TSC subpopulation with higher *Cdx2* and *Esrrb* expression levels, while the next cells along pseudotime values showed higher expression of *Elf5*, consistent with ExE identity (Figure 2H). Following in the trajectory were cells abundant for *Tfap2c* and *Ascl2* expression and TFs marking the ExE/EPC (Guillemot et al., 1994; Auman et al., 2002; Werling and Schorle, 2002; Latos et al., 2015), while the highest pseudotime values marked cells expressing the TR differentiation markers *Flt1* or *Gcm1*. Importantly, we identified differentiated TRs within TSCs (9%, Figure S2E), showing that FGF4/TGFβ1 consent to spontaneous differentiation. We confirmed the presence of subpopulations using smFISH with cells rich in either *Cdx2*, *Gsto1*, and *Esrrb* or *Ascl2*, *Gcm1*, and *Krt18* transcripts (Figure S2F). This was further confirmed at the protein level (CDX2/KRT18, Figure S2G). Taken together, these analyses show that FGF4/TGFβ1 consent to the maintenance of concomitant subpopulations reflecting the blastocyst TE, post-implantation ExE, and more differentiated TRs.

Trophoblast stem cells' subpopulations reflect functionally different and interconvertible stem cell states

Next, we examined whether CDX2^{high} and CDX2^{low} TSCs represent functionally different states. Using flow cytometry analysis, we observed that CDX2^{high} cells were present in all cell-cycle phases, while CDX2^{low} cells were predominantly in the G0/G1 phases (Figure 2I). Consistently, CDX2^{high} cells had a 30% clonogenicity rate, three times higher than that of CDX2^{low} cells (Figure 2J), which were more prone to differentiate upon removal of FGF4/TGFβ1 (*Pl1* and *Synb* mark TR giant cells and syncytiotrophoblasts, respectively; Figure 2K).

Protein fluctuation can occur stochastically but synchronously for members of the same biological pathway, which generates heterogeneity (Sigal et al., 2006). When we conducted live imaging of CDX2-eGFP TSCs, we observed transitions between the CDX2^{high} and CDX2^{low} states (Figure S2I and Video S1) reminiscent of fluctuations in ESCs (Chambers et al., 2007; Hayashi et al., 2008; Hastreiter et al., 2018). Thus, we investigated whether subpopulations were capable of interconversion. Within 5 days after sorting of CDX2^{high} or CDX2^{low} cells, these subpopulations re-established the initial heterogeneity (Figure 2L), and analysis of multiple sortings over 50 days showed that the initial transcriptome was restored (Figures S2I and S2J). We concluded that these states are reversible and that heterogeneity is an intrinsic, possibly regulated property of TSCs under minimal conditions. However, the CDX2^{low} cells proliferated more slowly than the CDX2^{high} cells (Figure S2K), suggesting a priming mechanism.

In ExE and TSCs, the *Cdx2* locus is marked with high levels of the activating H3K4me3 mark, while these levels decrease upon differentiation (Rugg-Gunn et al., 2010). Accordingly, H3K4me3 levels at the *Cdx2* promoter were 50% lower in CDX2^{low} TSCs, suggesting either reduced promoter activity or fewer active promoters (Figure S2L). In contrast, levels of the active transcription marker H3K9Ac were comparable between populations. We concluded that the *Cdx2* locus remains accessible and can be reactivated, for example in response to an environmental factor such as a growth factor, but is subjected to reversible epigenetic regulations that prime CDX2^{low} TRs for differentiation. This transcriptomic and epigenetic reversibility is consistent with the reversibility of the mural TE, as shown by blastocyst microdissection/recombination (Gardner et al., 1973; Gardner, 1983). Overall, we concluded that FGF4/TGFβ1 allow fluctuating, interconvertible, peri-implantation-like TR states with different proliferation and self-renewing potentials, a phenomenon that facilitates differentiation.

Exposure to optimal embryonic inducers generates stable CDX2^{high} trophoblast stem cells

Next, we investigated the impact of combined EPI inducers. We tested individual molecules acting on pathways found active in the TE (Figure S1D) for their capacity to induce CDX2 in TSCs (Figures 3A and S3A and Table S4). Nine molecules acted in a dose-dependent manner including IL11, Activin, BMP4/7, 1-Oleoyl Lysophosphatidic Acid (LPA) (Yu et al., 2012, 2021; Goto et al., 2015), 8-Br cAMP, XAV939, and the PPAR

(H) Pseudotime heatmap for visualization of expression patterns along with marker genes for various differentiation states. For clusters, see also Figure S2E.
(I) Cell-cycle analysis of TSCs shows a correlation between CDX2 expression (higher CDX2 content in red, lower in blue) and the cell-cycle state.
(J) Colony formation potential of single CDX2^{high} and CDX2^{low} cells based on three independent experiments. Data are means ± SEM, analyzed by Student's t test.
(K) mRNA expression of differentiated marker genes in CDX2^{high} andCDX2^{low} TSCs.
(L) Percentage of the different subpopulations upon pure subpopulation sorting and further independent culture, based on three independent experiments and a total of 96 wells of cells for each condition. Dark green for CDX2^{high}, gray for CDX2^{intermediate}, light green for CDX2^{low}.
For each panel, *p < 0.05, **p < 0.01, ***p < 0.001. See also Figure S2.

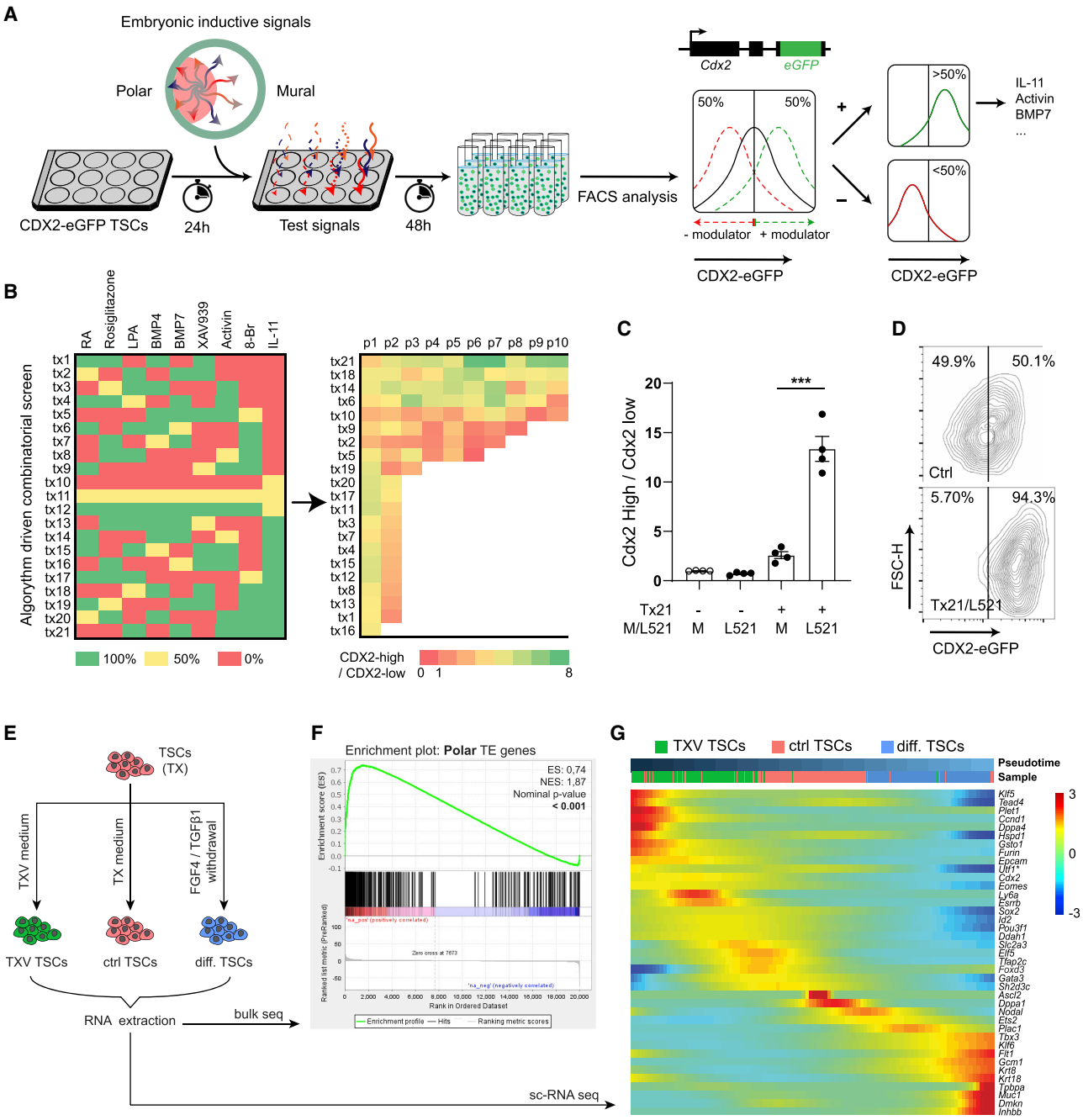

Figure 3. Optimal embryonic inducers capture TR stem cells with a transcriptome more akin to the TE

(A) Strategy to identify CDX2 expression regulators with CDX2-eGFP TSCs. Chemicals with a $CDX2^{high}/CDX2^{low}$ ratio bigger than 1.25 were considered positive modulators.

(B) List of 21 different cocktails using a combination of nine different CDX2 regulators (left). Green, yellow, and red color with percentage indicate the relative concentration of each modulator. Actual modulator concentrations are indicated in Figure S3A. The 21 cocktails were ranked based on the average $CDX2^{high}/CDX2^{low}$ ratio after 10 passages (right). Colors from 0 to eight indicate $CDX2^{high}/CDX2^{low}$ ratio based on flow cytometry.

(C) $CDX2^{high}/CDX2^{low}$ ratios of TSCs upon combination of the top cocktail (Tx21) with either Matrigel or Laminin 521 (L521) coated plates. Data are means ± SEM, analyzed by one-way ANOVA. ***$p < 0.001$.

(D) Flow cytometry showing that Tx21 compounds combined with L521 dramatically increase the percentage of $CDX2^{high}$ cells.

(E) Schematic view of each group preparation.

(F) GSEA for polar TE genes with TSCs exposed to optimal inducers for 15 days.

(G) Pseudotime heatmap for visualization of expression patterns along with self-renewal, polar, differentiated, and classical TSCs marker genes. Most self-renewal and polar genes are enriched in TXV TSCs compared to TX or differentiated TSCs.

See also Figure S3.

receptor agonist Rosiglitazone) ($CDX2^{high}/CDX2^{low}$ ratio >1.25, Table S4). We excluded the autocrine factor IGF2, previously proposed to guide TR differentiation (Lee et al., 2019) (Figure S3B). Because secreted molecules act synergistically during development, we explored combinations using factorial design (Hutchens et al., 2007) by culturing TSCs for 10 passages while monitoring CDX2 expression (Figure 3B). Although all combinations initially induced CDX2, most cultures (17/21) collapsed after two passages due to a lack of proliferation or attachment. The remaining four conditions supported a sustainable, long-term increase in CDX2 expression without apparent cell death. Through principal component analysis, we identified IL11, BMP7, LPA, Activin, and 8-Br cAMP (Tx21 medium) as most beneficial, evidenced by higher expression of self-renewal TFs (*Cdx2*, *Eomes*, *Esrrb*, and *Elf5*) and lack of upregulation of differentiation markers (e.g., ExE/EPC marker *Ascl2*) (Figures S3C–S3E). We then tested eight different laminin proteins to replace Matrigel, and we selected laminin L521 based on its expression in the blastocyst, its support of TSC proliferation, and an increase of CDX2 expression (Figures 3C, 3D, and S3F–S3H). An optimal set of molecules includes FGF4 (25 ng/mL), TGFβ1 (2 ng/mL), Activin (50 ng/mL), IL11 (50 ng/mL), BMP7 (25 ng/mL), 8-Br cAMP (200 μM), LPA (5 nM), and L521 coating, hereafter referred to as TXV (for TX plus five compounds).

Trophoblast stem cells exposed to optimal epiblast inducers maintain a trophectoderm-like transcriptome

We next analyzed the transcriptome of TXV TSCs. In-bulk analyses showed that a transcriptome shift occurred within 48 h and was further enhanced after 15 days (1,360 and 3,473 DEG, respectively, $p < 0.05$) (Figure S3I and Tables S5AA, Tables S6AS6B, and S7). After 15 days, GSEA showed that polar TE genes were significantly enriched, including *Cdx2*, *Eomes*, and *Ly6a*, whereas mural and ExE genes were not (Figures 3E, 3F, and S3J). Notably, transcripts for molecules reported to mediate mural TE/endometrium interactions (*Lgals1*, *Hb-egf*, and *Efna1*) (Fujii et al., 2006; Lim and Dey, 2009; Barrientos et al., 2014; You et al., 2018) (Figure S3K) and transcripts for molecules that increase upon ExE progression (*Elf5*, *Tead2*, *Id1*, *Ascl2*, and *Hand1*) (Figure S1J) were decreased (Table S6A). Gene ontology analysis showed differences in transcription (448 genes, Benjamini = 1.4×10^{-12}), cell-cell adhesion (79 genes, Benjamini = 3.9×10^{-12}), and cell cycle (159 genes, Benjamini = 8.7×10^{-6}) (Tables S5A and S6A). A transcriptome shift was confirmed in three lines from different genetic backgrounds (Figure S3L).

Exposure to increased FGF4 concentrations or genetic induction of *Cdx2* (48 h, Figure S3J) led to different transcriptome shifts as compared to TXV (Tables S5B, S6B, S6C, and S7), which suggests that the set of inducers acts more broadly, possibly on CDX2 upstream regulators such as Notch signaling (*Notch4* and *Rbpj*) (Figure S3I and Tables S5B, S6B, S6C, and S7). scRNA-seq analysis (unsupervised clustering and monocle analysis) assigned the lowest pseudotime values to TXV TSCs and reflected a developmental trajectory with initially high expression of TE TFs (*Cdx2*, *Eomes*, and *Elf5*) and polar markers (*Ly6a*, *Ddah1*, *Hspd1*, *Gsto1*, and *Utf1*) (Figures 3G, S3M, and S3N). Cells with the lowest pseudotime values expressed high levels of *Klf5* and *Tead4*, two TFs essential for early TE specification (Shindo et al., 2002; Yagi et al., 2007; Ema et al., 2008; Nishioka et al., 2008; Lin et al., 2010). These were followed by cells highly expressing the polar TE markers *Ly6a* and *Esrrb*, and *Duox2* and *Gsto1*, previously described as markers for *bona fide* TR progenitors (Kubaczka et al., 2014; Kuales et al., 2015) (Figure S3N). TE epithelia genes were also prominent at low pseudotime value (Figure S3O). Collectively, we concluded that an optimal set of EPI inducers (MAPK, Hippo, SMAD, and STAT; see Table S5A) maintain a state better reflecting the TE transcriptome and prevent the expression of blastocyst mural TE and post-implantation ExE genes.

Epiblast inducers enhance trophoblast stem cells' self-renewal, enhance derivation of lines, and repress differentiation

Culturing TSCs in TXV enhanced clonogenicity (40%, 2-fold, $p < 0.0028$; Figures 4A and 4B), mirroring levels of ground state ESCs (Ying et al., 2008). We also measured increased efficiency for TR progenitor derivation from blastocysts (percentage of $CDX2^{+}/EOMES^{+}$ cells, Figures 4C, S4A, and S4B) in the three different genetic backgrounds tested, including C57BL/6J mice (Ohinata and Tsukiyama, 2014). Cell line derivation was highly efficient from both E3.5 blastocysts and E6.5 isolated ExE (Figure S4C), showing the reversibility of ExE progenitors. In these lines, the number of differentiated $KRT8/18^{high}$ cells reduced (2%–8%) and increased upon exposure to the PPARd receptor agonist GW501516 that confers TE implantation competency (Xie et al., 2008) (Figures 4D and 4E). The polar protein LY6A was also increased (Figures 4F–4H and S4E). Upon growth factor removal, TXV TSCs differentiated as evidenced by a decrease in *Cdx2* expression (day 1) and upregulation of the ExE/EPC marker *Ascl2* (day 2–3) (Figure 4I). Although TX TSCs required a transition to serum-containing medium to chimerize the placenta (Kubaczka et al., 2014), TXV TSCs contributed to the TE when injected into morula-stage embryos (Figure S4F) and chimerized the $ELF5^{+}$ ExE compartment (E7.5, Figures 4J, 4K, and S4G–S4I). We did not observe embryonic contribution.

Epiblast inducers enhance the epithelial phenotype and morphogenetic potential of trophoblast stem cells

The transcriptome of TXV TSCs was enriched in epithelia transcripts including those related to extracellular matrix organization, cell adhesion, pathways related to ECM-receptor interaction, focal adhesion, cytoskeleton, and tight junctions (e.g., *Cldn4*, *Cldn6*, *Tjp2*, and *Jam2*) that contribute to TE morphogenesis (Moriwak et al., 2007) (Figure S3O). By quantifying phenotypic changes of single-cell morphologies using E-CADHERIN/Hoechst-staining segmentation, we extracted 161 morphometric features from both TX TCSs (502 cells) and TXV TSCs (297 cells) (Figure S5A). After being ranked based on the p value scores (Mann-Whitney; Methods S1), the top 20% morphometric features separated the two populations (Figures S5B and S5C). TXV TSCs had significantly larger cell size and nuclei areas and were more circular and less lobulated (Figure S5D). Cells reflecting the TE should efficiently undergo epithelial morphogenesis. As compared to TX TSCs, TXV TSCs more efficiently formed blastoids that were larger and more circular (Figures 5A–5D and S5E). This was partly due to an enhanced autonomous potential measured by a higher capacity to

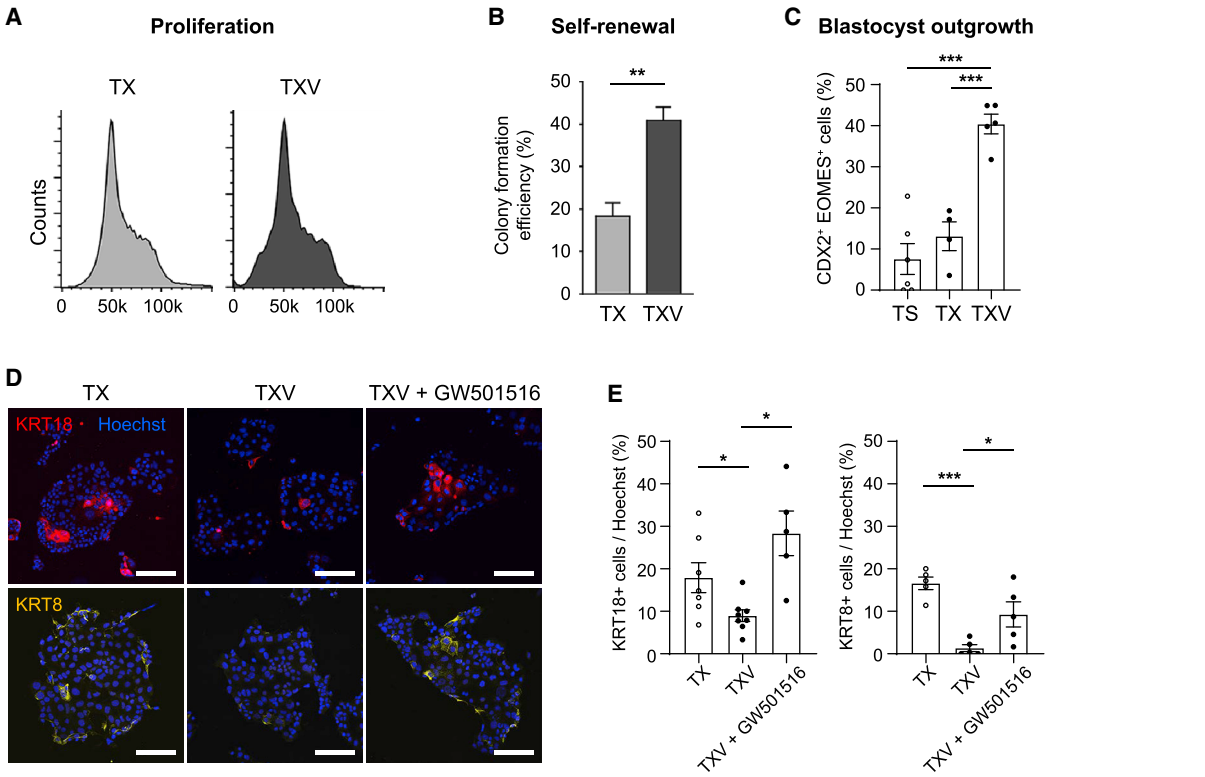

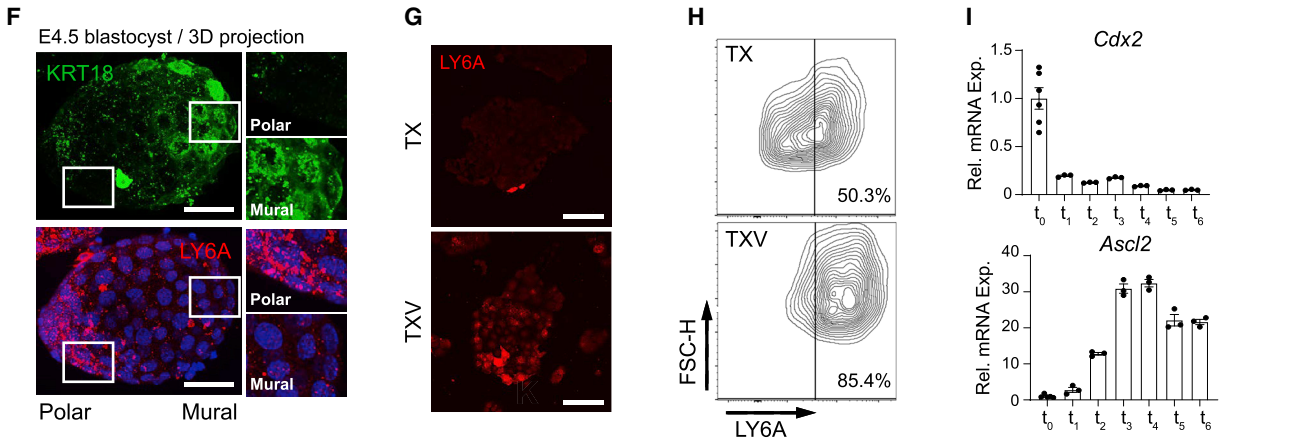

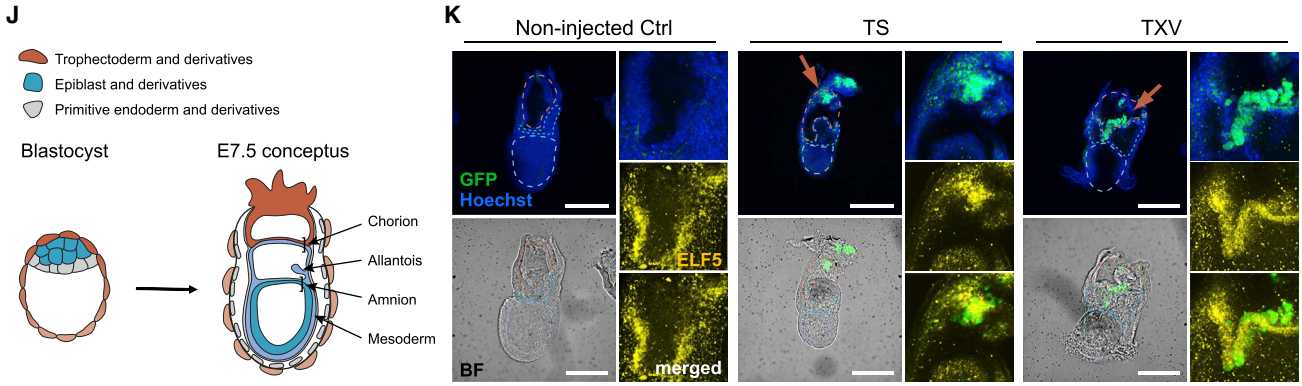

(legend on next page)

form trophospheres (cavitation efficiency and circularity) (Figures S5F–S5H). This was also due to an enhanced response to ESCs as TXV TSCs formed blastoids that had a larger diameter, a feature that did not occur in trophospheres (Figures 5B and S5G). Because TX and TXV TSCs proliferate at similar rates in blastoids (Figure S5I), we concluded that the increased diameter was due to enhanced swelling in response to inducers. Blastoids correctly localized the basal adherens junctions (E-CADHERIN [E-CAD]) and apical cytoskeletal protein (KRT8/18) (Figure 5E). Taken together, these observations show that TXV TSCs have an enhanced epithelial phenotype and morphogenetic functions, consistent with the TE.

Cumulatively, we showed that TSCs cultured in TXV (1) enhance their transcriptomic similarity to the TE, (2) enhance their self-renewal, (3) repress gene expression associated with differentiation, (4) maintain their potential to rapidly differentiate and chimerize the ExE, and (5) have an enhanced potential to recapitulate features of TE epithelial morphogenesis. Therefore, we call these cells TESCs.

Epiblast inducers spatially pattern the polar-mural axis

Next, we asked whether inducers spatially pattern the polar- and mural-like states that confer specific functions during implantation. Single TRs isolated from blastoids formed a pseudotime trajectory (Figure S5J) that included three transitioning clusters (Figure S5K). Cells with low pseudotime values more abundantly expressed transcripts for *Esrrb*, *Cdx2*, and *Ly6a* (Figures 5F and 5G) and numerous polar genes (*Ly6a*, *Gsto1*, *Ddah1*, *Utf1*, and *Duox2*). In contrast, the cluster with the highest pseudotime value showed enhanced expression levels of mural markers (*Krt8/18*, *Ndrg1*, *Basp1*, *Ctsb, Flt1*, and *Slc5a5*) and of *Lgals1*, which mediates endometrial interaction (Sood et al., 2006; Shi et al., 2013; Barrientos et al., 2014) (Figure 5F). Using smFISH, we confirmed that the polar marker *Ly6a* was more prominently expressed in the blastoid polar cells (7/10) (Figures 5H and S5L). At the protein level, the axis defined by CDX2 and KRT8/18 formed at a low efficiency similar to that in previously reported blastoids formed either with ESCs (Rivron et al., 2018) or with EPSCs (Sozen et al., 2019) (Figure S5M). However, this frequency increased when FGF4/TGFβ1 were removed from the medium (45.5% versus 28.6% for CDX2 and 73.2% versus 50.8% for KRT8/18, see method details) (Figures 5I, 5J, S5M, and S5N). We concluded that the absence of these molecules leaves the blastoid EPI-like cells as the main source of positional information, which facilitates mural differentiation. Accordingly, when exposed to TXV molecules, blastocysts maintained ELF5 and LY6A expression in the mural cells, which were less able to become KRT8/18^{high} (Figures 5K and S5O). Collectively, these data indicate that EPI inducers act locally to pattern the TE axis.

Proximity to inducers maintains the trophectoderm decidualization capacity

After the initial attachment (~E4.5–5.0), the blastocyst instructs the uterus to form an enveloping decidual tissue (~E5.0–7.5) but the contribution from different pools of TRs is unknown. Previous experiments showed that trophospheres are composed of differentiated TRs and have a diminished potential to induce decidualization (Gardner and Johnson, 1972; Rossant and Tamura-Lis, 1981; Rivron et al., 2018). Here, we examined whether the polar TE might be critical for decidua formation. To minimize signaling between conceptus and uterus, we first used fixed blastoids. They were incapable of inducing decidua formation (Figures 6A and 6B, $p < 0.0001$). Along with the diminished potential of trophospheres to decidualize the uterus (Rivron et al., 2018), this suggests that blastoids actively instruct decidualization. Blastoids formed with TESCs or with TSCs including a CDX2 inducible transgene (CDX2i-TSCs, Figure S6A) had an enhanced capacity for decidualization as compared to TSCs blastoids (Figures 6C and 6D, 18.7% versus 7.6%, $p = 0.0002$; Figure 6F, $p = 0.0128$). They formed larger deciduae similar in size to that of the blastocyst (Figure 6E) and achieved a higher receptivity rate (Figure S6B, 96.7% versus 64.9%). We concluded that inducers contribute in making the TE competent for decidualization. Blastoids formed from ESCs also had a higher potential to regulate decidualization as compared to blastoids formed from EPSCs (Figure 6E). Finally, a GW501516 treatment of blastoids reduced CDX2 expression and diminished their potential for decidualization (Figures 6G, 6H, and S6C). Overall, we concluded that EPI inducers regulate CDX2 expression, which endows TRs with the capacity to decidualize the uterine tissues, consistent with CDX2 genetic loss-of-function experiments in which null blastocysts fail to implant (Strumpf et al., 2005).

Figure 4. TXV TSCs have an enhanced capacity to self-renew, a lessened propensity to spontaneously differentiate, and a maintained potential to contribute to development

(A) Fluorescence-activated cell sorting (FACS) analysis of cell-cycle profiles of cells cultured in TX and TXV medium based on DNA content measured using Hoechst 34580.

(B) Colony formation efficiency of single sorted TX and TXV TSCs based on three independent experiments and a total 288 wells of cells for each condition.

(C) Ratio of CDX2/EOMES double-positive cells within outgrowths from C57BL/6J mouse blastocysts.

(D and E) Immunostaining against KRT18 and KRT8 (D) and quantification of KRT18- or KRT8-positive cells (E) in TX and TXV TSCs and in TXV TSCs treated with GW501516.

(F) LY6A and KRT18 expression in the E4.5 blastocysts. LY6A was enriched in the polar TE compared to the mural TE and shows clear contrast to KRT18.

(G and H) Immunostaining (G) and flow cytometry (H) analysis for LY6A of TX and TXV TSCs.

(I) Differentiation dynamics of TXV TSCs upon removal of optimal inducers. A sample was taken every 24 h for 6 days after compound removal at t0.

(J) Schematic view for the cell types in E3.5 blastocyst and their derivatives in E7.5 conceptus.

(K) Immunostaining against GFP and ELF5 in E7.5 chimeric embryos obtained upon the injection of blastocysts with serum-cultured TSCs, TX-cultured TSCs, and TXV-cultured TSCs. Non-injected Ctrl represents E7.5 conceptus, which developed from blastocysts that were not injected with TSCs but that, similar to injected blastocysts, underwent laser incision of the Zona Pellucida.

For each graph, data are means ± SEM, analyzed by Student's t test: $^{**}p < 0.01$, $^{***}p < 0.001$. Scale bars: 40 μm in (D); 150 μm in (F) and (G); 300 μm in (K). See also Figure S4.

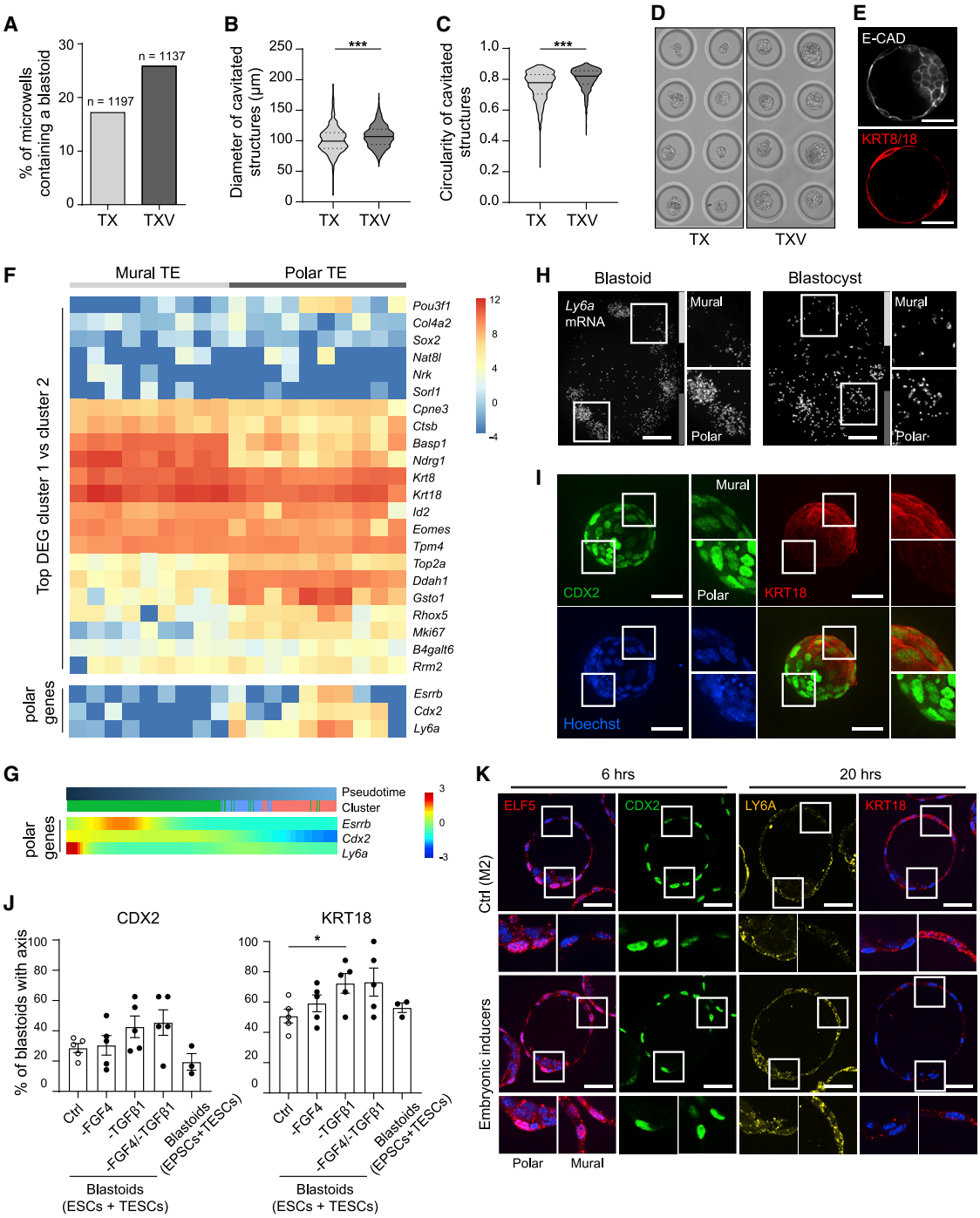

Figure 5. Embryonic inducers pattern the embryonic-abembryonic axis

(A) Percentage of microwells containing a blastoid (based on circularity, diameter, and presence of one single cavity).

(B and C) Diameter (B) and circularity (C) of all structures formed in all microwells for TSCs cultured in TX or TXV medium.

(D) Representative images of microwells containing TX and TXV blastoids.

(E) Blastoid formed from TXV TSCs stained for E-CAD and KRT8/18. Scale bars, 40 µm.

(F) The top differentially expressed genes when comparing clusters 1 and 2 (see Figure S5K) were plotted for the single cells obtained from polar and mural TE from Nakamura et al. (2015). Each column indicates a single cell from the respective group.

(G) Pseudotime heatmap for the polar genes *Esrrb* and *Cdx2* and *Ly6a* (see also Figures S5J and S5K).

(H) smFISH staining for *Ly6a* in a blastoid and blastocyst. Scale bars, 20 µm.

(legend continued on next page)

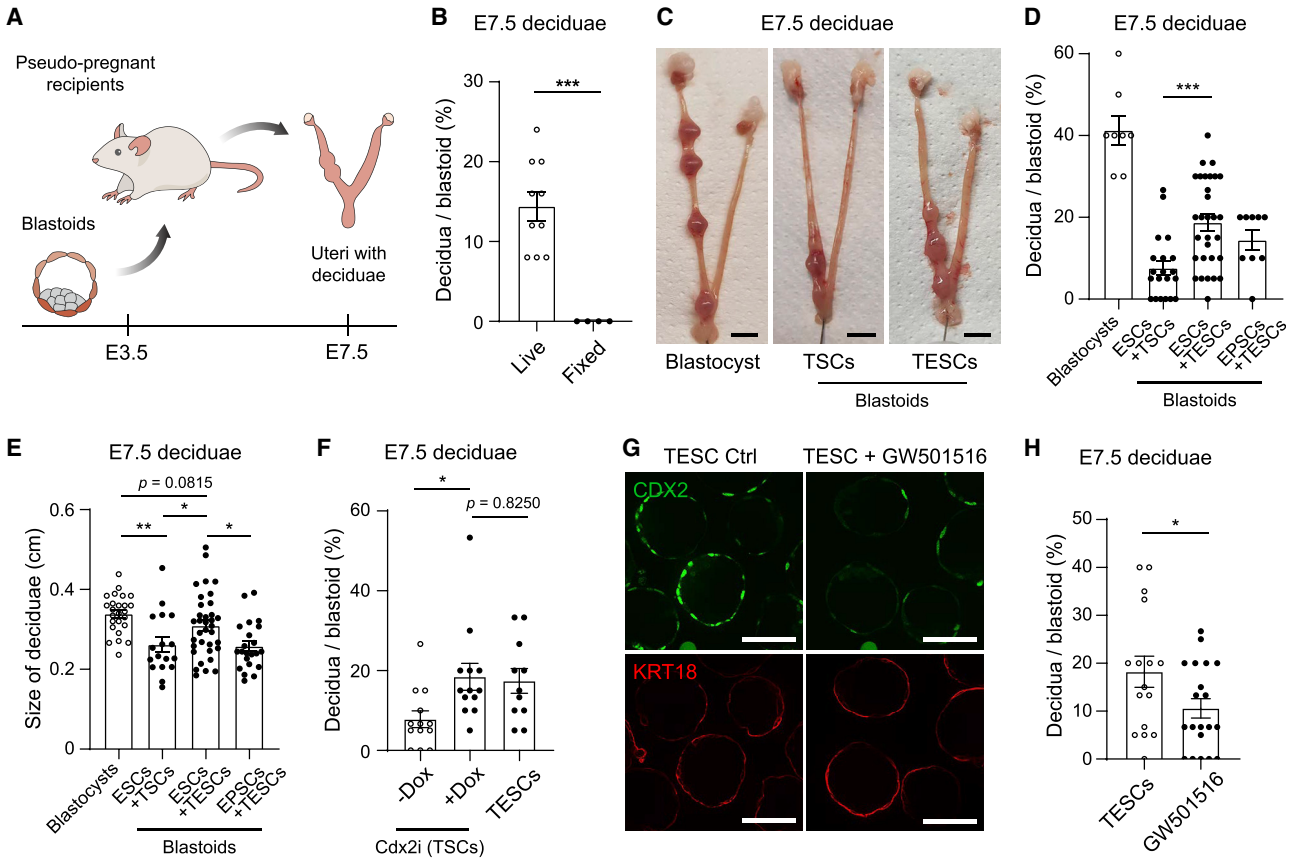

Figure 6. Embryonic inducers capacitate TRs for decidualization

(A) Timeline for uterus transfer and deciduae recovery.

(B) Decidua formation efficiency of live and fixed (dead) blastoids at E7.5. Fixed blastoids were chosen as a negative control instead of concanavalin A (ConA)-coated beads or sesame oil since the latter two have been reported to induce a uterine reaction by physical or signaling interactions (Cuatrecasas and Tell, 1973).

(C) E7.5 deciduae induced by blastocysts, TSCs blastoids, and TESCs blastoids.

(D) Quantification of the implantation efficiency.

(E) Quantification of the size of E7.5 decidua.

(F) Decidua formation efficiency of blastoids formed from CDX2 overexpression inducible TSCs (CDX2i) ± doxycycline (Dox) treatment.

(G) Immunostaining of blastoids formed from GW501516-treated TESCs showed reduced CDX2 expression as well as increased KRT18 expression.

(H) Quantification of the decidua formation efficiency at E7.5.

For (B), (D), (F), and (H), each dot represents an individual mouse. In (C)–(E), each dot represents one decidua. For each graph, data are means ± SEM, analyzed by Student's t test: *p < 0.05, **p < 0.01, ***p < 0.001. Scale bars: 0.5 cm in (C); 100 μm in (G). See also Figure S6.

WNT6/7B are downstream effectors of CDX2 contributing to decidualization

We sought to identify molecules (1) whose secretion is regulated by CDX2 and (2) that could contribute to decidualization. Using the computational framework SCENIC (Aibar et al., 2017), we identified multiple Wnt ligands (*Wnt6* and *Wnt7b*) and receptors (*Fzd2/7/10*) with promoter regions predicted to be bound by CDX2 (two interaction sites for *Wnt6*, one for *Wnt7b* promoter region; Figure 7A). In blastocysts, *Wnt7b* transcripts are the most abundant, followed by *Wnt6*. In addition, *Wnt7b* transcripts are enriched in CDX2^{high} relative to CDX2^{low} TSCs and upon *Cdx2* overexpression (Figure S7A). Consistent with a role for Wnt in decidualization (Mohamed et al., 2005), WNT7B is highly expressed in the TE and its derivatives (Figure 7B), and *Wnt6/7b* expression is maintained in the ExE (Figure S7B). This expression pattern is conserved in humans with *Wnt6/7b* transcripts being also abundant in the TE (Figure S7C) (). Consistent with a role for TE-secreted Wnt ligands in decidualization, 8-cell embryos cultured with porcupine inhibitor (IWP2, 2.5 μM, 48 h) formed blastocysts that had a significantly decreased potential for decidualization

(I) Immunostaining for CDX2 and KRT18 as marker proteins for axis formation in the blastoid. Shown is a representative 3D projection of a TESCs blastoid formed without addition of TGFβ1. Scale bar represents 50 μm.

(J) Percentage of blastoids with an axis for CDX2 or KRT18. Plotted are the mean percentages of five individual experiments (total 40–60 blastoids per group).

(K) Immunostaining of blastocysts cultured with TXV factors for 6 or 20 h. Scale bar, 40 μm.

For each graph, data are means ± SEM, analyzed by Student's t test and one-way ANOVA: *p < 0.05, **p < 0.01, ***p < 0.001. See also Figure S5.

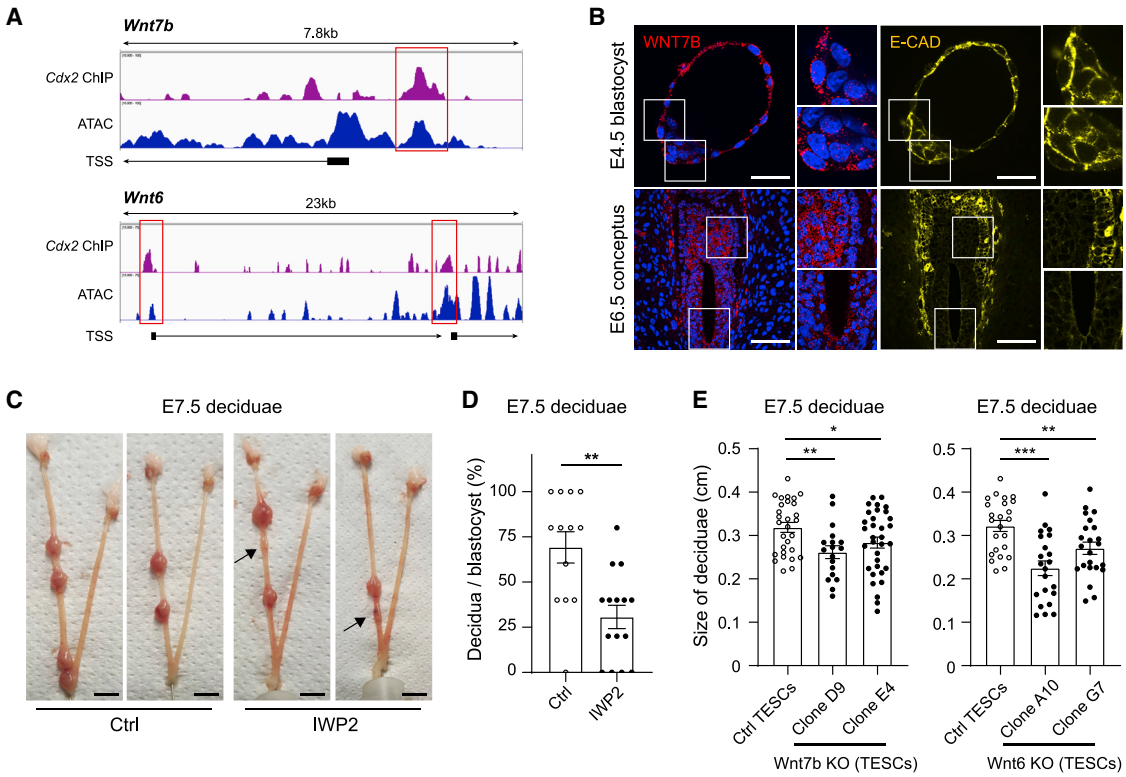

Figure 7. Decidualization by TRs proceeds partly through CDX2 and the secretion of WNT6/7B

(A) CDX2 ChIP-seq analysis of *Wnt7b* and *Wnt6* genes. Peaks in Assay for Transposase-Accessible Chromatin using sequencing (ATAC) show chromatin accessibility. TSS, transcription start site.

(B) Immunostaining of an E4.5 blastocyst and an E6.5 conceptus for WNT7B and E-CAD. WNT7B was detected in the TE rather than the EPI at E4.5. In the E6.5 conceptus, E-CAD^{+} cells surrounded WNT7B^{+} cells, reminiscent of the CDX2 and KRT18 expression pattern (Figure 1E). The data indicate that WNT7B is enriched in polar TE derivatives.

(C and D) E7.5 deciduae induced by IWP2-treated blastocysts (C) and quantification of the implantation efficiency (D). Arrows indicate resolving deciduae. Each dot represents an individual mouse.

(E) Quantification of the size of E7.5 decidua from *Wnt7b* KO blastoids (left) and *Wnt6* KO blastoids (right). Each dot represents one decidua.

For each graph, data are means ± SEM, analyzed by Student's t test: *p < 0.05, **p < 0.01, ***p < 0.001. Scale bars: 40 and 80 μm in (B) top and bottom, respectively; 0.5 cm in (C). See also Figure S7.

(Figures 7C and 7D). Many deciduae were immature or resorbed (Figure 7C, arrow). To first model the autocrine functions of Wnt ligands specifically in the TE, we formed trophospheres with *Wnt6* or *Wnt7b* knockout (KO) TESCs (Figures S7D–S7F) (Meistermann et al., 2021). Consistent with a role for WNT activity in TE formation (Rivron et al., 2018), these trophospheres had a decreased cavitation capacity (Figure S7G). This suggests an autocrine function for WNT/7B in TE morphogenesis. Of note, Wnt controls Hippo pathway activity in several other systems. Finally, we observed that blastoids formed with *Wnt6* or *Wnt7b* KO TESCs initially attached to the uterus comparably to wild type (E5.5, Figures S7H and S7I). Thus we did not detect an early attachment defect, often associated with mural TE functions. However, later (E7.5), the diameter of the deciduae was significantly decreased (Figures 7E and S7J). Note that a 20% decrease in sphere diameter correspond to a 2-fold decrease in volume. Taken together, we concluded that the EPI inducers not only locally maintain the TR progenitors, but also support the secretion of Wnt ligands for decidua formation.

DISCUSSION

For development to occur, embryos must maintain progenitors that fuel growth while allowing a subset of cells to differentiate in order to fulfill functions. Here, we show that a specific combination of EPI inductions increases the optimality of the TF network (CDX2, EOMES, and ESRRB), enhances self-renewal, and prevents differentiation. On the contrary, suboptimal exposure to inducers favors a fluctuation of the progenitor state, creating reversible subpopulations with facilitated differentiation. We propose that the dynamic regulation of this EPI/TR interface endows the progenitor pool with a flexible strategy for either maintaining more progenitors or generating differentiated cell types. We surmise that cellular heterogeneity arises as the embryo exploits a suboptimal environment to control an equilibrium between interconvertible TR populations. This EPI/TR interface and the reversibility of cellular states would endow the progenitor pool with adaptive and regulative properties to synchronize tissue development, thus acting as a checkpoint.

Conceivably, the rapid geometric changes (size and shape) of the developing embryo influence the exposure to EPI inducers, thus linking morphogenesis with the maintenance of TR progenitors.

The origin of the observed heterogeneity and plasticity of TSCs is unknown. Upstream CDX2 regulators (e.g., Hippo/Notch signaling components) can vary stochastically (Sigal et al., 2006) due to the properties of intracellular biochemical loops or to fluctuations in cell-cell membrane interactions. CDX2 expression might also be regulated by geometrical or mechanical cues as observed during the morula-to-blastocyst transition. Beyond inductions, both the intrinsic properties of biochemical networks and extrinsic geometric cues might thus contribute to distributing cell states. Signaling pathways act as CDX2 regulators but also as inducers of histone remodeling. For example, Notch activates target genes with trimethylation of H3K4 by inhibiting dimethyl-transferase (KDM5A) activity (Rayon et al., 2014; (Liefke et al., 2010)). Hippo signaling also controls histone remodeling (Hillmer and Link, 2019). Our data showed higher trimethylation of H3K4 (H3K4me3) in CDX2^{high} cells. Thus, in the CDX2^{low} TRs that are prone to differentiation, epigenetic mechanisms might act as feedforward loops engraving the differentiation path.

Blastoids formed from TESCs spontaneously generate a gene expression pattern along the axis. We conclude from these experiments of reconstruction that, following subtle early patterning events (Graham and Zernicka-Goetz, 2016; Zhang and Hiiragi, 2018), the EPI produces inductive signals that significantly contribute to axis formation. This process ultimately ensures the blastocyst/uterus interaction of implantation. We propose that inducers, including LPA, FGF4, Nodal, BMP4, BMP7, and IL6/11, contribute toward regulating CDX2 expression in the polar TE, which impacts proliferation, self-renewal, and epithelial morphogenesis but also the expression of WNT ligands that contribute to decidualization. The regulation of WNT ligands might be a mechanism with potential translational applicability to human implantation (Koler et al., 2009).

Altogether, this study provides a framework to explain how the conceptus leverages inductions and TR state fluctuation to maintain progenitors, facilitate differentiation, or allocate and balance the functions necessary for implantation to occur.

Limitation of study

Although blastoids formed with ESCs and TESCs implant better into the uterus and form decidua more efficiently than blastoids formed with ESCs and TSCs, we did not observe the formation of a fetus. The minimal requirements for development to occur are not yet met.

We selected WNT6 and WNT7b as downstream effectors of CDX2 based on RNA-seq, ChIP, TESC and CDX2 overexpression analysis in TSCs, and the expression pattern of these genes in the TE of human blastocysts. We propose that these WNT ligands follow the dynamical expression pattern of CDX2. However, decidualization is a complex process that involves multiple players. Beyond WNT6/7b, other molecules secreted by the conceptus might affect decidualization.

STAR★METHODS

Detailed methods are provided in the online version of this paper and include the following:

- KEY RESOURCES TABLE
- RESOURCE AVAILABILITY
  - Lead contact
  - Material availability
  - Data and code availability
- EXPERIMENTAL MODEL AND SUBJECT DETAILS
  - Stem cells and culture condition
  - Mouse lines and embryos
- METHOD DETAILS
  - Generation of inducible Caudal Type Homeobox 2 overexpression cell lines
  - Generation of WNT6 and WNT7B knockout trophoblast stem cells
  - Cell cycle analysis
  - Colony formation assay
  - Combinatorial screen
  - Immunofluorescence
  - Whole tissue staining/clearing and 3D imaging of embryos
  - Single-molecule FISH
  - Single-molecule FISH polarity quantification
  - High content imaging
  - Live cell imaging
  - Flow cytometry
  - qRT-PCR
  - RNA sequencing
  - Mapping and processing of single-cell mRNA sequencing data
  - Analysis of single-cell mRNA sequencing data
  - Caudal Type Homeobox 2 ChIP-seq analysis
  - Chromatin immunoprecipitation PCR (ChIP-PCR)
  - Chimeric embryo formation
  - Trophoblast stem cells line derivation and staining
  - Blastoid formation
  - Uterus transfer and decidua analysis
  - Blue band assay
  - Western Blot
  - SCOPE and PTUI
- QUANTIFICATION AND STATISTICAL ANALYSIS

SUPPLEMENTAL INFORMATION

Supplemental information can be found online at https://doi.org/10.1016/j.stem.2022.06.002.

ACKNOWLEDGMENTS

We would like to thank J. Deschamps for providing the CDX2-eGFP mice; A. Barve for preliminary data analysis; S. van der Elst and R. van der linden for helping with FACS assays; A. de Graaf for helping with microscopy; H. Begthel for helping with histology; H.C. Theussl for helping with both TSC injection into morula and uterine transfer of chimeric blastocysts; and all mouse caretaking staff, especially J. Patry, for their help. N.C.R. is supported by an ERC Consolidator grant (2020 ERC-CoG no. 101002317-BLASTOID). J.S. is supported by the European Union's Framework Program for Research and Innovation Horizon 2020 (2014–2020) under the Marie Curie Skłodowska Grant

Agreement no. 847548. V.H. is supported by a Boehringer Ingelheim Fonds Fellowship. H.H.K. is supported by the Austrian Science Fund (FWF), Lise Meitner Program M3131-B. H.K. is supported by the Japan Society for the Promotion of Science Overseas Research Fellowships. G.S. is supported by the HFSP number RGY0081/2019. S.P. is supported by the VIP2 program that has received funding from the European Union's Horizon 2020 research and innovation program under the Marie Skłodowska-Curie grant agreement no. 847548.

AUTHOR CONTRIBUTIONS

Conceptualization: J.S., J.F.A., V.H., H.K., and N.C.R.; formal analysis: J.S., J.F.A., V.H., G.S., A.A., and N.C.R; funding acquisition: J.S., V.H., and N.C.R.; investigation: J.S., J.F.A., V.H., H.K., H.H.K., Y.S.R.O., L.V., J.V., L.L., J.K., F.D., and A.v.O.; methodology: J.S., V.H., H.K., H.H.K., and M.K.; validation: J.S. and V.H.; visualization: J.S., J.F.A., and V.H.; writing – original draft: J.S., J.F.A., V.H., and N.C.R.; writing – review & editing: J.S., V.H., H.K., D.t.B., and N.C.R.; project administration: N.C.R.; supervision: N.C.R.

DECLARATION OF INTERESTS

N.C.R. and N.G. are inventors on a patent (EP2986711)filed on 2013-04-16 in the Netherlands, currently maintained by the IMBA in Austria, and entitled, "Blastoid, cell line based artificial blastocyst."

INCLUSION AND DIVERSITY

We worked to ensure sex balance in the selection of non-human subjects. We worked to ensure diversity in experimental samples through the selection of the cell lines. We worked to ensure diversity in experimental samples through the selection of the genomic datasets. One or more of the authors of this paper self-identifies as a member of the LGBTQ+ community. The author list of this paper includes contributors from the location where the research was conducted who participated in the data collection, design, analysis, and/or interpretation of the work.

Received: January 12, 2022
Revised: April 21, 2022
Accepted: June 2, 2022
Published: July 7, 2022

REFERENCES

Aibar, S., Gonzalez-Blas, C.B., Moerman, T., Huynh-Thu, V.A., Imrichova, H., Hulselmans, G., Rambow, F., Marine, J.C., Geurts, P., Aerts, J., et al. (2017). SCENIC: single-cell regulatory network inference and clustering. Nat. Methods *14*, 1083–1086. https://doi.org/10.1038/nmeth.4463.

Aubin, J., Davy, A., and Soriano, P. (2004). In vivo convergence of BMP and MAPK signaling pathways: impact of differential Smad1 phosphorylation on development and homeostasis. Genes Development *18*, 1482–1494. https://doi.org/10.1101/gad.1202604.

Auman, H.J., Nottoli, T., Lakiza, O., Winger, Q., Donaldson, S., and Williams, T. (2002). Transcription factor AP-2γ is essential in the extra-embryonic lineages for early postimplantation development. Development *129*, 2733–2747. https://doi.org/10.1242/dev.129.11.2733.

Azami, T., Bassalert, C., Allègre, N., Valverde Estrella, L., Pouchin, P., Ema, M., and Chazaud, C. (2019). Regulation of the ERK signalling pathway in the developing mouse blastocyst. Development *146*, dev177139.

Barrientos, G., Freitag, N., Tirado-Gonzalez, I., Unverdorben, L., Jeschke, U., Thijssen, V.L., and Blois, S.M. (2014). Involvement of galectin-1 in reproduction: past, present and future. Hum. Reprod. Update *20*, 175–193. https://doi.org/10.1093/humupd/dmt040.

Ben-Haim, N., Lu, C., Guzman-Ayala, M., Pescatore, L., Mesnard, D., Bischofberger, M., Naef, F., Robertson, E., and Constam, D.B. (2006). The nodal precursor acting via activin receptors induces mesoderm by maintaining a source of its convertases and BMP4. Dev. Cell *11*, 313–323. https://doi.org/10.1016/j.devcel.2006.07.005.

Cha, J., Sun, X., and Dey, S.K. (2012). Mechanisms of implantation: strategies for successful pregnancy. Nature Medicine *18*, 1754–1767. https://doi.org/10.1038/nm.3012.

Chai, N., Patel, Y., Jacobson, K., McMahon, J., McMahon, A., and Rappolee, D.A. (1998). FGF is an essential regulator of the fifth cell division in preimplantation mouse embryos. Developmental Biology *198*, 105–115.

Chambers, I., Silva, J., Colby, D., Nichols, J., Nijmeijer, B., Robertson, M., Vrana, J., Jones, K., Grotewold, L., and Smith, A. (2007). Nanog safeguards pluripotency and mediates germline development. Nature *450*, 1230–1234. https://doi.org/10.1038/nature06403.

Constam, D.B., and Robertson, E.J. (2000). SPC4/PACE4 regulates a TGFβ signaling network during axis formation. Genes Development *14*, 1146–1155. https://doi.org/10.1101/gad.14.9.1146.

Constância, M., Hemberger, M., Hughes, J., Dean, W., Ferguson-Smith, A., Fundele, R., Stewart, F., Kelsey, G., Fowden, A., Sibley, C., and Reik, W. (2002). Placental-specific IGF-II is a major modulator of placental and fetal growth. Nature *417*, 945–948. https://doi.org/10.1038/nature00819.

Copp, A.J. (1978). Interaction between inner cell mass and trophectoderm of the mouse blastocyst. J. Embryol. Exp. Morphol. *48*, 109–125. https://doi.org/10.1242/dev.48.1.109.

Corson, L.B., Yamanaka, Y., Lai, K.M.V., and Rossant, J. (2003). Spatial and temporal patterns of ERK signaling during mouse embryogenesis. Development *130*, 4527–4537. https://doi.org/10.1242/dev.00669.

Cuatrecasas, P., and Tell, G.P.E. (1973). Insulin-like activity of concanavalin A and wheat germ agglutinin–direct interactions with insulin receptors. Proceedings of the National Academy of Sciences of the United States of America *70*, 485–489. https://doi.org/10.1073/pnas.70.2.485.

Das, S.K., Wang, X., Paria, B., Damm, D., Abraham, J., Klagsbrun, M., Andrews, G., and Dey, S. (1994). Heparin-binding EGF-like growth factor gene is induced in the mouse uterus temporally by the blastocyst solely at the site of its apposition: a possible ligand for interaction with blastocyst EGF-receptor in implantation. Development *120*, 1071–1083. https://doi.org/10.1242/dev.120.5.1071.

Donnison, M., Beaton, A., Davey, H.W., Broadhurst, R., L'Huillier, P., and Pfeffer, P.L. (2005). Loss of the extraembryonic ectoderm in Elf5 mutants leads to defects in embryonic patterning. Development *132*, 2299–2308. https://doi.org/10.1242/dev.01819.

Ema, M., Mori, D., Niwa, H., Hasegawa, Y., Yamanaka, Y., Hitoshi, S., Mimura, J., Kawabe, Y., Hosoya, T., Morita, M., et al. (2008). Krüppel-like factor 5 is essential for blastocyst development and the normal self-renewal of mouse ESCs. Cell Stem Cell *3*, 555–567. https://doi.org/10.1016/j.stem.2008.09.003.

Frias-Aldeguer, J., Kip, M., Vivié, J., Li, L., Alemany, A., Korving, J., Darmis, F., van Oudenaarden, A., Geijsen, N., and Rivron, N.C. (2020). Embryonic signals perpetuate polar-like trophoblast stem cells and pattern the blastocyst axis. Preprint at bioRxiv. https://doi.org/10.1101/510362.

Fujii, H., Tatsumi, K., Kosaka, K., Yoshioka, S., Fujiwara, H., and Fujii, S. (2006). Eph-ephrin A system regulates murine blastocyst attachment and spreading. Dev. Dynam. *235*, 3250–3258.

Gao, H., Gao, R., Zhang, L., Xiu, W., Zang, R., Wang, H., Zhang, Y., Chen, J., Gao, Y., and Gao, S. (2018). Esrrb plays important roles in maintaining self-renewal of trophoblast stem cells (TSCs) and reprogramming somatic cells to induced TSCs. J. Mol. Cell Biol. *11*, 463–473. [Preprint]. https://doi.org/10.1093/jmcb/mjy054.

Gardner, R.L. (1983). Origin and differentiation of extraembryonic tissues in the mouse. Int. Rev. Exp. Pathol. *24*, 63–133.

Gardner, R.L. (2000). Flow of cells from polar to mural trophectoderm is polarized in the mouse blastocyst. Human Reproduction *15*, 694–701. https://doi.org/10.1093/humrep/15.3.694.

Gardner, R.L., and Johnson, M.H. (1972). An investigation of inner cell mass and trophoblast tissues following their isolation from the mouse blastocyst. J. Embryol. Exp. Morphol. *28*, 279–312. https://doi.org/10.1242/dev.28.2.279.

Gardner, R.L., Papaioannou, V.E., and Barton, S.C. (1973). Origin of the ectoplacental cone and secondary giant cells in mouse blastocysts reconstituted

from isolated trophoblast and inner cell mass. J. Embryol. Exp. Morphol. *30*, 561–572. https://doi.org/10.1242/dev.30.3.561.

Gardner, R.L., Squire, S., Zaina, S., Hills, S., and Graham, C.F. (1999). Insulin-like growth factor-2 regulation of conceptus composition: effects of the trophectoderm and inner cell mass genotypes in the mouse. Biol. Reprod. *60*, 190–195.

Gotoh, N., Manova, K., Tanaka, S., Murohashi, M., Hadari, Y., Lee, A., Hamada, Y., Hiroe, T., Ito, M., Kurihara, T., et al. (2005). The Docking protein FRS2α is an essential component of multiple fibroblast growth factor responses during early mouse development. Molecular and Cellular Biology *25*, 4105–4116. https://doi.org/10.1128/mcb.25.10.4105-4116.2005.

Goto, S., Shimizu, M., Kadowaki, T., Izumi, Y., and Shiotani, M. (2015). First Report of detection of Lysophosphatidic acids (LPAs) and analysis of LPA quantity in a human embryo-conditioned medium. J. Mammalian Ova Res. *32*, 57–66. https://doi.org/10.1274/jmor.32.57.

Graham, S.J.L., Wicher, K.B., Jedrusik, A., Guo, G., Herath, W., Robson, P., and Zernicka-Goetz, M. (2014). BMP signalling regulates the pre-implantation development of extra-embryonic cell lineages in the mouse embryo. Nat. Commun. *5*, 5667. https://doi.org/10.1038/ncomms6667.

Graham, S.J.L., and Zernicka-Goetz, M. (2016). The acquisition of cell fate in mouse development. Curr. Top. Dev. Biol. *117*, 671–695. https://doi.org/10.1016/bs.ctdb.2015.11.021.

Grün, D., Muraro, M., Boisset, J.C., Wiebrands, K., Lyubimova, A., Dharmadhikari, G., van den Born, M., van Es, J., Jansen, E., Clevers, H., et al. (2016). De Novo prediction of stem cell identity using single-cell transcriptome data. Cell Stem Cell *19*, 266–277. https://doi.org/10.1016/j.stem.2016.05.010.

Grün, D., Kester, L., and van Oudenaarden, A. (2014). Validation of noise models for single-cell transcriptomics. Nat. Methods *11*, 637–640. https://doi.org/10.1038/nmeth.2930.

Guillemot, F., Nagy, A., Auerbach, A., Rossant, J., and Joyner, A.L. (1994). Essential role of Mash-2 in extraembryonic development. Nature *371*, 333–336. https://doi.org/10.1038/371333a0.

Guo, G., Huss, M., Tong, G.Q., Wang, C., Li Sun, L., Clarke, N.D., and Robson, P. (2010). Resolution of cell fate decisions revealed by single-cell gene expression analysis from zygote to blastocyst. Dev. Cell *18*, 675–685. https://doi.org/10.1016/j.devcel.2010.02.012.

Gu, Z., Nomura, M., Simpson, B.B., Lei, H., Feijen, A., van den Eijnden-van Raaij, J., Donahoe, P.K., and Li, E. (1998). The type I activin receptor ActRIB is required for egg cylinder organization and gastrulation in the mouse. Genes Development *12*, 844–857. https://doi.org/10.1101/gad.12.6.844.

Guzman-Ayala, M., Ben-Haim, N., Beck, S., and Constam, D.B. (2004). Nodal protein processing and fibroblast growth factor 4 synergize to maintain a trophoblast stem cell microenvironment. Proceedings of the National Academy of Sciences of the United States of America *101*, 15656–15660. https://doi.org/10.1073/pnas.0405429101.

Hashimshony, T., Senderovich, N., Avital, G., Klochendler, A., de Leeuw, Y., Anavy, L., Gennert, D., Li, S., Livak, K.J., Rozenblatt-Rosen, O., et al. (2016). CEL-Seq2: sensitive highly-multiplexed single-cell RNA-Seq. Genome Biology *17*, 77. https://doi.org/10.1186/s13059-016-0938-8.

Hastreiter, S., Skylaki, S., Loeffler, D., Reimann, A., Hilsenbeck, O., Hoppe, P.S., Coutu, D.L., Kokkaliaris, K.D., Schwarzfischer, M., Anastassiadis, K., et al. (2018). Inductive and selective effects of GSK3 and MEK inhibition on Nanog heterogeneity in embryonic stem cells. Stem Cell Rep. *11*, 58–69. https://doi.org/10.1016/j.stemcr.2018.04.019.

Hatano, N., Mori, Y., Oh-hora, M., Kosugi, A., Fujikawa, T., Nakai, N., Niwa, H., Miyazaki, J., Hamaoka, T., and Ogata, M. (2003). Essential role for ERK2 mitogen-activated protein kinase in placental development. Gene Cell *8*, 847–856. https://doi.org/10.1046/j.1365-2443.2003.00680.x.

Hayashi, K., Lopes, S.M.C.S., Tang, F., and Surani, M.A. (2008). Dynamic equilibrium and heterogeneity of mouse pluripotent stem cells with distinct functional and epigenetic states. Cell Stem Cell *3*, 391–401. https://doi.org/10.1016/j.stem.2008.07.027.

Hillmer, R.E., and Link, B.A. (2019). The roles of hippo signaling Transducers Yap and Taz in chromatin remodeling. Cells *8*, 502. https://doi.org/10.3390/cells8050502.

Hutchens, S.A., Leon, R., O'Neill, H., and Evans, B. (2007). Statistical analysis of optimal culture conditions for Gluconacetobacter hansenii cellulose production. Lett. Appl. Microbiol. *44*, 175–180. https://doi.org/10.1111/j.1472-765x.2006.02055.x.

Ishisaki, A., Yamato, K., Hashimoto, S., Nakao, A., Tamaki, K., Nonaka, K., ten Dijke, P., Sugino, H., and Nishihara, T. (1999). Differential inhibition of Smad6 and Smad7 on Bone morphogenetic protein- and activin-mediated growth arrest and apoptosis in B cells. J. Biol. Chem. *274*, 13637–13642. https://doi.org/10.1074/jbc.274.19.13637.

Kiyozumi, D., Nakano, I., Sato-Nishiuchi, R., Tanaka, S., and Sekiguchi, K. (2020). Laminin is the ECM niche for trophoblast stem cells. Life Science Alliance *3*, e201900515. https://doi.org/10.26508/lsa.201900515.

Klaffky, E., Williams, R., Yao, C.C., Ziober, B., Kramer, R., and Sutherland, A. (2001). Trophoblast-specific expression and function of the integrin alpha 7 subunit in the peri-implantation mouse embryo. Developmental Biology *239*, 161–175. https://doi.org/10.1006/dbio.2001.0404.

Koler, M., Achache, H., Tsafrir, A., Smith, Y., Revel, A., and Reich, R. (2009). Disrupted gene pattern in patients with repeated in vitro fertilization (IVF) failure. Human Reproduction *24*, 2541–2548. https://doi.org/10.1093/humrep/dep193.

Kuales, G., Weiss, M., Sedelmeier, O., Pfeifer, D., and Arnold, S.J. (2015). A Resource for the Transcriptional Signature of Bona Fide Trophoblast Stem Cells and Analysis of Their Embryonic Persistence. *Stem Cells Int. 2015*, 218518.

Kubaczka, C., Senner, C., Araúzo-Bravo, M.J., Sharma, N., Kuckenberg, P., Becker, A., Zimmer, A., Brüstle, O., Peitz, M., Hemberger, M., and Schorle, H. (2014). Derivation and maintenance of murine trophoblast stem cells under defined conditions. Stem cell reports *2*, 232–242.

Latos, P.A., Sienerth, A.R., Murray, A., Senner, C.E., Muto, M., Ikawa, M., Oxley, D., Burge, S., Cox, B.J., and Hemberger, M. (2015). Elf5-centered transcription factor hub controls trophoblast stem cell self-renewal and differentiation through stoichiometry-sensitive shifts in target gene networks. Genes Development *29*, 2435–2448. https://doi.org/10.1101/gad.268821.115.

Lawson, K.A., Dunn, N.R., Roelen, B.A., Zeinstra, L.M., Davis, A.M., Wright, C.V., Korving, J.P., and Hogan, B.L. (1999). Bmp4 is required for the generation of primordial germ cells in the mouse embryo. Genes Development *13*, 424–436.

Lee, C., Bailey, A., Lopez-Tello, J., Sferruzzi-Perri, A.N., Okkenhaug, K., Moffett, A., Rossant, J., and Hemberger, M. (2019). Inhibition of Phosphoinositide-3-Kinase Signaling Promotes the Stem Cell State of Trophoblast. Stem Cells *37*, 1307–1318.

Lee, J.E., Pintar, J., and Efstratiadis, A. (1990). Pattern of the insulin-like growth factor II gene expression during early mouse embryogenesis. Development *110*, 151–159. https://doi.org/10.1242/dev.110.1.151.

Liefke, R., Oswald, F., Alvarado, C., Ferres-Marco, D., Mittler, G., Rodriguez, P., Dominguez, M., and Borggrefe, T. (2010). Histone demethylase KDM5A is an integral part of the core Notch-RBP-J repressor complex. Genes & development *24*, 590–601.

Lim, H.J., and Dey, S.K. (2009). HB-EGF: a unique mediator of embryo-uterine interactions during implantation. Experimental Cell Res. *315*, 619–626. https://doi.org/10.1016/j.yexcr.2008.07.025.

Lin, S.-C.J., Wani, M.A., Whitsett, J.A., and Wells, J.M. (2010). Klf5 regulates lineage formation in the pre-implantation mouse embryo. Development *137*, 3953–3963. https://doi.org/10.1242/dev.054775.

McDole, K., and Zheng, Y. (2012). Generation and live imaging of an endogenous Cdx2 reporter mouse line. Genesis *50*, 775–782. https://doi.org/10.1002/dvg.22049.

Meistermann, D., Bruneau, A., Loubersac, S., Reignier, A., Firmin, J., François-Campion, V., Kilens, S., Lelièvre, Y., Lammers, J., Feyeux, M., et al. (2021). Integrated pseudotime analysis of human pre-implantation embryo single-cell

transcriptomes reveals the dynamics of lineage specification. Cell Stem Cell *28*, 1625–1640.e6.

Mesnard, D., Donnison, M., Fuerer, C., Pfeffer, P.L., and Constam, D.B. (2011). The microenvironment patterns the pluripotent mouse epiblast through paracrine Furin and Pace4 proteolytic activities. Genes Development *25*, 1871–1880. https://doi.org/10.1101/gad.16738711.

Miura, S., Singh, A.P., and Mishina, Y. (2010). Bmpr1a is required for proper migration of the AVE through regulation of Dkk1 expression in the pre-streak mouse embryo. Developmental Biology *341*, 246–254. https://doi.org/10.1016/j.ydbio.2010.02.038.

Mohamed, O.A., Jonnaert, M., Labelle-Dumais, C., Kuroda, K., Clarke, H.J., and Dufort, D. (2005). Uterine Wnt/β-catenin signaling is required for implantation. Proceedings of the National Academy of Sciences of the United States of America *102*, 8579–8584. https://doi.org/10.1073/pnas.0500612102.

Moriwaki, K., Tsukita, S., and Furuse, M. (2007). Tight junctions containing claudin 4 and 6 are essential for blastocyst formation in preimplantation mouse embryos. Developmental Biology *312*, 509–522. https://doi.org/10.1016/j.ydbio.2007.09.049.

Motomura, K., Oikawa, M., Hirose, M., Honda, A., Togayachi, S., Miyoshi, H., Ohinata, Y., Sugimoto, M., Abe, K., Inoue, K., and Ogura, A. (2016). Cellular dynamics of mouse trophoblast stem cells: Identification of a persistent stem cell type. Biol. Reprod. *94*, 122. https://doi.org/10.1095/biolreprod.115.137125.

Murohashi, M., Nakamura, T., Tanaka, S., Ichise, T., Yoshida, N., Yamamoto, T., Shibuya, M., Schlessinger, J., and Gotoh, N. (2010). An FGF4-FRS2α-Cdx2 Axis in trophoblast stem cells induces Bmp4 to regulate proper growth of early mouse embryos. Stem Cells *28*, 113–121. https://doi.org/10.1002/stem.247.

Nakamura, T., Yabuta, Y., Okamoto, I., Aramaki, S., Yokobayashi, S., Kurimoto, K., Sekiguchi, K., Nakagawa, M., Yamamoto, T., and Saitou, M. (2015). SC3-seq: a method for highly parallel and quantitative measurement of single-cell gene expression. Nucleic Acids Research *43*, e60. https://doi.org/10.1093/nar/gkv134.

Nakao, A., Afrakhte, M., Morn, A., Nakayama, T., Christian, J.L., Heuchel, R., Itoh, S., Kawabata, M., Heldin, N.E., Heldin, C.H., and Dijke, P. (1997). Identification of Smad7, a TGFβ-inducible antagonist of TGF-β signalling. Nature *389*, 631–635. https://doi.org/10.1038/39369.

Natale, B.V., Schweitzer, C., Hughes, M., Globisch, M.A., Kotadia, R., Tremblay, E., Vu, P., Cross, J.C., and Natale, D.R.C. (2017). Sca-1 identifies a trophoblast population with multipotent potential in the mid-gestation mouse placenta. Sci. Rep. *7*, 5575. https://doi.org/10.1038/s41598-017-06008-2.

Nichols, J., and Smith, A. (2012). Pluripotency in the embryo and in culture. Cold Spring Harbor perspectives in biology *4*, a008128.

Nichols, J., Zevnik, B., Anastassiadis, K., Niwa, H., Klewe-Nebenius, D., Chambers, I., Scholer, H., and Smith, A. (1998). Formation of pluripotent stem cells in the mammalian embryo depends on the POU transcription factor Oct4. Cell *95*, 379–391. https://doi.org/10.1016/s0092-8674(00)81769-9.

Nishioka, N., Yamamoto, S., Kiyonari, H., Sato, H., Sawada, A., Ota, M., Nakao, K., and Sasaki, H. (2008). Tead4 is required for specification of trophectoderm in pre-implantation mouse embryos. Mech. Dev. *125*, 270–283. https://doi.org/10.1016/j.mod.2007.11.002.

Nishioka, N., Inoue, K., Adachi, K., Kiyonari, H., Ota, M., Ralston, A., Yabuta, N., Hirahara, S., Stephenson, R.O., Ogonuki, N., et al. (2009). The Hippo signaling pathway components Lats and Yap pattern Tead4 activity to distinguish mouse trophectoderm from inner cell mass. Dev. Cell *16*, 398–410. https://doi.org/10.1016/j.devcel.2009.02.003.

Ohinata, Y., and Tsukiyama, T. (2014). Establishment of trophoblast stem cells under defined culture conditions in mice. PLoS One *9*, e107308. https://doi.org/10.1371/journal.pone.0107308.

Ohnishi, Y., Huber, W., Tsumura, A., Kang, M., Xenopoulos, P., Kurimoto, K., Oles, A.K., Arauzo-Bravo, M.J., Saitou, M., Hadjantonakis, A.K., and Hiiragi, T. (2014). Cell-to-cell expression variability followed by signal reinforcement progressively segregates early mouse lineages. Nat. Cell Biol. *16*, 27–37. https://doi.org/10.1038/ncb2881.

Perez-Garcia, V., Lea, G., Lopez-Jimenez, P., Okkenhaug, H., Burton, G.J., Moffett, A., Turco, M.Y., and Hemberger, M. (2021). BAP1/ASXL complex modulation regulates epithelial-mesenchymal transition during trophoblast differentiation and invasion. Elife *10*. https://doi.org/10.7554/eLife.63254.

Posfai, E., Schell, J.P., Janiszewski, A., Rovic, I., Murray, A., Bradshaw, B., Yamakawa, T., Pardon, T., El Bakkali, M., Talon, I., et al. (2021). Evaluating totipotency using criteria of increasing stringency. Nat. Cell Biol. *23*, 49–60. https://doi.org/10.1038/s41556-020-00609-2.

Rayon, T., Menchero, S., Nieto, A., Xenopoulos, P., Crespo, M., Cockburn, K., Canon, S., Sasaki, H., Hadjantonakis, A.K., de la Pompa, J., et al. (2014). Notch and hippo converge on Cdx2 to specify the trophectoderm lineage in the mouse blastocyst. Dev. Cell *30*, 410–422. https://doi.org/10.1016/j.devcel.2014.06.019.

Rhee, C., Lee, B.K., Beck, S., LeBlanc, L., Tucker, H.O., and Kim, J. (2017). Mechanisms of transcription factor-mediated direct reprogramming of mouse embryonic stem cells to trophoblast stem-like cells. Nucleic acids research *45*, 10103–10114.

Rivron, N.C., Frias-Aldeguer, J., Vrij, E.J., Boisset, J.C., Korving, J., Vivie, J., Truckenmuller, R.K., van Oudenaarden, A., van Blitterswijk, C.A., and Geijsen, N. (2018). Blastocyst-like structures generated solely from stem cells. Nature *557*, 106–111. https://doi.org/10.1038/s41586-018-0051-0.

Roebroek, A.J., Umans, L., Pauli, I., Robertson, E., van Leuven, F., Van de Ven, W., and Constam, D. (1998). Failure of ventral closure and axial rotation in embryos lacking the proprotein convertase Furin. Development *125*, 4863–4876. https://doi.org/10.1242/dev.125.24.4863.

Rossant, J., and Tamura-Lis, W. (1981). Effect of culture conditions on diploid to giant-cell transformation in postimplantation mouse trophoblast. J. Embryol. Exp. Morphol. *62*, 217–227. https://doi.org/10.1242/dev.62.1.217.

Rugg-Gunn, P.J., Cox, B.J., Ralston, A., and Rossant, J. (2010). Distinct histone modifications in stem cell lines and tissue lineages from the early mouse embryo. Proceedings of the National Academy of Sciences of the United States of America *107*, 10783–10790. https://doi.org/10.1073/pnas.0914507107.

Saba-El-Leil, M.K., Vella, F.D., Vernay, B., Voisin, L., Chen, L., Labrecque, N., Ang, S.L., and Meloche, S. (2003). An essential function of the mitogen-activated protein kinase Erk2 in mouse trophoblast development. EMBO Rep *4*, 964–968.

Sebastiano, V., Dalvai, M., Gentile, L., Schubart, K., Sutter, J., Wu, G.M., Tapia, N., Esch, D., Ju, J.Y., Hubner, K., et al. (2010). Oct1 regulates trophoblast development during early mouse embryogenesis. Development *137*, 3551–3560. https://doi.org/10.1242/dev.047027.

Seong, J., Kim, N.S., Kim, J.A., Lee, W., Seo, J.Y., Yum, M.K., Kim, J.H., Park, I., Kang, J.S., Bae, S.H., et al. (2018). Side branching and luminal lineage commitment by ID2 in developing mammary glands. Development *145*. https://doi.org/10.1242/dev.165258.

Shindo, T., Manabe, I., Fukushima, Y., Tobe, K., Aizawa, K., Miyamoto, S., Kawai-Kowase, K., Moriyama, N., Imai, Y., Kawakami, H., et al. (2002). Krüppel-like zinc-finger transcription factor KLF5/BTEB2 is a target for angiotensin II signaling and an essential regulator of cardiovascular remodeling. Nat. Med. *8*, 856–863. https://doi.org/10.1038/nm738.

Shi, X.-H., Larkin, J.C., Chen, B., and Sadovsky, Y. (2013). The expression and localization of N-myc downstream-regulated gene 1 in human trophoblasts. PLoS One *8*, e75473. https://doi.org/10.1371/journal.pone.0075473.

Sigal, A., Milo, R., Cohen, A., Geva-Zatorsky, N., Klein, Y., Liron, Y., Rosenfeld, N., Danon, T., Perzov, N., and Alon, U. (2006). Variability and memory of protein levels in human cells. Nature *444*, 643–646. https://doi.org/10.1038/nature05316.

Sood, R., Zehnder, J.L., Druzin, M.L., and Brown, P.O. (2006). Gene expression patterns in human placenta. Proceedings of the National Academy of Sciences of the United States of America *103*, 5478–5483. https://doi.org/10.1073/pnas.0508035103.

Sozen, B., Cox, A.L., De Jonghe, J., Bao, M., Hollfelder, F., Glover, D.M., and Zernicka-Goetz, M. (2019). Self-organization of mouse stem cells into an Extended potential blastoid. Dev. Cell *51*, 698–712.e8. e8.

Strumpf, D., Mao, C.A., Yamanaka, Y., Ralston, A., Chawengsaksophak, K., Beck, F., and Rossant, J. (2005). Cdx2 is required for correct cell fate

specification and differentiation of trophectoderm in the mouse blastocyst. Development *132*, 2093–2102. https://doi.org/10.1242/dev.01801.

Sutherland, A. (2003). Mechanisms of implantation in the mouse: differentiation and functional importance of trophoblast giant cell behavior. Developmental Biology *258*, 241–251. https://doi.org/10.1016/s0012-1606(03)00130-1.

Tanaka, S., Kunath, T., Hadjantonakis, A.K., Nagy, A., and Rossant, J. (1998). Promotion of trophoblast stem cell proliferation by FGF4. Science *282*, 2072–2075. https://doi.org/10.1126/science.282.5396.2072.

Trapnell, C., Cacchiarelli, D., Grimsby, J., Pokharel, P., Li, S., Morse, M., Lennon, N.J., Livak, K.J., Mikkelsen, T.S., and Rinn, J.L. (2014). The dynamics and regulators of cell fate decisions are revealed by pseudotemporal ordering of single cells. Nat. Biotechnol. *32*, 381–386. https://doi.org/10.1038/nbt.2859.

Tsuji, A., Sakurai, K., Kiyokage, E., Yamazaki, T., Koide, S., Toida, K., Ishimura, K., and Matsuda, Y. (2003). Secretory proprotein convertases PACE4 and PC6A are heparin-binding proteins which are localized in the extracellular matrix. Potential role of PACE4 in the activation of proproteins in the extracellular matrix' Biochimica et biophysica acta *1645*, 95–104. https://doi.org/10.1016/s1570-9639(02)00532-0.

Ueno, M., Lee, L., Chhabra, A., Kim, Y., Sasidharan, R., Van Handel, B., Wang, Y., Kamata, M., Kamran, P., Sereti, K.I., et al. (2013). c-Met-dependent multipotent labyrinth trophoblast progenitors establish placental exchange interface. Dev. Cell *27*, 373–386. https://doi.org/10.1016/j.devcel.2013.10.019.

Weinstein, M., Yang, X., Li, C., Xu, X., Gotay, J., and Deng, C.X. (1998). Failure of egg cylinder elongation and mesoderm induction in mouse embryos lacking the tumor suppressor smad2. Proceedings of the National Academy of Sciences of the United States of America *95*, 9378–9383. https://doi.org/10.1073/pnas.95.16.9378.

Werling, U., and Schorle, H. (2002). Transcription factor gene AP-2 gamma essential for early murine development. Molecular and Cellular Biology *22*, 3149–3156. https://doi.org/10.1128/mcb.22.9.3149-3156.2002.

Wu, T., Wang, H., He, J., Kang, L., Jiang, Y., Liu, J., Zhang, Y., Kou, Z., Liu, L., Zhang, X., and Gao, S. (2011). Reprogramming of trophoblast stem cells into pluripotent stem cells by Oct4. Stem Cells *29*, 755–763. https://doi.org/10.1002/stem.617.

Xie, H., Tranguch, S., Jia, X., Zhang, H., Das, S.K., Dey, S.K., Kuo, C.J., and Wang, H. (2008). Inactivation of nuclear Wnt-β-catenin signaling limits blastocyst competency for implantation. Development *135*, 717–727. https://doi.org/10.1242/dev.015339.

Yagi, R., Kohn, M.J., Karavanova, I., Kaneko, K.J., Vullhorst, D., DePamphilis, M.L., and Buonanno, A. (2007). Transcription factor TEAD4 specifies the trophectoderm lineage at the beginning of mammalian development. Development *134*, 3827–3836. https://doi.org/10.1242/dev.010223.

Yang, W., Klaman, L.D., Chen, B., Araki, T., Harada, H., Thomas, S.M., George, E.L., and Neel, B.G. (2006). An Shp2/SFK/Ras/Erk signaling pathway controls trophoblast stem cell Survival. Dev. Cell *10*, 317–327. https://doi.org/10.1016/j.devcel.2006.01.002.

Ying, Q.L., Wray, J., Nichols, J., Batlle-Morera, L., Doble, B., Woodgett, J., Cohen, P., and Smith, A. (2008). The ground state of embryonic stem cell self-renewal. Nature *453*, 519–523.

You, J.-L., Wang, W., Tang, M.Y., Ye, Y.H., Liu, A.X., and Zhu, Y.M. (2018). A potential role of galectin-1 in promoting mouse trophoblast stem cell differentiation. Mol. Cell. Endocrinol. *470*, 228–239. https://doi.org/10.1016/j.mce.2017.11.003.

Yu, B., van Tol, H.T.A., Oei, C.H.Y., Stout, T.A.E., and Roelen, B.A.J. (2021). Lysophosphatidic acid Accelerates Bovine in vitro-produced blastocyst formation through the hippo/YAP pathway. Int. J. Mol. Sci. *22*, 5915. https://doi.org/10.3390/ijms22115915.

Yu, F.-X., Zhao, B., Panupinthu, N., Jewell, J., Lian, I., Wang, L., Zhao, J., Yuan, H., Tumaneng, K., Li, H., et al. (2012). Regulation of the hippo-YAP pathway by G-protein-Coupled receptor signaling. Cell *150*, 780–791. https://doi.org/10.1016/j.cell.2012.06.037.

Zechner, U., Hemberger, M., Constancia, M., Orth, A., Dragatsis, I., Luttges, A., Hameister, H., and Fundele, R. (2002). Proliferation and growth factor expression in abnormally enlarged placentas of mouse interspecific hybrids. an official publication of the American Association of Anatomists *224*, 125–134. https://doi.org/10.1002/dvdy.10094.

Zhang, H.T., and Hiiragi, T. (2018). Symmetry Breaking in the mammalian embryo. Annu. Rev. Cell Dev. Biol. *34*, 405–426. https://doi.org/10.1146/annurev-cellbio-100617-062616.

STAR★METHODS

KEY RESOURCES TABLE

REAGENT or RESOURCE	SOURCE	IDENTIFIER
Antibodies		
anti-CDX2	Abcam	Ab76541; RRID:AB_1523334
anti-CDX2	BioGenex	MU392A-5UC
anti-E-CADHERIN	BD Biosciences	610182; RRID:AB_397581
anti-ELF5	Santa Cruz	sc-9645; RRID:AB_640106
anti-TBR2/EOMES	Abcam	ab23345; RRID:AB_778267
anti-GFP	Abcam	ab13970; RRID:AB_300798
anti-KRT8/18	DAKO	M365201-2
anti-KRT8	Novus Biological	NBP2-44941-0.1mg
anti-KRT18	Thermo Scientific	MA1-06326
anti-LY6A	Abcam	ab51317; RRID:AB_1640946
anti-WNT7B	R&D Systems	AF3460; RRID:AB_2304437
anti-α-TUBULIN	Cell signaling	3873s
Hoechst	Invitrogen	H3570
WGA	Invitrogen	w11261
Bacterial and virus strains		
DH5a	In house	N/A
Chemicals, peptides, and recombinant proteins		
DMEM/F-12	In-house	N/A
L-ascorbic acid 2-phosphate (ASAP)	Sigma	A8960
Gibc Insulin Transferrin Selenium (ITS-G)	Gibco	12097549
GlutaMAX	Gibco	35050038
Sodium Pyruvate	Gibco	11360070
HEPES	In-house	N/A
β-mercaptoethanol	Gibco	31350010
Penicillin/streptomycin	Sigma	P0781
MEM Non-essential amino acid (NEAA)	Gibco	11140035
Human FGF-4	R&D system	235-F4
Human TGF-β1 (HEK293 derived)	PeproTech	100-21
Heparin	Sigma	H3149
Human/Murine/Rat Activin A (CHO derived)	PeproTech	120-14P
Murine IL11	PeproTech	220-11
human BMP7	PeproTech	120-03p
8-Br cAMP	BIOLOG	B 007-500
1-Oleoyl Lysophosphatidic Acid (LPA)	Tocris	2256236
Y-27632	MedChem Express	HY-10583
(Adv.) DMEM/F-12	Gibco	12634010
Neurobasal medium	Gibco	21103049
N-2 supplement	Gibco	17502048
B-27 supplement	Gibco	A1895602
CHIR 99021	MedChem Express	HY-10182
PD 0325901	MedChem Express	HY-10254
LIF (ESGRO)	Merck	ESG1107
BSA (35%)	Sigma	A7409
Doxycyclin	Sigma	D9891
GW501516	MedChem Express	HY-10838

(*Continued on next page*)

Continued

REAGENT or RESOURCE	SOURCE	IDENTIFIER
Laminin 521	Biolamina	LN521-05
Matrigel, GFR, Phenol red free	Corning	356231
Accutase	BioLegend	423201
TrypLE Express Enzyme (1x), no phenol red	Gibco	12604039
PMSG	Hölzel Diagnostika	OPPA01037
hCG	MSD	Chorulon 1500 IU
Tyrode's acid solution	Sigma	T1788
4-ring dish	Greiner CELLSTAR	627 170
Quickblasto	Janvier Lab	N/A
EmbryoMax M2 medium	Millipore Sigma	MR-015P-D
EmbryoMax KSOM medium	Millipore Sigma	MR-101-D
0.4% Trypan blue	Thermofisher Scientific	T10282
Critical commercial assays		
Quantigene ViewRNA kit	Affymetrix	QVC0001
RNeasy Mini Kit	Quiagen	74104
innuPREP RNA Mini Kit 2.0	Analytik Jena	845-KS-2040050
ChIP-IT High Sensitivity kit	Active Motif	53040 version A6
Deposited data		
Raw and Processed data	This paper	GEO: GSE200961
"Single cell transcriptome analysis of TSCs differentiated TSCs, pTSCs and pTSCs isolated from blastoid"	This paper and (Frias-Aldeguer et al., 2020)	GEO: GSE127754
"SC3-Seq: A Method for Highly Parallel and Quantitative Measurement of Single-Cell Gene Expression"	Nakamura et al., 2015	GEO: GSE63266
"Evaluating Totipotency Using Criteria of Increasing Stringency"	(Posfai et al., 2021)	GEO: GSE145609
"Mechanisms of transcription factor-mediated direct reprogramming of mouse embryonic stem cells to trophoblast stem-like cells"	(Rhee et al., 2017)	GSE90752 (GSM2412032, GSM2412027)
BirA cells_ChIP	Jonghwan Kim	GSM2412036
Codes for RNA-seq analysis	This paper	https://doi.org/10.5281/zenodo.6602725 (https://zenodo.org/record/6602725#.YpdYZqhBxaQ)
Experimental models: Cell lines		
F4-GFP TSCs	Gift obtained from Hospital for Sick Children, Toronto, ON, Canada (J. Rossant lab)	N/A
F4-GFP Cdx2-inducible TSCs	This paper	N/A
CDX2-eGFP TSCs	Gift obtained from Hospital for Sick Children, Toronto, ON, Canada (J. Rossant lab)	N/A
G4 ESCs	Gift obtained from Samuel Lunenfeld Research Institute, Mount Sinai Hospital, Toronto, ON, Canada (A. Nagy lab)	N/A
H2B-RFP ESCs	Gift obtained from the Whitehead Institute for Biomedical Research and Department of Biology, MIT, Cambridge (R. Jaenisch lab)	N/A
Experimental models: Organisms/strains		
Mouse_C57BL/6J	The Jackson Laboratory	RRID:IMSR_JAX:000,664
Mouse_CBA	The Jackson Laboratory	RRID:IMSR_JAX:000,656

(*Continued on next page*)

Continued

REAGENT or RESOURCE	SOURCE	IDENTIFIER
Mouse_B6CBAF1	CBA ♂ x C57BL/6J ♀	N/A
Mouse_FVB/N	The Jackson Laboratory	RRID:IMSR_JAX:001,800
Mouse_129/Sv	The Jackson Laboratory	RRID:IMSR_JAX:000,691
Oligonucleotides		
Primers for qRT-PCR, see Methods S3	This paper	N/A
Probes for Wnt6/7b knockout, see Table S15	This paper	N/A
Recombinant DNA		
PB-TAC-ERP2	Addgene	Add80478
pDONR211	Invitrogen	12536017
pENTR-mCDX2	This paper	N/A
PB-CAG-Pbase	Gift obtained from Center for iPS Cell Research and Application, Kyoto University, Kyoto, Japan, (K. Woltjen lab)	N/A
PB-TAC-mCDX2-ERP	This paper	N/A
Software and algorithms		
FlowJo_v10.6.2	FlowJo™	RRID:SCR_008520; https://www.flowjo.com/
Prism 8	GraphPad	RRID:SCR_002798; https://www.graphpad.com
Fiji	NIH	https://imagej.net/Fiji
Excel	Microsoft	https://www.microsoft.com/nl-nl/microsoft-365/excel
SCOPE	N/A	https://scope.aertslab.org/
PTUI	N/A	https://bird2cluster.univ-nantes.fr/demo/PseudoTimeUI/human/PTUI.html
Burrows-Wheeler Aligner (BWA)	N/A	http://bio-bwa.sourceforge.net/
Integrative Genomics Viewer (IGW)	Broad Institute and the Regents of the University of California	https://software.broadinstitute.org/software/igv/
Deeptools	Max Planck Institute for Immunobiology and Epigenetics, Freiburg	https://deeptools.readthedocs.io/en/develop/
RStudio version 1.3.1056	RStudio	https://www.rstudio.com/products/rstudio/download/
Adobe Illustrator 2022	Adobe	https://www.adobe.com/products/illustrator.html
Adobe Photoshop 2022	Adobe	https://www.adobe.com/nl/products/photoshop.html

RESOURCE AVAILABILITY

Lead contact

Further information and requests for resources and reagents should be directed to and will be fulfilled by the Lead Contact, Nicolas C. Rivron, Ph.D. (nicolas.rivron@imba.oeaw.ac.at).

Material availability

This study did not generate new unique reagents.

Data and code availability

- The raw data of the scRNA-seq, bulk RNA-seq, and ATAC-seq reported in this paper have been deposited to the GeneExpression Omnibus (GEO) database and are publicly available as of the date of publication. Accession numbers are also listed in the key resources table. Microscopy data reported in this paper will be shared by the lead contact upon request.
- All original code has been deposited at Zenodo (https://doi.org/10.5281/zenodo.6602725) and is publicly available as of the date of publication. Link is listed in the key resources table.

- Any additional information required to reanalyze the data reported in this paper is available from the lead contact upon request.

EXPERIMENTAL MODEL AND SUBJECT DETAILS

Stem cells and culture condition

TSCs (F4 GFP and CDX2-eGFP TSCs which were a kind gift from Janet Rossant (Hospital for Sick Children, Toronto, ON, Canada; Department of Molecular Genetics, University of Toronto, Toronto, ON, Canada) and Jacqueline Deschamps (Developmental Biology and Stem Cell Research, Hubrecht Institute, Utrecht, Netherlands), respectively) were cultured following a previously published protocol (Kubaczka et al., 2014). Dishes were coated with 0.1% Matrigel, and cells were cultured in basal TX medium, which consists of DMEM/F12 (phenol red-free, with l-glutamine, or made in house, Media Lab IMBA, Vienna) supplemented with insulin (19.4 μg/mL), l-ascorbic-acid-2-phosphate (64 μg/mL), sodium selenite (14 ng/mL), sodium bicarbonate (543 μg/mL), and holo-transferrin (10.7 μg/mL). For TX culture, basal TX medium was further supplemented with FGF4 (25 ng/mL), TGFβ1 (2 ng/mL), and heparin (1 μg/mL). TXV cultured cells were plated on laminin 521-coated plates (10 ug/ml diluted in PBS without $Mg2^{2+}$ and Ca^{2+}) in basal TX medium supplemented with FGF4 (25 ng/mL), TGFβ1 (2 ng/mL), heparin (1 μg/mL), IL11 (50 ng/mL), Activin (50 ng/mL), Bmp7 (25 ng/mL), LPA (5 nM) and 8-Br cAMP (200 μM). Upon TSCs seeding (both in TX and TXV), Rock inhibitor (Y-27632, 2 μM) was added to help the attachment of TSCs onto the plates. TSCs were differentiated by changing the medium to basal TX medium without FGF4, TGFβ1 nor any other CDX2 regulator. This medium was maintained for 6 days.

TS medium cultured cells were plated on MEF in RPMI-1640 medium supplemented with 20% FBS, GlutaMax (1x, Gibco, 35,050,038), Sodium pyruvate (1x, Gibco, 11,360,070), HEPES (10 mM, made in house, Media Lab IMBA, Vienna), 2-Mercaptoethanol (100 μM, Gibco, REF 31350010), FGF4 (25 ng/mL), and heparin (1 μg/mL). ESCs (G4 WT ESCs which were a kind gift from Andras Nagy (Samuel Lunenfeld Research Institute, Mount Sinai Hospital, Toronto, ON, Canada; Department of Molecular Genetics, University of Toronto, Toronto, ON, Canada)), and H2B-RFP V6.5 sub-clone (V6.5 cell line was derived from C57BL/6 × 129/Sv background and obtained from the laboratory of Rudolf Jaenisch (The Whitehead Institute for Biomedical Research and Department of Biology, MIT, Cambridge, MA 02142, USA)) were cultured under 2i conditions B27N2 medium (Ying et al., 2008) in gelatin-coated plates without MEF. Cells were routinely passaged using either accutase or trypsin which was quenched with trypsin soybean inhibitor.

Mouse lines and embryos

All animal experiments (e.g., blastocyst flushing and uterus transfer) were conducted using 8–20-week-old female mice on a B6CBAF1 background, unless noted otherwise (e.g., C57BL/6J, FVB/N, and 129/Sv background for the TSCs derivation experiment). Mice were maintained at the IMP/IMBA animal house. All animal experiments were approved by the IMP/IMBA animal house and performed in accordance with the guidelines of the institution.

For the blastocyst flushing, super-ovulation was performed. Briefly, PMSG (5-6 IU per mouse, Hölzel Diagnostika, OPPA01037) was injected into females between 14:00-15:00h and followed by hCG injection (5-6 IU per mouse, MSD, Chorulon 1500 IU) within 47–48 h. Mice were mated on the same night hCG was injected (19:00-20:00h) and checked for plugs the next morning. Three or four days after checking the plug (for E3.5 or E4.5 blastocysts, respectively), the uterus was explanted and flushed with M2 medium (Millipore Sigma, MR-015P-D). For further culture of blastocysts, M2 or M2 supplemented with TXV factors (doubled concentration) were used for six or 20 h.

Six days after checking the plug (for E6.5 embryos), the uterine wall was gently removed with forceps. The deciduae were fixed with 4% formaldehyde overnight at 4°C and washed with PBS (three to four x for 1 h each). After EtOH-xylene-paraffin dehydration processing, the deciduae were embedded in paraffin and sliced to 2-μm thickness.

METHOD DETAILS

Generation of inducible Caudal Type Homeobox 2 overexpression cell lines

Inducible CDX2 TSCs were generated in the F4 TSCs line. pCAG-PBase (5 μg) and PB-TAC-*Cdx2*-ERP (5 μg) were transfected by NEPA21 electroporation (Nepa Gene Co. Ltd) into $1x10^6$ cells in single-cell suspension. One day after transfection puromycin (1 μg/ml) was added for 7 days and the selected cells were maintained in a lower concentration of puromycin (0.1 μg/ml).

Generation of WNT6 and WNT7B knockout trophoblast stem cells

WNT6 and WNT7B KO TSCs were generated in the F4 TSCs line using a CRISPR-Cas9 system. Cells were electroporated (NEPA21 Super Electroporator, Nepa Gene Co., Ltd.) to transfect plasmids containing a specific guide RNA sequence (Figure S7D), as well as a Cas9, and BFP sequence. 10 μg of plasmid were used to transfect $1x10^6$ cells. BFP positive cells were FACS sorted the next day. After their expansion, BFP negative cells were FACS sorted individually onto inactivated MEFs for clonal expansion and cultured in TXV medium. MEFs were depleted and cells were genotyped by Sanger sequencing. The effect of genomic editing on gene expression was confirmed by qRT-PCR using primers that amplify the 3′UTR and Western Blot (Figure S7E and S7F). Sequence information for all primers and sgRNAs used in this study are available in Methods S3.

Cell cycle analysis

After trypsinization, 1x10^5 TSCs and TESCs were incubated in 0.5 mL of TX medium with 10 ug/ml Hoechst 34580 for 30 min at 37°C. After the incubation time, tubes with cells were placed on ice and analyzed on a FACS Canto II.

Colony formation assay

Single cells were sorted into MEF coated plates with either TX or TXV medium. Medium was changed every 48 h and the number of wells containing colonies was assessed 7 days after sorting.

Combinatorial screen

A library of all compounds tested in the combinatorial screen can be found in Table S4. To identify positive modulators for CDX2 induction, CDX2-eGFP TSCs were cultured in TX medium for 24 h and then exposed to new TX media containing the different concentrations of individual compounds. After 48 h, CDX2 expressions of TSCs in each condition were analyzed by flow cytometry (FACS Fortessa, and FlowJo). For the experiment in Figure S3B, IGF2 (50 ng/mL) and ZSTK474 (PI3K inhibitor, 200 nM) were added to the medium.

Immunofluorescence

Samples were fixed using 4% formaldehyde in PBS for 20-30 min at room temperature (RT) followed by three washing steps with PBS. A 0.3% triton solution in PBS (PBS-T) was used for permeabilization for 30-60 min at RT, followed by a 1-2 h blocking step with 0.1% PBS-T + 2% BSA +3% serum (goat or donkey serum complementary to the host of the secondary antibody). Samples were then incubated overnight with the primary antibody diluted in blocking solution at 4°C. A detailed summary of all primary antibodies used in this study is provided in Methods S4. The next day samples were washed three times in 0.1% PBS-T and incubated with the corresponding secondary antibodies for 1 h at RT. Hoechst was used for counterstaining with or without WGA. Images were taken with one of the following microscopes: PerkinElmer Ultraview VoX spinning disk microscope, confocal Axio Observer inverted microscope equipped with a Yokogawa CSU X1 Spinning disk, and Olympus IX3 Series (IX83) inverted microscope equipped with a dual-camera Yokogawa W1 spinning disk. The images were analyzed with Fiji and photoshop.

Whole tissue staining/clearing and 3D imaging of embryos

After checking the expression of naive GFP in the chimeric embryos, we performed whole tissue staining and clearing as previously reported ((Kubaczka et al., 2014); Seong et al., 2018). Briefly, the dissected E6.5 embryos were incubated in Reagent 1 [25% (w/w) urea, 25% (w/w) N,N,N′,N′- tetrakis (2-hydroxypropyl) ethylenediamine, 15% (w/w) Triton X-100 in distilled water] for 3 days at 37°C, and washed with PBS (1 h) and with 0.1% Triton X-100 in PBS (PBS-T) (1 h × 2 times) at RT. The embryos were incubated with a blocking buffer (10% donkey serum in 0.5% PBS-T) overnight at 4°C, and then incubated for 4 days at 4°C with gentle rocking and the GFP, Elf5 antibodies (Methods S4). The embryos were incubated with fluorescent probes for 2 days at 4°C with gentle rocking, and Hoechst was used to detect nuclei. A PBS-T (0.3%) wash followed each antibody and Hoechst incubation (1 h × 3 times). The embryos were incubated in Reagent 2 [44% (w/w) sucrose, 22% (w/w) urea, 9% (w/w) 2,2′,2″-nitrilotriethanol, 0.1% (w/w) Triton X-100 in distilled water] for tissue clearing at least 1 day at 37°C with gentle rocking. Immunofluorescence was detected using an Olympus IX83 inverted microscope equipped with a dual-camera Yokogawa W1 spinning disk.

Single-molecule FISH

TSCs plated on glass coverslips were allowed to grow and subsequently fixed using RNase free 4% PFA in PBS +1% Acetic Acid for 20 min. After fixation, all samples were processed as described in the Quantigene ViewRNA kit instructions (Affymetrix, QVC0001). Briefly, after three washes with RNase free PBS, samples were incubated for 10 min in a detergent solution. This was followed by three washes with RNase free PBS after which samples were incubated for 5 min at RT with Q protease. Samples were again washed three times with RNase free PBS, and incubated with the probes of interest diluted in Probe set diluent at 40°C for 3 h (in a humidified chamber). After three washes with wash buffer, samples were incubated at 40°C for 30 min with a preamplifier diluted in amplifier diluent and washed again for three times. Samples were then incubated at 40°C for 30 min with amplifier diluted in amplifier diluent. Samples were washed again three times with wash buffer and incubated at 40°C for 30 min with label diluted in label probe diluent. After two washes, they were washed once more for 10 min. Samples were then incubated for 15 min in RNase free PBS with Hoechst and WGA as counterstains followed by three washes with RNase free PBS. Blastocysts or blastoids were carefully placed in mounting media in glass bottom 3.5 mm plates. All samples were imaged with a 63x oil immersion objective on a PerkinElmer Ultraview VoX spinning disk microscope.

Single-molecule FISH polarity quantification

Single molecule fluorescence *in situ* hybridization (smFISH) confocal images were taken with a z-step of 0.3 μm. Given the complexity of an analysis performed in 3D that would require an algorithm capable of segmenting cells and quantifying the number of transcripts in 3D, we decided to quantify a 2D projection of the slices that included the ICM and blastocoel. Those z stack projections were oriented with the polar side on the left and the mural side on the right and then analyzed for average column pixel intensity, allowing us to plot an average pixel intensity histogram. An intensity profile was plotted for each embryo and gene. Each blastocyst is structurally different showing distinct cavity sizes, which implies that a different percentage of the TE is in contact with the ICM for each embryo.

In order to compare the expression of polar and mural TE, we divided the length of the embryo in three segments of equal distance, irrespective of the total diameter. The intermediate segment was considered a transition stage between the polar and mural regions and therefore was not included in the next analyses. The polar and mural segments of the profile were analyzed by comparing the average pixel intensities of each pixel column included in the segment.

High content imaging

Each colony was imaged for E-CADHERIN, CDX2 and Nuclei stainings. E-CADHERIN staining was used for manual cell segmentation in ImageJ. Cell profiler was used for analysis of cell segmentation and the other stainings. Measurements obtained in the Cell profiler were used for further analysis using a Python pipeline. After discarding dividing cells based on the nuclear staining, a total of 502 control cells and 297 TXV TSCs cells were analyzed.

Live cell imaging

For the live cell imaging, CDX2-eGFP TSCs were seeded in glass bottom 12 well plates coated with Matrigel in TX medium at 25,000/cm2 density and they were incubated for 24 h at 37°C, 5% CO2. At the end of the 24h the medium was replaced with fresh medium and then the well plate was transferred to UltraVIEW spinning disk confocal microscope (PerkinElmer) for live imaging analysis. The stage area was set up to 37°C, 5% CO2 prior to the experiment. Images were collected every 12 min (5 timepoints per hour) for a total of 60 h in the GFP channels. The analysis of the live imaging data was completed with ImageJ.

Flow cytometry

Dissociated TSCs/TESCs with 0.05% trypsin were stained for 30 min on ice with the 100 ng of LY6A antibody, and were incubated on ice with anti-rat Alexa 647 (See Methods S4). Each antibody incubation was followed by a wash with FACS buffer (PBS plus 2% FBS). After resuspension of cells with FACS buffer, flow cytometry was conducted using FACS LSR Fortessa (BD). We used at least 10,000 cells for gating. Data was analyzed by FlowJo software. With CDX2-eGFP TSCs/TESCs, we directly used the cells for the flow cytometry after dissociation.

Blastoids made by H2B-RFP ESCs and CDX2-GFP TSCs (see 'Blastoids formation' section below) were dissociated with 0.05% trypsin. By plotting them with GFP and RFP, GFP^+ TR cells were sorted out for further analysis.

For CDX2-high, -low cell sorting, we dissociated CDX2-GFP TSCs and sorted the cells with FACS aria III based on naive GFP signal. For CDX2-high and -low groups (H and L), we use top and bottom 10% of GFP^+ cells, respectively.

qRT-PCR

RNA was harvested using either the RNeasy Mini Kit (Quiagen, 74,104) or the innuPREP RNA Mini Kit 2.0 (Analytik Jena, 845-KS-2040050) according to the manufacturer's instructions. For cDNA synthesis RNA was incubated with 2.5 μM OligodT primer (New England Biolabs, S1316S) and 0.5 μM dNTPs (in house, Molecular Biology Service IMBA Vienna) at 65°C for 5 min. Reverse transcription was then performed using the SuperScript™ III Reverse Transcriptase (Invitrogen, 18,080,044) together with RNaseOUT™ Recombinant RNase Inhibitor (Invitrogen, 10,777,019) according to the protocol provided by the manufacturer. For the qPCR reactions GoTaq qPCR Master Mix (Promega, A6001) was used. All qPCRs were performed using a Bio-Rad CFX Connect Real-Time PCR System. Relative expression levels of target genes were calculated with the ΔΔCT method using *Hprt* as an endogenous reference gene for internal normalization. Sequence information for all primers can be found in Methods S3.

RNA sequencing

For bulk sequencing 1000 control and TXV cultured cells were used for Trizol RNA extraction. Both bulk and single cell sequencing was performed following the Cel Seq 2 protocol (Hashimshony et al., 2016). In-bulk samples were first normalized and then analyzed using the DESeq2 package in Rstudio. Triplicates for each group (F4 GFP in TX TXV, TX differentiated, and TXV differentiated) were analyzed. Genes were considered differentially expressed when showing a 1.5-fold expression change with a p value < 0.05. The DAVID gene ontology online tool was used for gene enrichment analysis.

Mapping and processing of single-cell mRNA sequencing data

Read one contains the cell or section barcode and the unique molecular identifier (UMI). Read two contains the biological information. Reads 2 with a valid cell barcode were selected and mapped using STAR-2.5.3a with default parameters to the mouse mm10 genome, and only reads mapping to gene bodies (exons or introns) were used for downstream analysis. Reads mapping simultaneously to an exon and to an intron were assigned to the exon. For each cell or section, the number of transcripts was obtained as previously described (Grün et al., 2014). We refer to transcripts as unique molecules based on UMI correction.

Analysis of single-cell mRNA sequencing data

To analyze CEL-Seq single cell sequencing experiments, mouse genomic sequence and annotation from NCBI GRCm38.p6 were used. Reads were trimmed using trim_galore v0.6.4 and subsequently aligned to the mouse genome (GRCm38.p6) using STAR v2.7.6a. UMI quantification and raw count matrixes generation were performed using umi_tools v1.0.1.

Further analysis was performed in R v4.0.4 with Seurat v3.2.3. Cells with a number of genes comprised between 200 and 2500 or with $\geq$ 5% mitochondrial genes were retained. Standardization of per gene expression values through the cells was performed using

NormalizeData, FindVariableFeatures and ScaleData; top 2000 variable genes were selected. Principal Component analysis was performed with RunPCA function whereas clusters were identified using FindNeighbours and FindClusters at a resolution of 0.8. Cluster marker genes and differentially expressed genes were detected with the Wilcox likelihood-ratio test using the FindMarkers function with logfc.threshold = 0.1. Uniform Mani-fold Approximation and Projection was used for the visualization.

Gene enrichment analysis was performed using GSEA V4.1.0 using the preranked function. Cluster genes identified using FindMarkers from the Seurat package were ranked according to the p value and the log fold change before conducting the gene enrichment analysis. Gene sets used in the preranked GSEA were obtained by performing differentially gene expression (as described above) between annotated polar and mural cells at the 4.5 blastocyst stage by (Nakamura et al., 2015) (GSE63266) and TE and ExE by (Posfai et al., 2021) (GSE145609). For the latter, annotations were kept as provided by the authors meaning that we included single TE cells from E2.5, E2.75, E3.0, E4.5 and ExE cells from E7.0 and E7.5 in our analyses.

Data was analyzed using the monocle and RaceID pipelines (Grün et al., 2014; Grün et al., 2016; Posfai et al., 2021) to organize cells into pseudotime trajectories (Trapnell et al., 2014) and generate unsupervised clustering heatmaps.

Caudal Type Homeobox 2 ChIP-seq analysis

Publicly available datasets for CDX2 ChIP-seq (GSM2412032), the corresponding input control (GSM2412036), and chromatin accessibility (ATAC-seq, GSM2412027) for mouse TSCs were reanalyzed. Briefly, raw sequencing reads were trimmed using Trimmomatic SE for Truseq2:SE adapters and were aligned to mouse mm10 reference genome using default parameters of Burrows-Wheeler Aligner. BigWig files were generated utilizing the bamCoverage function using RPKM normalization from deepTools 3.3.2. Reads from input signals were subtracted using bamCompare utilities. Normalized reads for both ChIP-seq and ATAC-seq were used for visualization with Integrative Genomics Viewer (IGV).

Chromatin immunoprecipitation PCR (ChIP-PCR)

Chromatin immunoprecipitation was performed using the ChIP-IT High Sensitivity kit (Active Motif, cat no 53040 version A6), following the included protocol. Briefly, the frozen cell pellets were resuspended in Chromatin Prep Buffer and nuclei isolated by douncing for 40 times on ice using a tight-fitting pestle. Samples were placed in an ice bath and sonicated to a size range of 200–800 base pairs using a probe sonicator. Input chromatin was prepared by treating a sample of the sonicated chromatin with RNAse A and Proteinase K, followed by de-crosslinking at 80°C for 2 h. The de-crosslinked DNA was precipitated using ethanol and the Precipitation Buffer and Carrier included in the kit, spun down, washed with 70% ethanol and resuspended in DNA Purification Elution Buffer (included in kit). Chromatin immunoprecipitation was performed using 0.7–2.5 μg chromatin and 4 μg anti-H3K9Ac (Active Motif 61,251) or anti-H3K4Me3 (Diagenode C15410003) antibody. After overnight incubation at 4°C with rotation, the reactions were incubated with Protein G agarose beads (included in kit) for 3 h at 4°C with rotation to capture the antibody/chromatin complexes. The beads were recovered and washed five times using the columns and wash buffer included in the kit, and the bound chromatin eluted twice using the included elution buffer. The eluded chromatin was treated with Proteinase K and de-crosslinked at 80°C for 2 h, after which the DNA was purified using the included purification columns and recovered in a 200 μL elution buffer (included).

qPCR was carried out on a BioRad CFX machine using a SYBRgreen based master mix. The amount of precipitated chromatin as a percentage of input for each analyzed region was determined using standard curves created from input chromatin in amounts ranging from 0.005 ng to 50 ng. Primer sequences are listed in Methods S2.

Chimeric embryo formation

Defrosted 8-cell embryos (Janvier Lab, Quickblasto) were cultured in KSOM medium (Sigma, MR-101D) for 4-5 h (37°C, 5% CO2). A micromanipulator was used to inject 8-12 F4 GFP TESCs or TSCs into the morula or early blastocyst cavity with the aid of a laser (Hamilton Throne, Xyrocos). TSCs/TESCs injected blastocysts were then transferred into the uterine horns of E2.5 pseudopregnant females. A maximum of seven blastocysts were used per horn. E6.5 embryos were isolated in PBS by gentle dissection and fixed with 4% formaldehyde. The embryos were stained using whole tissue staining and clearing methods described below.

Trophoblast stem cells line derivation and staining

E3.5 blastocysts were isolated from pregnant females. Zona pellucida was removed using Tyrode's acid solution before placing them in MEF-coated plates with TS, TX, or TXV medium. The medium was changed every 48 h. The outgrowth was monitored daily and was passaged on day 5–7 depending on cell growth. With proper size, the colonies were fixed, and immunofluorescence was performed as described above.

For TSCs line derivation from E6.5 conceptus in TXV medium, we isolated the ExE from E6.5 conceptus by manually cutting off the EPI, EPC, and visceral endoderm. The ExEs were placed on MEF in TXV medium, and the medium was changed every 48 h. The outgrowths were dissociated after 2 to 3 days and colonies became visible within the next 5 days. Both E3.5 and E6.5-derived TSCs were cultured on MEF for three passages, and then transferred to laminin-coated plates.

Blastoid formation

Full protocol link: https://protocolexchange.researchsquare.com/article/nprot-6579/v1). Agarose microwell arrays were casted using a custom PDMS stamp and incubated overnight in mES serum containing media. After washing the chips with PBS, an ESC solution of 150k cells/ml was dispensed in the central chip and allowed to settle. After 20 min, an additional 1 mL of mES medium was

added. 24-28 h later, mES medium was removed and a TSCs/TESCs solution of 150k cells/ml was dispensed. After allowing the cells to fall in the microwells, 1 mL of blastoid media was added to the wells. WNT7B or WNT6 KO blastoids were made from normal ESCs and WNT7b or WNT6 KO TSCs. The rest of the procedure was the same as the general protocol.

mES medium is DMEM high glucose medium (made in house, Media Lab IMBA, Vienna) supplemented with 10% FBS, GlutaMax (1x, Gioco, 35,050,038), Non-essential amino acid (1x, Gibco, 11,350,912), HEPES (10 mM, made in house, Media Lab IMBA, Vienna), 2-Mercaptoethanol (100 μM, Gibco, REF 31350-010), LIF (1000 U/ml, Sigma, ESG1107), and 1x Penicillin/streptomycin (Gibco, 15,140,122). Blastoid medium consisted of 50% basal TX medium and 50% WNT3A conditioned medium supplemented with 20 μM Y-27632 (MedChem Express, HY-10583), 3 μM CHIR99021 (MedChem Express, HY-10182), 1 mM 8-Br cAMP (BIOLOG, B 007-500), 25 ng/mL FGF4 (R&D systems, 5846F4), 15 ng/mL TGFβ1 (Peprotech 100-21), 30 ng/mL IL11 (Peprotech, 220-11), 1 μg/mL heparin (Sigma-Aldrich, H3149) and 1x Penicillin/streptomycin (Sigma, P0781). An additional shot of 8-Br cAMP was added to each well 24 h after TSCs/TESCs seeding to add another 1 mM per well. Blastoids were analyzed 65 h after TSCs/TESCs seeding unless noted otherwise.

To culture EPSCs and to make blastoids formed from the association of EPSC and TESCs, we followed the variation on our initial protocol as described in the reference (Sozen et al., 2019), at the exception of the initial TSCs culture conditions that were replaced by TESCs.

Uterus transfer and decidua analysis

Four hours before uterus transfer, the blastoid medium was replaced with DMEM high glucose medium. Picked blastoids from the microwells were placed on four ring-well plate and briefly washed with DMEM high glucose medium. With the few medium, 10-12 blastoids were transferred into the only one of the uterine horns of E3.5 pseudopregnant females, unless noted otherwise. E7.5 deciduae were explanted 4 days after uterus transfer. The bulb which has a clearly bigger diameter than the width of a normal uterus was considered as a decidua, and the number of deciduae was confirmed by three different scientists by performing blind test. We took decidua pictures with the ruler, and measured the length of deciduae from mesometrium side to anti-mesometrium side (perpendicular to the direction of the cervix from the ovary) with Fiji.

For the fixed blastoids transfer, blastoids were fixed with 4% formaldehyde in PBS for 30 min at RT. The blastoids in the control group were in the PBS for 30 min to be fair. After enough washing with PBS, the blastoids were transferred. For the Cdx2i blastoids, 225 nM (100 ng/mL) of doxycycline was added when the TSCs were seeded on the microwells with a blastoid medium. For the blastoids with GW501516, 3 μM of GW501516 was added 1 day before the uterus transfer (around 40-45 h after TSCs seeding).

For the comparison experiment of blastocysts with TSCs and TESCs blastoids, freshly isolated E3.5 blastocysts from pregnant females were directly transferred into the E3.5 pseudopregnant recipients. For IWP2 treatment before uterus transfer, we cultured eight cell-embryos in KSOM either with or without IWP2. After 2 days, they developed late blastocysts (E4.0-E4.5) and were transferred to the uterus.

Blue band assay

Two days after uterus transfer, 0.4% trypan blue (Thermofisher Scientific, T10282, 10 μL per 1g of mouse weight) was injected through intravenous (i.v.) injection. After 30 min, the mice were sacrificed and E5.5 uteri were analyzed. For Figure 7C, only four to six blastocysts were transferred to prevent overlap of individual blue bands.

Western Blot

For protein isolation, TSCs were lysed using RIPA buffer (Thermo Fisher Scientific, 89,900). For western blotting, proteins were transferred to 0.2μm Nitrocellulose membranes (Bio-Rad, 1,620,112), and membranes were then blocked with 0.1% PBS-T (PBS plus 0.1% Triton X-100) containing 5% skim milk at RT for 1 h. To detect specific proteins of interest, WNT7B and a-TUBULIN antibodies were used (See Methods S4). Horseradish peroxidase (HRP)-conjugated secondary antibodies were then used. Each antibody incubation was followed by washing with 0.1% PBS-T. Luminescence was detected with a Bio-Rad ChemiDoc MP Imaging System.

SCOPE and PTUI

Wnt family expression levels in the mouse embryo were analyzed with SCOPE (https://scope.aertslab.org/) using data resources from (Posfai et al., 2021) (GSE145609) for the analysis of transcriptomic differences between the TE and ExE. Wnt family expression levels in the human embryo were analyzed with PTUI (https://bird2cluster.univ-nantes.fr/demo/PseudoTimeUI/human/PTUI.html) by using data resources from ().

QUANTIFICATION AND STATISTICAL ANALYSIS

Statistical analyses were performed using GraphPad Prism 8 (GraphPad Software) and Excel (Microsoft). All error bars represent the SEM(SEM). Data were analyzed using a one-way ANOVA, a two-tailed t-test (for a difference in means), Mann-Whitney analysis, or Wilcox likelihood-ratio test. The statistical analysis used for each dataset is indicated in the figure legend. A p value < 0.05 was considered statistically significant at the 95% confidence level. The number of biological (non-technical) replicates for each experiment is indicated in the figure legends. All representative images shown are from experiments that have been performed in triplicate at least, except Figure S4H (two independent experiments with pooled 36-40 embryos).

Cell Stem Cell, Volume *29*

Supplemental Information

Epiblast inducers capture mouse trophectoderm stem cells *in vitro* and pattern blastoids for implantation *in utero*

Jinwoo Seong, Javier Frias-Aldeguer, Viktoria Holzmann, Harunobu Kagawa, Giovanni Sestini, Heidar Heidari Khoei, Yvonne Scholte Op Reimer, Maarten Kip, Saurabh J. Pradhan, Lucas Verwegen, Judith Vivié, Linfeng Li, Anna Alemany, Jeroen Korving, Frank Darmis, Alexander van Oudenaarden, Derk ten Berge, Niels Geijsen, and Nicolas C. Rivron

Figure S1. (Related to Figure 1)

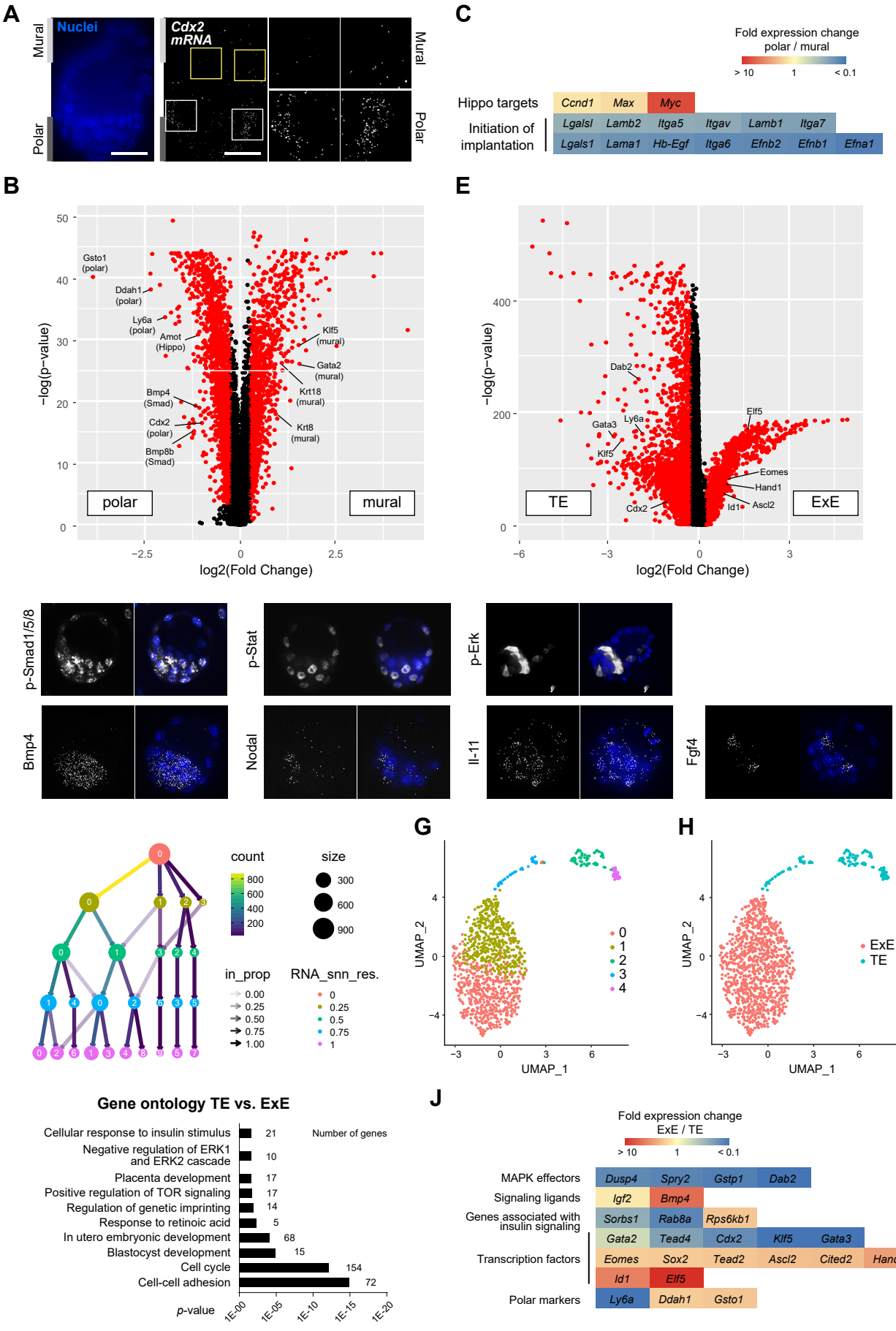

Figure S1. The transcriptomic transitions of pre- and post-implantation trophoblasts. Related to Figure 1.

A. smFISH for *Cdx2* mRNA in a E4.5 blastocyst. Scale bars represent 40 μm. **B**. Volcano plot showing differentially expressed genes between polar and mural TE cells. **C**. Heatmap showing the fold expression change of indicated genes in the polar TE compared to the mural TE. **D**. Immunofluorescence staining using antibodies specific to phosphorylated forms of proteins, and smFISH performed on freshly isolated blastocysts for key pathway effectors (pSMAD1/5/8, pSTAT, pERK) and ligands (BMP4, IL11, Nodal, FGF4). **E**. Volcano plot showing differentially expressed genes between ExE and TE. **F**. Using cluster tree, the data set published by Posfai et al. (2021) was reclustered. A resolution of 0.5 was chosen to generate the 5 clusters annotated in F. See also Material method (Analysis of scRNA-seq data). **G**. UMAP plot generated for the Posfai et al. (2021) data set. Unsupervised clustering showed distinct transcriptional differences between the cells from TE and ExE. **H**. UMAP plot with original annotations as published (Posfai et al. 2021). **I**. Gene ontology analysis based on differentially expressed genes between TE and ExE. **J**. Heatmap showing fold expression changes of indicated genes in the ExE compared to the TE.

Figure S2. (Related to Figure 2)

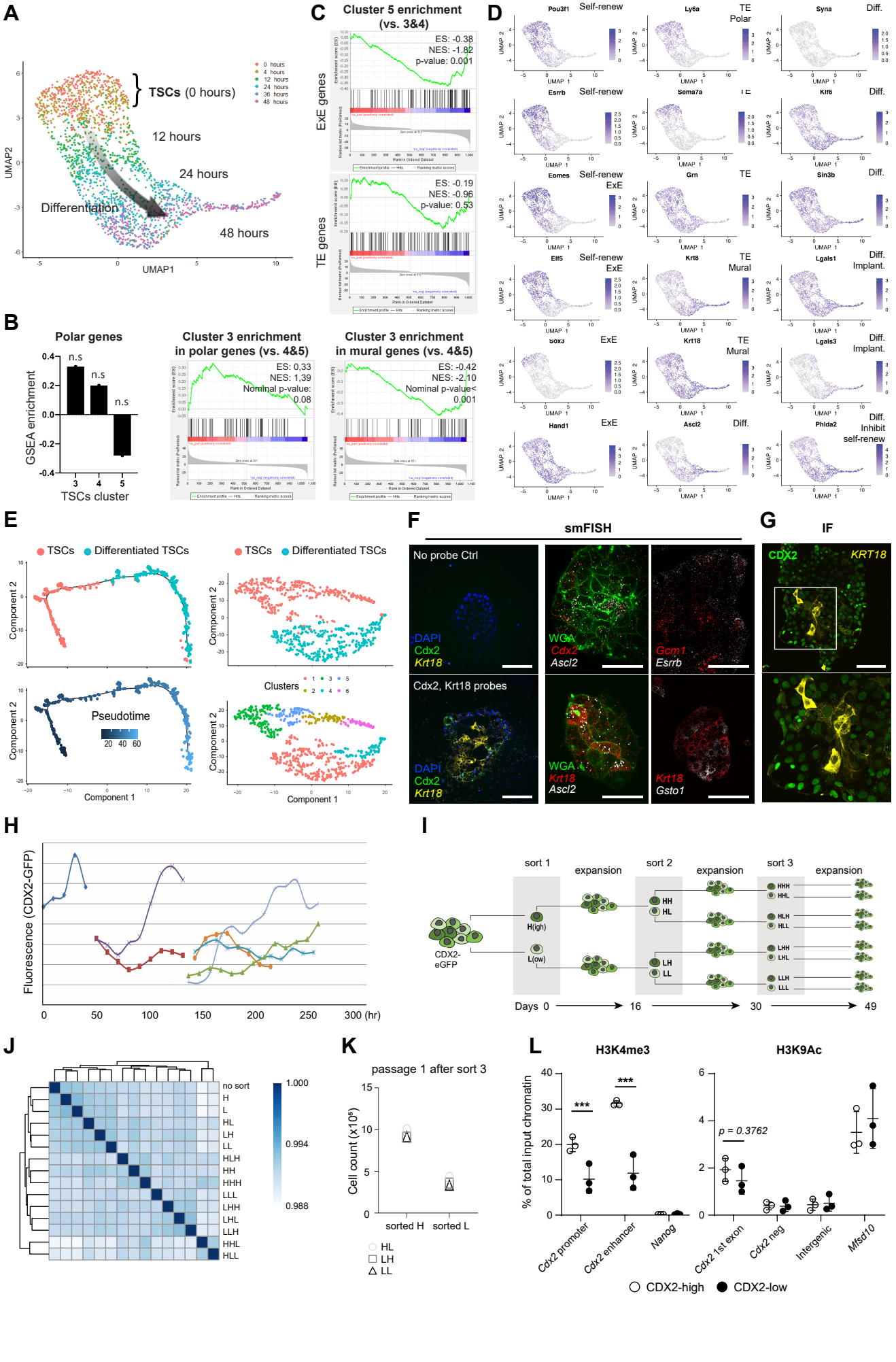

Figure S2. TSCs comprise heterogeneous and interconvertible states reflecting peri-implantation stages. Related to Figure 2.

A. Single cell transcriptome analysis upon removal of minimal inducers. The UMAP plot shows transcriptional shifts of differentiated TSCs over time. **B**. Gene set enrichment analysis (GSEA) for polar and mural genes in cluster 3 (vs.4 and 5), and **C**. ExE and TE genes in cluster 5 (vs.3 and 4). Data were analyzed by Wilcox likelihood-ratio test. **D**. UMAP plot showing distribution of various self-renewal, ExE, TE and differentiation-associated (Diff.) marker genes. **E**. Control TSCs and differentiated TSCs were located in a pseudotime trajectory by Monocle (left). Clustering analysis (t-SNE) of control TSCs and differentiated TSCs (right). Orange dots (TSCs) are clearly visible in clusters of blue dots or late pseudotime. **F**. smFISH for self-renewal, polar (*Cdx2*, *Esrrb*, *Gsto1*) and differentiated transcripts (*Ascl2*, *Gcm1*, *Krt18*) show heterogeneity of TSCs. No probes were used as a negative control. Scale bars represent 150 μm for the left column, and 40 μm for the middle and right column. **G**. Anti-correlation of CDX2 and KRT18 expression in TSCs. Scale bars: 150 μm. **H**. CDX2 intensity measurement from a TSCs and its descendants over time (one parent cell → two F1 cells → four F2 cells. Each line represents one cell tracked over time). Daughter cells from both divisions showed similar fluorescence levels right after division, but later oscillated substantially. **I**. Schematic view of serial cell sorting strategy for CDX2-high and -low TSCs. **J**. Pearson correlation map of TSCs sorted once, twice, or three times based on CDX2 expression. Even after several rounds of cell sorting, TSCs maintained their transcriptome with minor variation, and we could not distinguish the transcriptome of CDX2-high cells from that of CDX2-low cells. Notably, the shift of the transcriptome of TSCs that happens over time is more important than the difference between the transcriptome of cells recovered following a CDX2-high or CDX2-low sorting, suggesting plasticity between CDX2-high and -low cells. **K**. CDX2-low cells proliferate slower. The graph displays the cell numbers reached at the first passage after expansion of CDX2-high and low population sorted from the HL, LH, and LL population in the third sort. **L**. ChIP-PCR analysis of genomic DNA from flow cytometry-sorted CDX2-eGFP cells for H3K4me3 (left) and H3K9Ac (right) histone modifications. *Nanog*, *Cdx2* neg and Intergenic are negative controls; *Mfsd10* is a positive control. Data are means±s.e.m., analyzed by Student's t-test: ***$p<0.001$.

Figure S3. (Related to Figure 3)

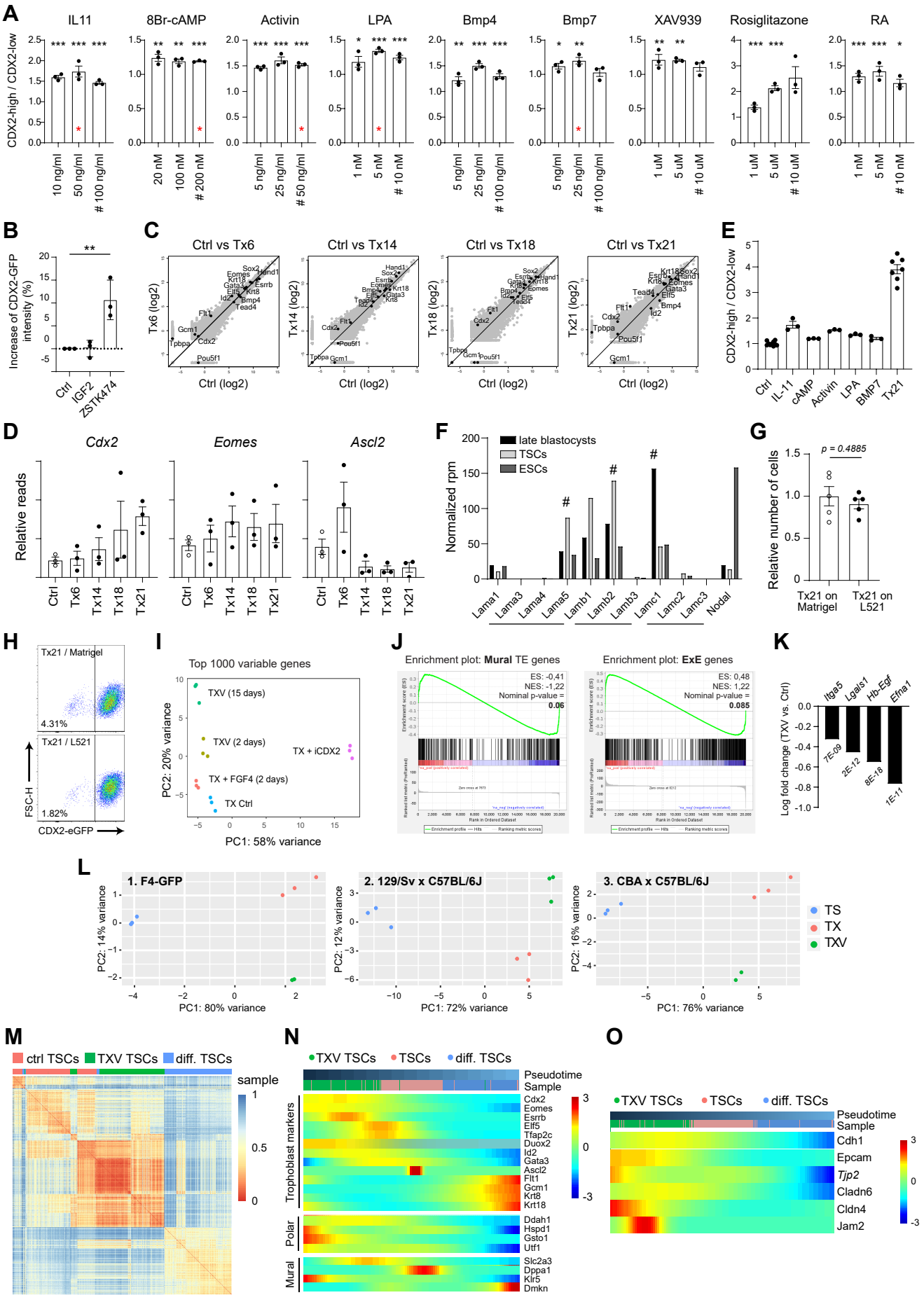

Figure S3. Optimal embryonic inducers capture trophoblast stem cells with a transcriptome more akin to the trophectoderm. Related to Figure 3.

A. Positive modulators which induce CDX2 expression. We assessed the CDX2-high/CDX2-low ratio of each condition by flow cytometry. Based on the results of an initial screen (Table S6), we identified 9 compounds as positive regulators of CDX2. For all graphs, control results (untreated groups, n = 10) were set to 1 and omitted from the graphs. Concentrations marked with # were considered as 100% in Figure 3B. Red asterisks indicate final compound concentrations used in TXV medium (concentration with highest induction and lowest *p*-value in each group). Data are means ± s.e.m., analyzed by Student's t-test: **p*<0.05, ***p*<0.01, ****p*<0.001. **B**. CDX2 (eGFP) intensity changes in CDX2-eGFP TSCs with IGF2 or PI3K inhibitor (ZSTK474) treatment. Each dot represents an independent experiment. Data are means±s.e.m., analyzed by one-way ANOVA. ***p*<0.01. **C**. Bulk transcriptome analysis allows us to compare the overall expression of key trophoblast markers for each culture condition. **D**. Expression of *Cdx2* and *Eomes* (as un-differentiated markers) and *Ascl2* (as a partially differentiated marker) for the 4 best compound combinations based on 3 independent bulk RNA-seq results. **E**. CDX2-high/CDX2-low ratio of single compounds or Tx21 (TXV) induction, highlighting a synergistic effect of compounds. **F**. Normalized rpm from bulk RNA-seq of late blastocysts, TSCs, and ESCs. Laminin alpha 5, beta 2, and gamma 1 (marked with #) were the most abundant laminins in blastocyst (*in vivo*) and TSCs culture (*in vitro*). Three numbers of laminin refer to the composition of laminin-alpha (*Lama*), -beta (*Lamb*), and -gamma (*Lamc*) chains (e.g., L521 = laminin-alpha 5, laminin-beta 2, and laminin-gamma 1). **G**. Quantification of proliferation of Tx21 TSCs on L521 compared to Matrigel control. **H**. Flow cytometry with CDX2-eGFP TSCs cultured in Tx21 on Matrigel or L521. Both conditions showed a high proportion of CDX2-high cells, but Tx21 TSCs on L521 had less CDX2-low cells compared to those on Matrigel (N = 4, *p = 0.0178*). **I**. Principal component analysis (PCA) of bulk RNA-seq with TXV TSCs (exposure to optimal inducers for 2 or 15 days), CDX2 overexpressed TX TSCs, and TX TSCs with high concentration of FGF4 (100 ng/ml). **J**. Gene set enrichment analysis (GSEA) for mural TE and ExE genes with TSCs exposed to optimal inducers for 15 days. **K**. Expression levels of transcripts associated with mural trophoblasts - endometrium interactions during implantation. The *p*-value is indicated below the respective bar. **L**. PCA of bulk RNA-seq of 3 different TSCs lines in TS, TX, and TXV medium. **M**. Unsupervised gene clustering analysis (distance map from RaceID pipelines) of single cells from control, TXV and differentiated TSCs. **N**. Pseudotime heatmap for visualization of expression patterns along with polar, mural, and classical trophoblast marker genes. **O**. Pseudotime heatmaps for epithelial and tight junction markers from control, TXV and differentiated TSCs.

Figure S4. (Related to Figure 4)

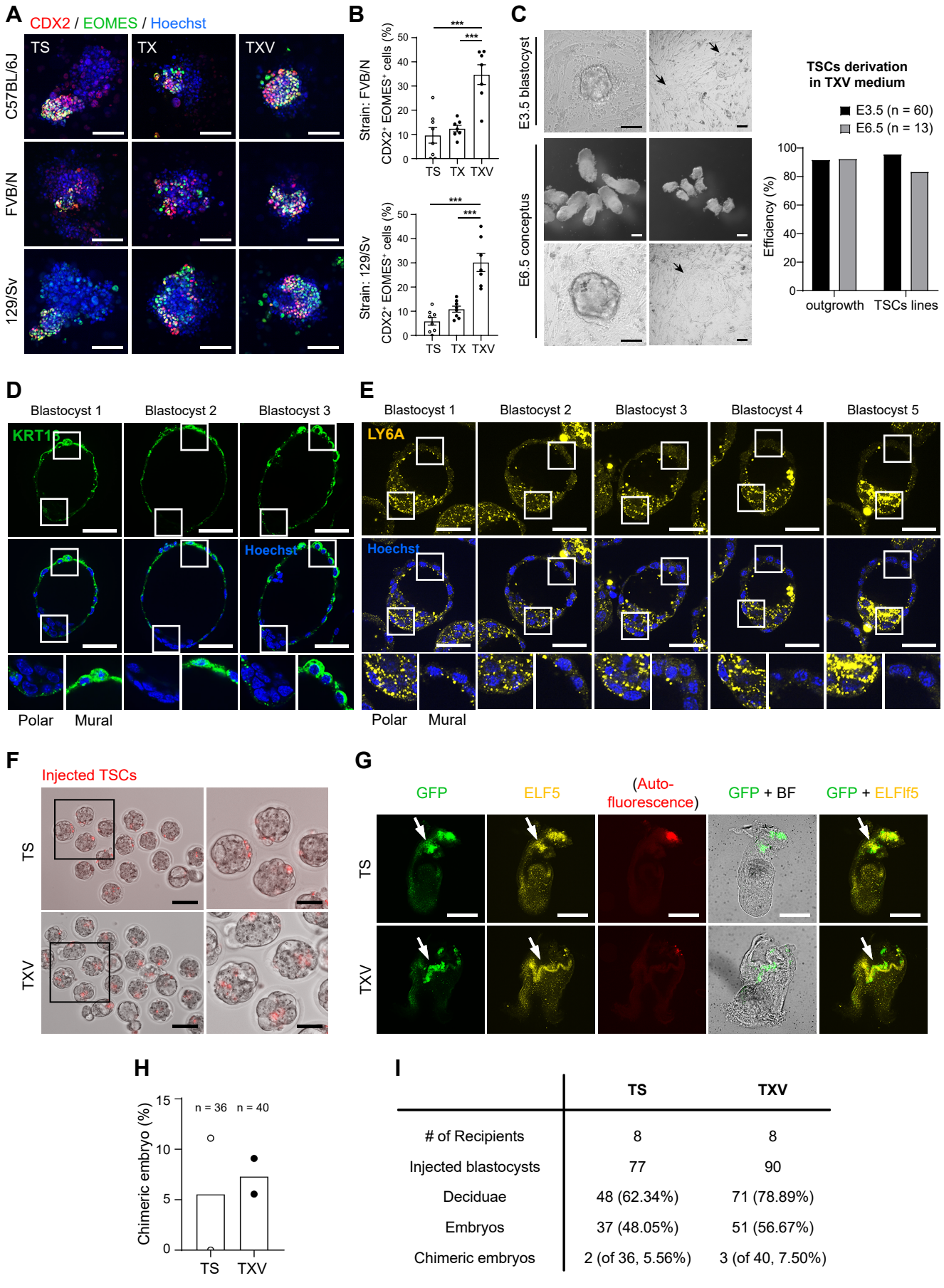

I

	TS	TXV
# of Recipients	8	8
Injected blastocysts	77	90
Deciduae	48 (62.34%)	71 (78.89%)
Embryos	37 (48.05%)	51 (56.67%)
Chimeric embryos	2 (of 36, 5.56%)	3 (of 40, 7.50%)

Figure S4. TXV TSCs have an enhanced capacity to self-renew, lessened propensity to spontaneously differentiate, and maintained potential to contribute to development. Related to Figure 4.

A. CDX2 and EOMES staining of blastocyst outgrowths 5-6 days after plating, and **B**. ratio of CDX2/EOMES double positive cells in 3 different mouse strains. Regardless of the mouse strain, TSCs cultured with optimal inducers maintained CDX2/EOMES double positive cells at higher levels than TSCs cultured in TS or TX medium. **C**. In the TXV medium, TSCs lines were derived from E3.5 blastocysts and E6.5 ExE, Outgrowth formation efficiency: 92% for both E3.5 blastocysts (55/60) and E6.5 isolated ExE (12/13); establishment of lines: 96% and 83%, (passage 4, 44/46 for E3.5; 10/12 for E6.5). The left figures show cell outgrowths and derived TSCs (from E3.5 and E6.5, arrows), and E6.5 conceptus and extracted ExE. **D**. Examples of immuno-stained blastocysts for KRT18 and **E**. LY6A. **F**. Morula and early blastocysts with injected TS and TXV TSCs. **G**. Immunostaining against GFP, ELF5, and images of auto-fluorescence and bright field (BF) in E7.5 chimeric embryos. We used auto-fluorescence controls to confirm the specificity of the signal. **H**. Efficiency of chimerism. 'n' is the total number of analyzed embryos from 2 independent experiments. **I**. Data listing the information on chimeric embryo formation. For each graph, data are means±s.e.m., analyzed by Student's t-test: *p<0.05, ***p<0.001. Scale bars: 100 μm in A, C and F (inset: 50 μm); 40 μm in D and E; 300 μm in G.

Figure S5. (Related to Figure 5)

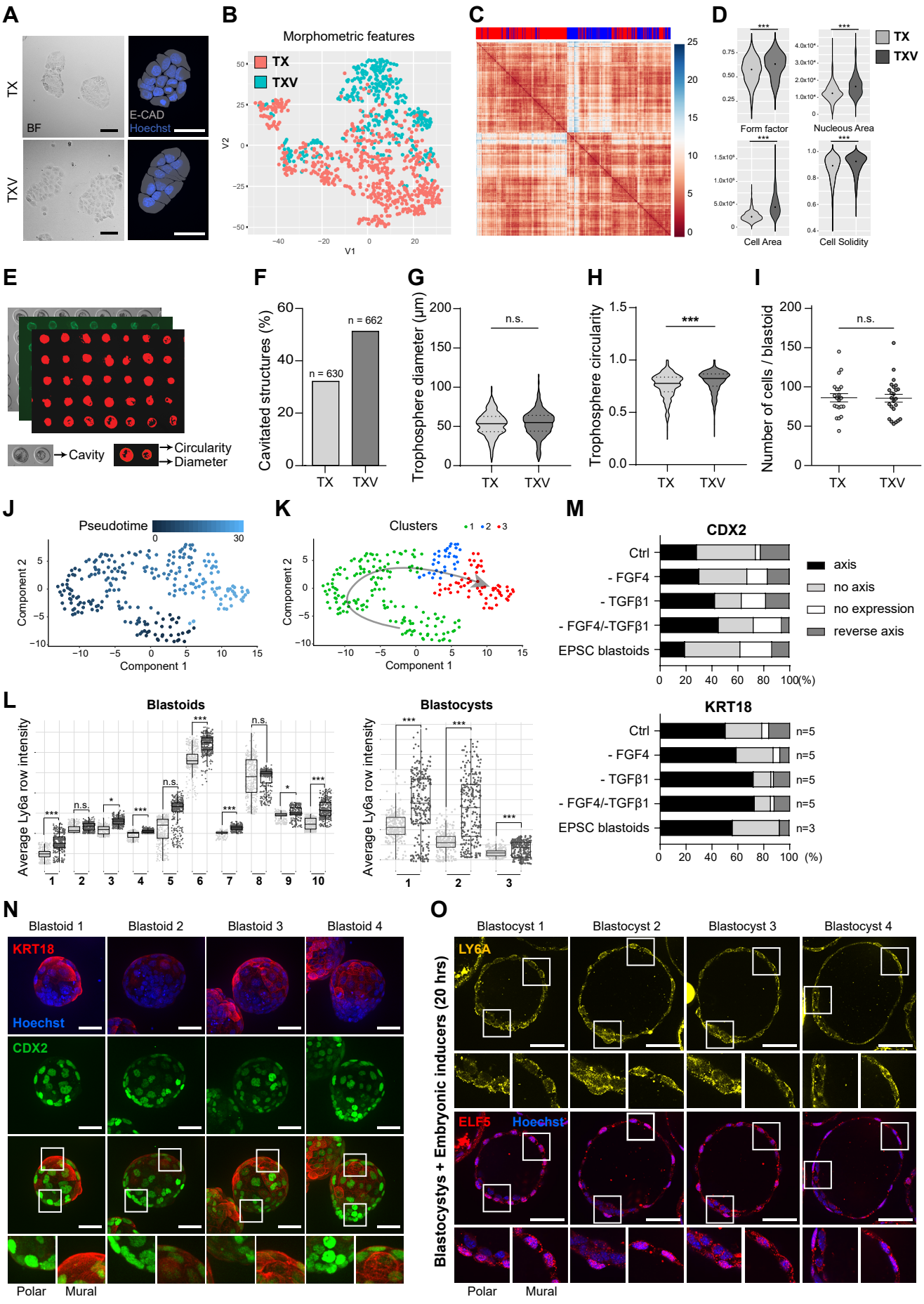

Figure S5. Embryonic inducers pattern the embryonic-abembryonic axis. Related to Figure 5.

A. Bright field (left) and high-content imaging of TX and TXV TSCs segmented based on Hoechst and E-CADHERIN (E-CAD) staining (right). We listed up the ranking of differential morphometric features based on the *p*-value after Mann-Whitney statistical analysis. The top 20% differential morphometric features were chosen for further analysis. Scale bars represent 100 μm and 40 μm for the left and right panel, respectively. **B**. Representative t-SNE map plotting each cell based on its morphological features. With some overlap, TX and TXV TSCs form distinct clusters, indicating differences in morphological features. **C**. Heatmap of unsupervised clustering (distance map) based on the top 20% differential morphometric features of TX TSCs (red) and TXV TSCs (blue). Well-clustered blue and red bands (top) indicate morphological differences between TX and TXV TSCs. **D**. Violin plots of the value distribution for some top-ranked differential morphometric features. Data were analyzed by Cell Profiler, and Student's t-test. **E**. WGA-stained structures allowed us to perform a semi-automated acquisition of morphological parameters. **F**. Percentage of microwells containing a cavitated trophosphere. **G**. Trophosphere diameter, and **H**. trophosphere circularity for TX and TXV TSCs. **I**. Number of cells per blastoid formed from either TX or TXV TSCs. **J**. Pseudotime trajectory of single TSCs isolated from blastoids with Monocle clustering analysis. **K**. The monocle clustering analysis groups the cells in three clusters. Grey arrow indicates directionality of pseudotime trajectory shown in G. **L**. *Ly6a* smFISH quantification for blastoids (left) and blastocysts (right). Bright and dark gray colored dots indicate the mural and polar cells, respectively. **M**. Quantification of axis formation. Based on the expression pattern of CDX2 or KRT18, blastoids either showed an axis, random expression (no axis), no expression, or a reverse axis. Bars represent the mean percentage of either 5 or 3 independent experiments as indicated by n. **N**. Immunostaining for CDX2 and KRT18 as marker proteins for axis formation in the blastoid. Shown are representative 3D projections of blastoids formed without addition of TGFβ1. Scale bar represents 50 μm. **O**. Immunostaining for LY6A and ELF5 in blastocysts that were cultured with TXV factors (embryonic inducers) for 20 hours. Scale bar represents 40 μm. Data are analyzed by Student's t-test: $*p<0.05$, $**p<0.01$, $***p<0.001$.

Figure S6. (Related to Figure 6)

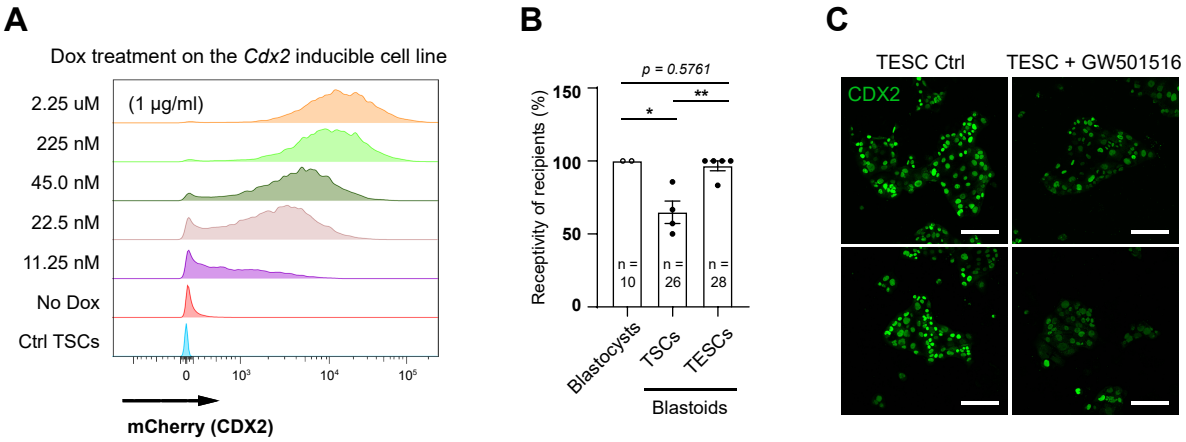

Figure S6. Embryonic inducers capacitate trophoblasts for decidualization. Related to Figure 6.

A. CDX2 overexpression according to different concentrations of doxycycline (Dox). We chose 225 nM of Dox to induce CDX2i cells, since levels of CDX2 overexpression plateaued at higher concentrations. **B**. Ratio of recipients with at least one decidua. Two to five independent experiments were performed, and 4-8 mice were analyzed for each experiment. 'n' is the total number of recipients. **C**. Immunostainings against CDX2 in TXV TSCs (TESCs) treated with GW501516 showed reduced CDX2 expression. Scale bar represents 40 μm. For each graph, data are means±s.e.m., analyzed by Student's t-test: *$p<0.05$, **$p<0.01$, ***$p<0.001$.

Figure S7. (Related to Figure 7)

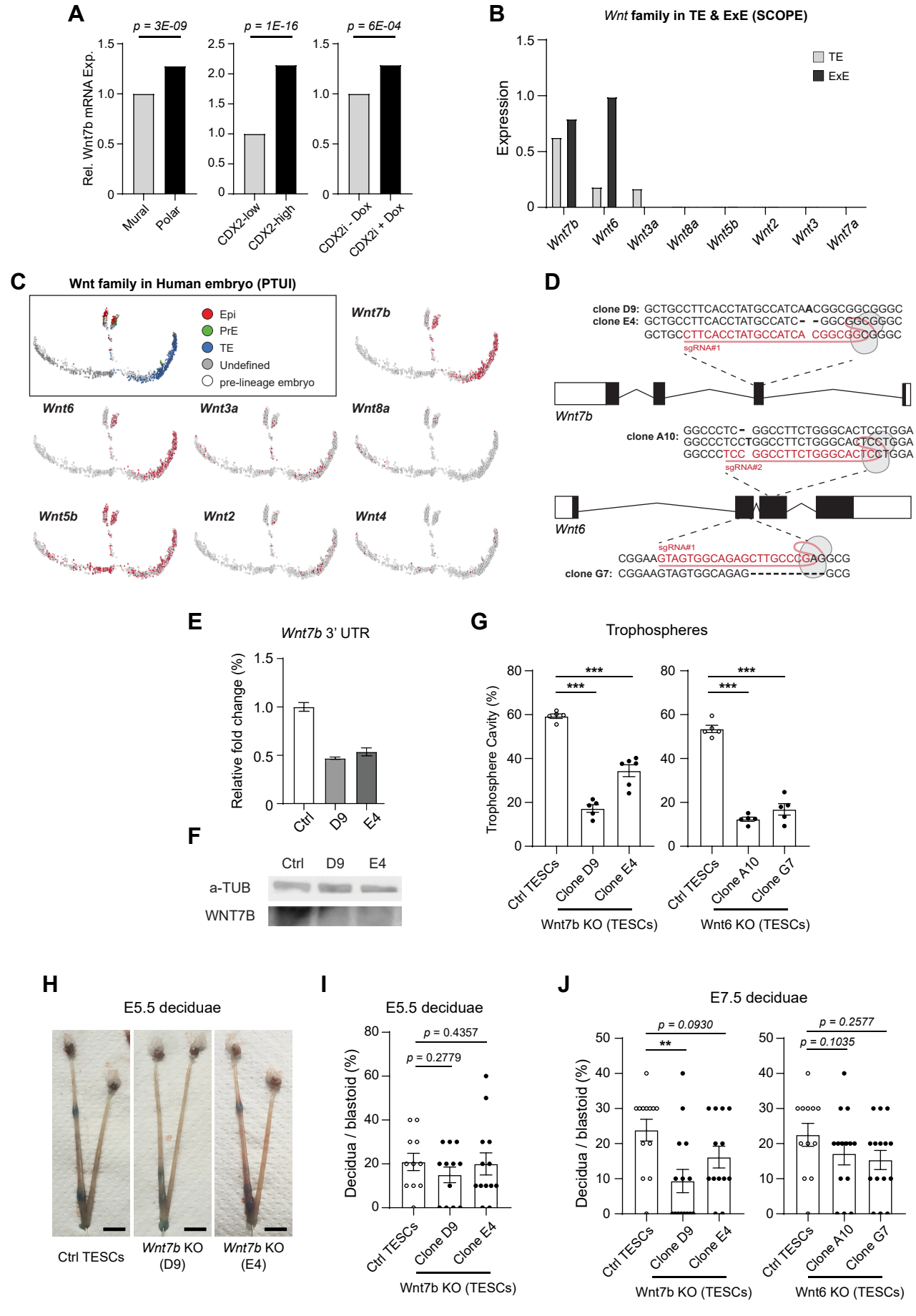

Figure S7. Decidualization by trophoblasts proceeds partly through CDX2 and the secretion of WNT6/7B. Related to Figure 7.

A. Comparison of *Wnt7b* mRNA expression between mural and polar, CDX2-high and -low, CDX2i TSCs ± Dox, based on bulk RNA-seq data (Tables S1, S3, and S11). **B**. Summary of Wnt family expression in mouse TE and ExE acquired using SCOPE. **C**. Summary of Wnt family expression in human embryos acquired using PTUI. **D**. Schematic view showing which exons were targeted using a CRISPR/Cas9 system to generate the indicated *Wnt* knock-out clones (clone D9 and E4 for *Wnt7b*; clone G7 and A10 for *Wnt6*). Although we used the same sgRNA for D9 and E4, they have different frameshift mutations. For WNT6 KO cell lines, A10 and G7 were generated from two different sgRNAs (see Table S15). **E**. Confirmation of *Wnt7b* KO with qRT-PCR, and **F**. western blot. Introduction of insertion-deletions is expected to elicit nonsense-mediated decay of the mutant mRNA, thus decreasing *Wnt7b* mRNA expression in D9 and E4 TSCs. a-TUB = alpha-TUBULIN. **G**. Cavity formation ratio of TESCs, D9, E4 (*Wnt7b* KO), and A10, G7 (*Wnt6* KO) trophospheres. **H**. E5.5 deciduae induced by TESCs and *Wnt7b* KO blastoids visualized by blue dye injection, and **I**. quantification of the implantation efficiency at E5.5. Scale bar represents 0.5 cm. **J**. Decidua maintenance at E7.5 with *Wnt7b* KO, and *Wnt6* KO blastoids. Each dot represents an individual mouse. For each graph, data are means±s.e.m., analyzed by Student's t-test: *p<0.05, **p<0.01, ***p<0.001.

CHAPTER 3:
A pendulum of induction between the epiblast and extra-embryonic endoderm supports post-implantation progression

Part of my PhD work was published in Development 149 (20), dev192310, October 15, 2022 (https://doi.org/10.1242/dev.192310), and this publication is included as the following chapter. A description of my contributions is provided at the end of this page.

3.1. Authors

Erik J. Vrij[1,2,5], Yvonne S. Scholte op Reimer[2], Laury Roa Fuentes[1], Isabel Misteli Guerreiro[3], Viktoria Holzmann[2], Javier Frias Aldeguer[1,3], Giovanni Sestini[2], Bon-Kyoung Koo[2], Jop Kind[3,4], Clemens A. van Blitterswijk[1] and Nicolas C. Rivron[2,5]

3.2. Affiliations

1 MERLN Institute for Technology-inspired Regenerative Medicine, Maastricht University, Universiteitssingel 40, 6229 ER Maastricht, Netherlands.
2 Institute of Molecular Biotechnology of the Austrian Academy of Sciences, Vienna Biocenter, Dr. Bohr-Gasse 3, 1030 Vienna, Austria.
3 Hubrecht Institute, Royal Netherlands Academy of Arts and Sciences (KNAW) and University Medical Center Utrecht, Uppsalalaan 8, 3584 CT Utrecht, Netherlands.
4 Department of Molecular Biology, Faculty of Science, Radboud Institute for Molecular Life Sciences, Radboud University Nijmegen, Geert Grooteplein Zuid 10, 6525 GA Nijmegen, Netherlands.
5 Correspondence: nicolas.rivron@imba.oeaw.ac.at and erikvrij@gmail.com

3.3. Contributions

In this study, my contribution was the experiment depicted in Figure S10, where I demonstrated that the chemically defined induction medium and its individual components did not interfere with the specification of epiblast and PrE cells in mouse blastocysts.

© 2022. Published by The Company of Biologists Ltd | Development (2022) 149, dev192310. doi:10.1242/dev.192310

STEM CELLS AND REGENERATION

RESEARCH ARTICLE

A pendulum of induction between the epiblast and extra-embryonic endoderm supports post-implantation progression

Erik J. Vrij[1,2,*], Yvonne S. Scholte op Reimer[2], Laury Roa Fuentes[1], Isabel Misteli Guerreiro[3], Viktoria Holzmann[2], Javier Frias Aldeguer[1,3], Giovanni Sestini[2], Bon-Kyoung Koo[2], Jop Kind[3,4], Clemens A. van Blitterswijk[1] and Nicolas C. Rivron[2,*]

ABSTRACT

Embryogenesis is supported by dynamic loops of cellular interactions. Here, we create a partial mouse embryo model to elucidate the principles of epiblast (Epi) and extra-embryonic endoderm co-development (XEn). We trigger naive mouse embryonic stem cells to form a blastocyst-stage niche of Epi-like cells and XEn-like cells (3D, hydrogel free and serum free). Once established, these two lineages autonomously progress in minimal medium to form an inner pro-amniotic-like cavity surrounded by polarized Epi-like cells covered with visceral endoderm (VE)-like cells. The progression occurs through reciprocal inductions by which the Epi supports the primitive endoderm (PrE) to produce a basal lamina that subsequently regulates Epi polarization and/or cavitation, which, in return, channels the transcriptomic progression to VE. This VE then contributes to Epi bifurcation into anterior- and posterior-like states. Similarly, boosting the formation of PrE-like cells within blastoids supports developmental progression. We argue that self-organization can arise from lineage bifurcation followed by a pendulum of induction that propagates over time.

KEY WORDS: Blastoids, Primitive endoderm, Extra-embryonic endoderm/epiblast rosette, Post-implantation development, Embryonic stem cells, Pro-amniotic cavity

INTRODUCTION

In certain species, extrinsic positional cues create a pre-pattern for development, e.g. through the local deposition of maternal RNA on one side of a *Drosophila* egg. However, mammalian development appears to rather favor decentralized and regulative principles, termed self-organizing, that prevail over more deterministic behaviors (e.g. pre-patterned hard-wired genetic programs). Accordingly, 16-cell stage mouse blastomeres can be dissociated and re-aggregated to form a competent blastocyst in minimal medium (Tarkowski et al., 2010; Suwińska et al., 2008; Posfai et al., 2017). Such a logic leverages the properties of gene regulatory networks and molecular noise to achieve cellular decision making (Semrau et al., 2017; Balázsi et al., 2011), and of non-linear cellular interactions to ensure lineage divergence and progression. In the mouse blastocyst, such principles are at play between the embryonic and extra-embryonic tissues (Arnold and Robertson, 2009), ensuring trophoblast/inner cell mass (Niwa et al., 2005) and epiblast (Epi)/primitive endoderm (PrE) development (Frankenberg et al., 2011; Bessonnard et al., 2014; Chazaud et al., 2006). This logic also supports organogenesis (Briscoe, 2019; Olson, 2006; Zuniga, 2015). To better understand these loops of cellular interactions, we created a partial mouse embryo model undergoing phenomenological self-organization and observed sequences of reciprocal inductions supporting its autonomous progression over time.

The early mammalian conceptus consists of three lineages: the pluripotent epiblast (Epi), which forms the embryo proper; and the two extra-embryonic lineages – the trophoblast and primitive endoderm (PrE) – that contribute to the placenta and yolk sac, respectively (Rossant and Tam, 2009; Lokken and Ralston, 2016). In mice, the bifurcation between PrE and Epi cells is established between E3.25 and E4.5 (Schrode et al., 2014; Onishi and Zandstra, 2015; Chazaud et al., 2006; Bassalert et al., 2018; Plusa et al., 2008), and is marked by the timed expression of the transcription factors Oct4, Nanog, Klf4 and Sox2 in the Epi (Neagu et al., 2020), and Gata6, Pdgfrα, Gata4, Sox17 and Sox7 in the PrE (Lokken and Ralston, 2016; Artus et al., 2013; Lo Nigro et al., 2017). Experiments suggest that PrE specification is initiated by lineage priming (Ohnishi et al., 2014) that exploits polycomb (Illingworth et al., 2016), chromatin modifier (Goolam and Zernicka-Goetz, 2017) and small-RNA (Ngondo et al., 2018) activities, along with the progression of gene regulatory networks (Lokken and Ralston, 2016) and intercellular signaling circuitries [e.g. FGF/Mapk/Erk (Azami et al., 2017; Kang et al., 2017; Molotkov et al., 2017; Ohnishi et al., 2014; Krawchuk et al., 2013; Schröter et al., 2015; Wigger et al., 2017; Chazaud et al., 2006; Yamanaka et al., 2010; Wicklow et al., 2014), Lif/Stat (Morgani and Brickman, 2015; Onishi and Zandstra, 2015), Nodal/Smad2/3 (Mesnard et al., 2006; Papanayotou and Collignon, 2014), Bmp4/Smad4 (Graham et al., 2014; Wang et al., 2004) and Wnt/β-catenin (Corujo-Simon et al., 2017; ten Berge et al., 2011) pathways]. The initial PrE cell specification is reinforced by Epi inductions made through FGF4 signaling (Mulvey et al., 2015; De Caluwé et al., 2019; Molotkov and Soriano, 2018; Artus et al., 2013; Frum and Ralston, 2015;

[1]MERLN Institute for Technology-inspired Regenerative Medicine, Maastricht University, Universiteitssingel 40, 6229 ER Maastricht, Netherlands. [2]Institute of Molecular Biotechnology of the Austrian Academy of Sciences, Vienna Biocenter, Dr. Bohr-Gasse 3, 1030 Vienna, Austria. [3]Hubrecht Institute, Royal Netherlands Academy of Arts and Sciences (KNAW) and University Medical Center Utrecht, UtrechtUppsalalaan 8, 3584 CT Utrecht, Netherlands. [4]Department of Molecular Biology, Faculty of Science, Radboud Institute for Molecular Life Sciences, Radboud University Nijmegen, Geert Grooteplein Zuid 10, 6525 GA Nijmegen, Netherlands.

*Authors for correspondence (nicolas.rivron@imba.oeaw.ac.at; erikvrij@gmail.com)

N.C.R., 0000-0003-1590-5964

Handling Editor: Matthias Lutolf
Received 6 May 2020; Accepted 23 June 2022

Development (2022) 149, dev192310. doi:10.1242/dev.192310

Houston, 2017) to progressively lock cell fates, to promote their physical segregation, and to promote the epithelialization and lining of the PrE along the blastocoel cavity (Meilhac et al., 2009; Burtscher and Lickert, 2009; Saiz et al., 2013; Brimson, 2016). This process is regulative as it senses and adjusts the mutually allocated cell numbers (Plusa and Hadjantonakis, 2018; Grabarek et al., 2012; Mathew et al., 2019; Yamanaka et al., 2010). Here, we further explore the extent by which the Epi and PrE co-develop.

The use of microsystems to control cell numbers (Vrij et al., 2016a) and of chemically defined medium (Kubaczka et al., 2014) opens possibilities to increase the control, throughput and screening capacities of embryo models (Vrij et al., 2016a; Rivron et al., 2018a). Previously, we induced the formation of blastocyst-like structures by combining trophoblast stem cells (TSCs) and ESCs, which we termed blastoids (Rivron et al., 2018a). Blastoids generate PrE-like cells from the ESCs, as confirmed in later studies (Sozen et al., 2019; Posfai et al., 2021), and thus make up the three founding cell lineages. However, the limited expansion of the PrE-like cells is likely to restrict their potential to develop. Here, we run combinatorial screens of proteins, GPCR ligands and small molecules in a microwell array platform and in chemically defined conditions. This directs ESCs to rapidly and efficiently co-form blastocyst-stage PrE- and Epi-like cells. These cells then develop synergistically in minimal medium to form a structure resembling the post-implantation Epi and extra-embryonic endoderm tissues (XEn), referred to as Epi/XEn. We apply this model to test the share of autonomous development of the Epi/XEn module. We observe mutual inductions between the Epi and PrE that support the potential for growth, viability, specification and morphogenesis that underlie aspects of post-implantation development. We propose that development can be driven by sequences of reciprocal interactions between progressively diverging cell types.

RESULTS

Naive pluripotency enhances the ESCs potential for PrE differentiation

Forming tissues of appropriate size is crucial to ensure relevant concentrations and distributions of biological parameters (e.g. molecules and mechanical forces). We used a high-content screening platform of non-adherent hydrogel microwells in 96-well plates (Vrij et al., 2016b) to reproducibly aggregate small and defined numbers of ESCs that reflected the number of inner cells within blastocysts (Fig. 1A). The cell number followed a Poisson distribution across the 430 microwells (7-12 cells per microwell) and the cells aggregated within 24 h (Fig. 1B, Fig. S1). We quantified PrE differentiation via *in situ* imaging of a fluorescent reporter under the promoter for Pdgfrα (ESCs$^{Pdgfr\alpha\text{-}h2b\text{-}gfp/+}$, Fig. 1A) (Artus et al., 2010; Plusa et al., 2008). EBs survived in serum-free N2B27 medium supplemented with leukemia inhibitory factor (Lif) but did not proliferate and formed only a few Pdgfrα$^+$ cells (yield of Pdgfrα$^+$ EBs: 1%, Fig. 1C, Fig. S2). In contrast, the addition of serum induced the appearance and proliferation of Pdgfrα$^+$ cells (44%, Fig. 1C, P<0.001). Consistent with a previous report (Schröter et al., 2015), we observed that an initial 2D expansion in chemically defined N2B27/2i/Lif medium supporting a naive pre-implantation-like state (Ying et al., 2008) enhanced the susceptibility for formation of Pdgfrα$^+$ cells, when compared with expansion in serum-containing medium that captures concomitant peri-implantation-like populations (Neagu et al., 2020) (Fig. 1C). We concluded that, similar to the blastocyst cells (Artus et al., 2010; Plusa et al., 2008), formation of Pdgfrα$^+$ cells is favored by an initial permissive state, along with signals present in serum that regulate specification and proliferation.

A three-dimensional screen reveals signaling pathways that regulate Pdgfrα expression

Signaling molecules have been proposed to influence PrE specification, including Lif (Morgani and Brickman, 2015), retinoic acid (Cho et al., 2012), FGF (Yamanaka et al., 2010; Chazaud et al., 2006; Goldin and Papaioannou, 2003), GSK3β/β-catenin (Krawetz and Kelly, 2008; Price et al., 2013) and Nodal (Niakan et al., 2013; Mesnard et al., 2006). In the conceptus, these molecules activate pathways that are likely to act synergistically but investigating their respective interactions and functions remains difficult. We thus modulated these pathways in EBs. Although Lif (10 ng/ml) increased the yield of Pdgfrα$^+$ EBs in serum cultures (30% yield, 3.6-fold increase, Fig. 1D), addition of retinoic acid (RA; 10 nM) further improved the process (91% yield, 3-fold increase, Fig. 1D) and increased the number of Pdgfrα$^+$ clusters per EB (5.5-fold increase, Fig. 1D, clusters are defined as Pdgfrα$^+$ cells found within the equatorial plane of EBs, see Materials and Methods). In contrast, the effect of these two molecules appeared restricted in serum-free N2B27/Lif medium (16% yield). Consistent with a synergistic action of multiple pathways, we concluded that Lif and RA support but are not sufficient to efficiently form Pdgfrα$^+$ cells.

We then created a small library of activators and inhibitors of signaling pathways that are active in the blastocyst (Table S1). We first tested them individually in a serum-containing medium and measured the percentage of Pdgfrα$^+$ EBs (yield) and the number of Pdgfrα$^+$ clusters per EB. FGF4 (100 ng/ml) and the GSK3β inhibitor CHIR99021 (6 μM), which act on pathways active in the blastocyst Epi (ten Berge et al., 2011; Azami et al., 2019), increased the yield (44% and 81%, respectively) and the number of clusters per EB (both 1.6-fold; Fig. 1E,J). Inhibiting Wnt secretion (IWP2) and Wnt processing (XAV939) did not significantly affect specification (Fig. 1E). We concluded that the FGF and GSK3β/β-catenin pathways regulate Pdgfrα$^+$ cell specification.

In contrast, although BMP signaling has been proposed to contribute to PrE development (Graham et al., 2014), activation of the SMAD pathway by activin A and Tgfβ1 elicited a decline, albeit non-statistically significant, of either the yield or Pdgfrα$^+$ cell number. Consistently, the Tgfβ receptor inhibitor SB431542 and the Alk1/2 inhibitor ML347 (BMP signaling) enhanced the formation of Pdgfrα$^+$ cells (Fig. 1I), whereas the BMP pathway inhibitor LDN193189 prevented proliferation (Fig. 1I). We concluded that ESCs might have lost the potential to respond to the Tgfβ signaling pathway or that this pathway acts on elements other than PDGFRa, thereby preventing detection of its effect. We concluded that the activation of the FGF and inhibition of the GSK3β and Tgfβ pathway facilitate the generation of Pdgfrα$^+$ cells from naive ESCs.

A three-dimensional screen reveals GPCR ligands inducing Pdgfrα expression

Next, to complement the action of classical developmental pathways, we investigated the potency of signaling through G-protein-coupled receptors (GPCR) by screening for 264 GPCR ligands, informed by previous findings that cAMP modulates Pdgfrα expression in EBs (Vrij et al., 2016a). DL-adrenaline, a β-adrenoceptor agonist acting upstream of the cAMP/PKA pathway, strongly increased the yield of Pdgfrα$^+$ EBs (206%) without affecting the overall size of EBs or the number of clusters (Fig. 1E). Accordingly, 8Br-cAMP (3200 μM) also increased the yield of Pdgfrα$^+$ EBs by 91% when compared with serum/Lif alone,

Development (2022) 149, dev192310. doi:10.1242/dev.192310

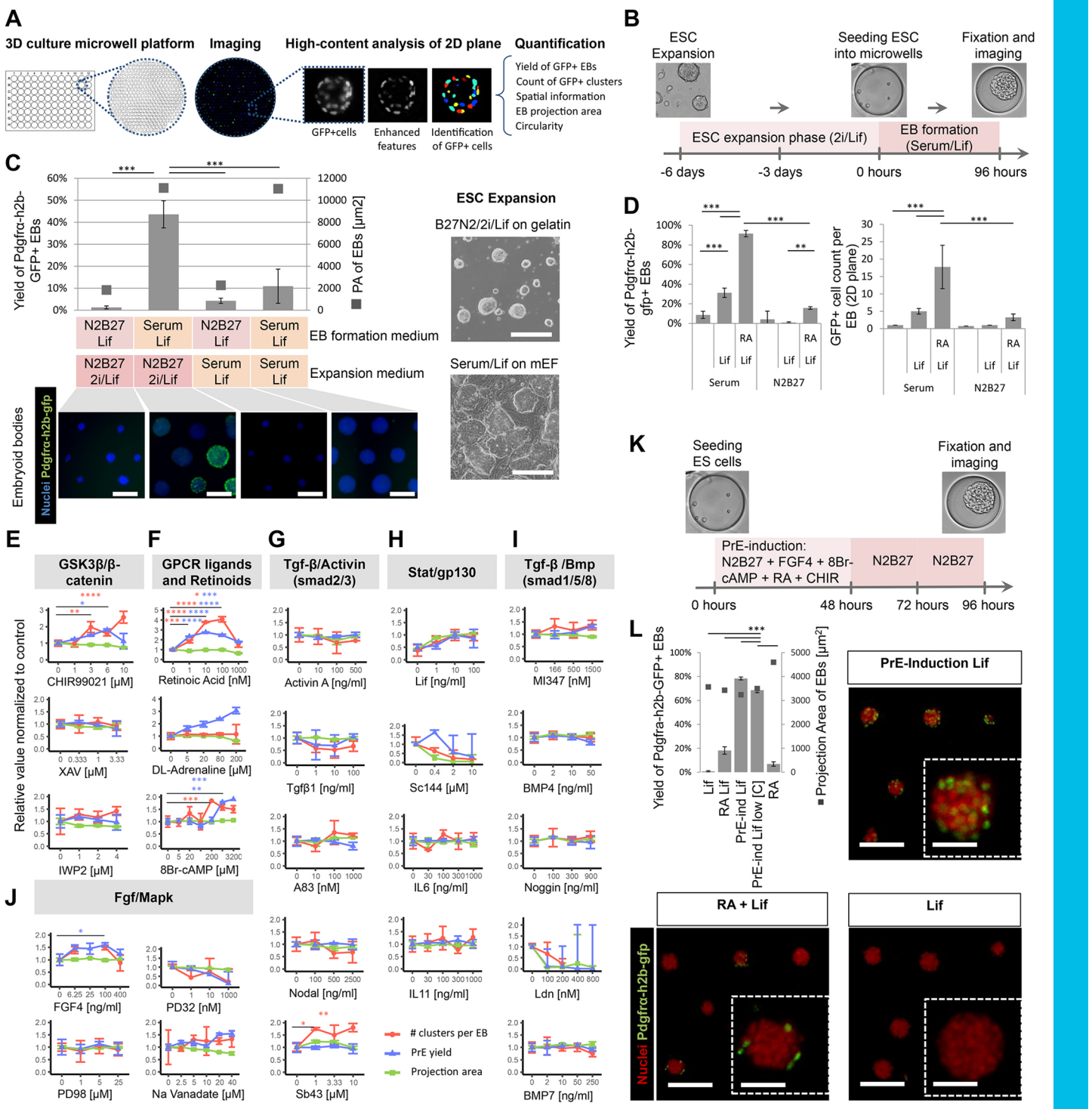

Fig. 1. See next page for legend.

Fig. 1E) (Vrij et al., 2016a) without affecting EBs size. We concluded that DL-adrenaline and cAMP potentiate naive ESCs for Pdgfrα expression independent of proliferation. Altogether, we concluded that FGF4, GSK3β/β-catenin, Lif, RA, DL-adrenaline and cAMP individually increase the expression of Pdgfrα.

A combinatorial screen delineates a chemically defined medium inducing Pdgfrα expression

Because signaling molecules often act in concert, we ran combinatorials of molecules, this time in serum-free medium (N2B27 medium, Fig. S3A,B). Using a factorial design screening approach (Hutchens et al., 2007), we tested combinations of 8Br-cAMP, DL-Adrenaline, Lif, FGF4, sodium orthovanadate, CHIR99021, ML347, SB431542, RA and activin A at effective concentration ranges. Specific combinations preserved EB viability and integrity, and induced PrE-like specification (measured by EB projection area, circularity, and Pdgfrα and Gata6 expression, respectively; Figs S3C and S4). Among the selected 21 combinations, a medium containing 8Br-cAMP (1 mM), RA (10 nM), FGF4 (100 ng/ml) and CHIR99021 (5 µM) led to a

Development (2022) 149, dev192310. doi:10.1242/dev.192310

Fig. 1. The initial naive state of ESCs and specific signaling pathways induce efficient co-development of the PrE-/Epi-like niche *in vitro*. (A) High-content screening (HCS) method for 96-well plates imprinted with agarose microwell arrays (430 microwells per well) in which EBs are formed (each microwell captures a single EB), cultured and imaged (2D mid-focal plane). (B) Schematic of experimental set-up, including ESC expansion and EB-based primitive endoderm (PrE) differentiation. (C) Top and right: quantified yield of PrE-differentiation (Pdgfrα$^+$, left axis) and proxy for EB size (2D projection area, right axis) derived from ESCs expanded in naive (N2B27/2i/Lif) versus serum/Lif conditions. Bottom: fluorescence images show the nuclei (blue) and Pdgfrα-h2b-gfp$^+$ clusters (green) within EBs formed by combinations of different formation and ESC expansion media. Bright-field images of ESCs expanded in N2B27/2i/Lif or serum/Lif [on mouse embryonic fibroblasts (mEFs)]. Scale bars: 200 µm. (D) Yield of Pdgfrα-h2b-gfp$^+$ EBs and the number of GFP$^+$ clusters per EB in N2B27 or serum media supplemented with or without Lif and with or without RA. Data are mean±s.d. obtained from n=4 wells, with each well containing ∼400 EBs. ANOVA with Bonferroni post-hoc test (***P<0.001, **P<0.01). (E-J) Dose-response curves showing the effect of different soluble pathway modulators after 96 h in culture on the yield of Pdgfrα-h2b-gfp$^+$ EBs (blue), the number of Pdgfrα-h2b-gfp$^+$ clusters per EB (red) in median focus plane (10× objective) and the EB projection area (as a proxy for EB size, green). All values were normalized to H_2O/DMSO controls. Mean and s.d. values were obtained from n=3 or 4 wells, with every well containing ∼400 EBs. ANOVA with Tukey's multiple comparison test (****P<0.0001, ***P<0.001, **P<0.01, *P<0.05). (K) Schematic for chemically induced differentiation of EBs towards PrE. (L) Graph shows yields for PrE differentiation (left axis) and EB projection area (right axis) using the induction cocktail. Low [C] indicates lower concentrations of cAMP (1 mM) and CHIR99021 (3 µM). Representative fluorescent images of indicated conditions. PrE inductions in Lif and RA/Lif media are shown for comparison. Scale bars: 200 µm; 40 µm (insets). Data are mean±s.d. obtained from n=4 wells, with each well containing ∼400 EBs. ANOVA with Tukey's multiple comparison test (***P<0.001). Images in C, K and L are taken after 96 h of culture.

stark upregulation of the yield of Pdgfrα$^+$ EBs (78%, Fig. 1K,L, Fig. S4C). Consistent with the important role of RA (Niakan et al., 2013; Cho et al., 2012), depleting this molecule from the induction medium reduced the yield significantly (Fig. 1L). However, the synergy with other factors was essential for robust and efficient induction (Fig. 1L). This chemically defined inductive medium also reduced the number of dead cells per EB to levels similar to serum-containing medium (Fig. S5B), and cells no longer required the presence of Lif for maintaining viability or Pdgfrα expression (Fig. S5A).

Formation of a partial blastocyst model with PrE- and Epi-like cells

Within 24 h of induction, double-positive (Nanog$^+$/Gata6$^+$) cells and double-negative cells emerged in a salt and pepper-like distribution between Nanog$^+$/Gata6$^-$ cells, as observed in the E3.5 blastocyst (Chazaud et al., 2006; Saiz et al., 2020) (Fig. 2A, Fig. S6). Over time, the relative number of Gata6$^+$ cells increased (Fig. 2A, Figs S6 and S7) and the initially intermingled cell types spontaneously segregated to form an outer layer of cells expressing Gata6 (Meng et al., 2018; Schrode et al., 2014; Wang et al., 2010; Cai et al., 2008; Lavial et al., 2012) and Sox17 (Qu et al., 2008; Kinoshita et al., 2015; Artus et al., 2011), and inner Nanog$^+$ cells (96 h, Fig. 2B and Fig. S8), consistent with the segregation of the PrE and Epi that occurs in the E4.5 blastocyst (Chazaud et al., 2006). The observation of robust proportioning of Nanog$^+$ and Gata6$^+$ cells, despite exposure to inductive molecules, might point at regulatory circuits ensuring a balance between the two cell types, as previously proposed (Raina et al., 2020), and was disturbed upon FGF/Mapk/Erk signaling inhibition (Fig. S9). Notably, the chemically defined inductive medium and its individual components did not interfere with Epi and PrE cell specification in mouse blastocysts (Fig. S10), thereby suggesting that additional layers of regulation prevent unbalancing of these cell numbers.

We then characterized the Epi- and PrE-like cells by isolating them based on Pdgfrα antibody labeling and analyzing them via single-cell transcriptomics (96 h). Principal component (PC) analysis showed two distinct subpopulations along the PC1 axis that corresponded to the Pdgfrα$^-$ and Pdgfrα$^+$ cells (Fig. 2C), with the top differentially expressed genes reminiscent of those for Epi- and PrE-like cells, respectively (Fig. S11A). The Pdgfrα$^+$ cells expressed *Gata6*, *Gata4*, *Pdgfra*, *Sox7*, *Fgfr2* and *Sox17* at higher levels than the Pdgfrα$^-$ cells, which preferentially expressed E4.5 Epi genes such as *Nanog*, *Sox2*, *Esrrb*, *Fgf4* and *Oct4* (Fig. 2D). Gene set enrichment analysis (GSEA) comparing the Pdgfrα$^+$ and Pdgfrα$^-$ cells with PrE cells from E4.5 mouse embryos (Mohammed et al., 2017) showed statistically significant (P<0.001) enrichment scores of 0.686 and −0.545, respectively (Fig. 2E). In contrast, these cells were not significantly enriched in the transcripts of peri-implantation stage VE cells (E5.5, enrichment score of 0.317, gene list in Table S3). We concluded that these two cellular populations best reflect the Epi and PrE at a peri-implantation blastocyst stage.

However, we observed that, in contrast to the relatively homogeneous transcriptome of the Epi-like cells, the PrE-like cells were scattered along the PC2 axis (Fig. S11A,B, Table S2). Additional analysis showed that, although they reflected E4.5 PrE rather than E5.5 visceral endoderm (VE) cells, they were primed for the peri-implantation divergence occurring around E5.0 between the parietal endoderm (PE)-expressing markers [such as *Fst* (follistatin) and *Vim* (vimentin)] and VE-expressing the markers [*Dab2* and *Podxl* (podocalyxin)] (Fig. 2F). tSNE clustering also revealed these two PrE subpopulations (Fig. 2G, Fig. S12A) with mutually distinct expression levels of PE genes (Edgar et al., 2013), such as *Vim*, *Fst*, *Thbd*, *Sema6* and *Nog*, and VE genes (Edgar et al., 2013; Pfister et al., 2007) such as *Amn*, *Cubn*, *Dab2*, *Podxl* and *Apoe* (Fig. 2H, Fig. S12B). Compared with the VE-like subpopulation, the PE-like subpopulation showed higher expression levels for extracellular matrix (ECM) proteins, including *Col4a1*, *Col4a2*, *Nid1*, *Lama1*, *Lamc1* and *Sparc* (Fig. S12A), which are necessary for the deposition of a thick multilayered basal lamina, named Reichert's membrane, along the inner side of the trophoblasts (Salamat et al., 1995). We produced a list of differentially expressed genes that may be used as potential early markers for PE and VE (Figs S11B and S12A, Table S2). From these data, we performed gene ontology term analysis (Table S2). In the VE-like subpopulation, genes encoding cell polarity regulators that are typical of an epithelium (e.g. *Jam3*, *Cfl1*, *Lmna*, *Amot* and *Gja1*) and of a response to Tgfβ pathway activation (*Dab2* and *Runx1*) were enriched when compared with those in the Epi. We concluded that, beyond an intrinsic program regulated by Gata6 (Morrisey et al., 1998; Cai et al., 2008), the Epi might induce Tgfβ activity in the VE, a pathway that often regulates epithelialization. Of note, a role for Nodal has previously been proposed later on (at E5.0) during the peri-implantation stage for VE specification (Mesnard et al., 2006; Edgar et al., 2013; Pfister et al., 2007). Altogether, this model points to the neutrality of Nodal, activin, Tgfb1, BMP4 or BMP7 in the initial specification of the PrE but to a possible role for Tgfβ pathways in the initiation of the VE.

Overall, we concluded that the chemically defined medium induced co-formation and spatial organization of blastocyst-stage PrE- and Epi-like cells, the former being primed for bifurcating into both VE and PE lineages. These populations recapitulate known intercellular signaling circuitries, including Epi-produced FGF4 that

Development (2022) 149, dev192310. doi:10.1242/dev.192310

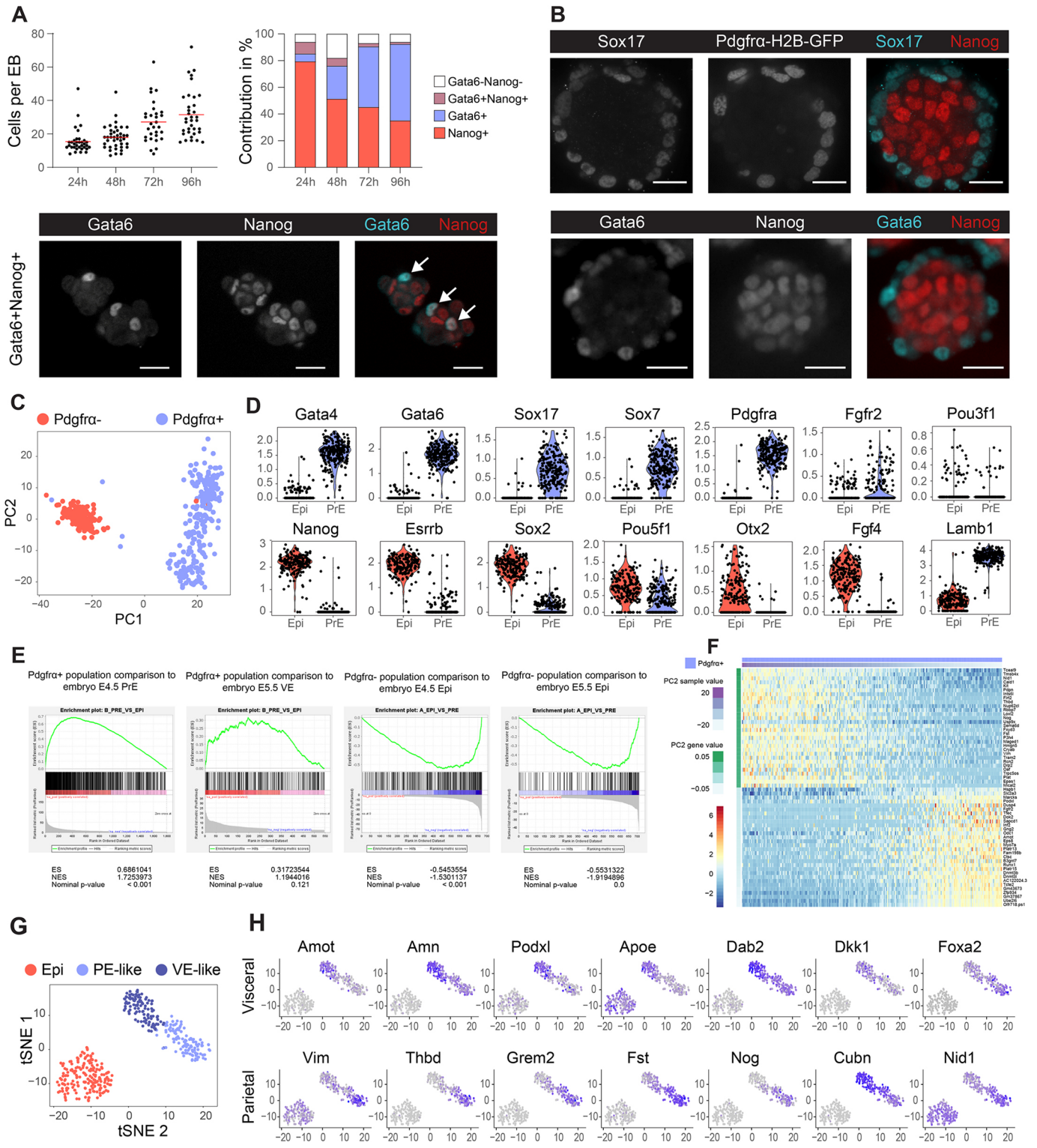

Fig. 2. EBs form a niche that includes both Epi- and PrE-like cells with putative PE and VE populations. (A) Total cell numbers per PrE-induced EB at 24, 48, 72 and 96 h (left), and associated average contribution of double-positive (Nanog$^+$, Gata6$^+$), double-negative (Gata6$^-$, Nanog$^-$), Gata6$^+$ and Nanog$^+$ cells per EB over time (right). The image depicts double-positive (Gata6$^+$ and Nanog$^+$, white arrows) cells found within PrE-induced EBs at 24 h (confocal spinning disk fluorescence image, single plane). EBs were randomly selected and pooled from *n*=3 wells. (B) Immunofluorescence images of Sox17, Pdgfrα-H2B-GFP, Nanog and Gata6 of PrE-induced EBs after 96 h of culture. Scale bars: 50 µm. (C) Principal component analysis of single-cell transcriptomics data for PrE-induced EBs after 96 h of culture in microwells. (D) Violin plots of RNA normalized transcript counts for PrE and Epi markers found in Pdgfrα$^+$ cells (PrE) and Pdgfrα$^-$ cells (Epi). (E) Gene set enrichment analysis (GSEA) comparing the gene expression signature of the Pdgfrα$^+$ (first and second images) and Pdgfrα$^-$ (third and fourth images) cell cluster to mouse embryo E4.5 PrE, E5.5 VE, E4.5 Epi and E5.5 Epi (Mohammed et al., 2017). ES, enrichment score; NES, normalized enrichment score. (F) Heatmap depicting single-cell RNA expression data of the top and bottom 30 most differentially expressed genes along the PC2 axis in the subpopulation of Pdgfrα$^+$ cells. (G) tSNE mapping delineates three putative subpopulations: E4.5 Epi, early VE and early PE. (H) tSNE maps for the early VE genes *Amot*, *Amn*, *Podxl*, *Apoe*, *Dab2*, *Dkk1* and *Foxa2*, and for the PE genes *Vim*, *Thbd*, *Grem2*, *Fst*, *Nog*, *Cubn* and *Nid1*. Axes labels are tSNE dimension 1 (vertical) and 2 (horizontal). Color intensity correlates with expression level.

Development (2022) 149, dev192310. doi:10.1242/dev.192310

contributes to PrE specification and Tgfβ superfamily members that shape the VE.

The PrE/Epi model progresses into a post-implantation rosette and pro-amniotic-like cavity in minimal conditions

In utero, Epi rosettes form at the time of blastocyst implantation. This coincides with the deposition of a laminin-rich basal lamina by the PrE that polarizes the underlying Epi and triggers the formation of the pro-amniotic cavity (Fig. 3A) (Li et al., 2003). Accordingly, Epi-like rosettes can form in the absence of PrE cells when ESCs are encapsulated in Matrigel and cultured in serum-containing medium (Moore et al., 2014; Bedzhov and Zernicka-Goetz, 2014). To assess the potential of the blastocyst PrE/Epi model to autonomously progress, we washed it and cultured it in minimal N2B27 medium. The cells proliferated and underwent morphogenesis by forming a rosette that progressed into a cavity morphologically resembling the polarized Epi/XEn tissue (Fig. 3A-C). We termed these structures EpiCs (Epi/XEn pro-amniotic-like cavities). On the contrary, the Epi/PrE-like model maintained in the initial specification culture medium did not efficiently undergo morphogenesis. In addition, aggregates of ESCs alone did not proliferate in such minimal medium (data not shown). Similar to post-implantation embryos, the rosette-like cells expressed Oct4 and Otx2, and accumulated F-actin and Podxl at the apical side (Fig. 3D,E), while the PrE-like cells produced a laminin-rich basal lamina and also became polarized (Podxl, Fig. 3E). Over time, the cavities increased in size (Fig. S13A). The process was both efficient (94%) and reproducible (Fig. 3F, Fig. S13B). We concluded that the two tissues mutually supported their proliferation and morphogenesis, and that a switch of signaling environment is necessary for post-implantation transition.

Lif signaling inhibits the formation of the pro-amniotic-like cavity

Because progression required a switch of signaling environment, we then tested factors that might act as developmental checkpoints. Lif has been shown to prevent the formation of the cavity in Matrigel-embedded/serum-cultured conditions (Shahbazi et al., 2017). Similarly, we observed that the presence of Lif during the first 3 days or for the entire 6 days of *in vitro* development reduced and abrogated, respectively, the formation of the pro-amniotic cavity, as seen by the absence of Podxl within the Epi-like cells and the arched bilateral/apical location of Podxl in the VE-like cells (Fig. 3F-H). In addition, as previously observed (Moore et al., 2014; Bedzhov and Zernicka-Goetz, 2014), the inhibition of apoptosis using Z-vad-fmk did not impair lumenogenesis (Fig. S13B). Finally, insulin has been reported to limit the initial specification of 2D cultured PrE-/VE-like cells termed nEND (Anderson et al., 2017; Zhong and Binas, 2019). Complementing the N2B27 medium with additional insulin or with the PI3K inhibitor ZSTK474 did not prevent Gata6^{+} cell specification and pro-amniotic-like cavity formation. However, additional insulin increased the overall size of EpiCs, consistent with a role in proliferation (Fig. S14). Differences between the 2D (Anderson et al., 2017) and 3D conformation might create additional layers of regulation of this pathway. Altogether, we concluded that, in chemically defined conditions, a restricted number of signaling pathways (GSK3β/β-catenin, Fgf, RA and cAMP) induces the specification of naive ESCs into PrE-like cells while maintaining Epi-like cells, and that a switch of signaling activity is necessary for the progression of the tissues, including a depletion of Lif for cavity formation and the putative presence of PI3K activators for growth. These data suggest that these two cell types provide each other with sufficient signals to support the morphogenetic transition.

Nodal signaling from the Epi is required for the VE/Epi bonding

In the early post-implantation embryo, the absence of Nodal signals originating from the Epi prevents the acquisition of an embryonic VE identity and incomplete adherence between the VE and Epi (Mesnard et al., 2006; Brennan et al., 2001). Likewise, EpiCs using a Nodal homozygous knockout ESCs showed an increased level of disorganization where the VE layer partly delaminated and separated from the Epi compartment (Fig. 3I,L). In addition, laminin staining appeared irregular and scattered around the VE cells that produce it, thus possibly preventing the proper deposition of a continuous basal lamina onto the Epi (Fig. 3I). Concomitantly, Epi pro-amniotic-like cavities, marked by F-actin and Podxl, were often not evident, reinforcing the importance of Epi adhesion to the basal lamina for the establishment of Epi apical-basal polarity. However, XEn specification, marked by Gata6 and Pdgfrα expression, was not significantly affected (Fig. S15). Moreover, we ran a small screen using soluble factors on 72 h EpiC structures (Fig. S16) and observed that inhibition of Nodal/activin signaling using SB431542 showed a similar response to that observed in the Nodal double knockout line (Fig. 3I,J). Of note, both the Epi and VE tissues express β1 integrins and, as previously shown, embryos and EBs deficient for β1 integrins also display Epi/PrE delamination (Moore et al., 2014). Complementing the initial findings that Tgfβ superfamily signals originating from the Epi regulate VE development (Fig. 1G), these data suggest that Nodal signaling instructs the transition between PrE and VE. This Tgfβ signaling might directly induce the production of the basal lamina that serves as a base for epithelialization, via β1 integrin (Moore et al., 2014); they also suggest that Epi induction at the peri-implantation stage is important for the formation of an abutting double epithelium of VE and Epi tissues. Altogether, this suggests the existence of a two-way circuit regulating the co-development of these two tissues.

EpiCs support both epiblast and visceral endoderm maturation

To more finely assess the state and reflected stage of the cells within the fully developed EpiCs, we performed additional single-cell RNA sequencing after 0, 24 and 64 h in plain N2B27 medium. We also included controls in the form of naive ESCs (2i/Lif), which are XEN cells that are thought to best reflect the parietal endoderm (Lin et al., 2016; Zhong and Binas, 2019), and of Matrigel-embedded ESCs, which form rosette-like cells undergoing lumenogenesis in the presence of serum but in the absence of XEn-like cells (Bedzhov and Zernicka-Goetz, 2014). We visualized single-cell distribution using uniform manifold approximation and projection (UMAP), and identified 10 distinct clusters (Fig. 4A,B). The top differentially expressed genes within each cluster was compared with expression maps of mouse gastrulation and early organogenesis (Pijuan-Sala et al., 2019) (Fig. 4C). We observed that the XEn compartment transitioned from a mixed parietal/visceral endoderm identity at 0 h (see also Fig. 2G,H) towards a more constrained VE identity at 64 h (*Amn*$^{+}$/*Dab2*$^{+}$, *Fst*$^{-}$/*Afp*$^{-}$; Fig. 4D, Fig. S17A). We concluded that the sustained contact with the Epi reduced the initial VE/PE heterogeneity and channeled the VE transcriptome. This transition was marked by initial Epi expression of known VE regulators *Nodal* and *Tdgf1* (*Crypto*) (Kimura et al., 2001; Kruithof-de Julio et al., 2011) and by the expression of genes involved in the STAT pathway (*Lifr* and *Stat3*), in epithelialization (*Crb3*, *Podxl*, *Cdh1*,

Development (2022) 149, dev192310. doi:10.1242/dev.192310

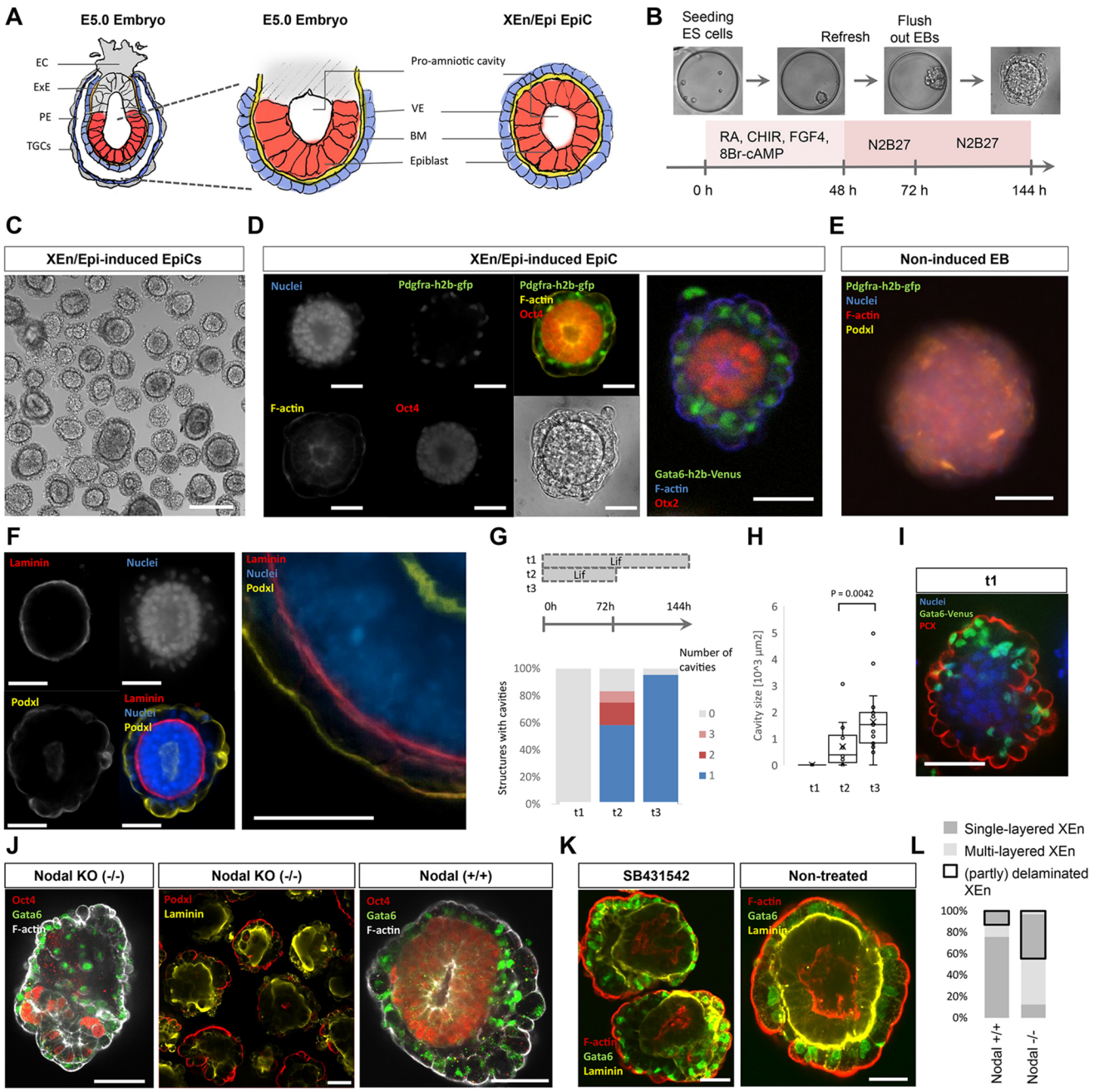

Fig. 3. The PrE-/Epi-like niche spontaneously progresses into a post-implantation extra-embryonic endoderm/epiblast epithelialized pro-amniotic-like cavity (XEn/Epi EpiC) in minimal culture conditions. (A) Schematic depicting an E5.0 conceptus (left, middle) and corresponding tissues in an XEn/Epi EpiC (right). EC, ectoplacental cone; ExE, extra-embryonic ectoderm; PE, parietal endoderm; TGCs, trophoblast giant cells; VE, visceral endoderm; BM, basal lamina. (B) Schematic for XEn/Epi EpiC formation. (C) Bright-field image of XEn/Epi rosettes and EpiCs. Scale bar: 200 µm. (D) Immunofluorescence and bright-field images of individual XEn/Epi rosette images after 120 h of culture. Staining for nuclei (DNA), F-actin (pro-amniotic cavity), Pdgfrα-h2b-gfp (PrE), Oct4 (pluripotent Epi) (left) and Otx2 (right). (E) EB cultured under the same basic conditions but without PrE-induction molecules. (F) Immunofluorescence images depicting cell nuclei (DNA), Podxl (polarization) and laminin (basal lamina) in a XEn/Epi pro-amniotic-like cavity. (G,H) Effect of Lif on (G) the percentage of structures forming a pro-amniotic cavity or multiple cavities and (H) the resulting integrated surface area of the cavities. *P*-value calculated according to the Mann–Whitney *U*-test. Boxes and whiskers indicate the first, median and third quartile, and minimum and maximum data points excluding outliers, respectively. This result was repeatedly replicated (>10 times) in other experiments as inclusion of a negative control. (I) Immunofluorescence image of a non-cavitated and non-polarized structure resulting from continuous Lif supplementation, labeled for nuclei, Gata6 (PrE) and Podxl (polarization). (J) Immunofluorescence images of 120 h XEn/Epi EpiCs from double Nodal knockout (–/–) and control (+/+) ESCs. (K) Immunofluorescence images of 120 h XEn/Epi EpiCs treated with the Nodal/activin signaling inhibitor SB431542 and non-treated controls. (L) Percentage of structures (32 in total) that contained a laminated or delaminated XEn layer (outlined in black) that is either single or multilayered. Scale bars in D-F,I-K: 50 µm.

Cldn6/7 and *Ezr*) possibly initiated by *Foxa2* (Burtscher and Lickert, 2009), and in the deposition of extracellular basal lamina proteins (*Col4a1/2*, *Lmna*, *Lama1/b1/c1*, *Dag1* and *Nid2*; Fig. 4D, Fig. S17B). Consistent with an inductive role of Nodal in VE epithelialization, genes related to apical/basal polarity (*Podxl* and *Crb3*) and epithelial cells (*Cdh1*, *Cldn6*, *Cldn7* and *Ezr*) became

Development (2022) 149, dev192310. doi:10.1242/dev.192310

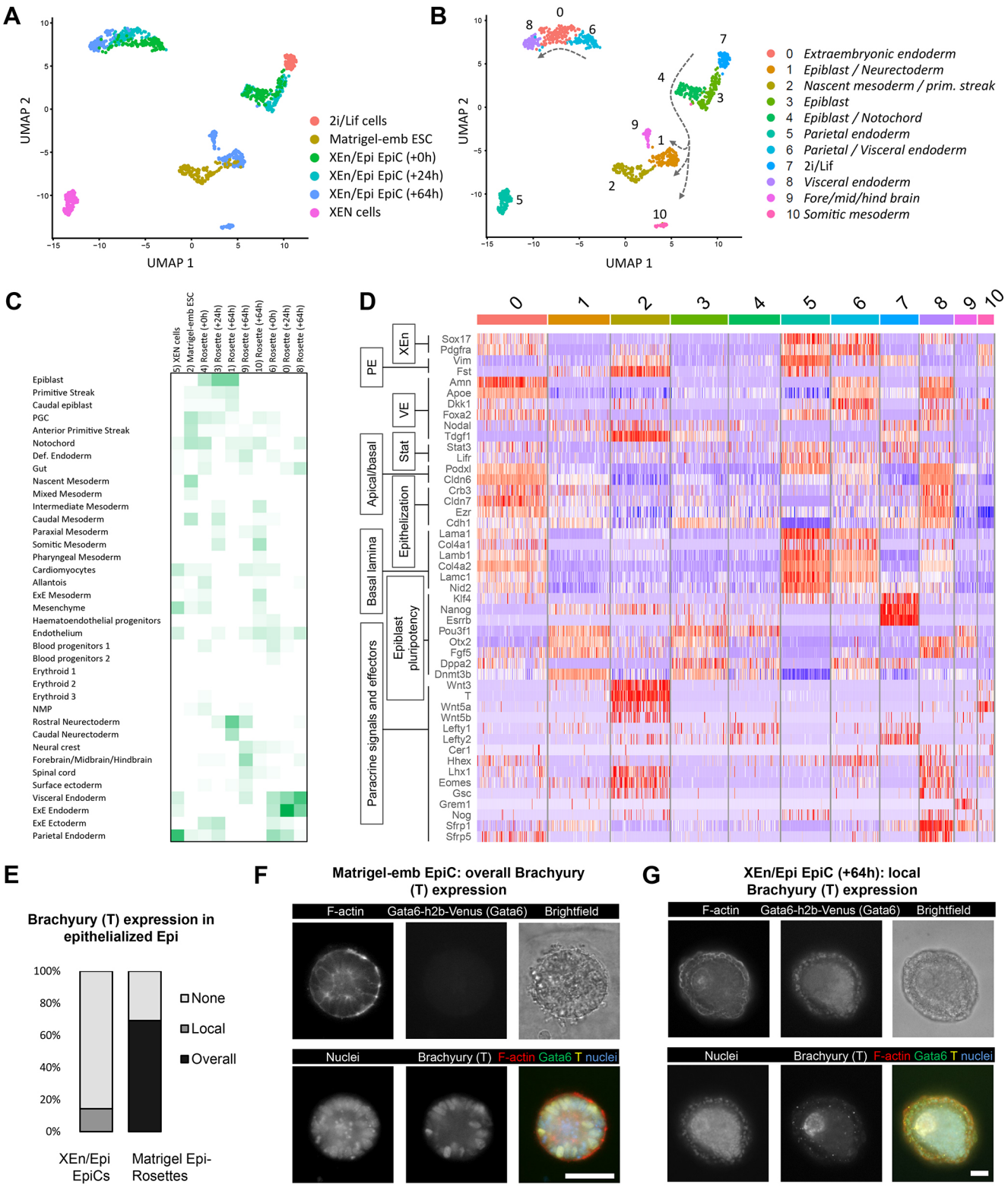

Fig. 4. Cellular identities of XEn/Epi EpiCs over time. (A) UMAP plot of single-cell RNA-seq data of indicated culture conditions. Timepoints indicate the number of hours after EpiCs were flushed out from the microwells. Matrigel-emb ESCs were cultured for 96 h in total. XEN and 2i/Lif cells were cultured as monolayers. (B) Cell points are numbered and colored based on their computationally assigned cluster, and annotated by tissue type. Lines with arrows indicate the trajectory over time of EpiCs (+0 till +64 h). (C) Inferred tissue types per cluster by comparing top gene list with embryo data from Pijuan-Sala et al. (2019). (D) Heatmap plot depicting differentially expressed genes for extra-embryonic endoderm (XEn), parietal endoderm (PE), visceral endoderm (VE), STAT signaling, apical/basal polarity, epithelialization and basal lamina formation, epiblast pluripotency, and paracrine signals and effectors in the Nodal, BMP and Wnt pathways. (E) Brachyury (T) immunofluorescence found in epithelial-like epiblast compartments in XEn/Epi EpiCs (24 structures total) and in Matrigel-embedded Epi-EpiCs (13 structures total). (F,G) Representative immunofluorescence images of overall and local brachyury expression in (F) Matrigel-embedded Epi-EpiCs and (G) XEn/Epi rosettes (+64 h), respectively. Scale bars: 50 µm.

Development (2022) 149, dev192310. doi:10.1242/dev.192310

progressively more prominently expressed over time. XEN cells clustered apart from the VE-like clusters, a distance that might reflect their PE identity (Fig. 4A,B, Fig. S17A). The Epi compartments at 0 and 24 h clustered largely together and expressed genes reflecting an early post-implantation Rosette-like identity (e.g. *Otx2*, *Fgf5*, *Oct6* and *Pou3f1*; Fig. 4D). The exit from naive pluripotency requires a transient downregulation of Wnt activity, possibly mediated by the Wnt inhibitor Dkk1 expressed by the PrE (Neagu et al., 2020). Accordingly, we observed a transient expression of Dkk1 in the PrE-like tissue (0 h) and its disappearance from 24 h onwards. The transience of Wnt inhibition would also subsequently allow the Epi to become receptive to autocrine and VE-secreted Wnt signals at gastrulation stage (Arnold and Robertson, 2009).

At 64 h, the Epi compartment spread into three different clusters with respective top-expressed genes found in native fore-, mid- and hindbrain, in Epi and neurectoderm tissues, and in somitic mesoderm. The first two clusters concomitantly expressed these germ layer-related genes along with post-implantation Epi-specific genes [*Klf4*$^{-}$, *Oct6*$^{+}$ (*Pou3f1*$^{+}$) and *Otx2*$^{+}$], suggesting a partial early anterior identity (Fig. 4D, Fig. S17C). The cluster expressing somitic mesoderm genes no longer expressed these Epi genes but was characterized by the expression of Wnt3 and Wnt5, which mark the posterior domain and are important for the gastrulation processes (Tortelote et al., 2013; Minegishi et al., 2017). When staining for brachyury (T), 14% of EpiCs (>64 h) contained brachyury-positive inner cells originating from an epithelium-like tissue (Fig. 4E-G). Additionally, the minority (20%) of structures that formed non-epithelized amorphous cell clumps, but included non-delaminated XEn layers, were all brachyury positive (Fig. S18). Of note, these amorphous structures were not included for single-cell transcriptomic analysis. To more finely assess the inductive role of the VE-like cells on the progression of the Epi-like cells, we compared the transcriptome with rosette-like cells embedded into Matrigel and cultured with serum (Bedzhov and Zernicka-Goetz, 2014). Most of these cells (96 h) clustered with the subpopulation reflecting a nascent mesoderm and/or primitive streak identity, while also partially overlapping with the Epi and neurectoderm (Fig. 4A,B). In comparison, Epi-like cells from the EpiCs also formed partial anterior-like cells (cluster 9, Fig. 4A,B,D, Fig. S17C). Consistent with a role for Epi epithelialization in facilitating the formation of the anterior Epi (Girgin et al., 2021), this suggests that the basal lamina regulates the formation of the posterior pre-gastrulation Epi, while additional signals originating from the XEn, possibly regulated by *Dkk1*, *Otx2*, *Lhx1* and *Foxa2* (Perea-Gomez et al., 2001), are conductive for the formation of the anterior cells. Overall, we concluded that reciprocal interactions between the Epi and VE are sufficient to initiate a program that reflects the formation of anterior and of posterior, gastrulating, Epi.

Induction of gene expression that originates from the trophoblasts, including *Bmp4*, regulates the expression of Wnt ligands and gastrulation (Rivera-Pérez and Magnuson, 2005). Although we observed Wnt3 and Wnt5 expression in the Epi-like tissue, we did not detect Wnt3 expression in the VE-like tissue, which is known to be produced first during development (Arnold and Robertson, 2009). In addition, trophoblast-secreted BMP4 maintains Nodal levels in the Epi first locally via a SMAD, which is a FoXH1 autoregulatory enhancer, and then through the activation of an autoregulatory posterior Wnt3 loop. Here, Nodal was initially not expressed in the VE and was expressed at low levels in the Epi (0/24 h), likely due to the absence of trophoblast signals; however, its expression later increased in both the VE- and Epi-like tissues (64 h). This suggests an alternative induction route separate from BMP and Wnt signals. Altogether, these data suggest that, although trophoblastic tissues are important for the anterior-posterior patterning of the Epi (Stephenson et al., 2012), Epi-VE interactions are sufficient to initiate part of the gastrulation program, including the expression of Wnt ligands in the Epi and Wnt inhibitors in the VE.

The VE is known to form a subpopulation of anterior VE that migrates toward the prospective anterior Epi, which, under the control of Foxa2 (Kimura-Yoshida et al., 2007) and Otx2 (Perea-Gomez et al., 2001), secretes inhibitors of the Wnt and Nodal signaling pathways to facilitate formation of the anterior tissues (Kimura-Yoshida et al., 2005; Arnold and Robertson, 2009). Accordingly, the 64 h VE-like tissue expressed *Foxa2*, *Otx2*, the Wnt ligand inhibitor *Sfrp1*, Wnt agonists *Hhex* and *Sfrp5*, and modulators of Nodal activity (*Gsc*, *Eomes* and *Lhx1*), but barely expressed the ensuing factors *Cer1*, *Dkk1*, *Tdgf1* (*Crypto*) and *Lefty1* (Fig. 4D, Fig. S17D). We concluded that, as previously observed (Rodriguez et al., 2005), the Epi/VE interaction is sufficient to promote the expression of some DVE genes regulating the expression of inhibitors, including *Sfrp1* and *Gsc*, but that is insufficient to regulate anterior Epi effector genes such as *Cer1*, *Dkk1*, *Tdgf1* (*Crypto*), *Lefty1*, *Spp1*, *Zbp1* and *Aire* (Cheng et al., 2019). Accordingly, microdissection of the ExE of E5.5 concepti showed that this tissue represses the expression of *Cer1* and *Lhx1* in the DVE (Rodriguez et al., 2005). EpiCs might be excluded from the element of the Epi/VE interaction that regulates *Cer1* and *Lhx1*, or there could be an earlier unreported role of the trophoblasts in inducing the formation of the VE and/or DVE. Altogether, we concluded that supervision of the DVE by its interaction with both the Epi and the trophoblast might ensure the expression of Wnt and Nodal inhibitors.

In blastoids, the four molecules prime ESCs to form primitive endoderm-like cells

Next, we tried to enhance the formation of PrE-like cells in blastoids to eventually model the impact of the two extra-embryonic tissues on Epi development. We thus modified the original blastoid protocol (Rivron et al., 2018a) by exposing ESCs, including a fluorescent reporter for Gata6 (ESCs$^{Gata6\text{-}h2b\text{-}venus/+}$) (Freyer et al., 2015), to the inductive molecules during the aggregation phase (0–24 h, Fig. 5A), i.e. before adding the TSCs. PrE-induction tempered the efficiency of blastoid formation (from 49% to 36%, specified as a single trophoblast cavity enveloping ESCs, Fig. 5B) by reducing the efficiency of TSCs to engulf the EBs (from 39% to 30% of non-engulfed structures, Fig. 5B). Although the underlying reasons are unknown, the specification of PrE-like cells might coincide with a change in their surface properties, reducing the capacity for TSCs to englobe them. Nevertheless, the molecules increased the overall percentage of blastoids, including Gata6^{+} and Nanog^{+} cells from 22% to 78% (Fig. 5C-F, Fig. S19). Concomitantly, the number of Gata6^{+} cells increased (P=0.00079, Fig. 5E,G). Notably, the total number of Epi plus PrE cells also increased (Fig. 5H) and the ratio of Gata6^{+} to Nanog^{+} cells in PrE-induced blastoids (Fig. 5I) was comparable with the one in blastocysts (0.83 versus 0.9 in 120 cells-stage blastocysts (Saiz et al., 2016). In accordance with our observations in EpiCs and with a previous study (Saiz et al., 2016; Nowotschin et al., 2019; Hiramatsu et al., 2013), PrE and Epi cells co-regulate their specification and proliferation.

Next, we examined the spatial organization of PrE-induced blastoids and observed that 21% of the blastoids, including PrE-like cells, showed a layer of Gata6^{+} cells lined up along the cavity of the

Development (2022) 149, dev192310. doi:10.1242/dev.192310

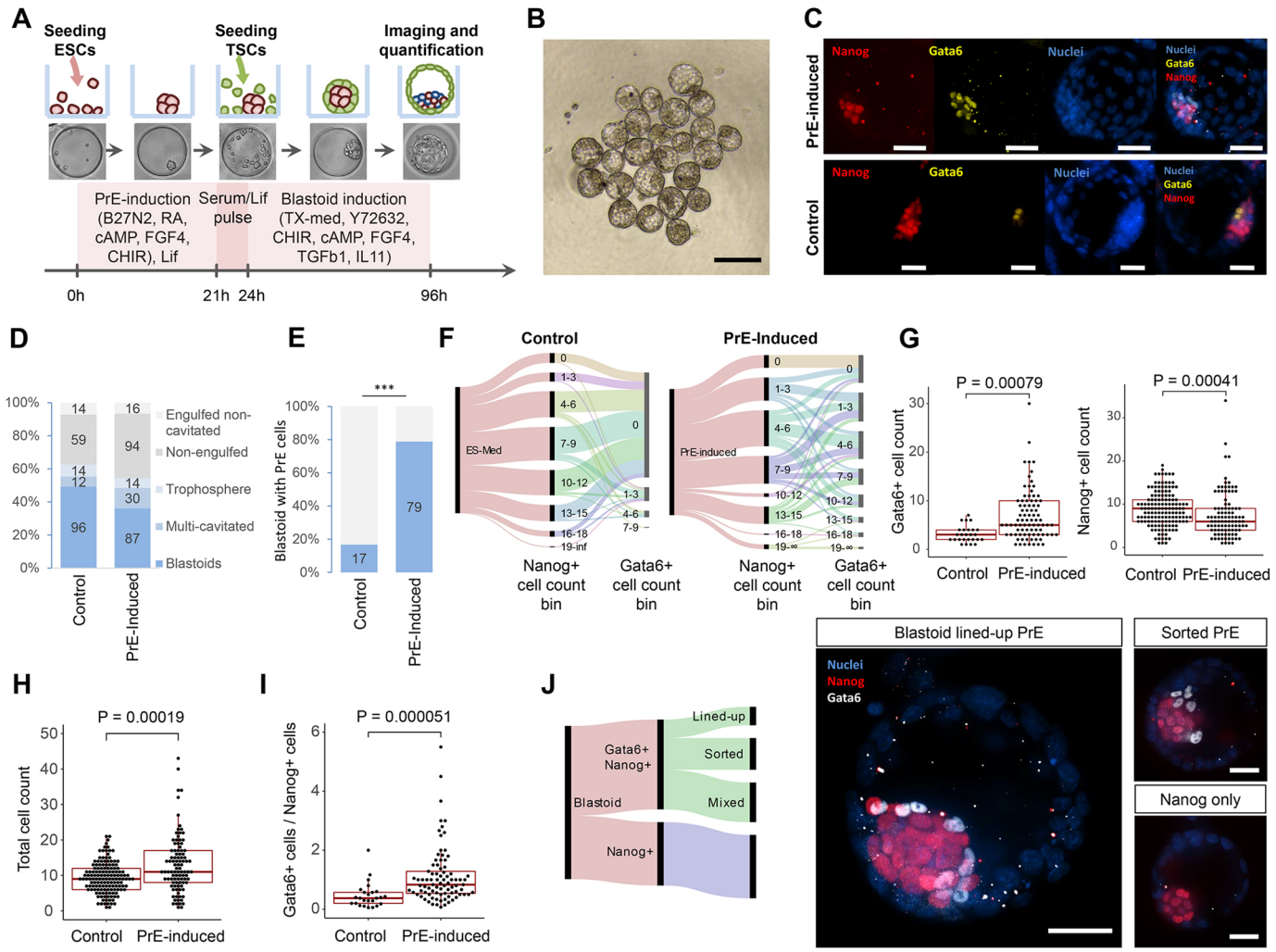

Fig. 5. The PrE/Epi priming of ESCs induces the formation of the niche in blastoids. (A) Schematic for PrE-induced blastoid formation. (B) Bright-field image of representative selection of PrE-induced blastoids. Structures with a single cavity and an inner cell compartment were classified as blastoids. (C) Maximum intensity confocal projection immunofluorescence images of representative PrE-induced and control blastoids stained for Nanog (red) and Gata6 (yellow). DAPI staining (blue) shows cell nuclei. Scale bars: 200 µm. (D) Percentages of the different structures found in microwell arrays in control (n=195) and PrE-induced (n=241) conditions, pooled from two wells per condition. (E) Percentage of blastoids including Gata6$^+$/Nanog$^+$ cells formed under the control of PrE-induced conditions (left). Pooled results from three datasets. ***P<0.001, Fisher's exact test. (F) Alluvial diagram displaying cell count of Nanog$^+$ and Gata6$^+$ dichotomy for control and PrE-induced blastoids (left). (G) Gata6$^+$ and Nanog$^+$ cell counts compared between control and PrE-induced blastoids that contain both Nanog$^+$ and Gata6$^+$ cells. (H) Total number of inner cells within blastoids. (I) Ratio of Gata6$^+$/Nanog$^+$ cells per blastoid containing both Gata6$^+$ and Nanog$^+$ cells. Boxes and whiskers indicate the first, median and third quartile, and minimum and maximum data points excluding outliers, respectively. (J) Alluvial diagram displaying contributions of resulting phenotypes following PrE-induced blastoid formation. Representative immunofluorescence images of PrE/Epi blastoid phenotypes. Scale bars: 50 µm. Data in D-I are derived from two independent experiments with three pooled wells each. In G-I, the P-values were determined using the Mann–Whitney U-test.

blastoid (Fig. 5J), similar to E4.5 blastocysts (Hermitte and Chazaud, 2014; Ohnishi et al., 2014). Among the other blastoids, 35% comprised sorted but not aligned Gata6$^+$ cells, while 44% had the salt and pepper phenotype of Gata6$^+$ and Nanog$^+$ cells (Fig. 5J) that is reminiscent of an earlier blastocyst stage (Frankenberg et al., 2011; Plusa et al., 2008; Meilhac et al., 2009).

In blastoids, the expansion of the primitive endoderm-like tissue supports the formation of post-implantation-like structures *in vitro*

Finally, we tested whether the PrE/Epi-like tissues within blastoids could support the formation of tissues reflecting the post-implantation stage. We cultured PrE-induced blastoids containing PrE cells (>2 Gata6$^+$ or Pdgfrα$^+$ cells) and non-induced blastoids *in vitro* (Bedzhov et al., 2014; Hsu et al., 1974). Induction of the ESCs at the onset of blastoid formation did not affect the final presence of Epi cells (96 h, 98% versus 100%, Fig. 6A) but enhanced the potential of the PrE-like cells to expand (96 h, Gata6$^+$, 60% versus 10%, Fig. 6A). This effect correlated with the initial number of PrE cells present in blastoids and is reminiscent of the FGF4 induction of PrE in blastocysts (Fig. 6C). The presence of the PrE-like cells did not improve the formation of non-organized 3D structures (experimental average of 18% versus 15%, Fig. 6B; pooled yields of 15% versus 19% from eight independent experiments) containing both Oct4$^+$ Epi and PrE cells (Fig. 6C, Fig. S20) but endowed some blastoids with the capacity to support the formation of EpiCs marked by Podxl expression (Fig. 6D, Fig. S20) (11% of blastoids, pooled yield in eight independent experiments; Fig. 6C), the Epi of which transitioned into a Oct6$^+$ post-implantation-like state (Fig. 6F); however, ExE-like tissue

Development (2022) 149, dev192310. doi:10.1242/dev.192310

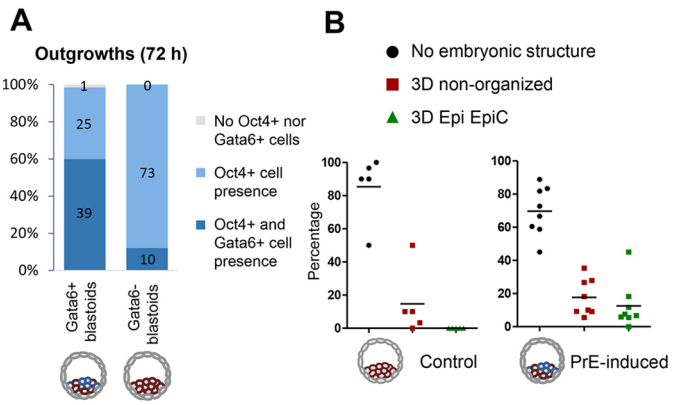

	Experiment:	1	2	3	4	5	6	7	8
Ctrl	Control								
	No embryonic structure	29/30	9/9	9/10	18/20	15/30	N/A	N/A	N/A
	3D non-organized	1/30	0/9	1/10	2/20	15/30	N/A	N/A	N/A
	3D Epi EpiC	0/30	0/9	0/10	0/20	0/30	N/A	N/A	N/A
PrE-ind	PrE-induced								
	No embryonic structure	10/17	9/11	10/15	16/18	9/20	8/11	100/120	26/43
	3D non-organized	6/17	2/11	4/15	1/18	2/20	1/11	11/120	12/43
	3D Epi EpiC	1/17	0/11	1/15	1/18	9/20	2/11	9/120	5/43

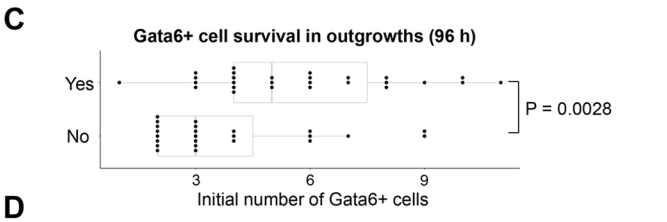

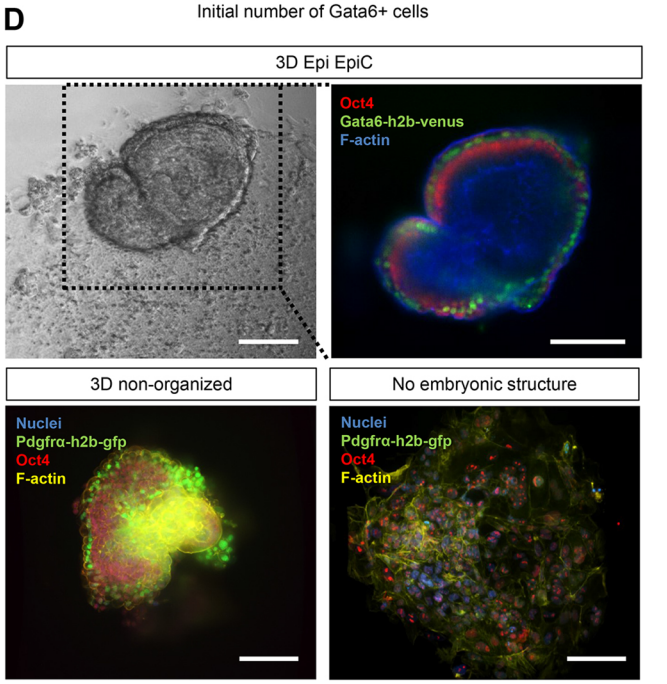

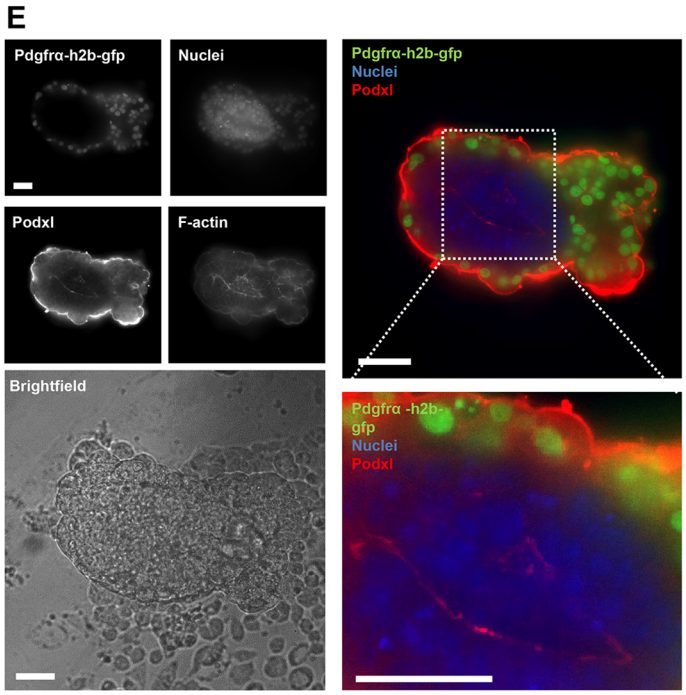

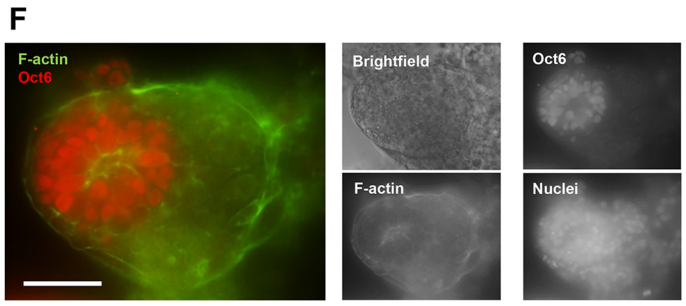

Fig. 6. The induction of the PrE-/Epi-like niche in blastoids supports the formation of post-implantation-like tissues. (A) Presence of Epi (Oct4$^+$) and PrE (Gata6$^+$) cells within *in vitro* outgrown (for 72 h) PrE-induced blastoids with and without Gata6$^+$ cells (96 h). Total number of structures pooled from four experiments are displayed within the bars. (B) Percentage (left) and number (right) of different tissue phenotypes arising from PrE-induced blastoids including two or more Gata6$^+$ cells compared with non-induced blastoids. Every data point represents an independent experiment. Monolayer outgrowths were classified as 'no embryonic structure'; structures with 3D outgrowths without a pro-amniotic-like cavity and irrespective of cell type were classified as '3D non-organized'. Structures with 3D outgrowths that contained Epi cells, PrE cells and had a pro-amniotic-like cavity, as observed by F-actin and/or Podxl staining, were classified as '3D Epi EpiC'. (C) The presence of PrE tissue (Gata6$^+$) within *in vitro* grown PrE-induced blastoids (yes/no, at 96 h) as a function of the numbers of Gata6$^+$ cells within the initial blastoids. Each point represents an individual cell aggregate. *P*-values were determined by a Mann–Whitney *U*-test. (D) Top: bright-field and immunofluorescence images of an *in vitro* grown blastoid with Oct4$^+$ Epi (red) and Gata6$^+$ PrE (green) cells surrounding a pro-amniotic cavity and growing on top of a TSC monolayer (96 h). Bottom: representative images of *in vitro* grown blastoid phenotypes with Oct4$^+$ Epi (red), Pdgfrα$^+$ PrE (green) and overall F-actin (yellow) and nuclei (blue). Scale bars: 200 µm. (E) Pdgfrα$^+$ cells surrounding an epiblast-like tissue, including a pro-amniotic-like cavity marked by Podxl expression (72 h). Scale bars: 50 µm. (F) Oct6$^+$ epiblast-like tissue blastoid outgrowth (48 h). Scale bar: 50 µm.

formation appeared absent. The non-induced blastoids lacked that potential (Fig. 6C). We concluded that a threshold in the number of PrE-like cells is crucial to support the progression of the post-implantation Epi-like tissue in blastoids.

Altogether, we concluded that the Epi/XEn tissues are sufficient to support aspects of specification and proliferation to the rosette and lumenogenesis stages through the deposition of a basal lamina (Fig. 7). During the early post-implantation stage, the Epi supports further progression of the VE through the secretion of Nodal and Tdgf1 that facilitates the progression of two abutting VE/Epi epithelia. At the post-implantation/pre-gastrulation stages, the VE not only provides structural support through the formation of a basal

Development (2022) 149, dev192310. doi:10.1242/dev.192310

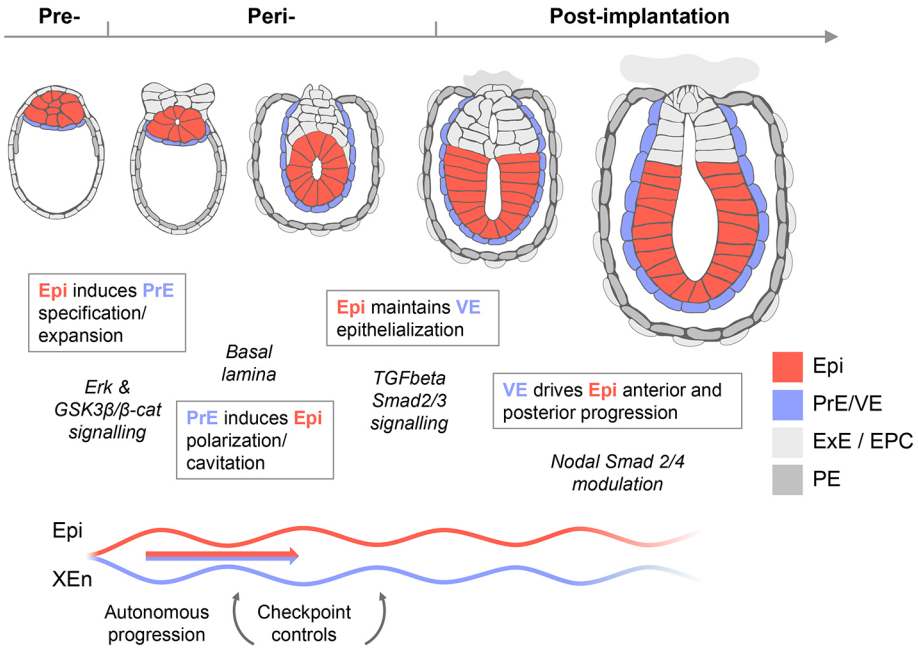

Fig. 7. Self-organized reciprocal inductions and pathways underpinning the co-developing XEn-/Epi-like tissues. Signals from the pre-implantation Epi (Erk and GSK3β/β-catenin signaling) support the primitive endoderm (PrE) to produce a basal lamina that subsequently regulates Epi polarization and cavitation. In exchange, the Epi channels the transcriptomic progression to VE through TGFβ signals. This VE then contributes to Epi bifurcation into anterior- and posterior-like states. In this model, self-organization arises from lineage bifurcation followed by a pendulum of induction that propagates over time.

lamina, but also appears to produce additional signals that contribute to the formation of both the anterior (e.g. *Lhx1*, *Otx2* and *Foxa2*) and posterior Epi.

DISCUSSION

High-content screening of a large number of EBs on a microwell array in chemically defined culture conditions allows for robust statistics necessary to delineate the effect of signaling pathways. Here, we observed that the combination of FGF4, Wnt, cAMP and RA is sufficient to rapidly and efficiently drive the co-formation of PrE- and Epi-like cells in gel-free and serum-free 3D cultures.

Upon transfer into plain N2B27 medium, these two cell types are capable of further growth and autonomous organization into a structure that undergoes aspects of post-implantation development. We found that the PrE cells in PrE/Epi-induced structures before forming a pro-amniotic cavity show an initial bifurcation into PE and VE precursors independently from trophoblastic tissues (Fig. 2F-H), suggesting this to be a cell-autonomous mechanism that could be stochastic or partly tuned by signals from the Epi. However, when Epi/PrE-like structures underwent rosette morphogenesis, the identity of PrE tissues was channeled into a VE-like identity, not a PE identity, suggesting that the PE-precursors are lost or transcriptionally normalized over time by contact with the Epi. This suggests the possibility that the cells can fluctuate between states at the time of specification, followed by a channeling of the state due to an inductive environment. This initial fluctuation could endow the embryo with adaptive and regulative capacities (Paca et al., 2012).

The single-cell RNA-sequencing data suggest an early peri-implantation Epi identity for the embryonic clusters in 0/24 h EpiCs (Fig. 4). In contrast, embryonic clusters in 64 h EpiCs showed four distinct clusters that, although they clearly express Epi markers (Oct4 and Otx2), appear already transcriptionally primed for mesodermal and ectodermal progression. Notably, a definitive endoderm cluster was not found, possibly due to low combined levels of activin/Nodal and the BMP inhibitor noggin (Fig. S16D), which suggests the requirement of additional supporting tissues (e.g. trophoblastic). Of note, XEN cells clustered separately, with a seemingly parietal endoderm identity.

Consistent with the idea that blastocysts are self-regulating systems adjusting the ratios and numbers of their three founding cell types (Saiz et al., 2016), the induction of PrE-like cells in blastoids triggers a regulation of the total cell number. The *in vitro* culture of blastoids (Hsu, 1971) additionally suggests that a threshold of PrE cells is necessary to sustain the expansion and morphogenetic capability of the Epi during the post-implantation stage. Accordingly, the insufficient formation of PrE and incomplete lining of the PrE epithelium between the Epi and blastocoel, e.g. in GATA6 KO conceptus, has been described to halt Epi expansion in blastocysts (Artus et al., 2010; Moore et al., 2014). Similarly, inappropriate specification of the extra-embryonic VE results in disorganized ectoderm and stagnated development (Barbacci et al., 1999).

Overall, these results argue, beyond the inductions originating from the Epi (e.g. FGF4), for the importance of the PrE tissue in supporting the Epi for survival and expansion. The mechanisms by which the PrE accomplishes this remain to be determined. One attractive possibility is that Epi proliferation and morphogenesis needed to form the amniotic cavity cannot occur unless the PrE deposits the required basal lamina, similar to laminin-KO embryos that exhibit aberrant peri-implantation morphogenesis and halted development (Miner and Yurchenco, 2004; Smyth et al., 1999). It delineates a critical switch of signaling activity necessary to transit from pre- to post-implantation development, and suggests that the deposition of a functional amount of basal lamina acts as a checkpoint for developmental progression. During post-implantation development, the VE appears to play an additional role, beyond the maintenance of the basal lamina that is controlled by Nodal originating from the Epi, to drive the progression of the different tissues emerging from the Epi. Considering that blastoids do not progress upon implantation *in utero*, it would be interesting to find out in future studies whether PrE-induced blastoids have an improved capacity to do so. Altogether, this study contributes to the establishment of stem cell-based embryo models amenable to high-throughput drug and genetic screens, which may alleviate the burden on animal use (Andersson-Rolf et al., 2017; Rivron et al., 2018b) and become a foundation for basic and biomedical

Development (2022) 149, dev192310. doi:10.1242/dev.192310

discoveries to elucidate the crucial and currently unknown processes of embryogenesis.

MATERIALS AND METHODS

Microfabrication

Elastomeric stamps for imprinting the agarose microwell arrays were fabricated using PDMS Sylgard 184 kit. Microwell arrays were molded as described previously (Vrij et al., 2016b) using a 2.2% w/v solution of Ultrapure agarose (ThermoFisher, 11560166). Each well of a 96-well plate with 430 microwells of 200 µm was molded. Each well contained a calculated liquid volume of 250 µl split between 225 µl medium and 25 µl hydrogel buffer.

Cell culture

The following lines were used for experiments: Pdgfrα h2b-gfp/+, h2b-rfp V6.5 sub-clone, Gata6-h2b-Venus/+;ColA1 TetO-Gata4-mCherry/+;R26 M2rtTA/+ ES cells and V6.5 Nodal KO (−/−) with corresponding wild types. The Gata6-h2b-Venus cell line was a kind gift from C. Schröters' laboratory (Max Planck Institute of Molecular Physiology, Dortmund, Germany; Freyer et al., 2015). The V6.5 cell line has a C57BL/6×129/Sv background and was obtained from the laboratory of R. Jaenisch (Whitehead Institute for Biomedical Research, Cambridge, MA, USA). The Pdgfrα h2b-gfp/+ cell line has an ICR background and was derived in the laboratory of A.-K. Hadjantonakis (Sloan Ketttering Institute, New York, USA).

ESCs were seeded as 25,000 per cm^2 and expanded on 0.1% w/v gelatin-coated tissue culture-treated polystyrene dishes (Nunc). Cell expansion medium was carried out in N2B27 2i/Lif conditions comprising 2% B27 (Gibco, 17504-044) and 1% N2 (Gibco, 17502-048) in a 1/1 mixture of DMEM/F12 (ThermoFisher, 11039021) or Advanced DMEM/F12 (ThermoFisher, 12634028) with Neurobasal (ThermoFisher, 12348017), including 2 mM Glutamax (Gibco), 10 mM NEAA (ThermoFisher, 11140050), 0.5% bovine serum albumin (Sigma-Aldrich, A7979), 10 mM HEPES (Gibco, 15630056), 1 mM sodium pyruvate (ThermoFisher, 11360070), supplemented immediately before use with 10 ng/ml leukemia inhibitory factor (Lif, Merck Millipore ESG1106), 1 µM PD0325901 (AxonMed, 1408), 3 µM CHIR99021 (AxonMed, 1386) and 50 µM 2-mercaptoethanol (Gibco, 11528926), as developed previously (Nichols et al., 2009).

ESCs were expanded for a minimum of two passages before aggregating into EBs within the agarose microwells. For cell banking and serum/Lif experiments, ESCs were expanded on a monolayer of mouse embryonic fibroblasts (mEF) in serum-medium consisting of DMEM containing sodium pyruvate and Glutamax (Thermo Fisher, 10569010) supplemented with 10% serum, 10 mM NEAA, 10 mM HEPES, 10 ng/ml Lif and 50 µM 2-mercaptoethanol.

TSCs were seeded and expanded as 25,000 per cm^2 on 3% Matrigel-coated dishes in chemically defined TX-medium, as developed previously (Kubaczka et al., 2014) or on TCPS with a Laminin-512 coating (Biolamina LN521-02, 5 µg/ml overnight incubation at 4°C) in TX-medium supplemented with activin A (Bio-techne, 338-AC-010), 50 ng/ml IL11 (Peprotech, 220-11), 200 µM 8Br-cAMP (Biolog, B007-500), 25 ng/ml BMP7 (R&D Systems, 5666-BP-010), 5 nM LPA (Tocris, 3854), 2 ng/ml TGFβ1 (Peprotech, 100-21), 25 ng/ml FGF4 (R&D Systems, 5846-F4-025 and 7486-F4), 1 µg/ml heparin (Sigma-Aldrich, H3149) and 100 µM 2-mercaptoethanol. Extra-embryonic endoderm (XEN) cells were expanded on 0.15% gelatine-coated TCPS culture plates in RPMI 1640 medium (ThermoFisher, 11875085), including L-glutamine, supplemented with 20% FBS (fetal bovine serum, embryonic stem cell-qualified, ThermoFisher, 16141061), 1 mM sodium pyruvate, 10 mM HEPES, 100 µM 2-mercaptoethanol. Y27632 (AxonMed, 1683; 0.5 µM) was added to the medium when cells were passaged. All cells were routinely checked for mycoplasma infection.

EB, PrE/Epi and XEn/Epi formation

EBs were formed by seeding an average of seven ESCs per microwell in either serum-containing medium, Lif/serum-containing medium or N2B27-based media, all supplemented with 50 µM of 2-mercaptoethanol. Lif/serum-containing medium consisted of DMEM containing sodium pyruvate and glutamax (Thermo Fisher, 10569010) supplemented with 10% serum, 10 ng/ml Lif, 10 mM NEAA, 10 mM HEPES and 100 U/ml penicillin/streptomycin. PrE-induction medium consisted of advanced N2B27 medium supplemented with 3 µM CHIR99021, 50-100 ng/ml FGF4, 10 nM RA, 1 mM 8Br-cAMP and 50 µM 2-mercaptoethanol. To induce XEn/Epi EpiCs from PrE-induced EBs, 14 ESCs were seeded per microwell supplemented with 2 µM Y27632 (AxonMed 1683). Occasionally, microwell arrays were pre-wetted in serum-medium containing 100 U/ml penicillin/streptomycin before use. For XEn/Epi EpiC formation using the Nodal double KO (−/−) line, 10% of serum was added to the medium. After 24 h or 48 h of culture, cells were washed once with advanced N2B27 medium and then refreshed with advanced N2B27 supplemented with 50 µM 2-mercaptoethanol. After 72 h, EBs were flushed out and transferred into non-TCPS six-well plates with 2 ml advanced N2B27 medium supplemented with 50 µM 2-mercaptoethanol. Then, after an additional 48 h of culture, structures were either fixated using a fresh solution in PBS of 2% formaldehyde and 0.1% glutaraldehyde, or half of the medium was refreshed and structures were cultured for an additional 24 h before fixation.

Epiblast-only rosettes (used as controls in the scRNAseq data) were formed by first seeding eight ESCs per microwell in serum-containing medium. After 12 h, the ESC aggregates were flushed out and resuspended in 15 µl Matrigel droplets cultured in serum-containing medium.

Blastoid formation

Blastoids were formed as described previously (Rivron et al., 2018a; Rivron, 2018). For control blastoids, an average of seven ESCs were seeded per microwell in serum/Lif medium (10 ng/ml Lif, control blastoids) with 50 µM 2-mercaptoethanol. For PrE-induced blastoids, an average of seven ESCs were seeded per microwell in either (1) N2B27 medium with PrE-induction compounds and 10 ng/ml Lif for 21 h incubation followed by serum/Lif for 3 h, or (2) serum/Lif medium with PrE-induction compounds. After 24 h of ESC aggregation an average of 17 TSC were added per microwell in TX medium with non-essential amino acids and the blastoid culture components (20 µM Y27632, 5 µM CHIR99021, 1 mM 8Br-cAMP, 25 nG/ml FGF4, 2 nG/ml TGFβ1, 30 nG/ml IL11, 1 µg/ml heparin and 100 µM 2-mercaptoethanol). In some experiments, after 24 h an additional 1 mM of 8Br-cAMP was added to the blastoid culture medium. Structures with a single cavity and an inner cell compartment were classified as blastoids. Full stacks using a spinning disk confocal with a 40× objective were made for the counting of PrE and Epi cells within blastoids (Fig. 5). The fluorescence images of seven blastoids in Fig. 5 were made by stacking three to five spinning disk confocal slides.

In vitro post-implantation assay

Blastoids cultured for 96 h (from the time of seeding ESC) were selected based on their morphology (cystic, roundness, presence of inner cell mass) and transferred from microwells onto tissue-culture glass or polystyrene plastic in IVC1 medium using mouth pipetting. IVC1 medium consisted of Advanced DMEM/F12 medium with non-essential amino acids and sodium pyruvate, 20% ESC-selected fetal bovine serum, 2 mM glutamax, penicillin/streptomycin, 1/100 ITS-X (ThermoFisher, 51500056), 8 nM β-estradiol (Sigma-Aldrich, E8875), 200 ng/ml progesterone (Sigma, P8783), 25 µM Acetyl-l-cysteine (Sigma-Aldrich, A9165-5G) and 50 µM 2-mercaptoethanol. Structures were fixated after 72 or 96 h of culture using a fresh solution in PBS of 2% formaldehyde and 0.1% glutaraldehyde.

Microscopy and image-based analysis

For the soluble factor screen, the fluorescence images were acquired in widefield on a widefield Nikon Eclipse Ti microscope using a 10×objective, Andor Zyla4.2 camera and a Lumencor SpectraX as light source with LED lines of 390, 490, 568 and 647 nm that were used in this study. The standard DAPI (DAPI-5060C), GFP (GFP-3035D-000), Txred (TXRED-4040C0360), Cy5 (Cy5-4040C) and Cy7 (Cy7-B) filter cubes from Semrock were used. Analysis of EBs was performed using a custom-made pipeline in CellProfiler2.0 or 3.1 (Broad Institute) (Lamprecht et al., 2007). The number of EBs and cells positive for Pdgfrα-h2b-gfp or

Development (2022) 149, dev192310. doi:10.1242/dev.192310

Gata6-h2b-venus were determined by thresholding on intensity. EBs were considered positive for Pdgfrα when one or more cells were positive for Pdgfrα-h2b-gfp. The number of Pdgfrα$^+$ cells was identified from widefield images acquired within the equatorial plane of EBs, and therefore reflect a proxy for the total number of Pdgfrα$^+$ cells per EB. Mouse blastocyst images were deconvolved using Huygens Professional software and quantified using Imaris x64 9.5.0.

Soluble factor screening

Serial dilutions of compounds were made in appropriate solvents (DMSO or H_2O) and corresponding carrier controls were included in the assays. Serial dilutions were made for single soluble factor titrations; FGF4, sodium (ortho)vanadate (Sigma-Aldrich, S6508), PD0325901, PD98059 (Sigma, P215), activin A, TGFβ1, A83-01 (Tocris, 2939), Nodal (R&D systems, 1315-ND-025), SB431542 (Tocris, 1614), retinoic acid (Sigma-Aldrich, R2625), DL-epinephrine HCl (Sigma-Aldrich, E4642), 8Br-cAMP, SC144 (Tocris, 4963/10), IL6 (Peprotech, 216-16), IL11, Lif, BMP4 (Peprotech, 315-27), BMP7, LDN 193189 (Tocris, 6053), ML347 (Selleckchem, S7148), Noggin (Peprotech, 250-38), CHIR99021, IWP2 (Selleckchem, S7085) and XAV-939 (Selleckchem, S1180). Compounds with end concentrations that were used for XEn/Epi EpiC modulation: PI3K inhibitor ZSTK474 (Selleckchem, S1072) at 1 µM, insulin at 50 ng/ml, XAV-939 at 20 µM.

Mouse embryo culture

Embryos were flushed from the uterus as compacted morulas and incubated at 37°C in basic KSOM medium (Sigma-Aldrich, MR-101-D). Upon cavity formation, the embryos were transferred to KSOM medium supplemented as listed in Fig. S9 and incubated in the respective media at 37°C. Control medium was KSOM only. After 42-48 h blastocysts were fixed in 4% formaldehyde in PBS. If they had not hatched or were in the process of hatching, the zona pellucida was removed before fixation using Tyrode's solution.

Immunofluorescence

Blastoids and blastocysts were fixed in 4% formaldehyde solution in PBS for 15 min at room temperature. XEn/Epi EpiCs and *in vitro* implantation cultures were fixated in 2% formaldehyde solution with 0.1% glutaraldehyde in PBS for 15 min at room temperature. After fixation, samples were washed three times in washing buffer (0.1% Triton-X with 2% BSA in PBS), permeabilized in a 1% Triton-X solution in PBS and blocked in blocking buffer (2% BSA, 5% serum of host secondary antibody species, 0.5% glycine, 0.1% Triton-X, 0.2% Tween-20) for 30 min. Samples were incubated in antibody solution (25% blocking buffer with 50% PBS and 25% 0.1% Triton-X in PBS) with primary antibodies for 12 h at 4°C, washed three times for 10 min with washing buffer followed by incubation with secondary antibodies in antibody solution for 4 h at 4°C. Some samples were also stained with DAPI (0.2 µg/ml) and phalloidin (ThermoFisher, A22287 or A12380, 1/100 dilution). A list of used antibodies can be found in Table S4.

Single-cell sequencing

EBs were washed twice in PBS before collagenase IV (600 U/ml) was added. Plates were shaken at 350 rpm for 30 min before being transferred to TrypLE 10X (Thermofisher, A1217701, no dilution) and shaken again for 20 min. EBs were dissociated into single cell suspensions using a small capillary. The resulting suspension was quenched using PBS with 50% FBS, centrifuged at 200 ***g*** and resuspended in 230 µl of PBS with 10% FBS. Cells were stained with Pdgfrα antibody (1:150 dilution) for 30 min at 4°C followed by three PBS (+10% FBS) washes and secondary antibody incubation (1:400) for 30 min. Cells were washed three times in PBS and sorted for further processing.

XEn/Epi EpiCs were manually picked and placed in a round-bottomed 96-well plate containing 100 µl PBS+0.5% BSA. When sufficient numbers were collected, they were transferred to an Eppendorf tube with 600 µl Accumax and incubated at 37°C for 30 min. Every 5-10 min the mixture was resuspended using a 200 µl pipette. When single cells were observed under the microscope, the suspension was centrifuged at 200 ***g*** for 4 min, supernatant was removed, and cells were resuspended in staining solution in PBS (2 µM Di-I+0.1% Dead-stain-647) and incubated for 20 min at room temperature in the dark.

Epiblast-only rosettes were washed once with PBS before domes were disrupted using 150 µl of a 1:1 DipaseII:N2B27 mixture and incubated for 20 min at 37°C in a 1.5 ml Eppendorf tube (four domes per tube). Solution was resuspended every 5-10 min using a 200 µl pipette tip. Finally, the cell suspension was resuspended in 700 µl Accumax with 100 µl of PBS with 0.5% BSA and incubated for 25 min at 37°C. Single cells were stained with 2 µM Di-I+0.1% Dead-stain-647 and incubated for 20 min at room temperature in the dark.

Single-cell sequencing experiments

For single-cell sequencing, EBs, Matrigel-embedded Epi rosettes and XEn/Epi EpiCs were manually picked and incubated in AccuMax solution at 37°C for 30 min and resuspended every 5 to 10 min to aid single-cell dissociation. For Matrigel-embedded Epi rosettes, the basal lamina gel was first removed by one time washing with PBS followed by Cultrex organoid harvesting solution (R&D Systems, 3700-100-01) or a 1:1 mix of DispaseII: N2B27 medium and incubated for 25 min at room temperature or 37°C, respectively. Dissociated cells were stained for a live staining (Vybrant DiI Cell-Labeling Solution, ThermoFisher, V22885) and dead staining (LIVE/DEAD Fixable Near-IR Dead Cell Stain Kit, ThermoFisher, L34975) to improve selection of viable cells. Gata6-h2b-Venus$^+$ cells, which are indicative of PrE/VE, and non-fluorescent single cells were sorted in 384-well-plates for further RNA sequencing.

SORT-seq, sequencing and mapping of scRNA-seq data

The sorted 384-well plates were processed using the SORT-seq protocol (Muraro et al., 2016) and sequenced on an Illumina NextSeq500 sequencing platform yielding paired-end reads of 75 bp. The second sequencing run (associated with data in Fig. 4) was performed by SingleCellDiscoveries. The first six nucleotides of the read unique molecular identifier were followed by a unique cell barcode that was used to perform demultiplexing. After demultiplexing, read 2 was used to map to the mouse genome (mm10) using TopHat (v2.1.1) (Kim et al., 2013). The count table per single cell was obtained as previously described (Markodimitraki et al., 2020).

scRNA-seq data processing

scRNA-seq data was processed using Seurat (v3) (Stuart et al., 2019). Cells with more than 1000 genes detected were selected and genes present in fewer than three cells were removed from the analysis. Expression was normalized to 10,000 transcripts and the 3500 most variable transcripts were used for downstream analysis. Data were then scaled to the total number of transcripts per cell. After principal component analysis, 20 principal components were used for downstream analysis. Clustering, t-distributed stochastic neighbor embedding (t-SNE) and uniform manifold approximation and projection (UMAP) were performed using Seurat default parameters.

Data analysis and reproducibility

Sample sizes and statistical tests for every experiment are provided in the figure legends. Sample sizes were not predetermined using statistical methods. If not stated otherwise, all data are displayed as mean±s.d.

PrE-induced blastoid formation and *in vitro* implantation assays were repeated at least five times using two ESC and two TSC lines. Alluvial figures were created using RAW – an open source project by DensityDesign Lab and Calibro (Mauri et al., 2017).

Single-cell transcriptome analysis, including clustering and heatmaps, was performed in R (https://www.r-project.org/) using the Seurat package for R (https://satijalab.org/seurat/). A minimal detection threshold of 5000 genes per cell was selected for cells to be included for analysis. Gene ontology enrichment analysis was performed using GOrilla (Eden et al., 2009).

Bar plots were created using Microsoft Excel. SPRING Louvain clustering was performed using Kleintools (Weinreb et al., 2018). Scatter plots in Fig. 2 were generated using GraphPad Prism 5. Scatter plots in Fig. 4, violin plots and dose-response curves were generated using R with

the packages 'ggplot2', 'reshape2', 'ggsignif' and 'ggbeeswarm'. Statistical analysis was performed using the package 'stats'.

Acknowledgements
The authors thank Christian Schröter for providing the Gata6-Venus mouse ES cells; Valerie Prideaux, Jodi Garner and Janet Rossant for providing the F4 mouse TS cell lines; Anna-Katerina Hadjantonakis for providing the Pdgfrα-h2b-gfp mouse ES cells; and Single Cell Discoveries for providing de-multiplexed sequencing files. The Oncode Institute is partially funded by the KWF Kankerbestrijding.

Competing interests
N.C.R., E.J.V. and C.A.v.B. are inventors on the patents US14/784,659 and PCT/NL2014/050239, which describe the formation of mouse blastoids (April 2014). All rights and duties are maintained by the Institute for Molecular Biotechnology, Austrian Academy of Science.

Author contributions
Conceptualization: E.J.V., B.-K.K., J.K., N.C.R.; Methodology: E.J.V., Y.S.S.o.R., J.F.A., I.M.G., N.C.R.; Validation: E.J.V., Y.S.S.o.R., J.F.A., I.M.G., N.C.R.; Formal analysis: E.J.V., Y.S.S.o.R., J.F.A., I.M.G., J.K., N.C.R.; Investigation: L.R.F., V.H.; Validation: L.R.F., G.S., V.H.; Methodology: L.R.F., G.S., V.H.; Formal analysis: L.R.F., V.H.; Data curation: E.J.V.; Writing - original draft: E.J.V., N.C.R.; Writing - review & editing: E.J.V., N.C.R.; Supervision: B.-K.K., J.K., N.C.R.; Funding acquisition: E.J.V., B.-K.K., C.A.v.B., J.K., N.C.R.

Funding
This project has received funding from the European Research Council under the European Union's Horizon 2020 research and innovation program (2015 ERC-AdG number 694801-ORCHESTRATE) and from the Stichting De Weijerhorst ('Synthetic Embryos' PC0089). N.C.R. is funded by the European Research Council (2020 ERC-CoG number 101002317-BLASTOID). V.H. is funded by a Boehringer Ingelheim Fonds PhD fellowship. J.K. is funded by the European Research Council (2016 ERC-StG 678423-EpiID). I.M.G. is supported by a European Molecular Biology Organization Long-Term Fellowship (ALTF1214-2016), by the Schweizerischer Nationalfonds zur Förderung der Wissenschaftlichen Forschung (P400PB_186758) and by a Nederlandse Organisatie voor Wetenschappelijk Onderzoek-ZonMW Veni grant (VI.Veni.202.073). Open access funding provided by the Institute of Molecular Biotechnology of the Austrian Academy of Sciences. Deposited in PMC for immediate release.

Data availability
The single-cell transcriptomic datasets generated and analyzed during the current study have been deposited in GEO (Edgar et al., 2002) under accession number GSE129655. The data used to create Fig. 3G (time lapse of cavitated structures) can be found at https://doi.org/10.34894/GSOHSD.

Peer review history
The peer review history is available online at https://journals.biologists.com/dev/lookup/doi/10.1242/dev.192310.reviewer-comments.pdf.

References

Anderson, K. G. V., Hamilton, W. B., Roske, F. V., Azad, A., Knudsen, T. E., Canham, M. A., Forrester, L. M. and Brickman, J. M. (2017). Insulin fine-tunes self-renewal pathways governing naive pluripotency and extra-embryonic endoderm. *Nat. Cell Biol.* **19**, 1164-1177. doi:10.1038/ncb3617

Andersson-Rolf, A., Mustata, R. C., Merenda, A., Kim, J., Perera, S., Grego, T., Andrews, K., Tremble, K., Silva, J. C. R., Fink, J. et al. (2017). One-step generation of conditional and reversible gene knockouts. *Nat. Methods* **14**, 287-289. doi:10.1038/nmeth.4156

Arnold, S. J. and Robertson, E. J. (2009). Making a commitment: cell lineage allocation and axis patterning in the early mouse embryo. *Nat. Rev. Mol. Cell Biol.* **10**, 91-103. doi:10.1038/nrm2618

Artus, J., Panthier, J.-J. and Hadjantonakis, A.-K. (2010). A role for PDGF signaling in expansion of the extra-embryonic endoderm lineage of the mouse blastocyst. *Development* **137**, 3361-3372. doi:10.1242/dev.050864

Artus, J., Piliszek, A. and Hadjantonakis, A.-K. (2011). The primitive endoderm lineage of the mouse blastocyst: sequential transcription factor activation and regulation of differentiation by Sox17. *Dev. Biol.* **350**, 393-404. doi:10.1016/j.ydbio.2010.12.007

Artus, J., Kang, M., Cohen-Tannoudji, M. and Hadjantonakis, A.-K. (2013). PDGF signaling is required for primitive endoderm cell survival in the inner cell mass of the mouse blastocyst. *Stem Cells* **31**, 1932-1941. doi:10.1002/stem.1442

Azami, T., Waku, T., Matsumoto, K., Jeon, H., Muratani, M., Kawashima, A., Yanagisawa, J., Manabe, I., Nagai, R., Kunath, T. et al. (2017). Klf5 maintains the balance of primitive endoderm versus epiblast specification during mouse embryonic development by suppression of Fgf4. *Development* **144**, 3706-3718. doi:10.1242/dev.150755

Azami, T., Bassalert, C., Allègre, N., Valverde Estrella, L., Pouchin, P., Ema, M. and Chazaud, C. (2019). Regulation of ERK signalling pathway in the developing mouse blastocyst. *Development* **146**, dev177139. doi:10.1242/dev.177139

Balázsi, G., van Oudenaarden, A. and Collins, J. J. (2011). Cellular decision making and biological noise: from microbes to mammals. *Cell* **144**, 910-925. doi:10.1016/j.cell.2011.01.030

Barbacci, E., Reber, M., Ott, M. O., Breillat, C., Huetz, F. and Cereghini, S. (1999). Variant hepatocyte nuclear factor 1 is required for visceral endoderm specification. *Development* **126**, 4795-4805. doi:10.1242/dev.126.21.4795

Bassalert, C., Valverde-Estrella, L. and Chazaud, C. (2018). Primitive endoderm differentiation: from specification to epithelialization. *Curr. Top. Dev. Biol.* **128**, 81-104. doi:10.1016/bs.ctdb.2017.12.001

Bedzhov, I. and Zernicka-Goetz, M. (2014). Self-organizing properties of mouse pluripotent cells initiate morphogenesis upon implantation. *Cell* **156**, 1032-1044. doi:10.1016/j.cell.2014.01.023

Bedzhov, I., Leung, C. Y., Bialecka, M. and Zernicka-Goetz, M. (2014). In vitro culture of mouse blastocysts beyond the implantation stages. *Nat. Protoc.* **9**, 2732-2739. doi:10.1038/nprot.2014.186

Bessonnard, S., De Mot, L., Gonze, D., Barriol, M., Dennis, C., Goldbeter, A., Dupont, G. and Chazaud, C. (2014). Gata6, Nanog and Erk signaling control cell fate in the inner cell mass through a tristable regulatory network. *Development* **141**, 3637-3648. doi:10.1242/dev.109678

Brennan, J., Lu, C. C., Norris, D. P., Rodriguez, T. A., Beddington, R. S. P. and Robertson, E. J. (2001). Nodal signalling in the epiblast patterns the early mouse embryo. *Nature* **411**, 965-969. doi:10.1038/35082103

Brimson, C. A. (2016). *The Role of Hippo Signalling in Cell Fate Decisions in Mouse Embryonic Stem Cells and Pre-Implantation Development*.

Briscoe, J. (2019). Understanding pattern formation in embryos: experiment, theory, and simulation. *J. Comput. Biol.* **26**, 696-702. doi:10.1089/cmb.2019.0090

Burtscher, I. and Lickert, H. (2009). Foxa2 regulates polarity and epithelialization in the endoderm germ layer of the mouse embryo. *Development* **136**, 1029-1038. doi:10.1242/dev.028415

Cai, K. Q., Capo-Chichi, C. D., Rula, M. E., Yang, D.-H. and Xu, X.-X. (2008). Dynamic GATA6 expression in primitive endoderm formation and maturation in early mouse embryogenesis. *Dev. Dyn.* **237**, 2820-2829. doi:10.1002/dvdy.21703

Chazaud, C., Yamanaka, Y., Pawson, T. and Rossant, J. (2006). Early lineage segregation between epiblast and primitive endoderm in mouse blastocysts through the Grb2-MAPK pathway. *Dev. Cell* **10**, 615-624. doi:10.1016/j.devcel.2006.02.020

Cheng, S., Pei, Y., He, L., Peng, G., Reinius, B., Tam, P. P. L., Jing, N. and Deng, Q. (2019). Single-Cell RNA-seq reveals cellular heterogeneity of pluripotency transition and X chromosome dynamics during early mouse development. *Cell Rep.* **26**, 2593-2607.e3. doi:10.1016/j.celrep.2019.02.031

Cho, L. T. Y., Wamaitha, S. E., Tsai, I. J., Artus, J., Sherwood, R. I., Pedersen, R. A., Hadjantonakis, A.-K. and Niakan, K. K. (2012). Conversion from mouse embryonic to extra-embryonic endoderm stem cells reveals distinct differentiation capacities of pluripotent stem cell states. *Development* 139, 2866-2877. doi:10.1242/dev.078519

Corujo-Simon, E., Lilao-Garzon, J. and Muñoz-Descalzo, S. (2017). Wnt/B-catenin signalling facilitates cell fate decision making in the early mouse embryo. *Mech. Dev.* **145**, S159. doi:10.1016/j.mod.2017.04.453

De Caluwé, J., Tosenberger, A., Gonze, D. and Dupont, G. (2019). Signalling-modulated gene regulatory networks in early mammalian development. *J. Theor. Biol.* **463**, 56-66. doi:10.1016/j.jtbi.2018.12.008

Eden, E., Navon, R., Steinfeld, I., Lipson, D. and Yakhini, Z. (2009). GOrilla: a tool for discovery and visualization of enriched GO terms in ranked gene lists. *BMC Bioinformatics* **10**, 48. doi:10.1186/1471-2105-10-48

Edgar, R., Domrachev, M. and Lash, A. E. (2002). Gene expression omnibus: NCBI gene expression and hybridization array data repository. *Nucleic Acids Res.* **30**, 207-210. doi:10.1093/nar/30.1.207

Edgar, R., Mazor, Y., Rinon, A., Blumenthal, J., Golan, Y., Buzhor, E., Livnat, I., Ben-Ari, S., Lieder, I., Shitrit, A. et al. (2013). LifeMap discovery™: the embryonic development, stem cells, and regenerative medicine research portal. *PLoS ONE* **8**, e66629. doi:10.1371/journal.pone.0066629

Frankenberg, S., Gerbe, F., Bessonnard, S., Belville, C., Pouchin, P., Bardot, O. and Chazaud, C. (2011). Primitive endoderm differentiates via a three-step mechanism involving Nanog and RTK signaling. *Dev. Cell* **21**, 1005-1013. doi:10.1016/j.devcel.2011.10.019

Freyer, L., Schröter, C., Saiz, N., Schrode, N., Nowotschin, S., Martinez-Arias, A. and Hadjantonakis, A.-K. (2015). A loss-of-function and H2B-venus transcriptional reporter allele for Gata6 in mice. *BMC Dev. Biol.* **15**, 38. doi:10.1186/s12861-015-0086-5

Frum, T. and Ralston, A. (2015). Cell signaling and transcription factors regulating cell fate during formation of the mouse blastocyst. *Trends Genet.* **31**, 402-410. doi:10.1016/j.tig.2015.04.002

Girgin, M. U., Broguiere, N., Hoehnel, S., Brandenberg, N., Mercier, B., Arias, A. M. and Lutolf, M. P. (2021). Bioengineered embryoids mimic post-

implantation development in vitro. *Nat. Commun.* **12**, 5140. doi:10.1038/s41467-021-25237-8

Goldin, S. N. and Papaioannou, V. E. (2003). Paracrine action of FGF4 during periimplantation development maintains trophectoderm and primitive endoderm. *Genesis* **36**, 40-47. doi:10.1002/gene.10192

Goolam, M. and Zernicka-Goetz, M. (2017). The chromatin modifier Satb1 regulates cell fate through Fgf signalling in the early mouse embryo. *Development* **144**, 1450-1461. doi:10.1242/dev.144139

Grabarek, J. B., Żyżyńska, K., Saiz, N., Piliszek, A., Frankenberg, S., Nichols, J., Hadjantonakis, A.-K. and Plusa, B. (2012). Differential plasticity of epiblast and primitive endoderm precursors within the ICM of the early mouse embryo. *Development* **139**, 129-139. doi:10.1242/dev.067702

Graham, S. J. L., Wicher, K. B., Jedrusik, A., Guo, G., Herath, W., Robson, P. and Zernicka-Goetz, M. (2014). BMP signalling regulates the pre-implantation development of extra-embryonic cell lineages in the mouse embryo. *Nat. Commun.* **5**, 5667. doi:10.1038/ncomms6667

Hermitte, S. and Chazaud, C. (2014). Primitive endoderm differentiation: from specification to epithelium formation. *Philos. Trans. R. Soc. Lond. Ser. B Biol. Sci.* **369**, 20130537. doi:10.1098/rstb.2013.0537

Hiramatsu, R., Matsuoka, T., Kimura-Yoshida, C., Han, S.-W., Mochida, K., Adachi, T., Takayama, S. and Matsuo, I. (2013). External mechanical cues trigger the establishment of the anterior-posterior axis in early mouse embryos. *Dev. Cell* **27**, 131-144. doi:10.1016/j.devcel.2013.09.026

Houston, D. W. (2017). *Cell Polarity in Development and Disease*. Academic Press.

Hsu, Y.-C. (1971). Post-blastocyst differentiation in vitro. *Nature* **231**, 100-102. doi:10.1038/231100a0

Hsu, Y.-C., Baskar, J., Stevens, L. C. and Rash, J. E. (1974). Development in vitro of mouse embryos from the two-cell egg stage to the early somite stage. *J. Embryol. Exp. Morphol.* **31**, 235-245. doi:10.1242/dev.31.1.235

Hutchens, S. A., León, R. V., O'Neill, H. M. and Evans, B. R. (2007). Statistical analysis of optimal culture conditions for gluconacetobacter Hansenii cellulose production. *Lett. Appl. Microbiol.* **44**, 175-180. doi:10.1111/j.1472-765X.2006.02055.x

Illingworth, R. S., Hölzenspies, J. J., Roske, F. V., Bickmore, W. A. and Brickman, J. M. (2016). Polycomb enables primitive endoderm lineage priming in embryonic stem cells. *eLife* **5**, e14926. doi:10.7554/eLife.14926

Kang, M., Garg, V. and Hadjantonakis, A.-K. (2017). Lineage establishment and progression within the inner cell mass of the mouse blastocyst requires FGFR1 and FGFR2. *Dev. Cell* **41**, 496-510.e5. doi:10.1016/j.devcel.2017.05.003

Kim, D., Pertea, G., Trapnell, C., Pimentel, H., Kelley, R. and Salzberg, S. L. (2013). TopHat2: Accurate alignment of transcriptomes in the presence of insertions, deletions and gene fusions. *Genome Biol.* **14**, R36. doi:10.1186/gb-2013-14-4-r36

Kimura, C., Shen, M. M., Takeda, N., Aizawa, S. and Matsuo, I. (2001). Complementary functions of Otx2 and Cripto in initial patterning of mouse epiblast. *Dev. Biol.* **235**, 12-32. doi:10.1006/dbio.2001.0289

Kimura-Yoshida, C., Nakano, H., Okamura, D., Nakao, K., Yonemura, S., Belo, J. A., Aizawa, S., Matsui, Y. and Matsuo, I. (2005). Canonical Wnt signaling and its antagonist regulate anterior-posterior axis polarization by guiding cell migration in mouse visceral endoderm. *Dev. Cell* **9**, 639-650. doi:10.1016/j.devcel.2005.09.011

Kimura-Yoshida, C., Tian, E., Nakano, H., Amazaki, S., Shimokawa, K., Rossant, J., Aizawa, S. and Matsuo, I. (2007). Crucial roles of Foxa2 in mouse anterior-posterior axis polarization via regulation of anterior visceral endoderm-specific genes. *Proc. Natl. Acad. Sci. USA* **104**, 5919-5924. doi:10.1073/pnas.0607779104

Kinoshita, M., Shimosato, D., Yamane, M. and Niwa, H. (2015). Sox7 is dispensable for primitive endoderm differentiation from mouse ES cells. *BMC Dev. Biol.* **15**, 37. doi:10.1186/s12861-015-0079-4

Krawchuk, D., Honma-Yamanaka, N., Anani, S. and Yamanaka, Y. (2013). FGF4 is a limiting factor controlling the proportions of primitive endoderm and epiblast in the ICM of the mouse blastocyst. *Dev. Biol.* **384**, 65-71. doi:10.1016/j.ydbio.2013.09.023

Krawetz, R. and Kelly, G. M. (2008). Wnt6 induces the specification and epithelialization of F9 embryonal carcinoma cells to primitive endoderm. *Cell. Signal.* **20**, 506-517. doi:10.1016/j.cellsig.2007.11.001

Kruithof-de Julio, M., Alvarez, M. J., Galli, A., Chu, J., Price, S. M., Califano, A. and Shen, M. M. (2011). Regulation of extra-embryonic endoderm stem cell differentiation by Nodal and Cripto signaling. *Development* **138**, 3885-3895. doi:10.1242/dev.065656

Kubaczka, C., Senner, C., Araúzo-Bravo, M. J., Sharma, N., Kuckenberg, P., Becker, A., Zimmer, A., Brüstle, O., Peitz, M., Hemberger, M. et al. (2014). Derivation and maintenance of murine trophoblast stem cells under defined conditions. *Stem Cell Rep.* **2**, 232-242. doi:10.1016/j.stemcr.2013.12.013

Lamprecht, M. R., Sabatini, D. M. and Carpenter, A. E. (2007). CellProfiler™: free, versatile software for automated biological image analysis. *BioTechniques* **42**, 71-75. doi:10.2144/000112257

Lavial, F., Bessonnard, S., Ohnishi, Y., Tsumura, A., Chandrashekran, A., Fenwick, M. A., Tomaz, R. A., Hosokawa, H., Nakayama, T., Chambers, I. et al. (2012). Bmi1 facilitates primitive endoderm formation by stabilizing Gata6 during early mouse development. *Genes Dev.* **26**, 1445-1458. doi:10.1101/gad.188193.112

Li, S., Edgar, D., Fässler, R., Wadsworth, W. and Yurchenco, P. D. (2003). The role of laminin in embryonic cell polarization and tissue organization. *Dev. Cell* **4**, 613-624. doi:10.1016/S1534-5807(03)00128-X

Lin, J., Khan, M., Zapiec, B. and Mombaerts, P. (2016). Efficient derivation of extraembryonic endoderm stem cell lines from mouse postimplantation embryos. *Sci. Rep.* **6**, 39457. doi:10.1038/srep39457

Lo Nigro, A., de Jaime-Soguero, A., Khoueiry, R., Cho, D. S., Ferlazzo, G. M., Perini, I., Abon Escalona, V., Aranguren, X. L., Chuva de Sousa Lopes, S. M., Koh, K. P. et al. (2017). PDGFRα cells in embryonic stem cell cultures represent the in vitro equivalent of the pre-implantation primitive endoderm precursors. *Stem Cell Rep.* **8**, 318-333. doi:10.1016/j.stemcr.2016.12.010

Lokken, A. A. and Ralston, A. (2016). The genetic regulation of cell fate during preimplantation mouse development. *Curr. Top. Dev. Biol.* **120**, 173-202. doi:10.1016/bs.ctdb.2016.04.006

Markodimitraki, C. M., Rang, F. J., Rooijers, K., de Vries, S. S., Chialastri, A., de Luca, K. L., Lochs, S. J. A., Mooijman, D., Dey, S. S. and Kind, J. (2020). Simultaneous quantification of protein–DNA interactions and transcriptomes in single cells with scDam&T-Seq. *Nat. Protoc.* **15**, 1922-1953. doi:10.1038/s41596-020-0314-8

Mathew, B., Muñoz-Descalzo, S., Corujo-Simon, E., Schröter, C., Stelzer, E. H. K. and Fischer, S. C. (2019). Mouse ICM organoids reveal three-dimensional cell fate clustering. *Biophys. J.* **116**, 127-141. doi:10.1016/j.bpj.2018.11.011

Mauri, M., Elli, T., Caviglia, G., Uboldi, G. and Azzi, M. (2017). RAWGraphs: A Visualisation Platform to Create Open Outputs. In Proceedings of the 12th Biannual Conference on Italian SIGCHI Chapter, Vol. 28, pp. 1-5. https://doi.org/10.1145/3125571.3125585

Meilhac, S. M., Adams, R. J., Morris, S. A., Danckaert, A., Le Garrec, J.-F. and Zernicka-Goetz, M. (2009). Active cell movements coupled to positional induction are involved in lineage segregation in the mouse blastocyst. *Dev. Biol.* **331**, 210-221. doi:10.1016/j.ydbio.2009.04.036

Meng, Y., Moore, R., Tao, W., Smith, E. R., Tse, J. D., Caslini, C. and Xu, X.-X. (2018). GATA6 Phosphorylation by Erk1/2 propels exit from pluripotency and commitment to primitive endoderm. *Dev. Biol.* **436**, 55-65. doi:10.1016/j.ydbio.2018.02.007

Mesnard, D., Guzman-Ayala, M. and Constam, D. B. (2006). Nodal specifies embryonic visceral endoderm and sustains pluripotent cells in the epiblast before overt axial patterning. *Development* **133**, 2497-2505. doi:10.1242/dev.02413

Minegishi, K., Hashimoto, M., Ajima, R., Takaoka, K., Shinohara, K., Ikawa, Y., Nishimura, H., McMahon, A. P., Willert, K., Okada, Y. et al. (2017). A Wnt5 activity asymmetry and intercellular signaling via PCP proteins polarize node cells for left-right symmetry breaking. *Dev. Cell* **40**, 439-52.e4. doi:10.1016/j.devcel.2017.02.010

Miner, J. H. and Yurchenco, P. D. (2004). Laminin functions in tissue morphogenesis. *Annu. Rev. Cell Dev. Biol.* **20**, 255-284. doi:10.1146/annurev.cellbio.20.010403.094555

Mohammed, H., Hernando-Herraez, I., Savino, A., Scialdone, A., Macaulay, I., Mulas, C., Chandra, T., Voet, T., Dean, W., Nichols, J. et al. (2017). Single-cell landscape of transcriptional heterogeneity and cell fate decisions during mouse early gastrulation. *Cell Rep.* **20**, 1215-1228. doi:10.1016/j.celrep.2017.07.009

Molotkov, A. and Soriano, P. (2018). Distinct mechanisms for PDGF and FGF signaling in primitive endoderm development. *Dev. Biol.* **442**, 155-161. doi:10.1016/j.ydbio.2018.07.010

Molotkov, A., Mazot, P., Brewer, J. R., Cinalli, R. M. and Soriano, P. (2017). Distinct requirements for FGFR1 and FGFR2 in primitive endoderm development and exit from pluripotency. *Dev. Cell* **41**, 511-26.e4. doi:10.1016/j.devcel.2017.05.004

Moore, R., Tao, W., Smith, E. R. and Xu, X.-X. (2014). The primitive endoderm segregates from the epiblast in β1 integrin-deficient early mouse embryos. *Mol. Cell. Biol.* **34**, 560-572. doi:10.1128/MCB.00937-13

Morgani, S. M. and Brickman, J. M. (2015). LIF supports primitive endoderm expansion during pre-implantation development. *Development* **142**, 3488-3499. doi:10.1242/dev.125021

Morrisey, E. E., Tang, Z., Sigrist, K., Lu, M. M., Jiang, F., Ip, H. S. and Parmacek, M. S. (1998). GATA6 regulates HNF4 and is required for differentiation of visceral endoderm in the mouse embryo. *Genes Dev.* **12**, 3579-3590. doi:10.1101/gad.12.22.3579

Mulvey, C. M., Schröter, C., Gatto, L., Dikicioglu, D., Fidaner, I. B., Christoforou, A., Deery, M. J., Cho, L. T. Y., Niakan, K. K., Martinez-Arias, A. et al. (2015). Dynamic proteomic profiling of extra-embryonic endoderm differentiation in mouse embryonic stem cells. *Stem Cells* **33**, 2712-2725. doi:10.1002/stem.2067

Muraro, M. J., Dharmadhikari, G., Grün, D., Groen, N., Dielen, T., Jansen, E., van Gurp, L., Engelse, M. A., Carlotti, F., de Koning, E. J. P. et al. (2016). A single-cell transcriptome atlas of the human pancreas. *Cell Systems* **3**, 385-94.e3. doi:10.1016/j.cels.2016.09.002

Neagu, A., van Genderen, E., Escudero, I., Verwegen, L., Kurek, D., Lehmann, J., Stel, J., Dirks, R. A. M., van Mierlo, G., Maas, A. et al. (2020). In vitro capture

and characterization of embryonic rosette-stage pluripotency between naive and primed states. *Nat. Cell Biol.* **22**, 534-545. doi:10.1038/s41556-020-0508-x

Ngondo, R. P., Cirera-Salinas, D., Yu, J., Wischnewski, H., Bodak, M., Vandormael-Pournin, S., Geiselmann, A., Wettstein, R., Luitz, J., Cohen-Tannoudji, M. et al. (2018). Argonaute 2 is required for extra-embryonic endoderm differentiation of mouse embryonic stem cells. *Stem Cell Rep.* **10**, 461-476. doi:10.1016/j.stemcr.2017.12.023

Niakan, K. K., Schrode, N., Cho, L. T. Y. and Hadjantonakis, A.-K. (2013). Derivation of extraembryonic endoderm stem (XEN) cells from mouse embryos and embryonic stem cells. *Nat. Protoc.* **8**, 1028-1041. doi:10.1038/nprot.2013.049

Nichols, J., Silva, J., Roode, M. and Smith, A. (2009). Suppression of Erk signalling promotes ground state pluripotency in the mouse embryo. *Development* **136**, 3215-3222. doi:10.1242/dev.038893

Niwa, H., Toyooka, Y., Shimosato, D., Strumpf, D., Takahashi, K., Yagi, R. and Rossant, J. (2005). Interaction between Oct3/4 and Cdx2 determines trophectoderm differentiation. *Cell* **123**, 917-929. doi:10.1016/j.cell.2005.08.040

Nowotschin, S., Setty, M., Kuo, Y.-Y., Liu, V., Garg, V., Sharma, R., Simon, C. S., Saiz, N., Gardner, R., Boutet, S. C. et al. (2019). The emergent landscape of the mouse gut endoderm at single-cell resolution. *Nature* **569**, 361-367. doi:10.1038/s41586-019-1127-1

Ohnishi, Y., Huber, W., Tsumura, A., Kang, M., Xenopoulos, P., Kurimoto, K., Oleś, A. K., Araúzo-Bravo, M. J., Saitou, M., Hadjantonakis, A.-K. et al. (2014). Cell-to-cell expression variability followed by signal reinforcement progressively segregates early mouse lineages. *Nat. Cell Biol.* **16**, 27-37. doi:10.1038/ncb2881

Olson, E. N. (2006). Gene regulatory networks in the evolution and development of the heart. *Science* **313**, 1922-1927. doi:10.1126/science.1132292

Onishi, K. and Zandstra, P. W. (2015). LIF signaling in stem cells and development. *Development* **142**, 2230-2236. doi:10.1242/dev.117598

Paca, A., Séguin, C. A., Clements, M., Ryczko, M., Rossant, J., Rodriguez, T. A. and Kunath, T. (2012). BMP signaling induces visceral endoderm differentiation of XEN cells and parietal endoderm. *Dev. Biol.* **361**, 90-102. doi:10.1016/j.ydbio.2011.10.013

Papanayotou, C. and Collignon, J. (2014). Activin/Nodal signalling before implantation: setting the stage for embryo patterning. *Philos. Trans. R. Soc. Lond. Ser. B Biol. Sci.* **369**, 20130539. doi:10.1098/rstb.2013.0539

Perea-Gomez, A., Lawson, K. A., Rhinn, M., Zakin, L., Brulet, P., Mazan, S. and Ang, S. L. (2001). Otx2 is required for visceral endoderm movement and for the restriction of posterior signals in the epiblast of the mouse embryo. *Development* **128**, 753-765. doi:10.1242/dev.128.5.753

Pfister, S., Steiner, K. A. and Tam, P. P. L. (2007). Gene expression pattern and progression of embryogenesis in the immediate post-implantation period of mouse development. *Gene Expr. Patterns* **7**, 558-573. doi:10.1016/j.modgep.2007.01.005

Pijuan-Sala, B., Griffiths, J. A., Guibentif, C., Hiscock, T. W., Jawaid, W., Calero-Nieto, F. J., Mulas, C., Ibarra-Soria, X., Tyser, R. C. V., Ho, D. L. L. et al. (2019). A single-cell molecular map of mouse gastrulation and early organogenesis. *Nature* **566**, 490-495. doi:10.1038/s41586-019-0933-9

Plusa, B. and Hadjantonakis, A.-K. (2018). (De)constructing the blastocyst: lessons in self-organization from the mouse. *Curr. Opin. Syst. Biol.* **11**, 98-106. doi:10.1016/j.coisb.2018.08.002

Plusa, B., Piliszek, A., Frankenberg, S., Artus, J. and Hadjantonakis, A.-K. (2008). Distinct sequential cell behaviours direct primitive endoderm formation in the mouse blastocyst. *Development* **135**, 3081-3091. doi:10.1242/dev.021519

Posfai, E., Petropoulos, S., Oliveira de Barros, F. R., Schell, J. P., Jurisica, I., Sandberg, R., Lanner, F. and Rossant, J. (2017). Position- and Hippo signaling-dependent plasticity during lineage segregation in the early mouse embryo. *eLife* **6**, e22906. doi:10.7554/eLife.22906

Posfai, E., Schell, J. P., Janiszewski, A., Rovic, I., Murray, A., Bradshaw, B., Yamakawa, T., Pardon, T., El Bakkali, M., Talon, I. et al. (2021). Evaluating totipotency using criteria of increasing stringency. *Nat. Cell Biol.* **23**, 49-60. doi:10.1038/s41556-020-00609-2

Price, F. D., Yin, H., Jones, A., van Ijcken, W., Grosveld, F. and Rudnicki, M. A. (2013). Canonical Wnt signaling induces a primitive endoderm metastable state in mouse embryonic stem cells. *Stem Cells* **31**, 752-764. doi:10.1002/stem.1321

Qu, X.-B., Pan, J., Zhang, C. and Huang, S.-Y. (2008). Sox17 facilitates the differentiation of mouse embryonic stem cells into primitive and definitive endoderm in vitro. *Dev. Growth Differ.* **50**, 585-593. doi:10.1111/j.1440-169X.2008.01056.x

Raina, D., Bahadori, A., Stanoev, A., Protzek, M., Koseska, A. and Schröter, C. (2020). Cell-Cell Communication through FGF4 Generates and Maintains Robust Proportions of Differentiated Cell Types in Embryonic Stem Cells. *Development* 148, dev199926. doi:10.1101/2020.02.14.949701

Rivera-Pérez, J. A. and Magnuson, T. (2005). Primitive streak formation in mice is preceded by localized activation of Brachyury and Wnt3. *Dev. Biol.* **288**, 363-371. doi:10.1016/j.ydbio.2005.09.012

Rivron, N. (2018). Formation of blastoids from mouse embryonic and trophoblast stem cells. *Nature* **557**, 106-111. doi:10.1038/protex.2018.051

Rivron, N. C., Frias-Aldeguer, J., Vrij, E. J., Boisset, J.-C., Korving, J., Vivié, J., Truckenmüller, R. K., van Oudenaarden, A., van Blitterswijk, C. A. and Geijsen, N. (2018a). Blastocyst-like structures generated solely from stem cells. *Nature* **557**, 106-111. doi:10.1038/s41586-018-0051-0

Rivron, N., Pera, M., Rossant, J., Martinez Arias, A., Zernicka-Goetz, M., Fu, J., van den Brink, S., Bredenoord, A., Dondorp, W., de Wert, G. et al. (2018b). Debate ethics of embryo models from stem cells. *Nature* **564**, 183-185. doi:10.1038/d41586-018-07663-9

Rodriguez, T. A., Srinivas, S., Clements, M. P., Smith, J. C. and Beddington, R. S. P. (2005). Induction and migration of the anterior visceral endoderm is regulated by the extra-embryonic ectoderm. *Development* **132**, 2513-2520. doi:10.1242/dev.01847

Rossant, J. and Tam, P. P. L. (2009). Blastocyst lineage formation, early embryonic asymmetries and axis patterning in the mouse. *Development* **136**, 701-713. doi:10.1242/dev.017178

Saiz, N., Grabarek, J. B., Sabherwal, N., Papalopulu, N. and Plusa, B. (2013). Atypical protein kinase C couples cell sorting with primitive endoderm maturation in the mouse blastocyst. *Development* **140**, 4311-4322. doi:10.1242/dev.093922

Saiz, N., Williams, K. M., Seshan, V. E. and Hadjantonakis, A.-K. (2016). Asynchronous fate decisions by single cells collectively ensure consistent lineage composition in the mouse blastocyst. *Nat. Commun.* **7**, 13463. doi:10.1038/ncomms13463

Saiz, N., Mora-Bitria, L., Rahman, S., George, H., Herder, J. P., Garcia-Ojalvo, J. and Hadjantonakis, A.-K. (2020). Growth-factor-mediated coupling between lineage size and cell fate choice underlies robustness of mammalian development. *eLife* **9**, e56079 . doi:10.7554/eLife.56079

Salamat, M., Miosge, N. and Herken, R. (1995). Development of Reichert's membrane in the early mouse embryo. *Anat. Embryol.* **192**, 275-281. doi:10.1007/BF00184752

Schrode, N., Saiz, N., Di Talia, S. and Hadjantonakis, A.-K. (2014). GATA6 levels modulate primitive endoderm cell fate choice and timing in the mouse blastocyst. *Dev. Cell* **29**, 454-467. doi:10.1016/j.devcel.2014.04.011

Schröter, C., Rué, P., Mackenzie, J. P. and Martinez Arias, A. (2015). FGF/MAPK signaling sets the switching threshold of a bistable circuit controlling cell fate decisions in embryonic stem cells. *Development* **142**, 4205-4216. doi:10.1101/015404

Semrau, S., Goldmann, J. E., Soumillon, M., Mikkelsen, T. S., Jaenisch, R. and van Oudenaarden, A. (2017). Dynamics of lineage commitment revealed by single-cell transcriptomics of differentiating embryonic stem cells. *Nat. Commun.* **8**, 1096. doi:10.1038/s41467-017-01076-4

Shahbazi, M. N., Scialdone, A., Skorupska, N., Weberling, A., Recher, G., Zhu, M., Jedrusik, A., Devito, L. G., Noli, L., Macaulay, I. C. et al. (2017). Pluripotent state transitions coordinate morphogenesis in mouse and human embryos. *Nature* **552**, 239-243. doi:10.1038/nature24675

Smyth, N., Vatansever, H. S., Murray, P., Meyer, M., Frie, C., Paulsson, M. and Edgar, D. (1999). Absence of basement membranes after targeting the LAMC1 gene results in embryonic lethality due to failure of endoderm differentiation. *J. Cell Biol.* **144**, 151-160. doi:10.1083/jcb.144.1.151

Sozen, B., Cox, A. L., De Jonghe, J., Bao, M., Hollfelder, F., Glover, D. M. and Zernicka-Goetz, M. (2019). Self-organization of mouse stem cells into an extended potential blastoid. *Dev. Cell* **51**, 698-712.e8. doi:10.1016/j.devcel.2019.11.014

Stephenson, R. O., Rossant, J. and Tam, P. P. L. (2012). Intercellular interactions, position, and polarity in establishing blastocyst cell lineages and embryonic axes. *Cold Spring Harbor Perspect. Biol.* **4**, a008235. doi:10.1101/cshperspect.a008235

Stuart, T., Butler, A., Hoffman, P., Hafemeister, C., Papalexi, E., Mauck, W. M., Hao, Y., Stoeckius, M., Smibert, P. and Satija, R. (2019). Comprehensive integration of single-cell data. *Cell* **177**, 1888-1902.e21. doi:10.1016/j.cell.2019.05.031

Suwińska, A., Czołowska, R., Ożdżeński, W. and Tarkowski, A. K. (2008). Blastomeres of the mouse embryo lose totipotency after the fifth cleavage division: expression of Cdx2 and Oct4 and developmental potential of inner and outer blastomeres of 16- and 32-cell embryos. *Dev. Biol.* **322**, 133-144. doi:10.1016/j.ydbio.2008.07.019

Tarkowski, A. K., Suwińska, A., Czołowska, R. and Ożdżeński, W. (2010). Individual blastomeres of 16- and 32-cell mouse embryos are able to develop into foetuses and mice. *Dev. Biol.* **348**, 190-198. doi:10.1016/j.ydbio.2010.09.022

ten Berge, D., Kurek, D., Blauwkamp, T., Koole, W., Maas, A., Eroglu, E., Siu, R. K. and Nusse, R. (2011). Embryonic stem cells require Wnt proteins to prevent differentiation to epiblast stem cells. *Nat. Cell Biol.* **13**, 1070-1075. doi:10.1038/ncb2314

Tortelote, G. G., Manuel Hernández-Hernández, J., Quaresma, A. J. C., Nickerson, J. A., Imbalzano, A. N. and Rivera-Pérez, J. A. (2013). Wnt3 function in the epiblast is required for the maintenance but not the initiation of gastrulation in mice. *Dev. Biol.* **374**, 164-173. doi:10.1016/j.ydbio.2012.10.013

Vrij, E. J., Espinoza, S., Heilig, M., Kolew, A., Schneider, M., van Blitterswijk, C. A., Truckenmüller, R. K. and Rivron, N. C. (2016a). 3D high throughput screening and profiling of embryoid bodies in thermoformed microwell plates. *Lab. Chip* **16**, 734-742. doi:10.1039/C5LC01499A

Vrij, E., Rouwkema, J., LaPointe, V., van Blitterswijk, C., Truckenmüller, R. and Rivron, N. (2016b). Directed assembly and development of material-free tissues

with complex architectures. *Adv. Mater.* **28**, 4032-4039. doi:10.1002/adma.201505723

Wang, Q. T., Piotrowska, K., Ciemerych, M. A., Milenkovic, L., Scott, M. P., Davis, R. W. and Zernicka-Goetz, M. (2004). A genome-wide study of gene activity reveals developmental signaling pathways in the preimplantation mouse embryo. *Dev. Cell* **6**, 133-144. doi:10.1016/S1534-5807(03)00404-0

Wang, Y., Smedberg, J. L., Cai, K. Q., Capo-Chichi, D. C. and Xu, X.-X. (2010). Ectopic expression of GATA6 bypasses requirement for Grb2 in primitive endoderm formation. *Dev. Dyn.* **240**, 566-576. doi:10.1002/dvdy.22447

Weinreb, C., Wolock, S. and Klein, A. (2018). SPRING: a kinetic interface for visualizing high dimensional single-cell expression data. *Bioinformatics* **34**, 1246-1248. doi:10.1093/bioinformatics/btx792

Wicklow, E., Blij, S., Frum, T., Hirate, Y., Lang, R. A., Sasaki, H. and Ralston, A. (2014). HIPPO pathway members restrict SOX2 to the inner cell mass where it promotes ICM fates in the mouse blastocyst. *PLoS Genet.* **10**, e1004618. doi:10.1371/journal.pgen.1004618

Wigger, M., Kisielewska, K., Filimonow, K., Plusa, B., Maleszewski, M. and Suwińska, A. (2017). plasticity of the inner cell mass in mouse blastocyst is restricted by the activity of FGF/MAPK pathway. *Sci. Rep.* **7**, 15136. doi:10.1038/s41598-017-15427-0

Yamanaka, Y., Lanner, F. and Rossant, J. (2010). FGF signal-dependent segregation of primitive endoderm and epiblast in the mouse blastocyst. *Development* **137**, 715-724. doi:10.1242/dev.043471

Ying, Q.-L., Wray, J., Nichols, J., Batlle-Morera, L., Doble, B., Woodgett, J., Cohen, P. and Smith, A. (2008). The ground state of embryonic stem cell self-renewal. *Nature* **453**, 519-523. doi:10.1038/nature06968

Zhong, Y. and Binas, B. (2019). Transcriptome analysis shows ambiguous phenotypes of murine primitive endoderm-related stem cell lines. *Genes Cells* **24**, 324-331. doi:10.1111/gtc.12678

Zuniga, A. (2015). Next generation limb development and evolution: old questions, new perspectives. *Development* **142**, 3810-3820. doi:10.1242/dev.125757

S1

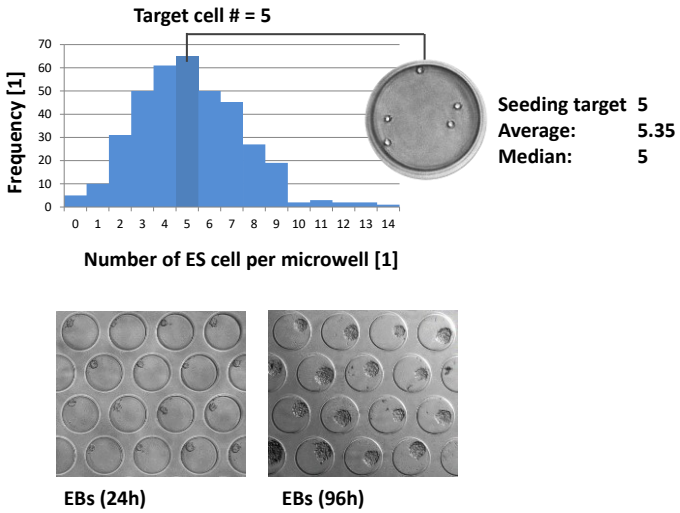

Fig. S1. Distribution of ESC numbers within microwells with a target seeding number of 7 cells per microwell (top). Brightfield images of EBs at 24 and 96 h of culture.

S2

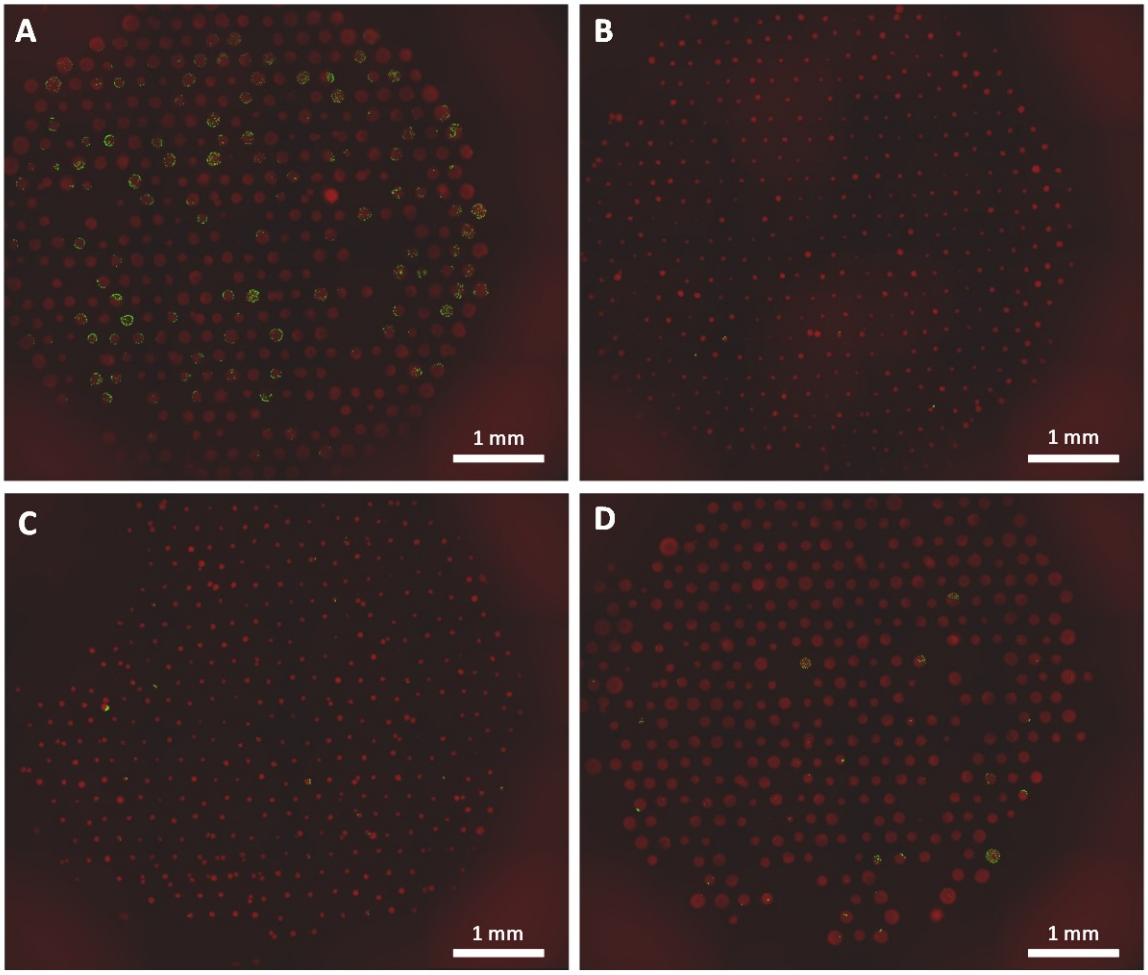

Fig. S2. Fluorescent montage images of EB cultures within hydrogel microwell screening arrays. Red color depicts the projection area of EBs identified by nuclear staining (Dapi). Green color depicts Pdgfra-h2b-gfp reporter expression.

A) B27N2 2i/lif expansion followed by serum/lif EB culture.
B) B27N2 2i/lif expansion followed by B27N2/lif EB culture.
C) Serum/lif expansion on mEF followed by B27N2/lif EB culture.
D) Serum/lif expansion on mEF followed by serum/lif EB culture.

S3A

Combinatorial screening for serum-free differentiation into primitive endoderm.

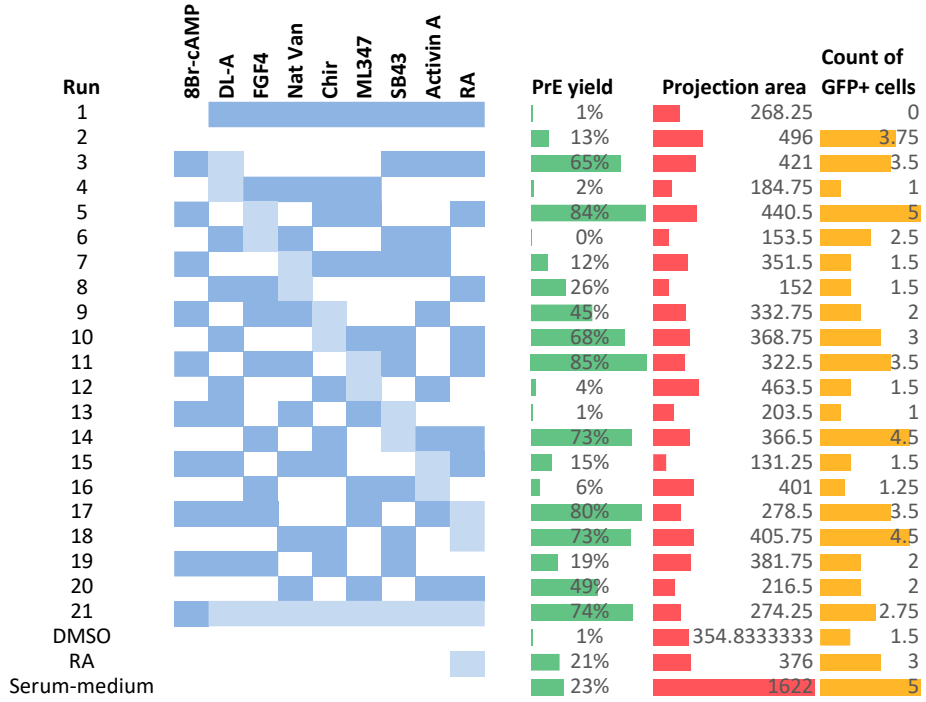

Fig. S3A. Experimental layout of Definitive Screening Design and the results of factor combinations on the yield of PrE-differentiation in EBs (PrE-yield), EB projection area (Projection area) and count of GFP+ cells per EB on selected Z plane (Count of GFP+ cells). In contrast to all other conditions, Serum-medium includes 10% FBS.

S3B

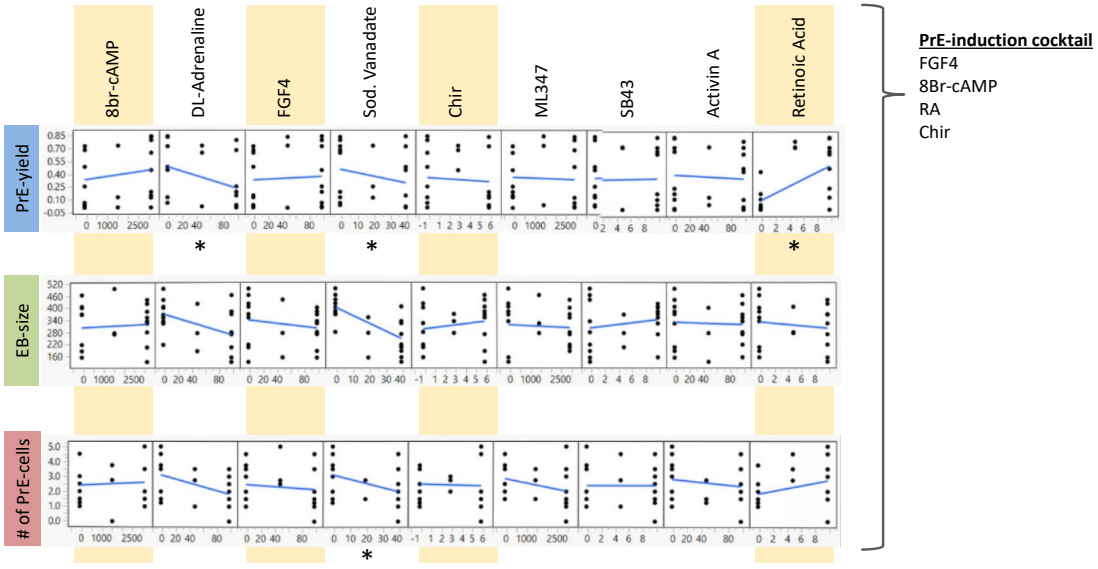

Fig. S3B. Main effect plots for the 9 factors in the combinatorial definitive screening design (DSD) assay shows a positive correlation with PrE-yield for 8Br-cAMP, FGF4 and RA, a positive correlation with EB projection area (EB-size) for CHIR99021 (Chir), SB43 and 8Br-cAMP, and a positive correlation with the number of PrE+ cells for RA. All conditions were supplemented with Lif and β-mercaptoethanol. Asterisks indicate statistical significance. Yellow-marked compounds; FGF4, 8Br-cAMP, RA and chir were selected for final induction cocktail.

S3C

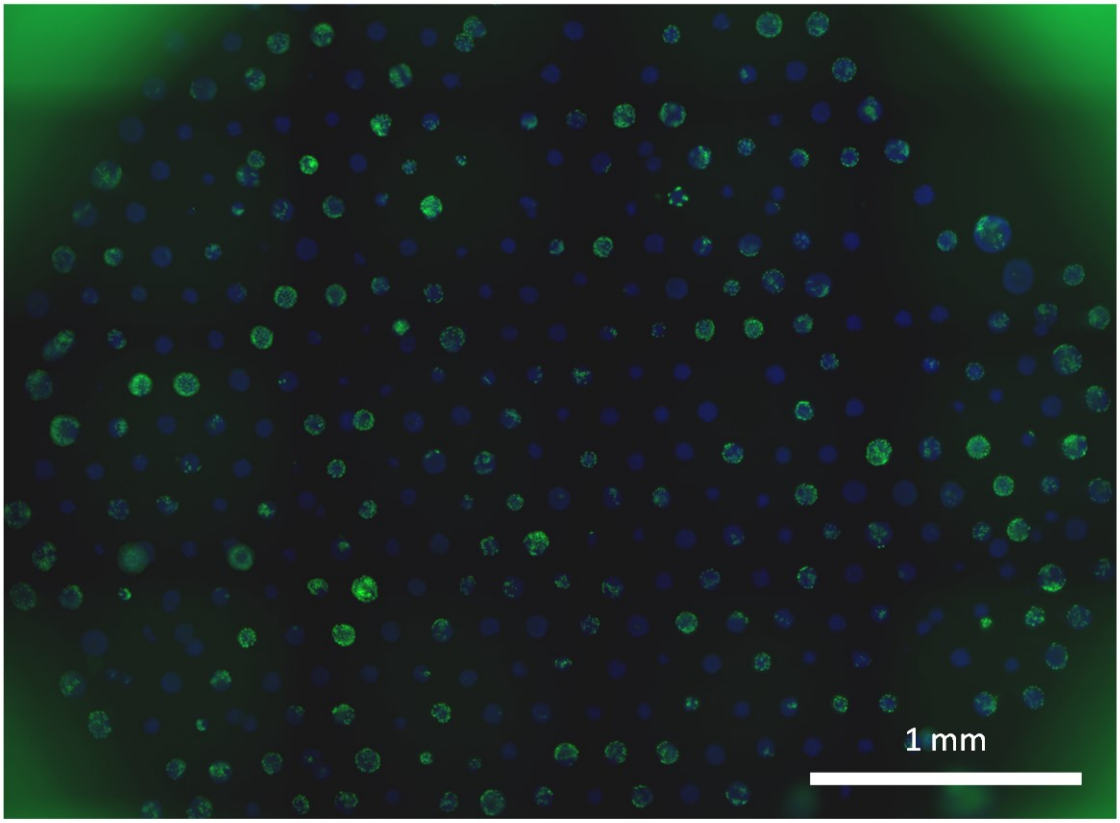

Fig. S3C. Cropped fluorescent montage image of EB cultures within a single well of a 96-wellplate that was induced for primitive endoderm differentiation using the PrE-induction cocktail (image readout at 96 hours of EB culture). Blue color indicates labelling of cell nuclei (Dapi). Green color depicts Pdgfra-h2b-gfp reporter expression.

S4

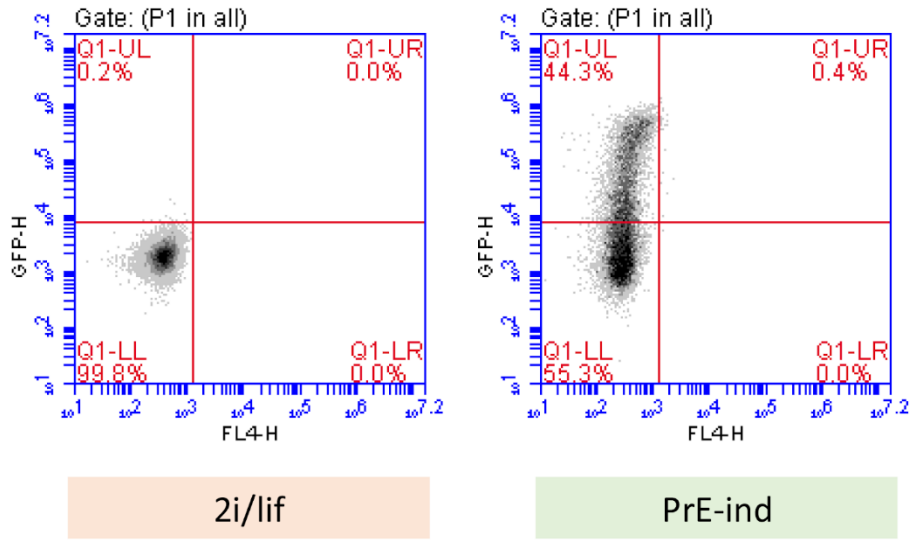

Fig. S4. Bulk flow cytometry shows that after 72 hours of PrE-induction 55.3% of cells is Gata6-h2b-Venus negative and 44.7% of cells is Gata6-h2b-Venus positive, compared to 2i/lif expanded cells that show 99.8% of cells gata6-h2b-Venus negative. The PrE-induction cocktail included 8Br-cAMP, RA, Fgf4, CHIR99021 (Chir) and Lif. 5 wells with each 430 EBs were pooled and dissociated.

S5

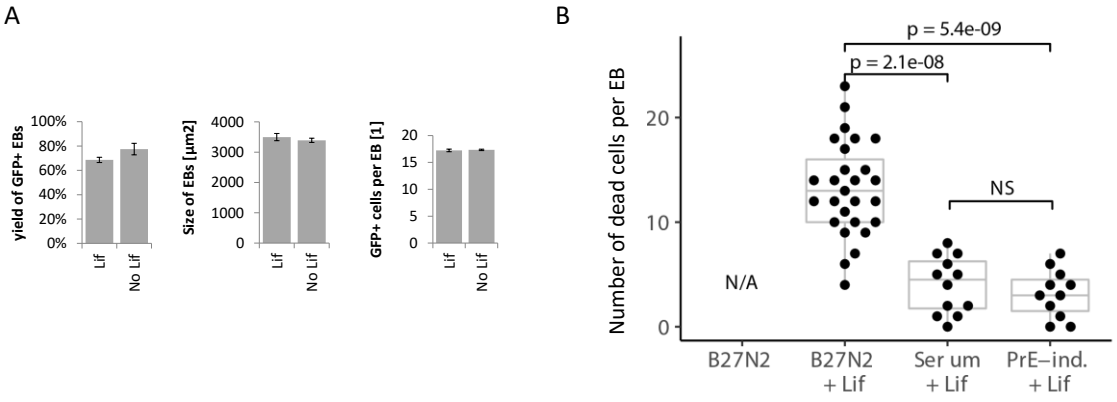

Fig. S5.A) Yield of Pdgfrα++ EBs, size of EBs and number of Pdgfrα+ cells per EB with the PrE induction cocktail with and without Lif.

B) B) Cell viability assay; quantifying the number of dead cells (Ethidium homodimer-positive cells) per EB comparer for standard per EB after culture in the different media: serum-free B27N2 without and with Lif, serum with Lif, and the PrE-induction cocktail including Lif. EB culture Serum + Lif and serum-free B27N2 minus Lif, with Lif and with PrE-induction cocktail including Lif.

S6

24 hours after induction

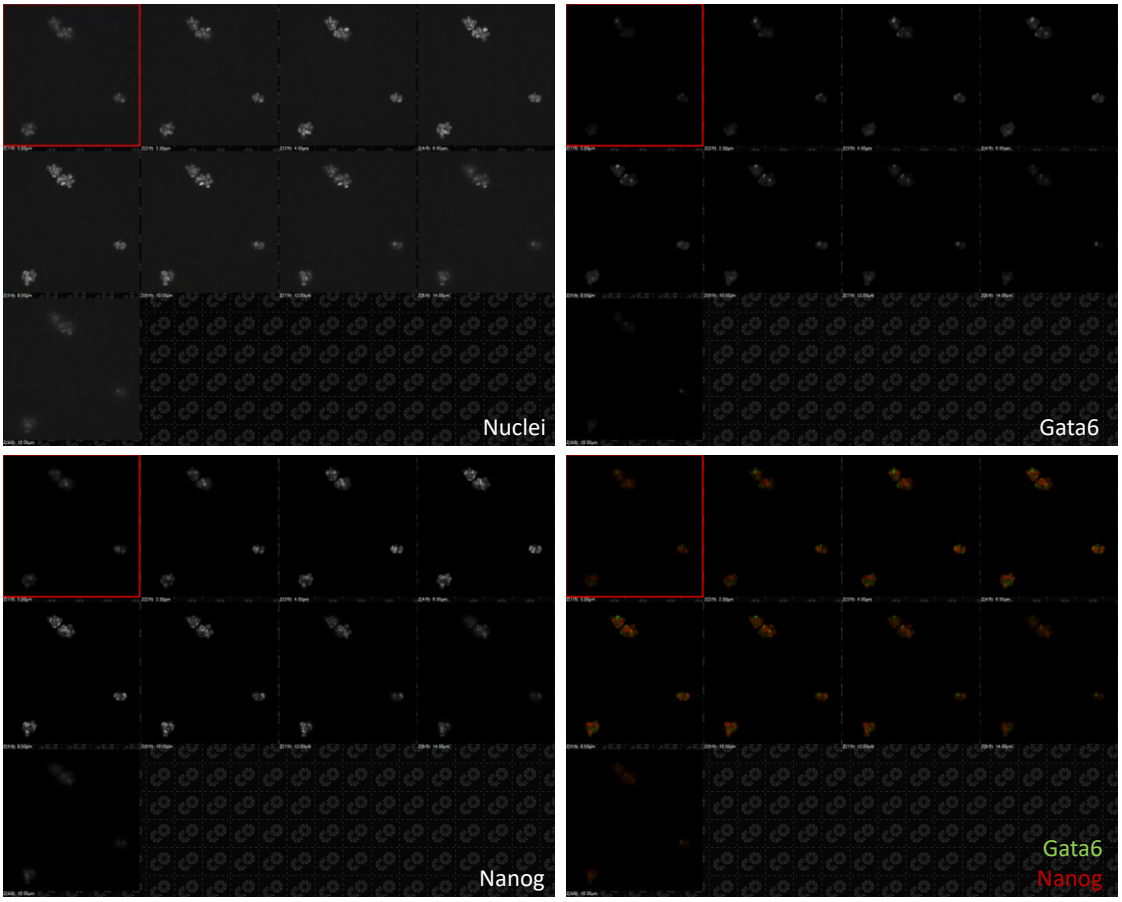

48 hours after induction

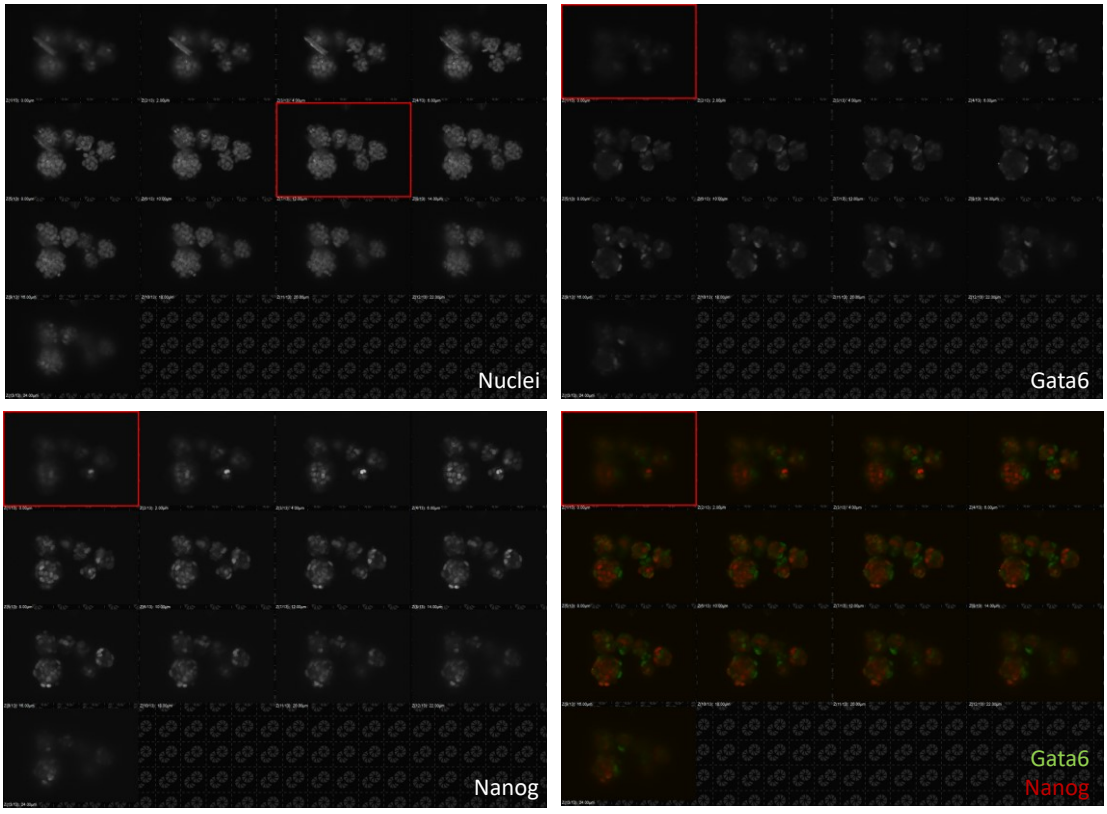

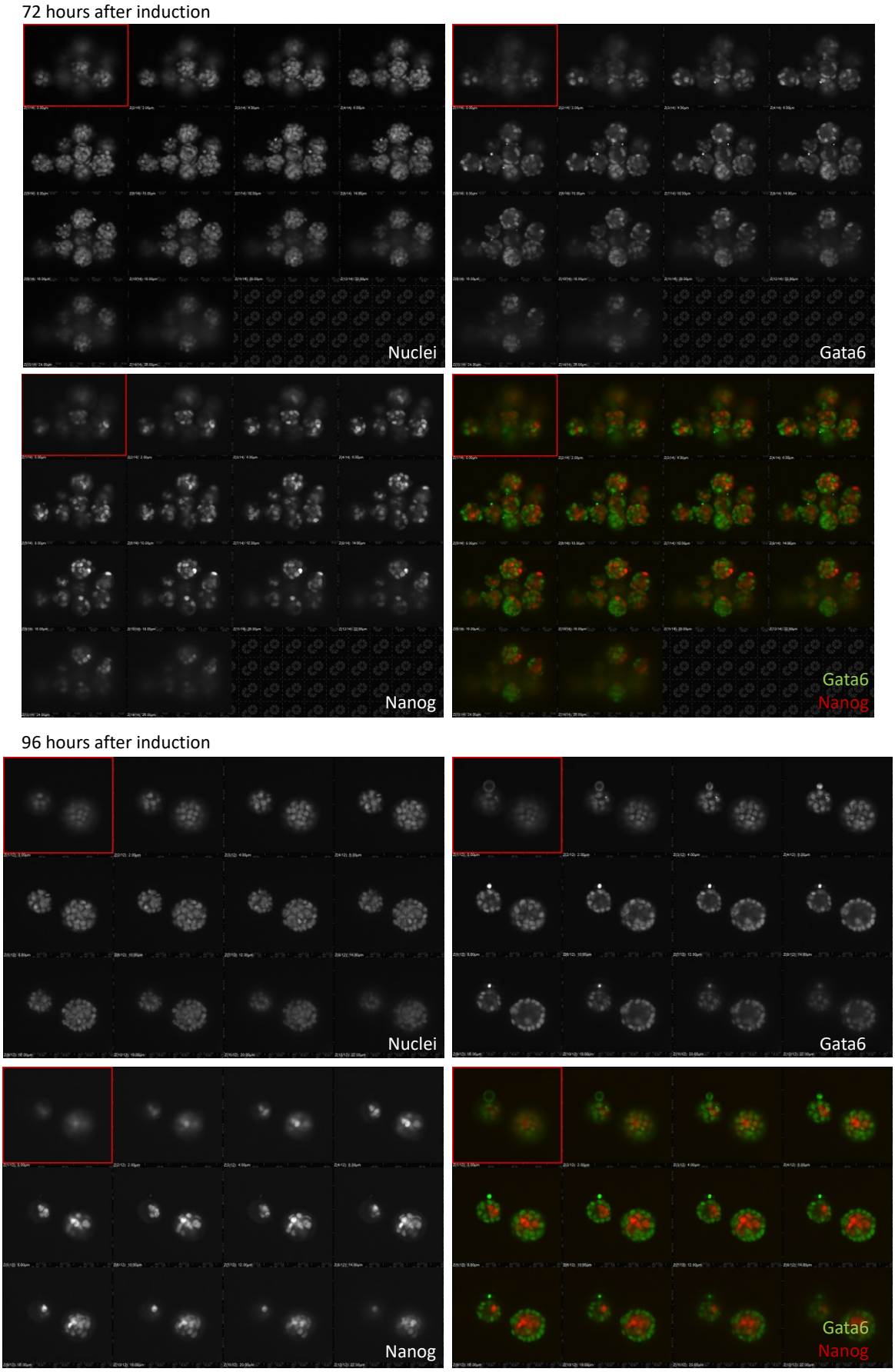

Fig. S6. Z-stack tiles showing Gata6 and Nanog immunofluorescence in PrE-induced ESC aggregates over time.

S7

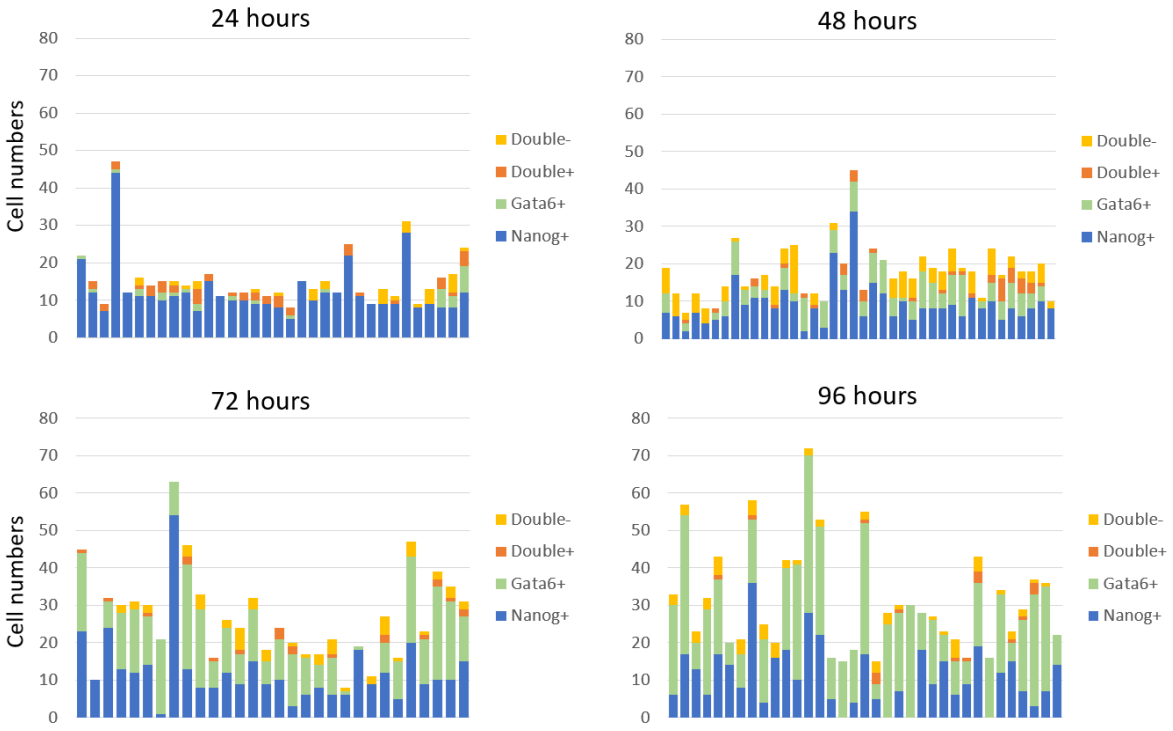

Fig. S7A. Number of cells in PrE/Epi-induced structures with Gata6+, Nanog+, double+ or double- protein expression over time. Cells were labelled using antibody staining.

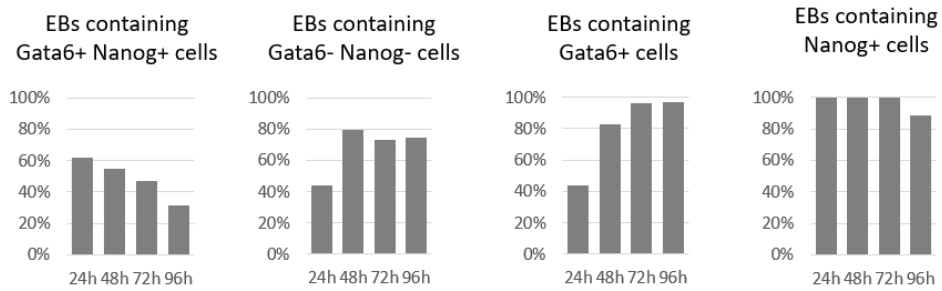

Fig. S7B. Percentages of EBs containing cells with Gata6+ and Nanog+, no Gata6 and Nanog (Gata6- and Nanog-), Gata6+, and Nanog+ protein expression over time.

S8

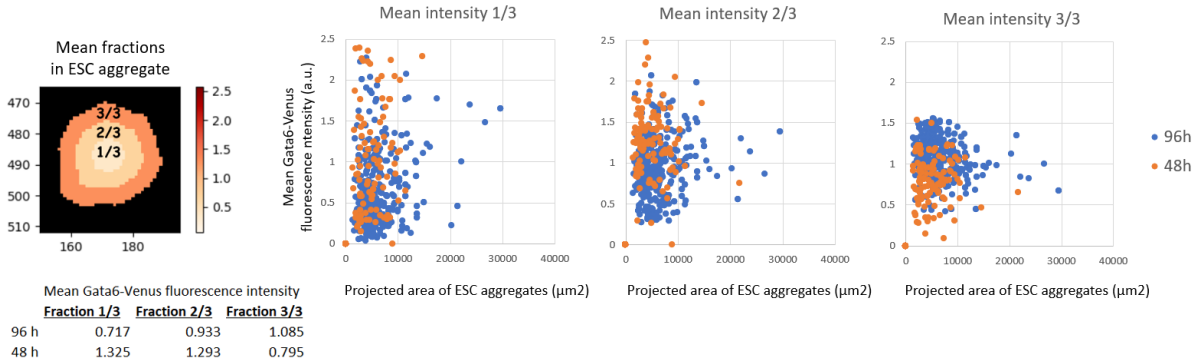

Mean Gata6-Venus fluorescence intensity

	Fraction 1/3	Fraction 2/3	Fraction 3/3
96 h	0.717	0.933	1.085
48 h	1.325	1.293	0.795

Fig. S8. The mean fluorescence intensity of Gata6-Venus expression was measured in three radial fractions of PrE-induced ESC aggregates as a function of the total projected area (size) per aggregate at 48 and 96 hours after induction.

S9

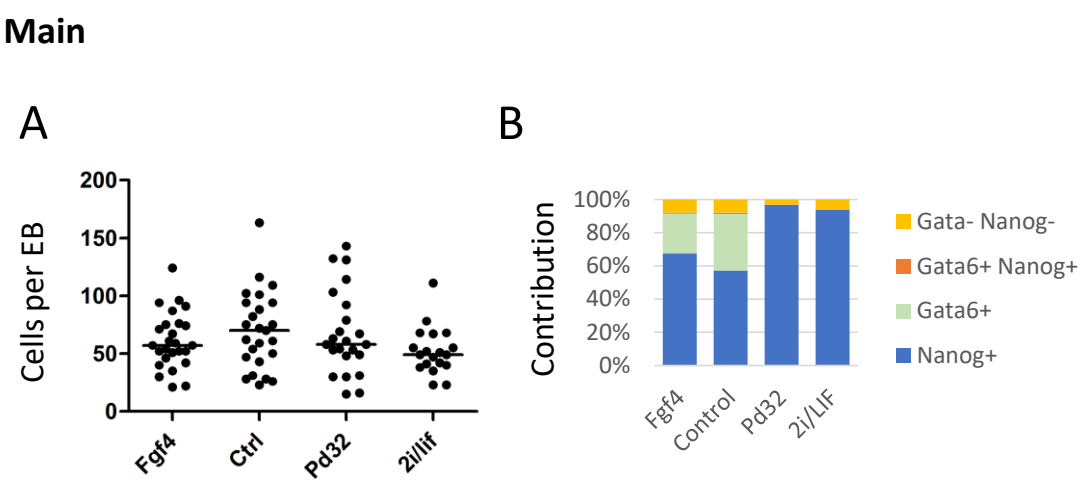

Fig. S9. Fgf4/mapk signalling was hyperactivated through the addition of 500 ng/ml Fgf4 or inhibited by addition of 2i/lif in PrE-induced ESC aggregates till 96 hours of culture. The addition of only Pd32 was included as an additional control (A) The total cell number that was counted per EB. (B) The relative number of Gata6 and Nanog antibody labelled cells per EB.

S10

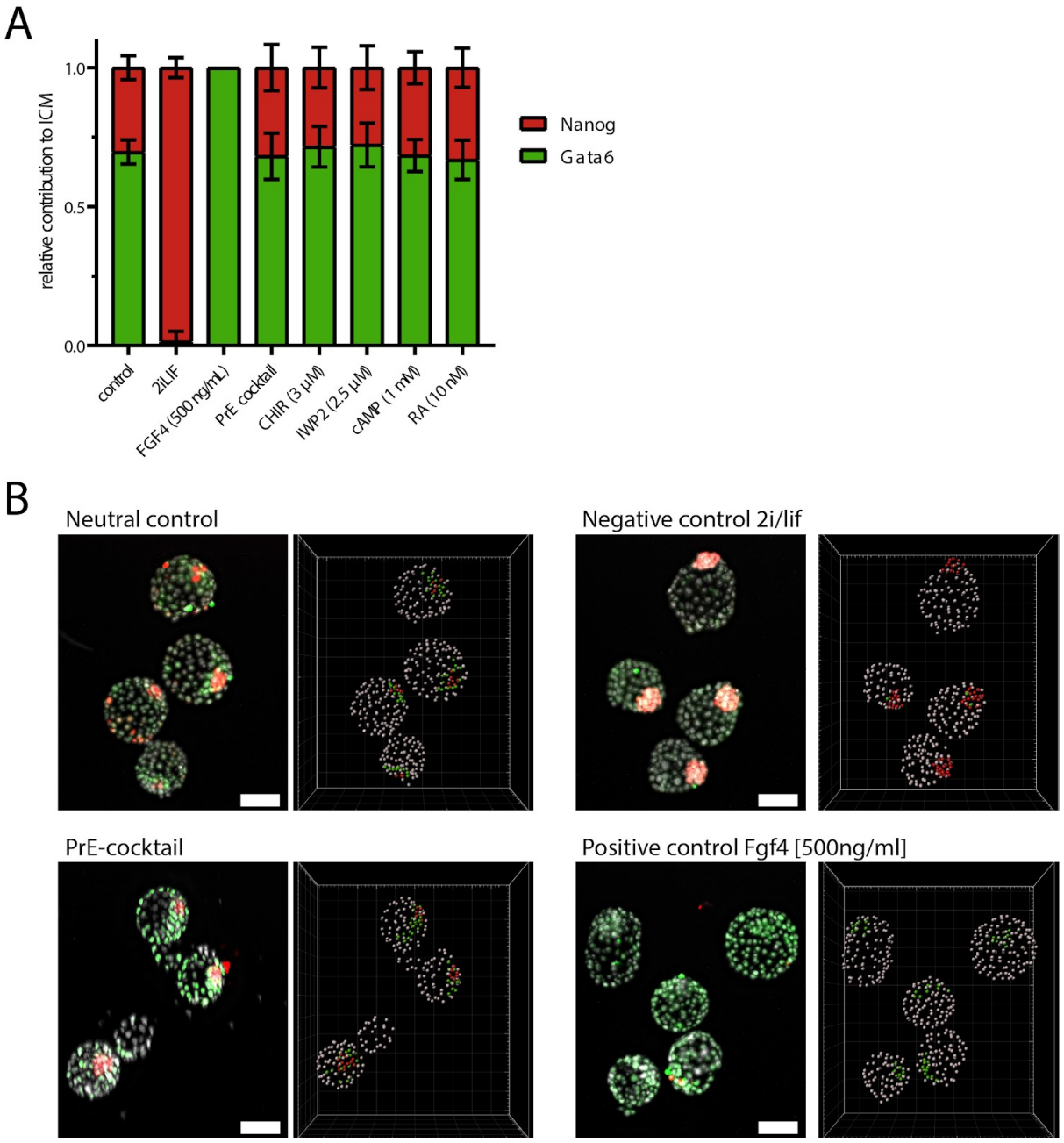

Fig. S10. Blastocyst culture under PrE-induction conditions and Fgf/Mapk modulation. A) Relative contribution of ICM cell numbers to either the epiblast (Nanog+) or PrE (Gata6+). B) Maximum intensity projections and identification of cell numbers using confocal fluorescence images of blastocysts (Imaris version x64 9.5.0) that were cultured in KSOM, KSOM with PrE-induction cocktail, KSOM with 2i/lif and KSOM with 500ng/ml Fgf4. All experimental conditions were assessed in the same experiment except for the full PrE cocktail, which was performed in a separate experiment. N = 4 or 5 blastocysts per condition.

S11A

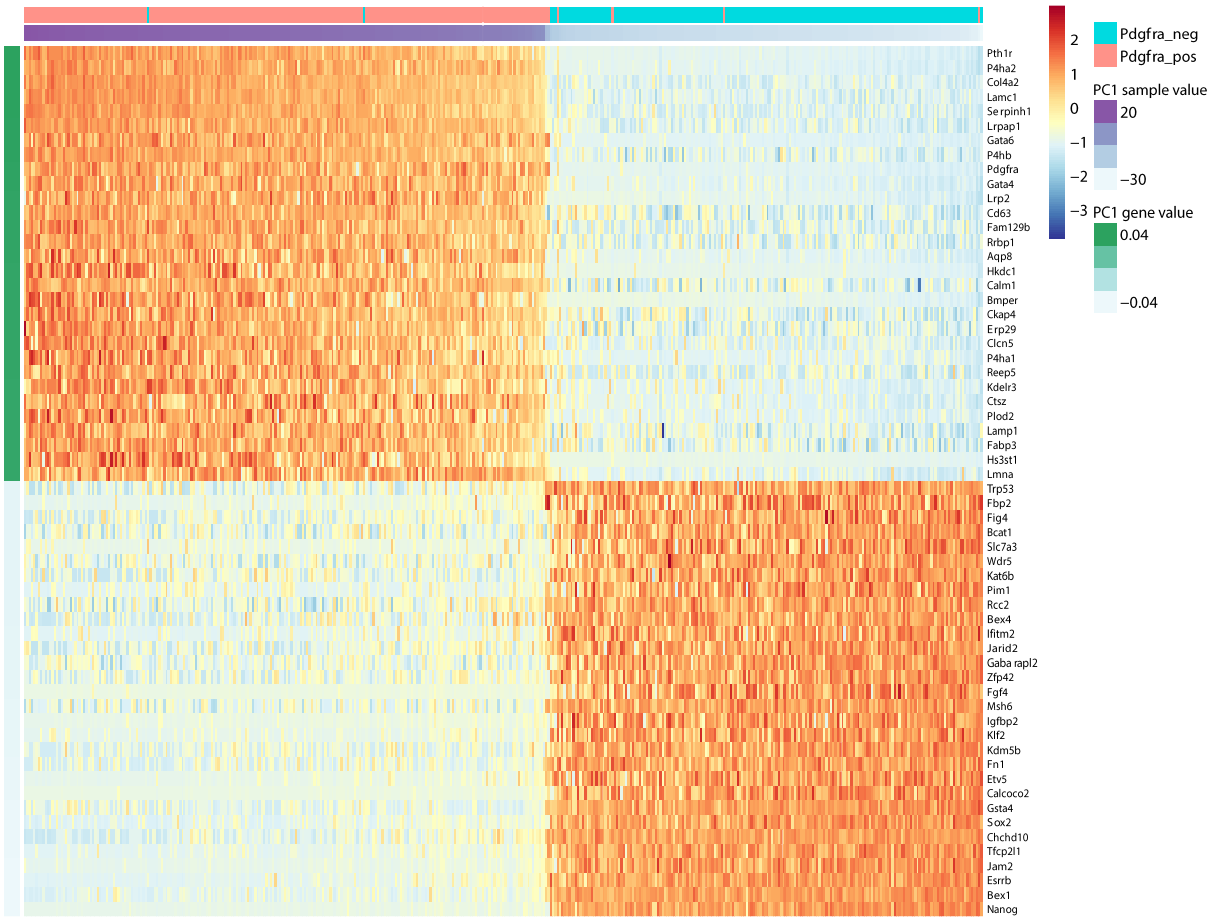

Fig. S11. Top and bottom differentially expressed genes along principle component axis 1 of both the Pdgfra- and Pdgfra+ subpopulations.

S11B

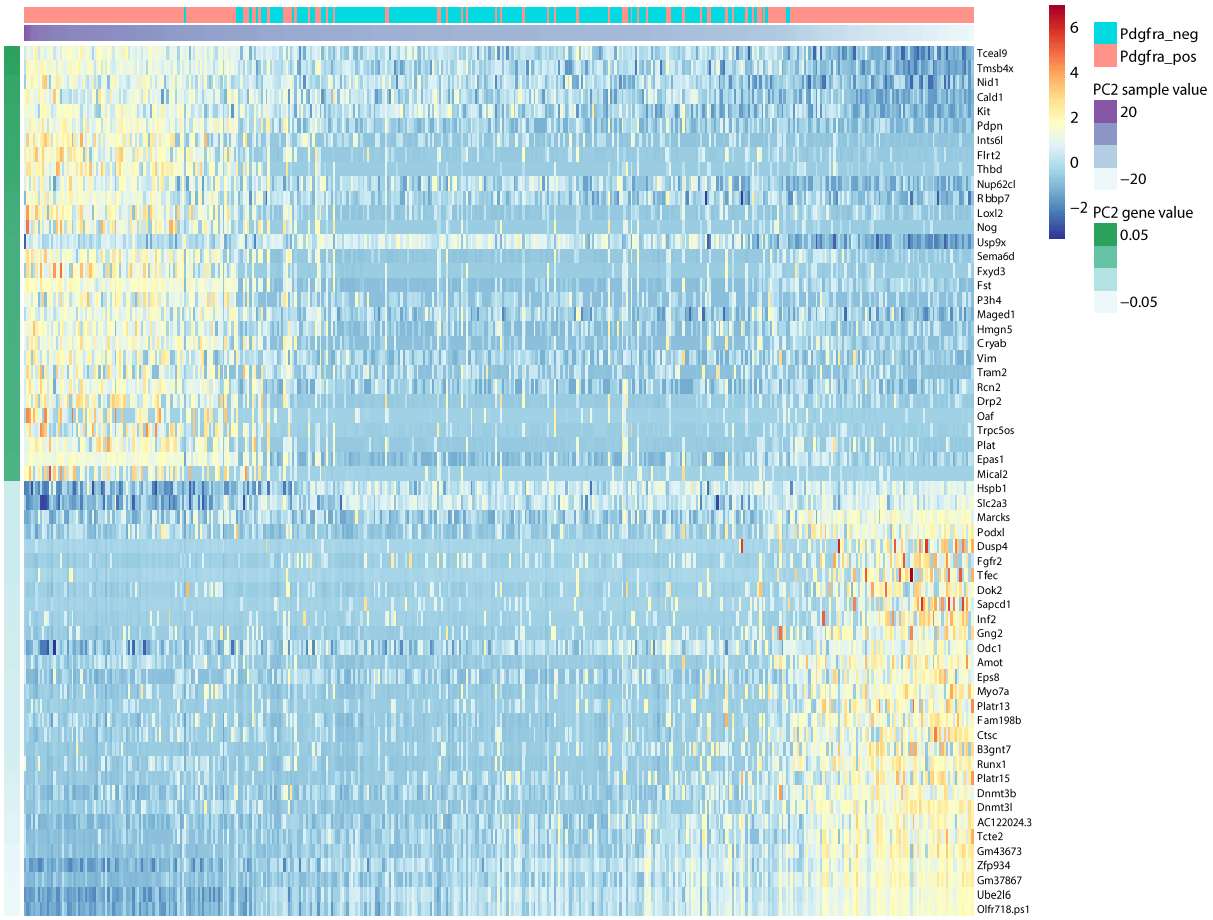

Fig. S11B. Top and bottom differentially expressed genes along principle component axis 2 of both the Pdgfra- and Pdgfra+ subpopulations.

S12A

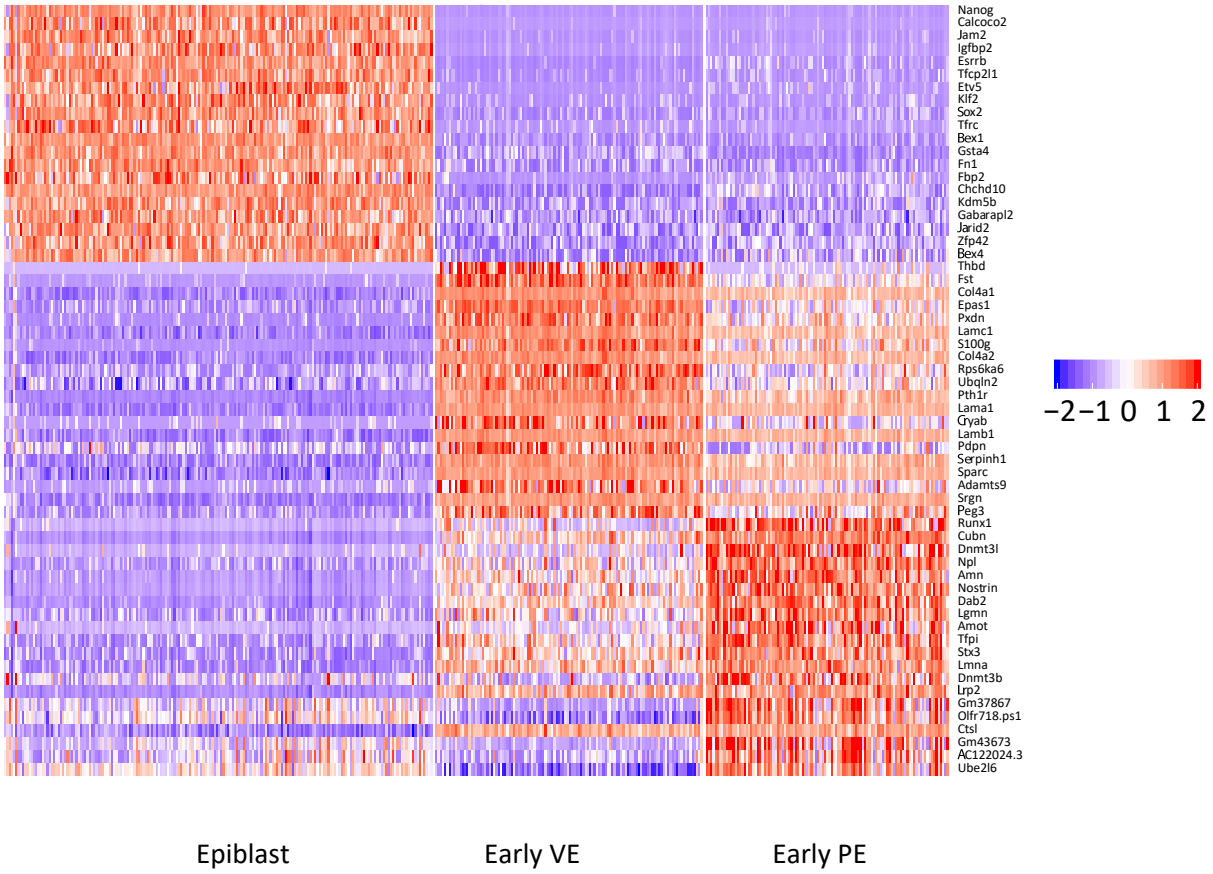

Fig. S12A. Top 20 most differentially expressed genes between the three groups: Epiblast, early PE and early VE.

S12B

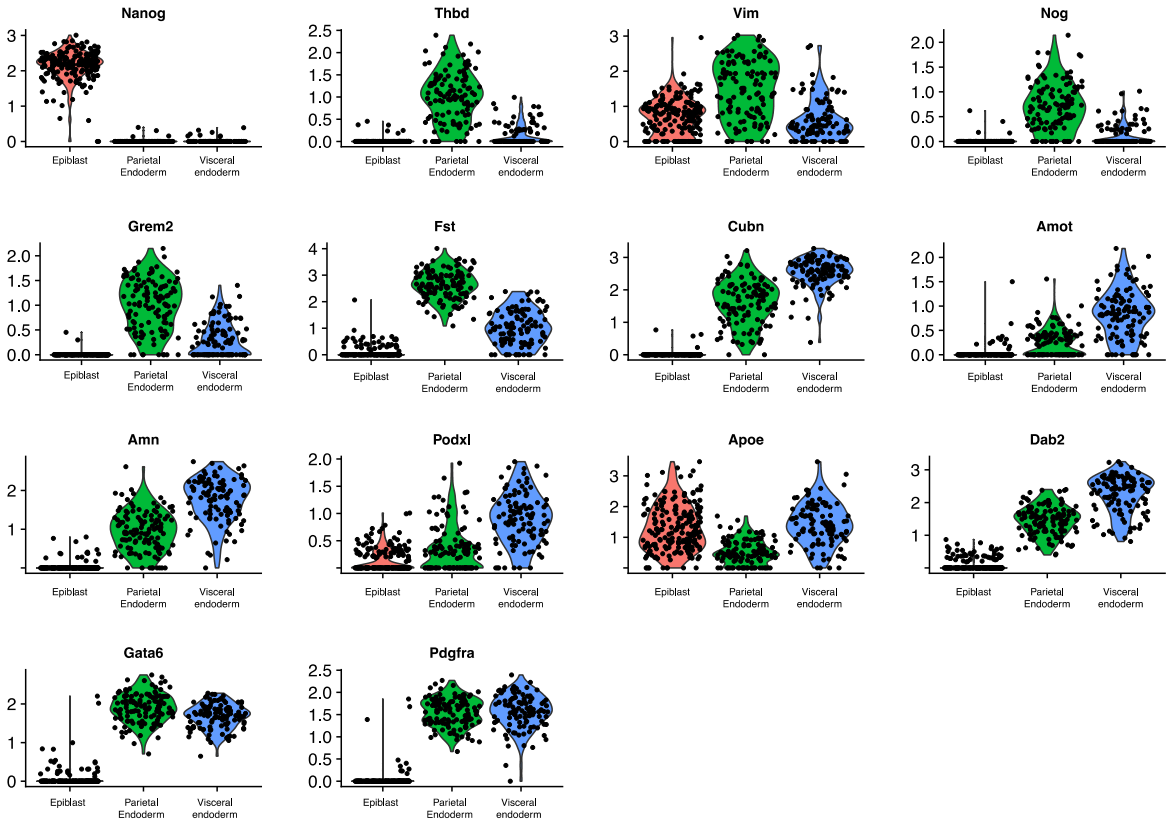

Fig. S12B. Relative expression levels for VE and PE genes within the three subpopulations (putative early PE, putative early VE and Epi) of 96h PrE-induced aggregates.

S13A

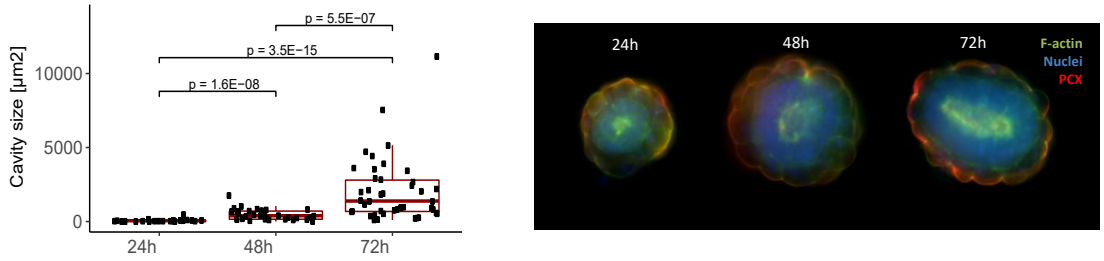

Fig. S13A. Size of cavities in XEn/Epi EpiCs over time (left) with accompanying representative fluorescence images (right). P-values were calculated according to the Mann – Whitney U test.

S13B

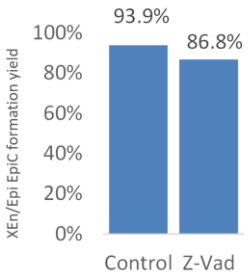

Fig. S13B. Formation efficiency of XEn/Epi EpiCs with and without addition of apoptotic inhibitor Z-vad-fmk (Z-Vad).

S14

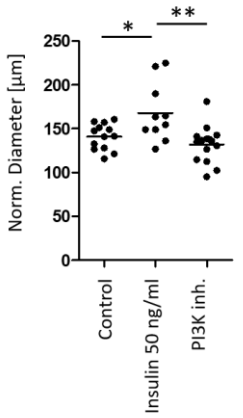

Fig. S14. Normalized diameter of controls Epi/XEn EpiCs and those exposed to insulin and a PI3K inhibitor ZSTK474 for the full culture time window. One-way ANOVA with Tukey's multiple comparison test; * denotes a $p < 0.05$ and ** denotes a $p < 0.01$.

S15

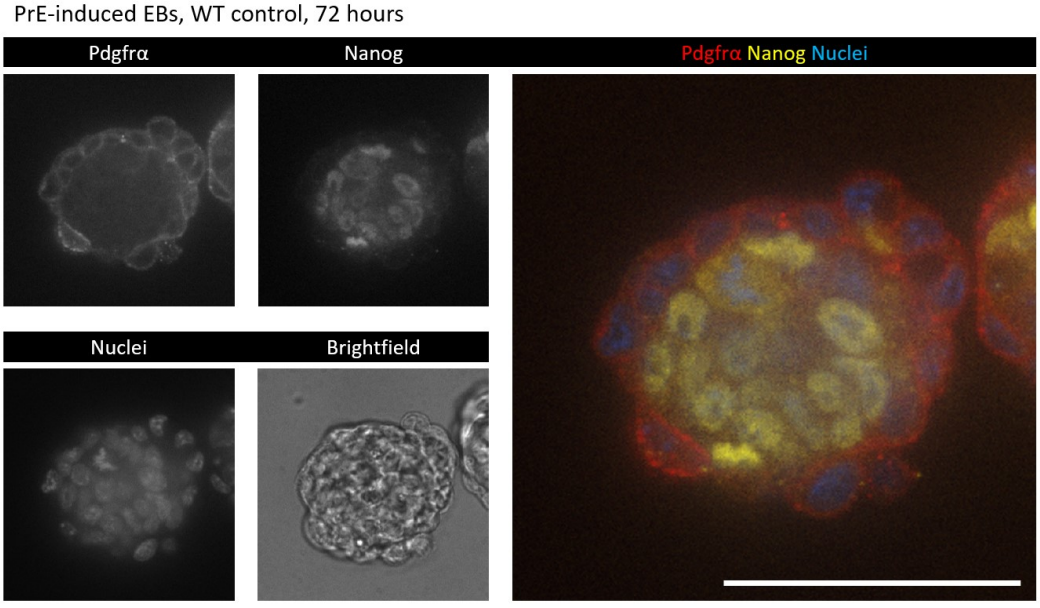

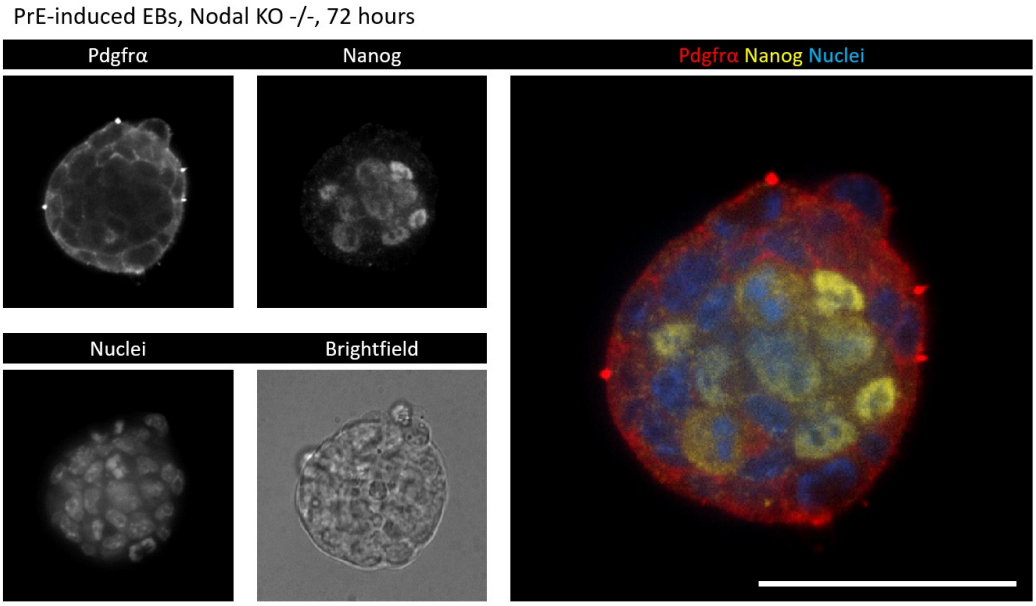

Fig. S15. Immunofluorescence staining for PrE (Pdgfra) and Epi (Nanog) in 72-hours PrE-induced structures formed with both the V6.5 ESC Nodal KO -/- line and its corresponding WT (+/+) control. Scale bars depict 50 micrometer.

S16

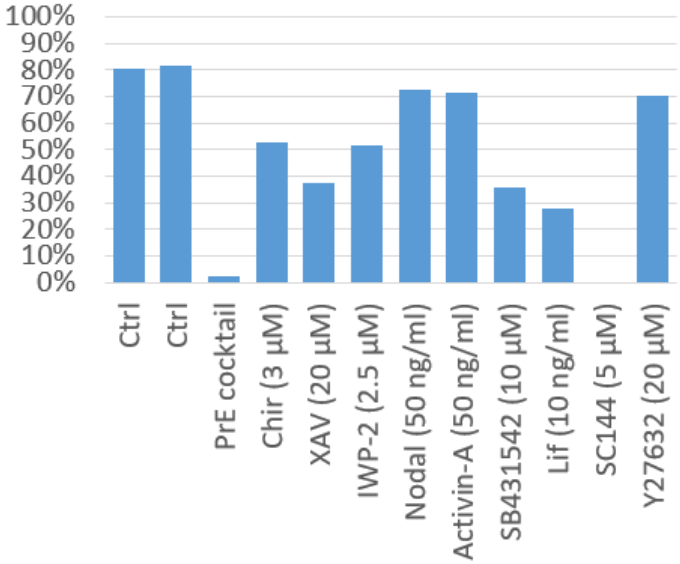

Fig. S16. Efficiency of XEn/Epi EpiC formation in response to addition of soluble pathway modulators starting at 72 h after cell seeding.

S17A

DVE/AVE

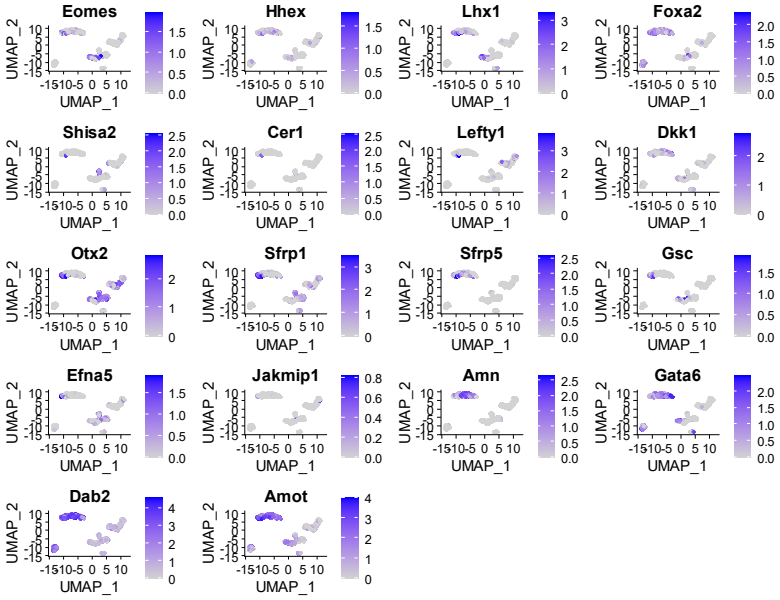

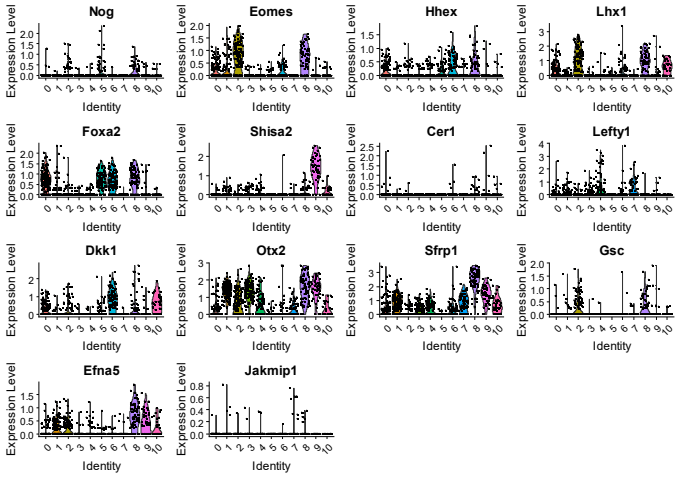

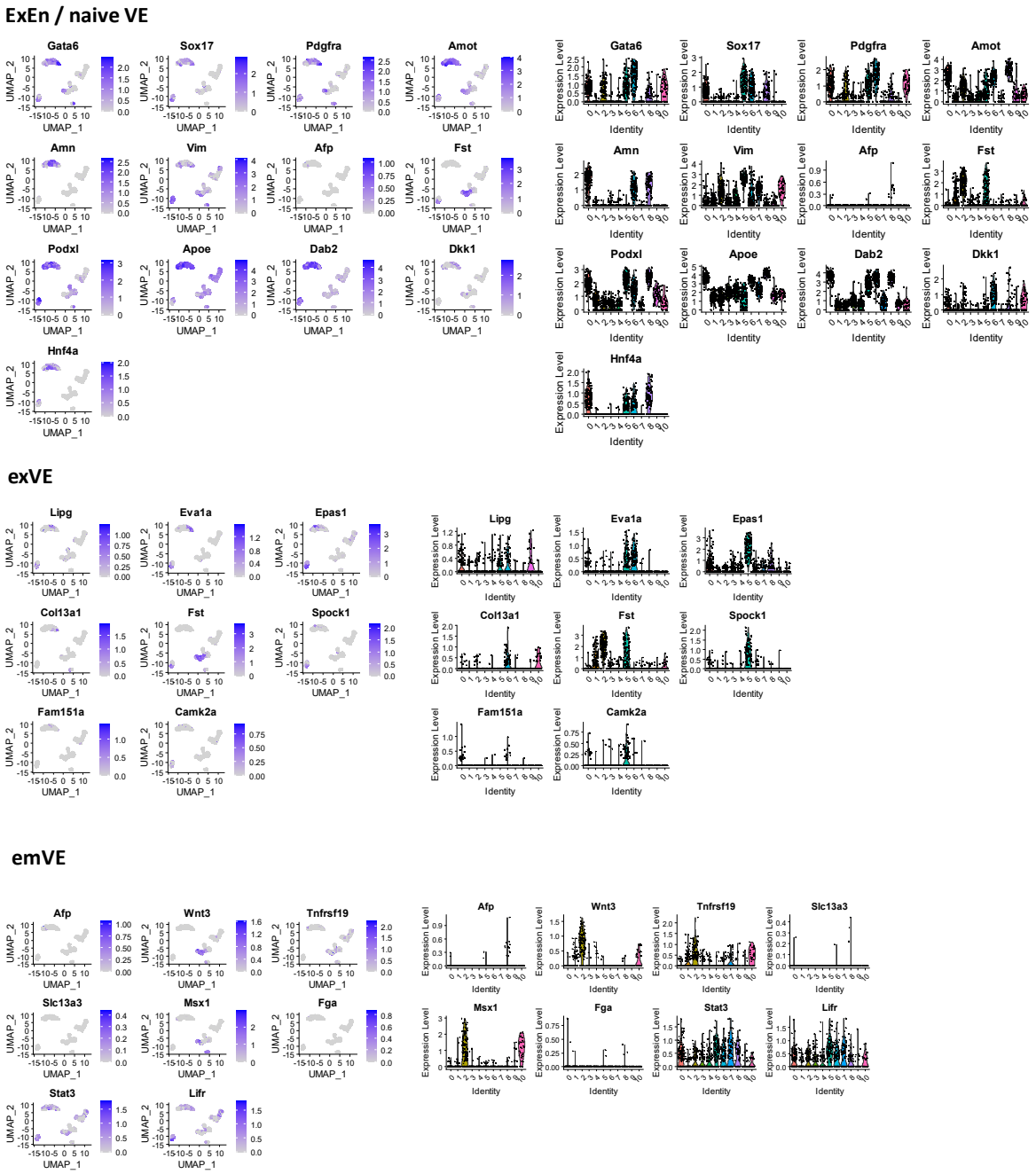

Gene expression plots involved in Extraembryonic endoderm (naïve VE), embryonic VE, extraembryonic VE and distal/anterior VE.

S17B

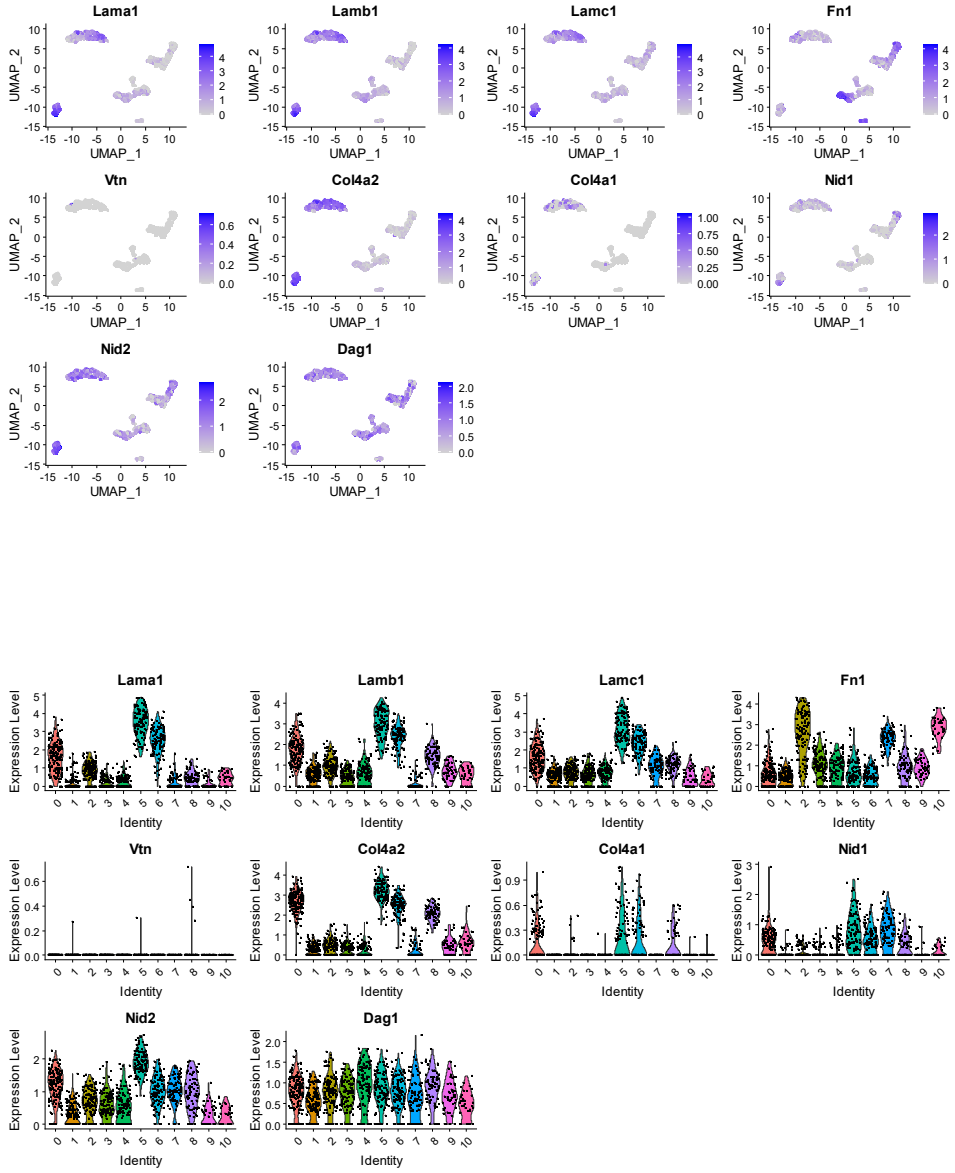

Fig. S17. Gene expression plots involved in expression of extracellular matrix proteins of the basal lamina.

S17C

posterior Epiblast

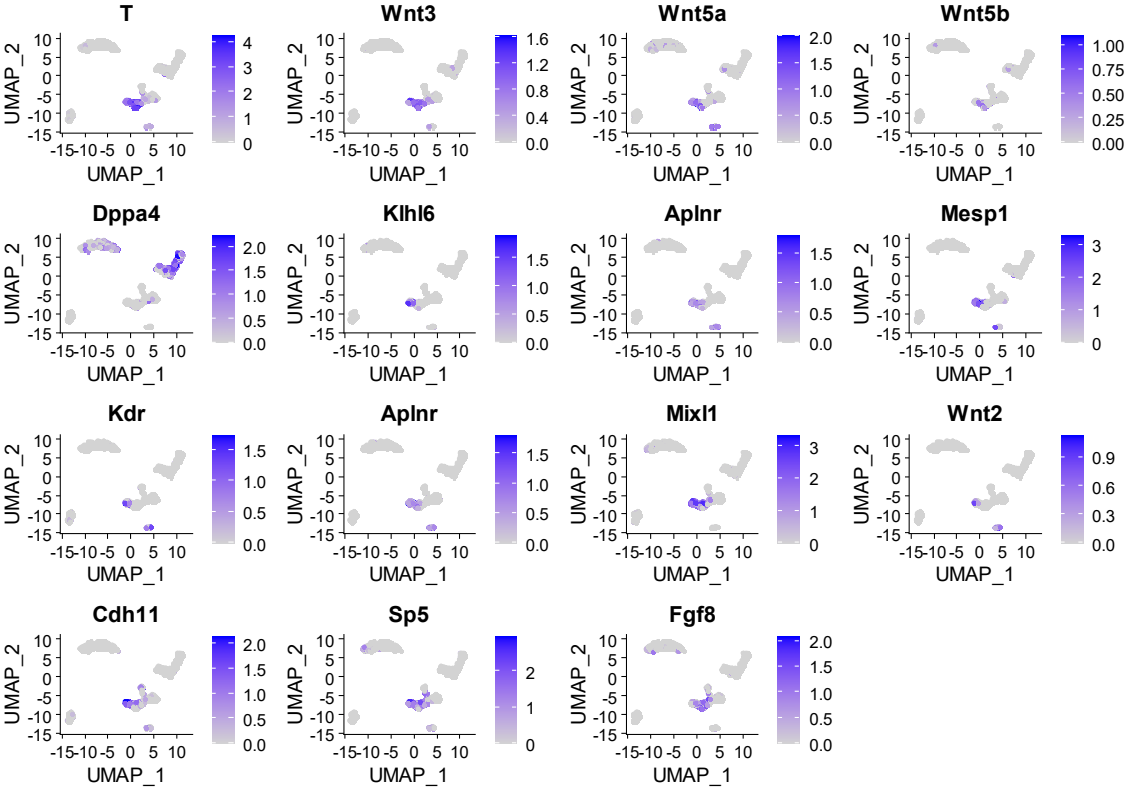

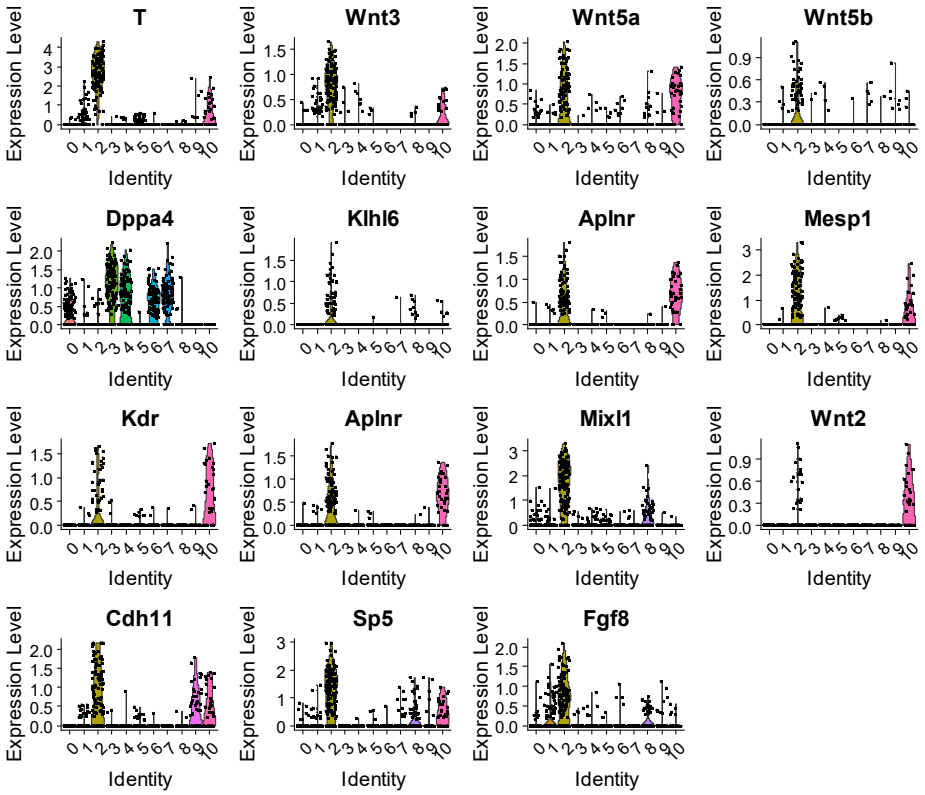

Anterior Epiblast

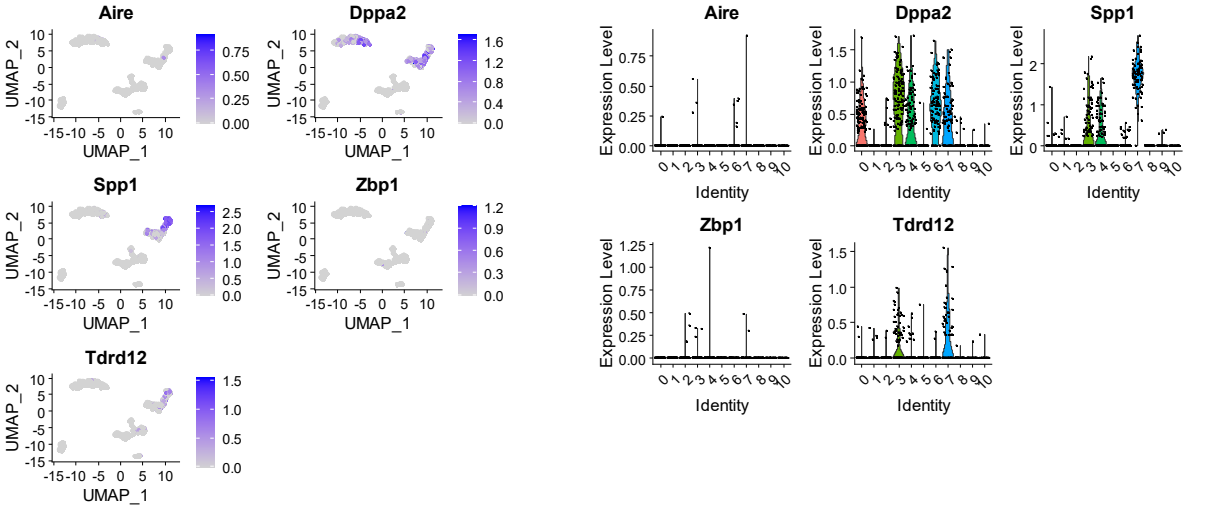

Transition Epiblast

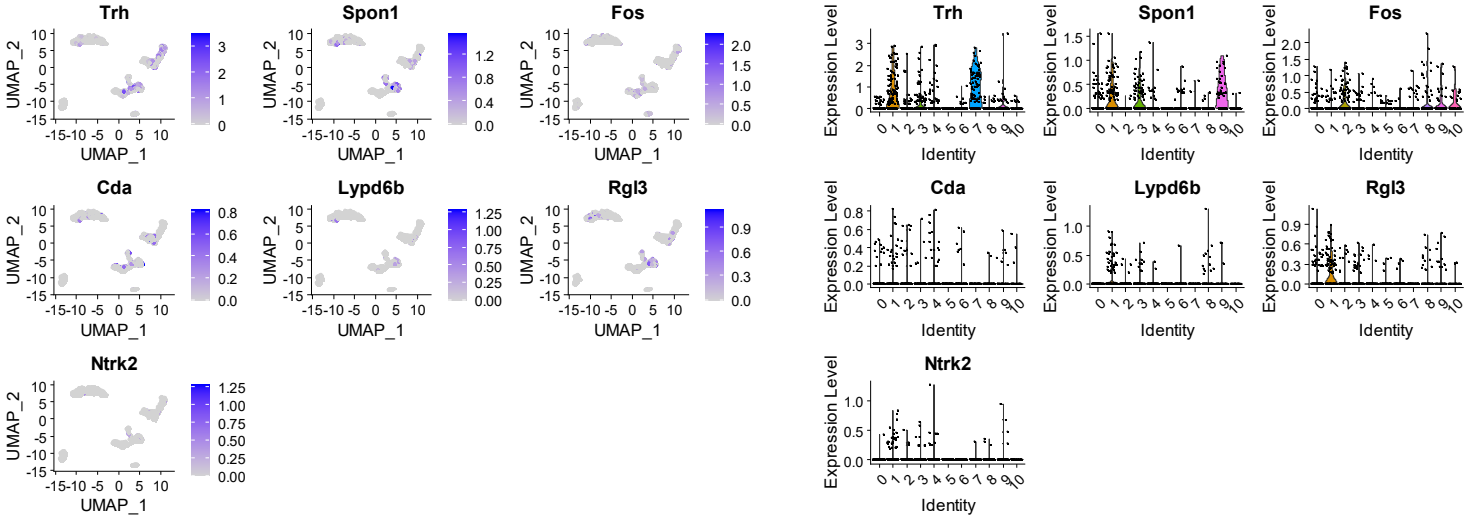

Gene expression plots involved in the anterior, transition and posterior epiblast

S17D

TGFbeta/Activin/Nodal signalling pathway

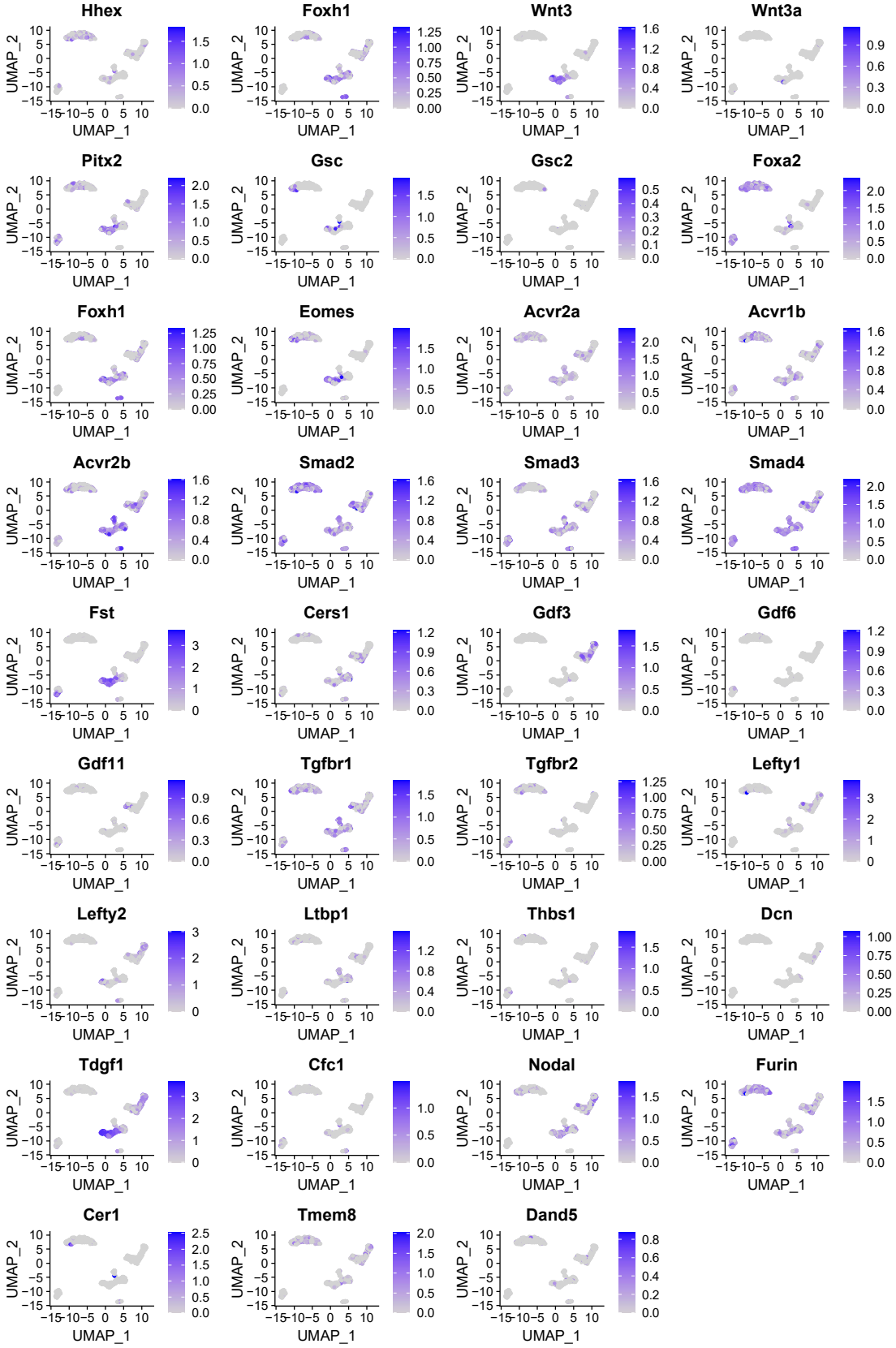

TGFbeta/Activin/Nodal signalling pathway

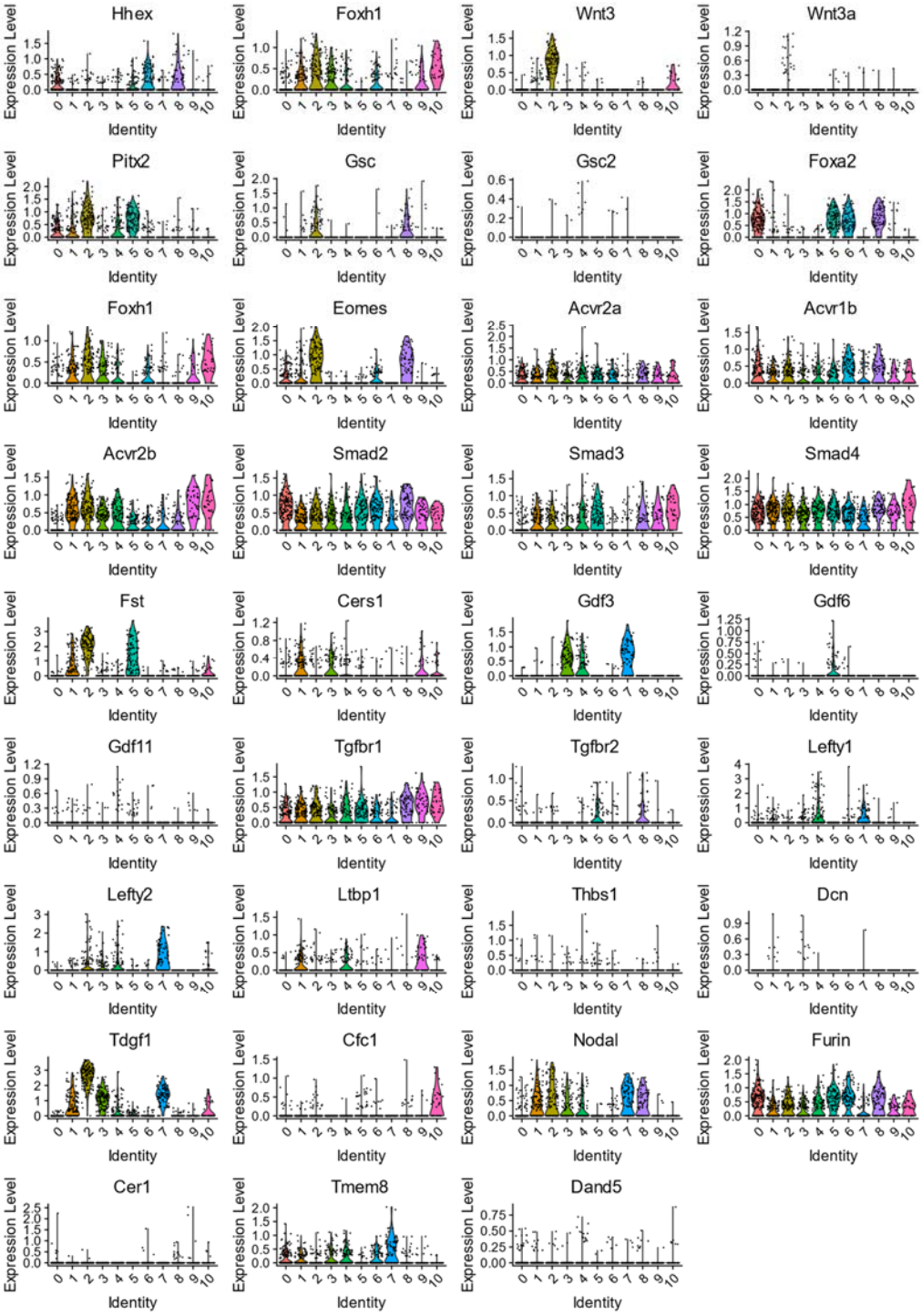

Wnt

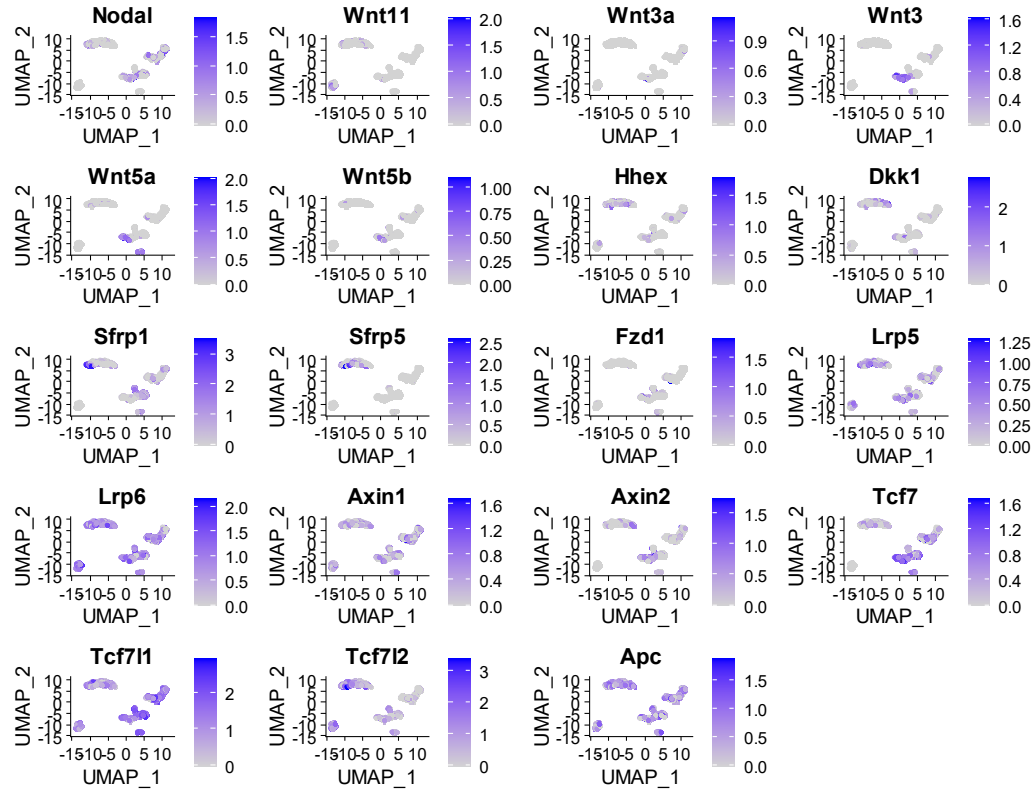

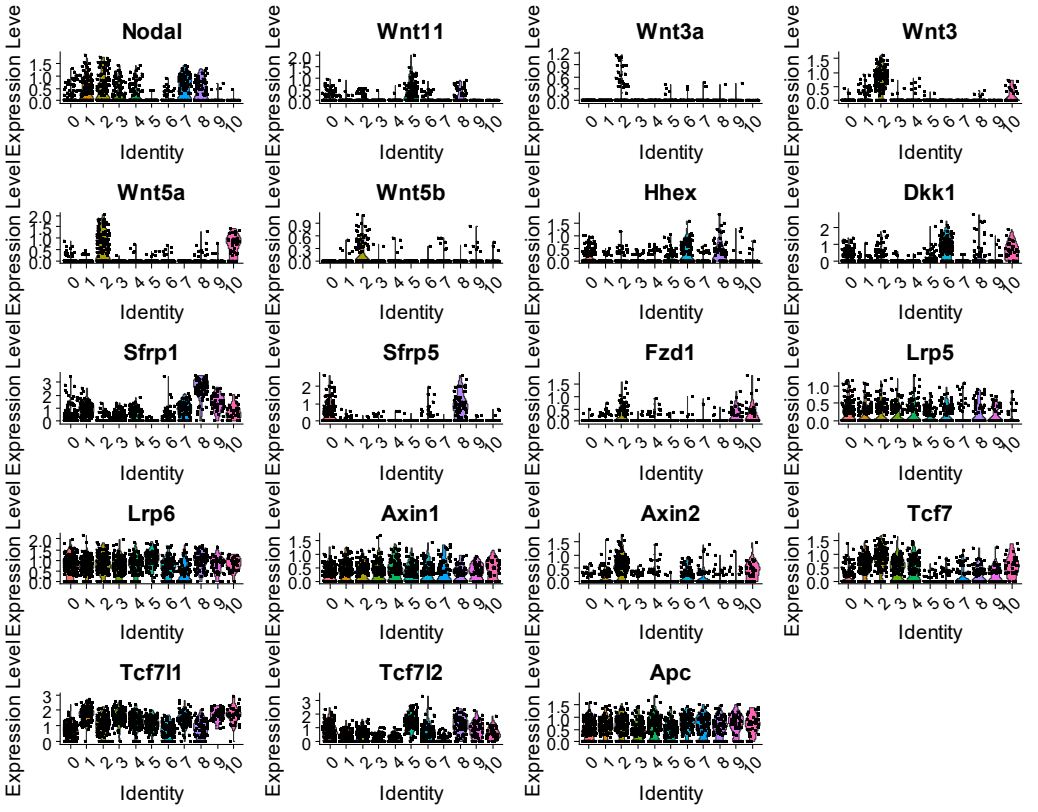

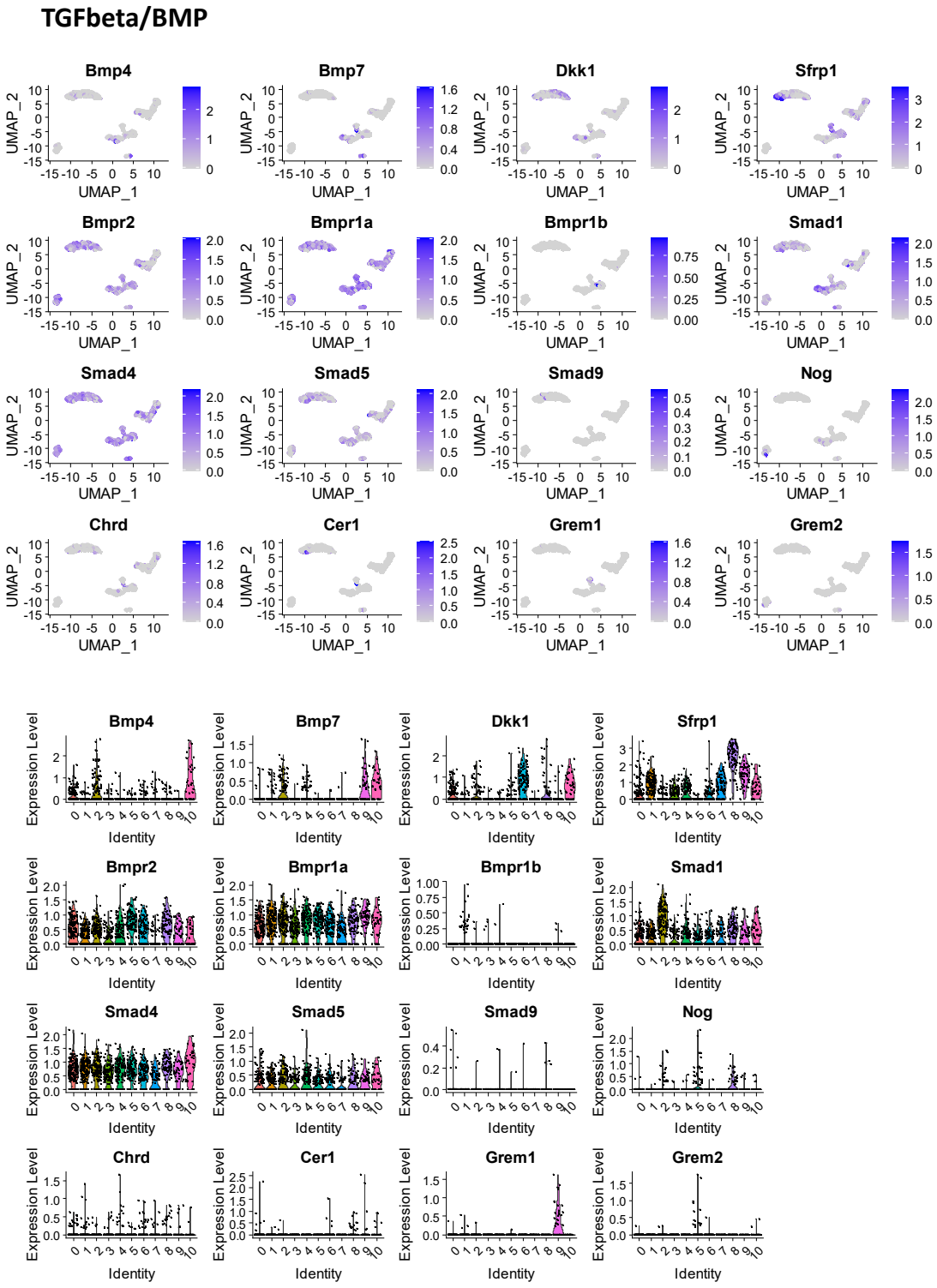

Fig. S17. Gene expression plots involved in the TGFbeta/Activin/Nodal, Wnt and TGFbeta/BMP signalling pathways.

S18

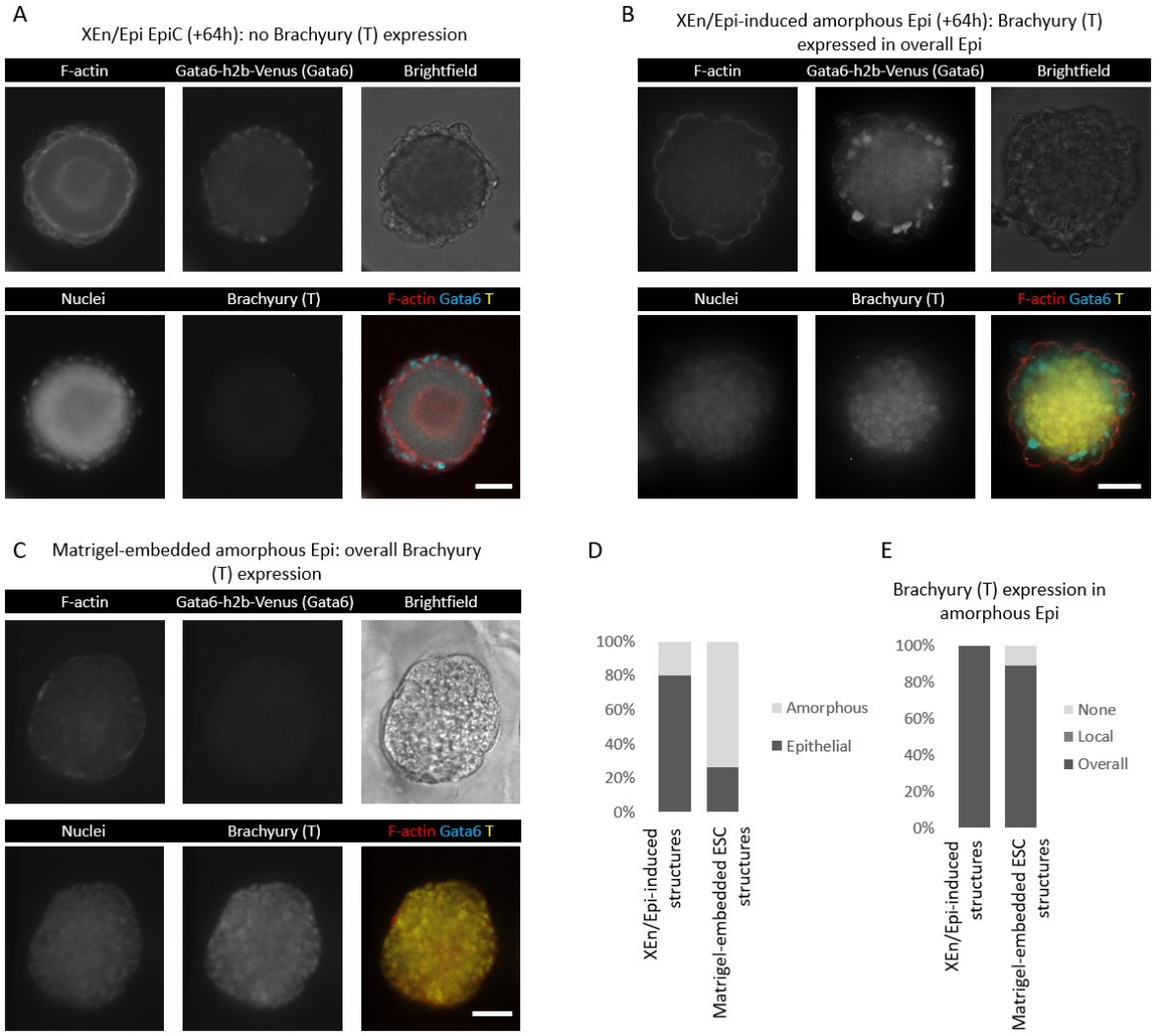

Fig. S18. Representative immunofluorescence images for Brachyury in A) Xen/Epi EpiCs (+64h) showing no apparent Brachyury (T) expression, B) Xen/Epi-induced structures with an amorphous Epi (64+) showing overall Epi Brachyury expression, and C) Matrigel-embedded structures with an amorphous Epi showing overall Brachyury expression. D) Percentage of structures with either an epithelialized or amorphous Epi compartment. E) Percentage of structures with No (None), local or overall expression of Brachyury in the amorphous Epi compartment.

S19

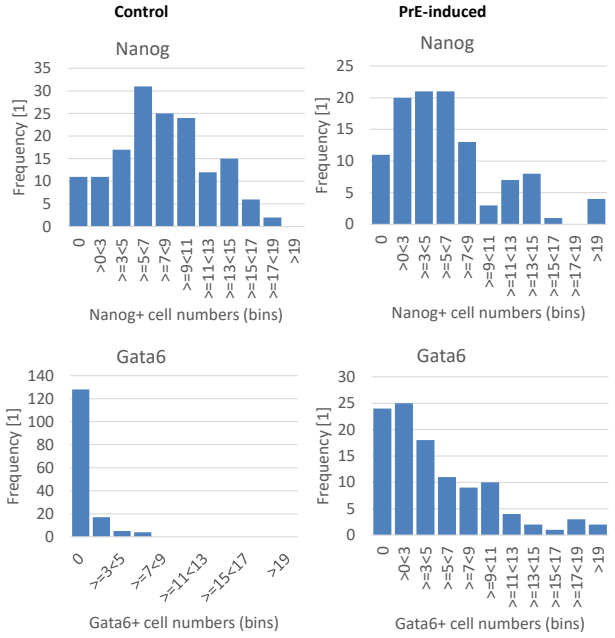

Fig. S19. Histograms displaying numbers of either Nanog+ or Gata6+ cells within control and PrE-induced blastoids.

S20

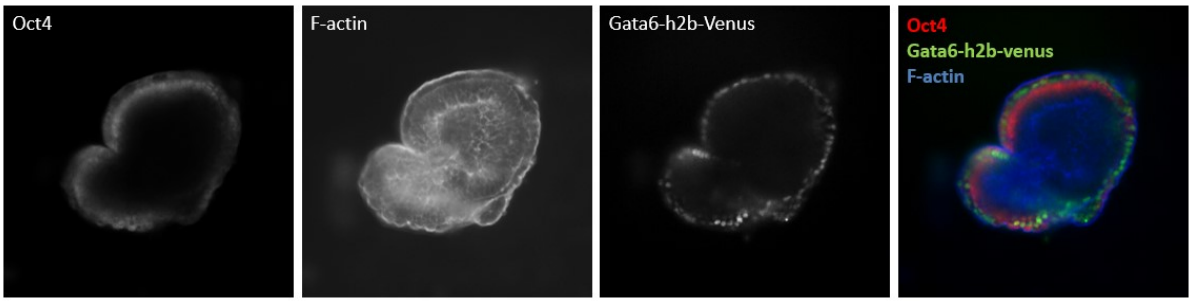

Fig. S20. Blastoid outgrowth (96 hours) showing separate immunofluorescence channels for gata6-h2b-Venus+ cells surrounding an Epi-like Oct4+ tissue.

Table S1. Titration of soluble factors

Click here to download Table S1

Table S2. Differential gene expression

Click here to download Table S2

Table S3. Enriched genes Epi and PrE in induced EBs

Click here to download Table S3

CHAPTER 4:
Canonical Wnt activity blocks the developmental progression of the primitive endoderm at early implantation stages

4.1. Abstract

In placental mammals, the differentiation and morphogenesis of the three blastocyst lineages is tightly orchestrated during the pre- to post-implantation transition. Which signalling interactions between the blastocyst lineages coordinate their peri-implantation development is only partially understood. In this study, we illustrate that the trophectoderm is a possible source of canonical WNT ligands, presumably activating Wnt signalling in the epiblast and primitive endoderm (PrE) at the blastocyst stage. We demonstrate that high canonical Wnt activity blocks the differentiation of PrE-like cells *in vitro*, reminiscent of what is known for epiblast-like embryonic stem cells. Specifically, Wnt counteracts differentiation of the pre-implantation PrE into the post-implantation visceral endoderm and influences the response of cells to the differentiation signals BMP4 and Activin A. Using a stem cell-based model of PrE and epiblast co-development at peri-implantation stages, we further show that high cellular Wnt activity prevents basement membrane formation by PrE-like cells, an essential step guiding epiblast morphogenesis in the embryo. Collectively, our work uncovers a significance of active canonical Wnt signalling in maintaining the pre-implantation potency of PrE-like cells *in vitro*. We argue that this might exploit an *in vivo* mechanism by which the blastocyst can halt development at pre-implantation stages if needed.

4.2. Introduction

In the development of placental mammals, the blastocyst undergoes drastic morphogenetic and cell fate changes during the pre- to post-implantation transition (Rossant & Tam, 2009; Takaoka & Hamada, 2012; Rossant, 2018). These peri-implantation changes must be precisely regulated to successfully set up the embryo for subsequent gastrulation. At the onset of implantation in mouse, cells of the extra-embryonic trophectoderm and primitive endoderm (PrE) deposit a basement membrane around the epiblast which induces epiblast polarisation, epithelialisation, and consecutive lumen formation, eventually creating the characteristic epiblast cup morphology (Bedzhov & Zernicka-Goetz, 2014). Coinciding with these changes in shape, the epiblast transitions from naïve to primed pluripotency (Nichols & Smith, 2009), while the PrE gives rise to the parietal and visceral endoderm (VE) lineages (Filimonow & de la Fuente, 2022). The VE largely engulfs the epiblast cup and fulfils a critical role in nutrient uptake and transport (Bielinska *et al*, 1999). Subsequently, a fraction of the VE specifies the distal and later anterior VE (DVE and AVE), thereby establishing an anterior-posterior axis that lays down the blueprint for the posterior initiation of gastrulation (Rossant & Tam, 2009; Takaoka & Hamada, 2012). Despite having identified many of the signalling pathways that control these sequential

developmental events, our understanding of how signalling interactions between the blastocyst lineages regulate differentiation and morphogenesis during the peri-implantation window remains incomplete.

In the epiblast, changes in canonical Wnt signalling activity have been suggested as a mechanism for regulating differentiation and morphogenesis during early post-implantation development. A range of WNT ligands are expressed at the blastocyst stage (Kemp *et al*, 2005), and Wnt is detectably active in the blastocyst and is later downregulated at early post-implantation stages (ten Berge *et al*, 2011). Accordingly, active Wnt signalling blocks the differentiation of murine embryonic stem cells (ESCs) and the glycogen synthase kinase-3 (GSK3) inhibitor, and Wnt agonist, CHIR99021 is routinely exploited to lock ESCs in a transcriptional state resembling the naïve E4.5 epiblast (ten Berge *et al*, 2011; Ying *et al*, 2008; Wray *et al*, 2011; Boroviak *et al*, 2014). Moreover, it has been shown that active Wnt signalling counteracts epiblast polarisation and must be shut down to allow epiblast morphogenesis (Neagu *et al*, 2020; Fan *et al*, 2020). On the contrary, which pathways regulate the concurrent differentiation of the adjacent PrE into VE remains elusive. Although there is recent evidence that Wnt activity initially affects PrE fate specification (Athanasouli *et al*, 2023), and it has been established that Nodal and bone morphogenetic protein (BMP) signalling later specifies DVE in the VE (Brennan *et al*, 2001; Rodriguez *et al*, 2005; Stower & Srinivas, 2018), what regulates the transition from the pre-implantation PrE to the post-implantation VE in the first place is unclear.

Here, to understand which signalling pathways are involved in PrE differentiation, we first used single-cell RNA sequencing data of blastocyst embryos to gain a comprehensive picture of the signalling interactions that the PrE is subjected to at the onset of implantation. We show that at the blastocyst stage, the trophectoderm is the main source of WNT ligands which are predicted to signal to the epiblast but also to the PrE. Using recently published *in vitro* culture systems of the PrE lineage (Raina *et al*, 2021; Yasuhide *et al*, 2022), we follow up on this prediction and reveal that canonical Wnt signalling blocks PrE differentiation into the VE lineage and influences the response to the known differentiation signals BMP4 and Activin A. Wnt activity also blocks the formation of a basement membrane by PrE cells in a stem cell-based model of PrE and epiblast co- development. Thus, while Wnt is active, the PrE cannot progress in its development and, at the same time, does not provide the mechanical cues that guide the morphogenesis of the adjacent epiblast. We suggest that at the blastocyst stage, the trophectoderm induces canonical Wnt activity which acts as a “developmental checkpoint”. Such a checkpoint may avert the premature developmental progression of the epiblast and PrE and their indispensable peri-implantation interactions.

4.3. Results

4.3.1. Trophectoderm-secreted Wnt ligands are predicted to act on the epiblast and primitive endoderm at the blastocyst stage

To determine which signalling pathways might affect PrE differentiation during implantation, we first aimed to get a more comprehensive picture of the ligand-receptor-mediated signalling that the PrE is subjected to at the blastocyst stage. For this, we used CellphoneDB (Garcia-Alonso *et al*, 2022) to predict active signalling interactions between cells of the PrE, trophectoderm, and epiblast from previously published single-cell RNA sequencing data (Nowotschin *et al*, 2019). We separately analysed two datasets for both E3.5 and E4.5 blastocysts and identified an overall of 508 significant interactions ($p \leq 0.05$) at E3.5 and 443 significant interactions at E4.5, of which 231 and 212 interactions were shared between both datasets of the same time point, respectively (Figure 1A, Table S1 and S2). Fibroblast growth factor 4 (FGF4) and platelet derived growth factors (PDGFs) were among the ligands expressed by the epiblast and predicted to bind to the corresponding receptors transcribed by the PrE and the trophectoderm at E3.5 and E4.5 (Figure 1B). This is in accordance with the importance of FGF4 and PDGFs for PrE and trophectoderm development at the blastocyst stage, which has been described extensively (Tanaka *et al*, 1998; Nichols *et al*, 2009; Artus *et al*, 2013). Consistent with the necessary deposition of a basement membrane by the PrE for epiblast polarisation (Bedzhov & Zernicka-Goetz, 2014), CellphoneDB also predicted interactions between laminin and collagen expressed by the PrE and integrin complexes expressed by the epiblast at E4.5 (Figure 1B). Overall, the recapitulation of previously identified interactions gave us confidence that this analysis predicts some signalling interactions as they occur at the blastocyst stage.

Notably, we also found a large amount of WNT mediated interactions at both E3.5 and E4.5. WNT ligands are known to be expressed at the blastocyst stage, and the pathway was shown to be active prior to implantation (Kemp *et al*, 2005; ten Berge *et al*, 2011). In our analysis, the trophectoderm was the major source of Wnt ligands, specifically WNT3A, WNT6, and WNT7B at E3.5 and WNT7B at E4.5 (Figure 1C-E). These WNT ligands are predicted to interact with a variety of FZD receptors of the epiblast and of the PrE. In turn, DKK1, a known inhibitor of Wnt signalling, is expressed by the PrE and is predicted to signal to all other blastocyst lineages (Figure 1F). Wnt has been described to be involved in PrE fate commitment (Athanasouli *et al*, 2023), however, our analysis suggests that the PrE is still receptive to Wnt ligands at E4.5, after PrE specification has already been completed. We conclude that Wnt ligands are largely produced by the trophectoderm and predicted to induce signalling activity in both the epiblast and PrE, which could fulfil a role in PrE lineage development at the onset of implantation.

4.3.2. Wnt activity affects the morphology of PrE-like cells *in vitro*, suggesting developmental progression

To further investigate the role of Wnt signalling in the PrE, we employed two different stem cell culture systems that model the PrE lineage *in vitro*. First, we opted to use the recently published PrE stem cells (PrESCs), which are directly derived from the blastocyst (Yasuhide *et al*, 2022). PrESCs are derived and maintained in the presence of FGF4, Heparin, PDGF-AA, and notably the GSK3 inhibitor CHIR99021 (CHIR), a potent activator of the Wnt pathway (Figure 2A). To complement the use of PrESCs, we also took advantage of a genetic approach where GATA binding protein 4 (GATA4), a major PrE transcription factor, is overexpressed in ESCs to generate PrE-like cells *in vitro*. Upon PrE differentiation, these cells are maintained in medium substituted solely with FGF4 and Heparin, without a Wnt pathway activator. We used previously established doxycycline-inducible *Gata4* (Gata4i) ESC lines (Raina *et al*, 2021) and adapted the published protocol for differentiation. In brief, we used a 5-hour doxycycline pulse to induce *Gata4* overexpression before changing the culture medium to N2B27 supplemented with FGF4 and Heparin (Figure 2B and Figure S2A). Already 24 hours after doxycycline induction, almost all cells started expressing the PrE marker proteins GATA6 and PDGF receptor alpha (PDGFRA) (Figure S2B). At the same time, endogenous *Gata4* was highly upregulated, while exogenous *Gata4* transcripts and GATA4 protein levels sharply decreased (Figure 2C). We also monitored the differentiation in more detail by whole transcriptome analysis. Expression of other PrE marker genes plateaued at 48 hours (Figure 2E and 2F), yet there was still a clear transcriptomic shift between samples collected 48 or 72 hours after doxycycline induction for bulk mRNA sequencing (Figure 2D and Figure S2C). We suspected that cells might differentiate further, and when looking at the expression pattern of VE marker genes, we found many of them highly expressed at 48 hours and even more so at 72 hours after doxycycline induction (Figure 2E). Thus, while PrESCs reflect the undifferentiated PrE at E4.5 (Yasuhide *et al*, 2022), Gata4i cells cultured with FGF4/Heparin, but in the absence of a Wnt activator, appear to transition through a PrE-like state 24 hours after doxycycline induction and continue to upregulate VE markers at later time points. Despite certainly being inherently different stem cell systems, a considerable divergence in the culture conditions is the use of a Wnt activator, hinting at a role of Wnt signalling to explain the variations in the developmental states.

To follow up on the role of Wnt for the culture of PrE-like cells *in vitro*, we cultured PrESCs and Gata4i cells with a range of different Wnt pathway effectors for up to 72 hours. To activate Wnt we used CHIR but also WNT Surrogate-Fc Fusion Proteins (WntS-Fc) or Wnt3a conditioned medium for receptor-mediated Wnt activation. This ensured that observed effects could be attributed to cellular Wnt activity and were not specific to CHIR. R-spondins (Rspo) are known to amplify Wnt signalling (Kim *et al*, 2008), and we therefore also used WntS-Fc in combination with Rspo1 conditioned medium. Moreover, to prevent the confounding effects of WNT ligands, produced by the cells themselves, we blocked their biosynthesis by including the porcupine inhibitor IWP2. We confirmed that Wnt could be induced in all experimental conditions by checking *Axin2* expression levels as a readout for Wnt activity (Figure 3A and

Figure S3A). While Wnt S-Fc alone induced *Axin2* expression, this effect was enhanced by the addition of Rspo1 conditioned medium. Noticeably, the levels of Wnt activity seemingly correlated with the extent to which cells spread out within PrESC colonies (Figure 3C). At high Wnt activity (10μM CHIR and WntS-Fc+Rspo1 conditioned medium), PrESCs formed tight colonies, whereas lower Wnt activity was permissive for the formation of cells with larger cytoplasmic area (Figure 3C). Strikingly, we observed that upon culture in Wnt OFF conditions, cells not only had a larger cytoplasmic area but also accumulated large vacuoles in their cytoplasm (Figure 3B and Figure S3B). We initially hypothesised that the vacuoles might be lipid droplets, as an enhanced lipid metabolism was found to be characteristic of the VE lineage (Farese *et al*, 1996; Watanabe *et al*, 2010). However, despite detecting significantly more lipid droplets in colonies cultured with the Wnt inhibitor XAV939, the lipid droplets did not match the size nor localisation of the cytoplasmic vacuoles (Figure S3C). Upon further examination, we noticed that in GFP-labelled PrESCs, GFP was excluded from the vacuoles, suggesting that they might be endosomes (Figure 3D). Since increased endocytosis is another feature of the VE (Perea-Gomez *et al*, 2019), we tested endocytic activity using a dextran uptake assay. We observed a dramatic increase in the uptake of dextran following the withdrawal of WNT agonists, which was repressed by the endocytic inhibitor LatrunculinA (Figure 3E). Collectively, the changes in cell morphology, in combination with the appearance of a VE characteristic phenotype with apparent endocytic activity in the absence of Wnt agonists, point at a role of Wnt signalling activity in blocking PrE differentiation.

4.3.3. Release from Wnt signalling induces visceral endoderm differentiation

To test if a decrease in Wnt signalling activity in fact promotes the differentiation of the PrE into VE, we first assessed the expression levels of VE marker genes in PrESCs and Gata4i cells under Wnt ON versus Wnt OFF culture conditions. For both cell lines, the absence of Wnt activators resulted in an upregulation of VE genes such as *Afp*, *Apob*, *Dab2*, and *Hnf4a*, while *Pdgfra* and *Pou5f1*, which mark an early PrE state (Linneberg-Agerholm *et al*, 2023), were downregulated (Figure 4A and Figure S4A and S4B). These expression patterns were consistent on the protein level in PrESCs, with cells in Wnt OFF culture conditions expressing the VE marker hepatocyte nuclear factor 4 alpha (HNF4A) and downregulating PDGFRA and octamer-binding transcription factor 4 (OCT4, the product of *Pou5f1*) (Figure 4C and Figure S4D). To gain a more holistic understanding of gene expression changes dependent on altered Wnt activity levels, we performed bulk mRNA sequencing of PrESCs cultured with CHIR, WntS-Fc, or without Wnt activators. By employing gene set enrichment analysis (GSEA), we found a positive enrichment of VE-specific genes among the differentially expressed genes (DEGs) between cells cultured with or without Wnt activators (Figure 4B). DEGs between cells cultured with CHIR or WntS-Fc also exhibited a positive enrichment for VE-specific genes which might be explained by the substantially higher Wnt signalling response that is achieved by 10 μM CHIR compared to the receptor-mediated signalling through WntS-Fc (see also Figure 3A). Conversely, there was a

negative or no enrichment of PrE-specific genes among the DEGs between cells cultured with or without Wnt activators (Figure S4C). Finally, to verify that the effects of Wnt signalling on PrE extend to the embryo, we isolated blastocysts at E3.7 and treated them with 10 µM CHIR from E4.2 before fixing them at E5.5. As anticipated, PrE cells of CHIR-treated embryos largely failed to upregulate the VE marker HNF4A (Figure 4D and 4E). Taking all together, we conclude that canonical Wnt signalling prevents the differentiation of the PrE into the VE.

4.3.4. Wnt activity influences cellular response to differentiation signals BMP4 and Activin A

BMP4 signalling is required for the differentiation of PrE into VE and subsequently specifies the embryonic VE (emVE) overlying the epiblast, which is distinct from the extra-embryonic VE (exVE) adjacent to the extra-embryonic ectoderm (Figure 5A)(Yamamoto *et al*, 2009). Given our results that Wnt prevents VE differentiation, we wondered if BMP4 signalling could override the inhibitory effect of Wnt. To understand this, we cultured cells with or without the receptor-mediated Wnt activator WntS-Fc and treated them with BMP4 for 24 hours before performing bulk mRNA sequencing (Figure 5B). Cells cultured with CHIR and without BMP4 were included as a control. In a principal component analysis (PCA), PC1 captured the PrE developmental trajectory that negatively correlated with the levels of Wnt activity (Figure 5C). VE marker genes *Apob*, and *Amot* were under the genes with highest positive loading value on PC1, while Wnt target *Axin2*, and early PrE marker *Pdgfra* and *Pou5f1* were among the genes with highest negative loading value (Figure S5A). BMP4 treatment caused a positive shift along PC2 that was independent of Wnt activity (Figure 5C). Genes with high positive PC2 loading scores included the VE marker genes *Apob* and *Hnf4a*, indicating that BMP4 indeed induces VE differentiation (Figure S5A). Independent of cellular Wnt activity, GSEA confirmed a positive enrichment for VE specific genes among the DEGs between BMP4 treated and untreated cells (Figure 5D). More specifically, we found a positive enrichment for emVE as opposed to exVE genes (Figure S5C and S5D), which is in line with what has been reported previously (Yamamoto *et al*, 2009). Although BMP4 induced an upregulation of VE-specific genes regardless of cellular Wnt activity, the expression of PrE-specific genes was maintained when Wnt signalling was active (Figure 5E). Furthermore, the expression levels of VE-specific genes were lower in cells treated with BMP4 and cultured with WntS-Fc as compared to those treated with BMP4 and cultured without WntS-Fc (Figure 5E). Thus, BMP4 can induce VE specification also in the presence of Wnt signalling, however, Wnt must be shut down to decrease PrE-specific gene expression and boost the upregulation of VE-specific genes.

In addition to its role in (em)VE specification from PrE, BMP signalling is also known to counteract the differentiation of VE into DVE (Figure 5A)(Rodriguez *et al*, 2005; Yamamoto *et al*, 2009; Stower & Srinivas, 2018). Interestingly, while the positive shift of BMP4 treated cells along PC2 appeared to be related to VE differentiation, the top genes with negative PC2 loading included the DVE marker genes *Otx2*, *Sfrp1*, and *Lefty1* (Figure 5C and Figure S5A). This

suggests that PC2 captures the transcriptomic differences between VE and the more specialised DVE, which is driven by BMP4 signalling (Figure 5C). In line with this, the expression levels of DVE markers such as *Otx2*, *Sfrp1*, *Cer1*, and *Lefty1* were downregulated in BMP4 treated samples compared to cells cultured without BMP4 under the same Wnt signalling condition (Figure 5E). Moreover, independent of Wnt activity, we found a negative enrichment for DVE specific genes (similar to the later AVE) among the DEGs between BMP4 treated and untreated cells (Figure S5B). Taken together, BMP4 counteracts the expression of DVE related genes, irrespective of cellular Wnt activity.

While our transcriptomic data showed that BMP4 can antagonise the expression of DVE-specific genes, these genes were still expressed at significantly higher levels in conditions where Wnt was inactive (Figure 5E). This indicates that VE differentiation, resulting from reduced Wnt activity, is accompanied by spontaneous DVE specificiation. Indeed, under Wnt OFF culture conditions, the DVE/AVE markers OTX2 and CER1 were expressed by patches of cells within PrESC colonies, while these proteins could not be detected in cells cultured with Wnt activators (Figure 5F). In the embryo, Nodal, a SMAD2/3 effector originating from the epiblast, induces DVE fate (Brennan *et al*, 2001). We wondered whether providing this signal could induce DVE differentiation in cells cultured under Wnt ON conditions, or if initial differentiation through Wnt inactivation is necessary for DVE specification. To test this, we exposed PrESCs to Activin A or TGFβ1 for SMAD2/3 activation under either Wnt ON or Wnt OFF conditions. Unlike TGFβ1, Activin A treatment very clearly increased the fraction of OTX2 positive cells in the absence of Wnt activators (Figure 5G and Figure S5E). However, while cells were also subjected to CHIR or WntS-Fc, Activin A treatment did not upregulate OTX2 expression, which is in accordance with what was published earlier last year (Figure 5G)(Schumacher *et al*, 2023). We therefore conclude that cells must be released from Wnt signalling to enable their initial differentiation into a VE-like state before they become receptive to Activin A as a DVE differentiation signal. Taking everything together, this implies a signalling hierarchy for differentiation where Wnt initially maintains PrE-specific gene expression while repressing VE-specific genes. BMP4, on the other hand, can induce VE differentiation despite cellular Wnt activity. However, Wnt must eventually be shut down to reinforce VE fate and to make cells receptive to additional differentiation signals, such as Activin A for DVE specification.

4.3.5. Wnt signalling prevents PrE differentiation and basement membrane formation in a 3D model of epiblast/PrE peri-implantation development

In the embryo, VE differentiation is tightly coupled to the morphogenesis and differentiation of the adjacent epiblast during epiblast cup formation. However, if PrE to VE differentiation affects epiblast morphogenesis is unclear. Therefore, we wanted to test the effect of Wnt on the co-development of the epiblast and PrE during peri-implantation stages. Modulating Wnt activity during peri-implantation development *in vivo* is technically challenging, and *in vitro* post-

implantation culture of blastocysts is inefficient and limited by the number of available blastocysts. To circumvent these constraints, we decided to broadly adopt a 3D stem cell model that we described previously, which models epiblast and PrE co-development from approximately E3.5 to E5.5 (Vrij *et al*, 2022). In brief, we mixed wild type ESCs with PrESCs or doxycycline-treated Gata4i cells and seeded them in CHIR containing medium into agarose microwells to form free-floating cell aggregates. 24 hours after seeding, the medium was changed to basal N2B27 medium to allow for unguided self-organisation of the two different cell types (Figure S6A). Cells within the aggregates were initially distributed in a salt and pepper manner, however, the PrE-like cells reliably sorted to the outside of the aggregates before depositing a basement membrane between themselves and the ESCs. This in turn triggerd polarisation and subsequent lumenogenesis of the ESCs between 72 and 96 hours. As this system models PrE-induced epithelialisation and cavity formation of epiblast-like cells, we refer to the structures as EpiCs. Using EpiCs, we can investigate the impact of Wnt signalling on the co-development of PrE-like and epiblast-like cells by simply adding Wnt activators and inhibitors when performing the protocol (Figure 6A and Figure S6B). We again used 10 µM CHIR or WntS-Fc ± Rspo1 conditioned medium as Wnt agonists, and the porcupine inhibitor IWP2 to limit the secretion of Wnt ligands between cells. Sorting of the PrE-like cells to the outside of aggregates was not affected by Wnt activity as we observed a clear segregation between outer GATA6+ and inner OCT4+ cells after 96 hours (Figure 6C and Figure S6D). However, continuous culture of EpiCs with CHIR or WntS-Fc+Rspo1 conditioned medium resulted in a very compact and smooth aggregate morphology, while in Wnt OFF conditions (IWP2 or Rspo1 conditioned medium alone) the PrE-like cells in the outer layer of EpiCs became noticeably blebby (Figure 6B and Figure S6C). Noteworthy, EpiCs cultured solely with WntS-Fc looked similar to EpiCs cultured under Wnt OFF conditions probably due to insufficient activation of the Wnt pathway by WntS-Fc alone (see also Figure 3A and Figure S3A). The outer blebby cells of Gata4i-EpiCs also showed high expression levels of HNF4A, indicating their differentiation into VE-like cells (Figure 6C). This suggests that active Wnt affects morphology and differentiation of the PrE lineage, also in a 3D co-culture model with epiblast-like cells.

The deposition of a basement membrane by the maturing PrE is one of the key steps that instructs epithelialisation of the epiblast during epiblast cup formation (Bedzhov & Zernicka-Goetz, 2014). Most interestingly, when EpiCs were cultured with CHIR or WntS-Fc+Rspo1 conditioned medium, we did not observe the formation of a dark ring between the PrE-like and epiblast-like cells after 96 hours (Figure 6B and Figure S6C). We suspected a defect in basement membrane formation and performed immunofluorescence stainings for the basement membrane component laminin. Indeed, the PrE-like cells failed to establish a basement membrane as evidenced by the absence of a distinct laminin layer between PrE-like cells and ESCs (Figure 6D and Figure S6E). As a consequence, ESCs of these EpiCs were disorganised and did not undergo lumenogenesis (Figure 6C). Since Wnt signals inhibit the differentiation and polarisation of ESCs and epiblast (Neagu *et al*, 2020; Fan *et al*, 2020), we cannot dismiss the possibility that the failure of basement membrane formation by the PrE/VE-

like cells may be indirectly regulated by the effect of Wnt on ESCs. To clarify this, we aggregated PrESCs alone in different Wnt ON and OFF conditions (Figure 6E). Similar to what we had observed in EpiCs, active Wnt signalling resulted in visibly tight aggregates, while aggregates cultured under Wnt OFF conditions were of irregular, blebby morphology (Figure S6F). To see how Wnt signalling affected the extracellular deposition of laminin, we fixed the aggregates and performed immunofluorescence stainings for laminin without permeabilization before primary antibody incubation. Permeabilised aggregates were included as controls. Aggregates cultured without Wnt or with Wnt inhibitors assembled extracellular laminin "sheets" between cells, which was not apparent in aggregates cultured under Wnt ON conditions (Figure 6F and Figure S6G). On the contrary, the levels of total laminin expression, as determined by quantifying the laminin signal of permeabilised aggregates, were comparable between all conditions. This suggests a defect in basement membrane formation, but not in membrane components production, as a result of Wnt signalling acting on the PrE-like cells directly. However, in contradiction, the transcription levels of basement membrane associated genes (*Lama1*, *Lamb1*, *Lamc1*, *Col4a1*, and *Col4a2*) negatively correlated with cellular Wnt activity (Figure S6H). Finally, since establishment of a basement membrane is tightly linked to cells acquiring apical-basal polarity (O'Brien *et al*, 2001), we checked if Wnt signalling interfered with establishment of cell polarity. Yet, no matter the culture condition, apical polarity was always acquired as marked by the apical expression of Podocalyxin (PODXL), atypical protein kinase C-zeta (PKCζ), and Zonula occludens-1 (ZO1) in the outer cells of PrESC aggregates (Figure 6G and Figure S6I). Overall, our results suggest that high canonical Wnt activity not only prevents the differentiation of the PrE into VE, but also blocks the associated formation of a basement membrane, thereby interfering with an essential developmental step necessary to guide epiblast morphogenesis.

4.4. Discussion

Cells of the three blastocyst lineages must precisely coordinate their differentiation and morphogenesis during peri-implantation development. Yet, our understanding of the signalling pathways involved, and the origins of the required signalling ligands remains incomplete. Here, using CellphoneDB (Garcia-Alonso *et al*, 2022), we identify the trophectoderm as a source of canonical WNT ligands, in line with what we have reported previously (Seong *et al*, 2022). Based on our analysis, WNT ligands from the trophectoderm are predicted to bind a variety of FZD receptors expressed by the epiblast and PrE, presumably activating the canonical Wnt pathway in these tissues. Activation of Wnt signalling in ESCs, the *in vitro* equivalent of the epiblast, has been widely employed to indefinitely maintain cells in a state of naïve pluripotency (Ying *et al*, 2008; Wray *et al*, 2011; Boroviak *et al*, 2014). In the present study, we investigated a potential role of Wnt signalling in the PrE lineage and show that canonical Wnt activity also blocks the differentiation of PrE-like cells *in vitro*. Moreover, high cellular Wnt activity prevents PrE-like cells from depositing a basement membrane between themselves and ESCs in a 3D model of

epiblast/PrE co-development at peri-implantation stages. Therefore, active canonical Wnt signalling evidently blocks the differentiation and morphogenetic progression of both ESCs and PrE-like cells *in vitro*.

This raises the question if there is a physiological relevance for a mechanism that can block developmental progression of cells in the embryo. Arguably, embryogenesis is a continuous process and naturally cells of the embryo would not arrest in a certain developmental state but steadily progress. However, in some mammalian species, including rodents, diapause provides an exception during which development is halted at the blastocyst stage (Mantalenakis & Ketchel, 1966; Mead, 1993; Renfree & Shaw, 2000). Recently, it was shown that canonical Wnt activity maintains naïve pluripotency in the epiblast during diapause and counteracts its polarisation through the Wnt downstream factor Esrrb (Fan *et al*, 2020). In fact, Wnt signalling had been suggested previously as a way to sustain naïve pluripotency in the dormant epiblast (Boroviak *et al*, 2015). The authors also found similarities in signalling activity between ESCs and the diapaused epiblast (Boroviak *et al*, 2015). This led them to speculate that using Wnt agonists to capture naïve pluripotency of ESCs *in vitro* engages the same pathways that allow the epiblast to undergo developmental arrest during diapause. Our findings that active Wnt signalling also inhibits the differentiation of the PrE could imply that Wnt plays a similar role in maintaining the PrE during diapause. Noticeably, *in vitro* equivalents of the PrE lineage, like PrESCs or naïve, extra-embryonic endodermal progenitor (nEnd) cells use either CHIR or WNT3A, respectively, to establish stable PrE-like cell lines (Anderson *et al*, 2017; Yasuhide *et al*, 2022). Taken together, we speculate that similarly to what has been proposed for ESCs, canonical Wnt activity could hinder differentiation of the PrE lineage during diapause, a mechanism that can be exploited for the capture of pre-implantation PrE-like cells *in vitro*.

Consistent with the idea of Wnt activity serving as a mechanism to pause embryonic development prior to implantation if needed, ablation of functional WNT ligands through a knockout of Porcupine (*Porcn*) does not cause obvious developmental defects before gastrulation (Biechele *et al*, 2013). However, WNT ligands are clearly expressed at the blastocyst stage (Kemp *et al*, 2005) and our analysis suggests activation of the Wnt pathway through interactions between the trophectoderm and the epiblast and PrE in non-diapause blastocysts. Moreover, using an *Axin2*^{LacZ} reporter, it has been shown that Wnt is active in the PrE and epiblast at the blastocyst stage, but is immediately shut down at early post-implantation stages (ten Berge *et al*, 2011). The reason for this transient Wnt activation as well as the mechanism by which it is shut down are unknown. We propose that Wnt activity might be downregulated through the secretion of Wnt inhibitors such as DKK1 by the PrE, as predicted by our analysis (Figure 1F). Supposing that the pre-implantation wave of Wnt must be downregulated to allow the progression of peri-implantation development, we speculate that Wnt activity levels in the blastocyst could act as a "developmental checkpoint". In other words, Wnt activity induced through WNT ligands coming from the TE could keep the epiblast and PrE undifferentiated until production of Wnt inhibitors surpasses a threshold, thereby shutting down Wnt activity and enabling development to proceed. Hitting said threshold could rely on the

maturity level of PrE cells, or simply on reaching an appropriate ratio of PrE cells in comparison to the epiblast and trophectoderm (Neagu *et al*, 2020). This would be an elegant solution by which the developing blastocyst lineages use signalling interactions to synchronise their development and avoid premature developmental progression.

Differentiation of PrE and epiblast is coupled to the formation of a basement membrane between the two tissues which facilitates their morphogenesis into the post-implantation egg cylinder (Bedzhov & Zernicka-Goetz, 2014). Conforming to the notion that Wnt inhibits developmental progression of the epiblast and PrE, high Wnt signalling activity also prevented the establishment of a basement membrane by PrE-like cells in our stem cell-based models. Nevertheless, the mechanism by which Wnt signalling obstructs basement membrane formation remains unclear. The generation of a basement membrane in developing epithelia is interlinked with the acquisition of an apical-basal cell polarity (O'Brien *et al*, 2001). However, in our experiments, PrESCs readily formed apical poles despite high cellular Wnt activity levels, suggesting that Wnt does not disrupt the establishment of cell polarity. While we did observe differences in the gene expression of basement membrane components (Figure S6H), expression of laminin proteins could be detected at similar levels irrespective of Wnt signalling activity (Figure S6G). Considering these conflicting results, we cannot exclude that Wnt might prevent the synthesis of basement membrane components. However, the failure to form a basement membrane could also be attributed to an inadequate supramolecular assembly of secreted laminin. Assembly of extracellular laminin into a basement membrane is mediated by cell surface laminin receptors (Hohenester & Yurchenco, 2013). Dystroglycan initially clusters laminin to the cell surface and, together with β1 integrins (*Itgb1*) and Perlecan, further organises it into increasingly complex structures (Henry *et al*, 2001). Interestingly, Dystroglycan is expressed at the basement membrane between the VE and epiblast cup, and a knockout of Dystroglycan (*Dag1*) disrupts the formation of the Reichert's membrane in the E6.5 embryo as well as the formation of a basement membrane in embryoid bodies (Williamson *et al*, 1997; Henry & Campbell, 1998). Moreover, *Itgb1* was significantly upregulated when culturing PrESCs in the absence of Wnt activators (Figure S6H). We speculate that elevated Wnt signalling activity might affect the regulators of laminin assembly, thereby counteracting the formation of a basement membrane. More experiments, also confirming an effect of Wnt on basement membrane formation *in vivo*, are needed.

In summary, our study shows that canonical Wnt signalling counteracts VE and DVE differentiation of PrE-like cells *in vitro*. Blockage of VE differentiation is accompanied by a failure to deposit a basement membrane in EpiCs, and therefore an absence of the mechanical cue that would guide the morphogenesis of the epiblast *in vivo*. Using Wnt agonists for the culture of PrE-like stem cells thus preserves cells in a state of pre-implantation potency, potentially harnessing *in vivo* mechanisms that halt development during diapause or prevent premature differentiation as a "developmental checkpoint".

4.5. Limitations of the study

While the presented work provides evidence that canonical Wnt signalling blocks the differentiation of the PrE into VE and DVE, the underlying mechanism remains to be determined and was outside the scope of this study. Additionally, the striking changes in cell morphology upon withdrawal of Wnt agonists from the culture were reminiscent of a VE phenotype, prompting us to solely investigate the differentiation of the PrE into VE. Consequently, we cannot comment on whether Wnt activity levels also affect the differentiation of the PrE into the parietal endoderm (PE), its second derivative lineage (Filimonow & de la Fuente, 2022). It will be interesting to see if Wnt signalling must also be shut down for PE differentiation, and if so, to identify which other signals determine either a VE or PE fate.

4.6. Figures

Continued on the next page.

Figure 1

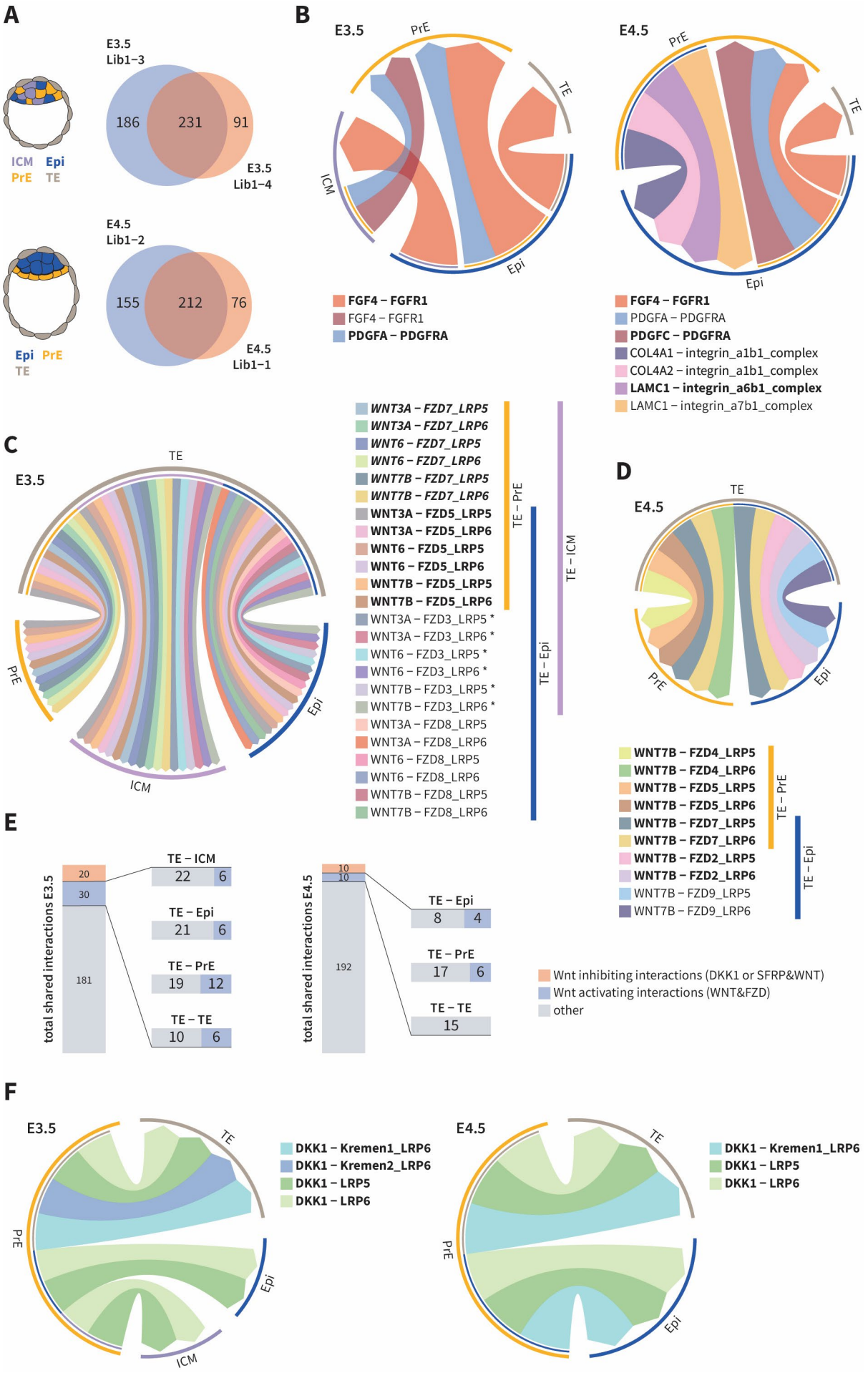
A
E3.5
Lib1–3
186
231
91
E3.5
Lib1–4
ICM Epi
PrE TE
E4.5
Lib1–2
155
212
76
E4.5
Lib1–1
Epi PrE
TE
B
E3.5
PrE
TE
ICM
Epi
FGF4 – FGFR1
FGF4 – FGFR1
PDGFA – PDGFRA
E4.5
PrE
TE
Epi
FGF4 – FGFR1
PDGFA – PDGFRA
PDGFC – PDGFRA
COL4A1 – integrin_a1b1_complex
COL4A2 – integrin_a1b1_complex
LAMC1 – integrin_a6b1_complex
LAMC1 – integrin_a7b1_complex
C
E3.5
TE
PrE
Epi
ICM
WNT3A – FZD7_LRP5
WNT3A – FZD7_LRP6
WNT6 – FZD7_LRP5
WNT6 – FZD7_LRP6
WNT7B – FZD7_LRP5
WNT7B – FZD7_LRP6
WNT3A – FZD5_LRP5
WNT3A – FZD5_LRP6
WNT6 – FZD5_LRP5
WNT6 – FZD5_LRP6
WNT7B – FZD5_LRP5
WNT7B – FZD5_LRP6
WNT3A – FZD3_LRP5 *
WNT3A – FZD3_LRP6 *
WNT6 – FZD3_LRP5 *
WNT6 – FZD3_LRP6 *
WNT7B – FZD3_LRP5 *
WNT7B – FZD3_LRP6 *
WNT3A – FZD8_LRP5
WNT3A – FZD8_LRP6
WNT6 – FZD8_LRP5
WNT6 – FZD8_LRP6
WNT7B – FZD8_LRP5
WNT7B – FZD8_LRP6
TE – PrE
TE – Epi
TE – ICM
D
E4.5
TE
PrE
Epi
WNT7B – FZD4_LRP5
WNT7B – FZD4_LRP6
WNT7B – FZD5_LRP5
WNT7B – FZD5_LRP6
WNT7B – FZD7_LRP5
WNT7B – FZD7_LRP6
WNT7B – FZD2_LRP5
WNT7B – FZD2_LRP6
WNT7B – FZD9_LRP5
WNT7B – FZD9_LRP6
TE – PrE
TE – Epi
E
total shared interactions E3.5
20
30
181
TE – ICM
22
6
TE – Epi
21
6
TE – PrE
19
12
TE – TE
10
6
total shared interactions E4.5
10
10
192
TE – Epi
8
4
TE – PrE
17
6
TE – TE
15
Wnt inhibiting interactions (DKK1 or SFRP&WNT)
Wnt activating interactions (WNT&FZD)
other
F
E3.5
TE
PrE
Epi
ICM
DKK1 – Kremen1_LRP6
DKK1 – Kremen2_LRP6
DKK1 – LRP5
DKK1 – LRP6
E4.5
TE
PrE
Epi
DKK1 – Kremen1_LRP6
DKK1 – LRP5
DKK1 – LRP6

Figure 1. Trophectoderm-secreted Wnt ligands are predicted to act on the epiblast and primitive endoderm at the blastocyst stage.

(**A**) Number of significant interactions predicted by CellphoneDB (Garcia-Alonso *et al*, 2022) for each analysed data set. Two data sets of E3.5 and two datasets of E4.5 blastocysts (Nowotschin *et al*, 2019) were each analysed individually. Cells were annotated as inner cell mass (ICM), epiblast (Epi), primitive endoderm (PrE), and trophectoderm (TE) at E3.5 and as Epi, PrE, and TE cells at E4.5. (**B**) Predicted significant interactions of ligands known to be involved in signalling at E3.5 and E4.5. The arrow indicates the direction of the interaction, with the first signalling partner being expressed in the cell type at the base of the arrow and the second signalling partner being expressed in the cell type at the tip of the arrow. Signalling partners are separated by dashes ("–"). Underscores ("_") indicate a multi-subunit signalling partner. Chord diagrams were generated using results of datasets Lib1-3 (E3.5) and Lib1-2 (E4.5). Bold interactions were predicted for both datasets of the respective timepoint. (**C**) Predicted significant interactions involving the ligands WNT3A, WNT6, and WNT7B at E3.5. Chord diagram was generated using results of the E3.5 dataset Lib1-3. Bold interactions were predicted for both datasets at E3.5. Bold and italic interactions were found in both datasets for TE – PrE, but not for TE – ICM. Interactions marked with asterisks were also predicted as autocrine interactions between TE – TE for both datasets. (**D**) Predicted significant interactions involving the ligands WNT3A, WNT6, and WNT7B at E4.5. Chord diagram was generated using results of the E4.5 dataset Lib1-1. Bold interactions were predicted for both datasets at E4.5. (**E**) Number of significant interactions classified as canonical Wnt activating or Wnt inhibiting as part of the overall number of identified interactions shared between both datasets of the respective time point. Wnt activating interactions are further broken down by interacting tissues. (**F**) Predicted significant interactions involving the Wnt inhibitor DKK1. The predicted significant autocrine interactions DKK1 – LRP5 and DKK1 – LRP6 between PrE – PrE at E3.5 and E4.5 are not plotted in the chord diagrams.

Figure 2

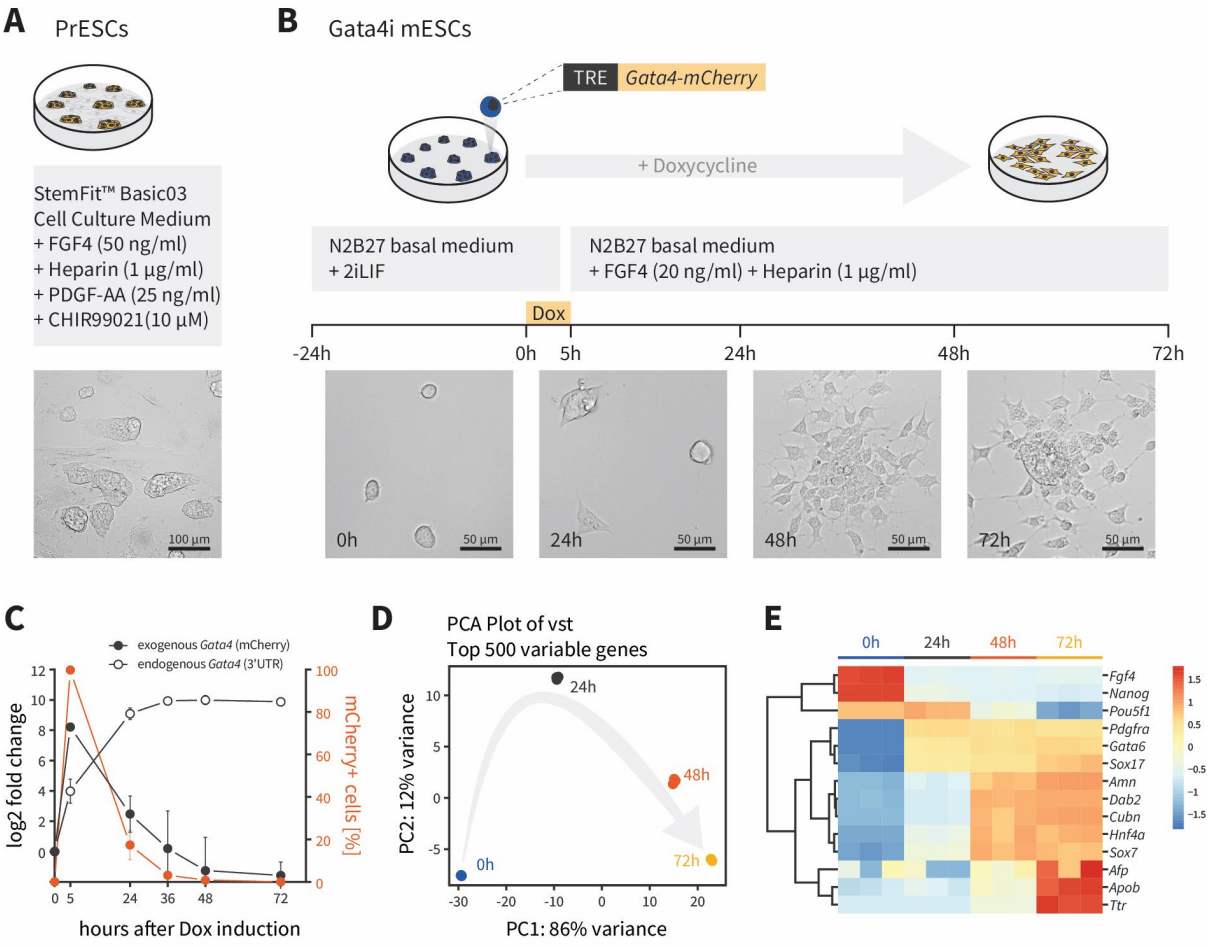
A
PrESCs
StemFit™ Basic03
Cell Culture Medium
+ FGF4 (50 ng/ml)
+ Heparin (1 µg/ml)
+ PDGF-AA (25 ng/ml)
+ CHIR99021(10 µM)
100 µm
B
Gata4i mESCs
TRE
Gata4-mCherry
+ Doxycycline
N2B27 basal medium
+ 2iLIF
N2B27 basal medium
+ FGF4 (20 ng/ml) + Heparin (1 µg/ml)
Dox
-24h
0h
5h
24h
48h
72h
0h
24h
48h
72h
50 µm
C
exogenous Gata4 (mCherry)
endogenous Gata4 (3'UTR)
log2 fold change
mCherry+ cells [%]
hours after Dox induction
D
PCA Plot of vst
Top 500 variable genes
PC2: 12% variance
PC1: 86% variance
0h
24h
48h
72h
E
0h
24h
48h
72h
Fgf4
Nanog
Pou5f1
Pdgfra
Gata6
Sox17
Amn
Dab2
Cubn
Hnf4a
Sox7
Afp
Apob
Ttr
F
NANOG
GATA6
overlay + Hoechst
NANOG
PDGFRA
overlay + Hoechst
2iLIF control
48h after Dox
100 µm

Figure 2. 2D model systems used to study primitive and visceral endoderm.

(**A**) PrESCs are cultured on feeders in StemFit™ Basic03 Cell Culture Medium supplemented with FGF4, Heparin, PDGF-AA and CHIR99021 (CHIR). (**B**) Gata4i mESCs were maintained on gelatin in standard 2iLIF medium (*i.e.*, 1 µM PD0325901, 3 µM CHIR, 20 ng/ml mLIF) and differentiated by a 5-hour doxycycline (Dox) pulse, followed by culture in N2B27 basal medium supplemented with FGF4 and Heparin for up to 72 hours. (**C**) Relative mRNA levels (normalised to 0h) for exogenous and endogenous GATA4 expression. Protein levels of exogenous GATA4-mCherry were traced by flow cytometry analysis at indicated time points. Data shown are mean ±SD of three independent experiments. (**D**) PCA clustering of bulk mRNA sequencing replicates (n=3) of Gata4i cells at indicated time points after Dox-induced differentiation. (**E**) Scaled gene expression heatmap of epiblast (*Fgf4*, *Nanog*), pluripotency (*Pou5f1*), PrE (*Gata6*, *Pdgfra*, *Sox17*, *Sox7*), and VE (*Amn*, *Dab2*, *Cubn*, *Hnf4a*, *Afp*, *Apob*, *Ttr*) markers at the indicated time points after Dox-induced differentiation. (**F**) Immunofluorescence stainings for PrE markers GATA6 and PDGFRA and epiblast marker NANOG at 48 hours after Dox-induction.

Figure 3

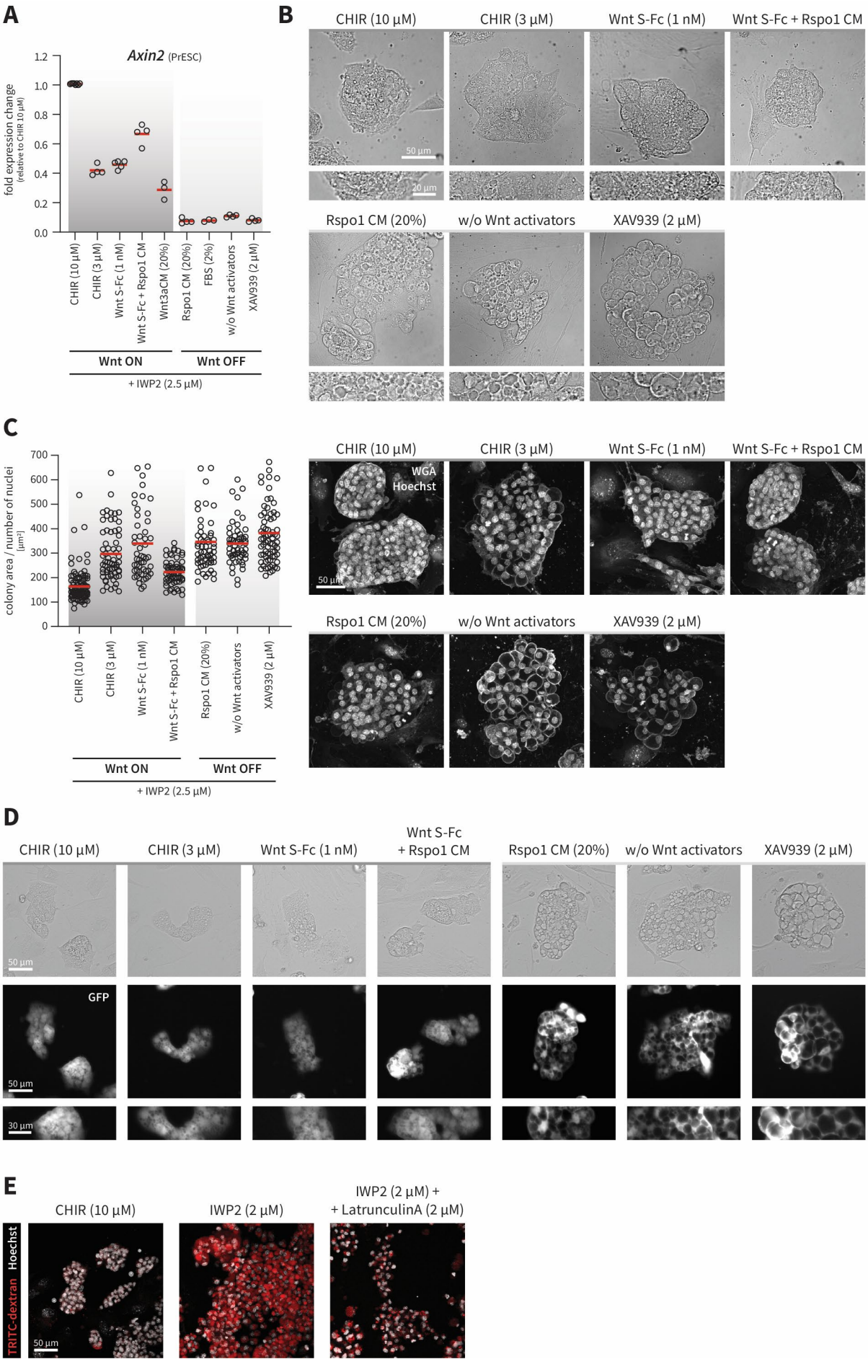
A
Axin2 (PrESC)
fold expression change (relative to CHIR 10 µM)
1.2
1.0
0.8
0.6
0.4
0.2
0.0
CHIR (10 µM)
CHIR (3 µM)
Wnt S-Fc (1 nM)
Wnt S-Fc + Rspo1 CM
Wnt3aCM (20%)
Rspo1 CM (20%)
FBS (2%)
w/o Wnt activators
XAV939 (2 µM)
Wnt ON
Wnt OFF
+ IWP2 (2.5 µM)
B
CHIR (10 µM)
CHIR (3 µM)
Wnt S-Fc (1 nM)
Wnt S-Fc + Rspo1 CM
50 µm
20 µm
Rspo1 CM (20%)
w/o Wnt activators
XAV939 (2 µM)
C
colony area / number of nuclei [µm²]
700
600
500
400
300
200
100
0
CHIR (10 µM)
CHIR (3 µM)
Wnt S-Fc (1 nM)
Wnt S-Fc + Rspo1 CM
Rspo1 CM (20%)
w/o Wnt activators
XAV939 (2 µM)
Wnt ON
Wnt OFF
+ IWP2 (2.5 µM)
CHIR (10 µM)
CHIR (3 µM)
Wnt S-Fc (1 nM)
Wnt S-Fc + Rspo1 CM
WGA
Hoechst
50 µm
Rspo1 CM (20%)
w/o Wnt activators
XAV939 (2 µM)
D
CHIR (10 µM)
CHIR (3 µM)
Wnt S-Fc (1 nM)
Wnt S-Fc + Rspo1 CM
Rspo1 CM (20%)
w/o Wnt activators
XAV939 (2 µM)
50 µm
GFP
50 µm
30 µm
E
CHIR (10 µM)
IWP2 (2 µM)
IWP2 (2 µM) +
+ LatrunculinA (2 µM)
TRITC-dextran
Hoechst
50 µm

Figure 3. Wnt activity affects the morphology of PrE-like cells *in vitro*, suggesting developmental progression.

(**A**) *Axin2* mRNA expression levels of PrESCs cultured for 72 hours in PrESC medium without CHIR99021 (CHIR), supplemented with Wnt activators or inhibitors as indicated. PrESCs cultured with 10 μM CHIR were used as a control. 2% FBS was chosen as a control for Wnt3a conditioned medium (CM) which contains 10% FBS. Rspo1 CM alone should not induce Wnt signalling and was included as a control for WntS-Fc+Rspo1 CM. Data shown are from at least three independent experiments; mean is indicated by red bar. (**B**) Brightfield images of PrESC colonies cultured for 72 hours in PrESC medium without CHIR, with IWP2 (2.5 μM), and supplemented with Wnt activators or inhibitors as indicated. (**C**) Left: Average area per cell (calculated by PrESC colony area / number of nuclei per PrESC colony) after 72 hours of culture in PrESC medium without CHIR, with IWP2 (2.5 μM), and supplemented with Wnt activators or inhibitors as indicated. Colony area and number of nuclei were determined based on WGA and Hoechst stainings as shown on the right. See also Figure S3C. Data shown are from four independent experiments; mean is indicated by red bar. (**D**) Intrinsic GFP signal of GFP-PrESCs cultured for 72 hours in PrESC medium without CHIR, with IWP2 (2.5 μM), and supplemented with Wnt activators or inhibitors as indicated. (**E**) Endocytosis assay using TRITC-dextran for 30 minutes on PrESCs. As a control PrESCs cultured for 72 hours with IWP2 were treated with LatrunculinA for 5 hours prior to TRITC-dextran incubation. This experiment was performed by Jolien Jacobs at Erasmus MC, Rotterdam, the Netherlands.

Figure 4

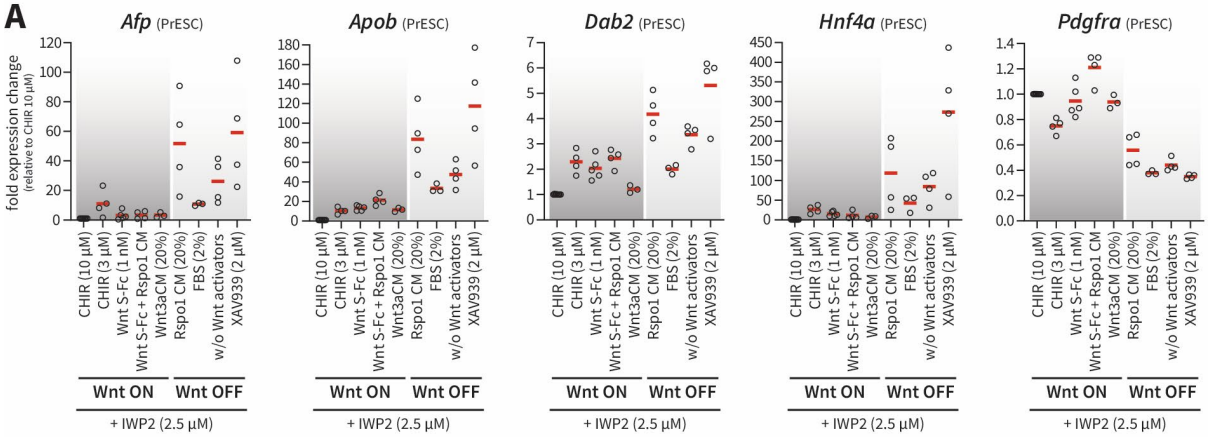
A
Afp (PrESC)
Apob (PrESC)
Dab2 (PrESC)
Hnf4a (PrESC)
Pdgfra (PrESC)
fold expression change
(relative to CHIR 10 µM)
CHIR (10 µM)
CHIR (3 µM)
Wnt S-Fc (1 nM)
Wnt S-Fc + Rspo1 CM
Wnt3aCM (20%)
Rspo1 CM (20%)
FBS (2%)
w/o Wnt activators
XAV939 (2 µM)
Wnt ON
Wnt OFF
+ IWP2 (2.5 µM)

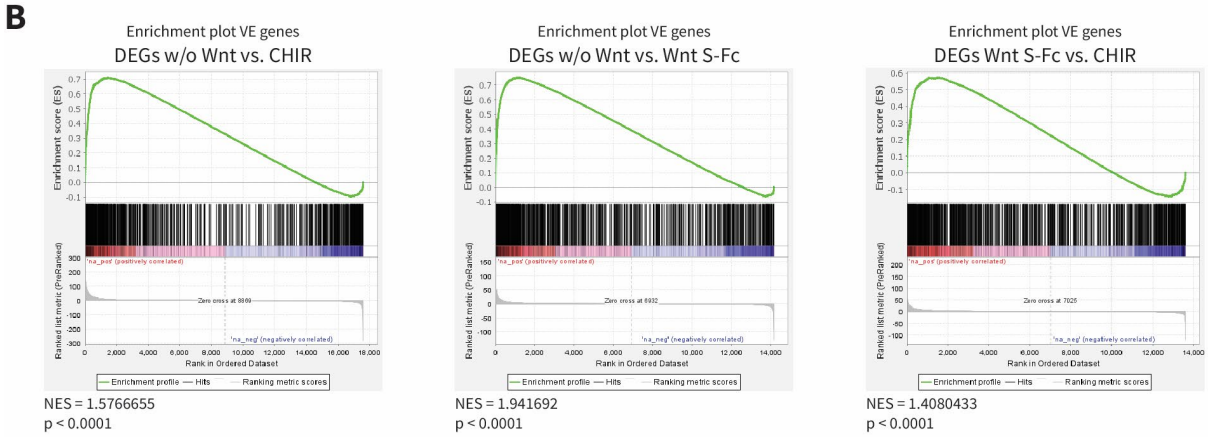
B
Enrichment plot VE genes
DEGs w/o Wnt vs. CHIR
NES = 1.5766655
p < 0.0001
Enrichment plot VE genes
DEGs w/o Wnt vs. Wnt S-Fc
NES = 1.941692
p < 0.0001
Enrichment plot VE genes
DEGs Wnt S-Fc vs. CHIR
NES = 1.4080433
p < 0.0001
Enrichment score (ES)
Ranked list metric (PreRanked)
Rank in Ordered Dataset
Enrichment profile
Hits
Ranking metric scores

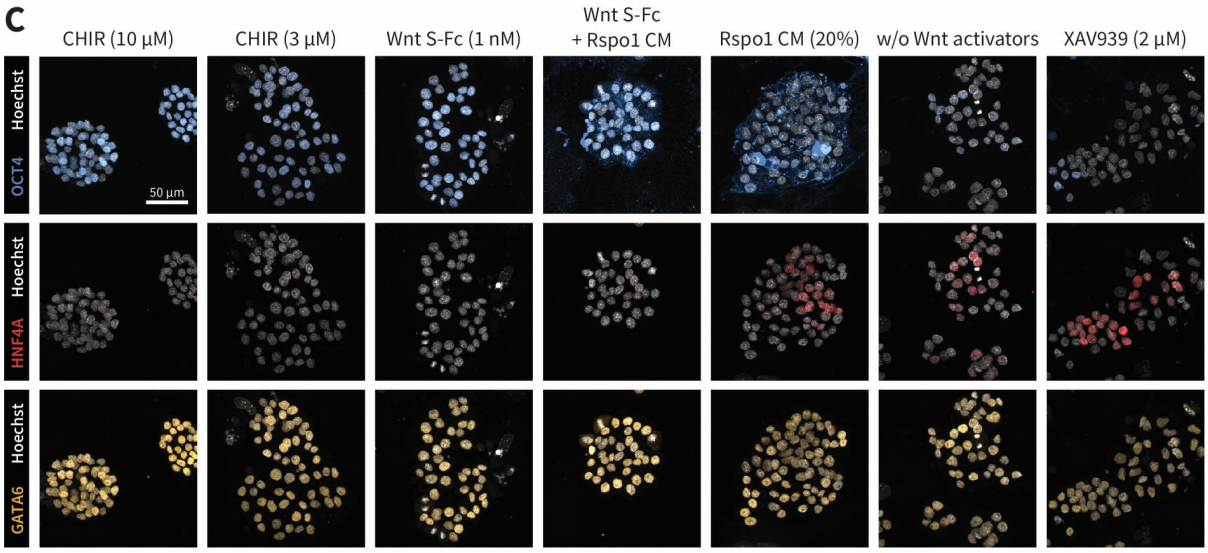
C
CHIR (10 µM)
CHIR (3 µM)
Wnt S-Fc (1 nM)
Wnt S-Fc + Rspo1 CM
Rspo1 CM (20%)
w/o Wnt activators
XAV939 (2 µM)
Hoechst
OCT4
HNF4A
GATA6
50 µm

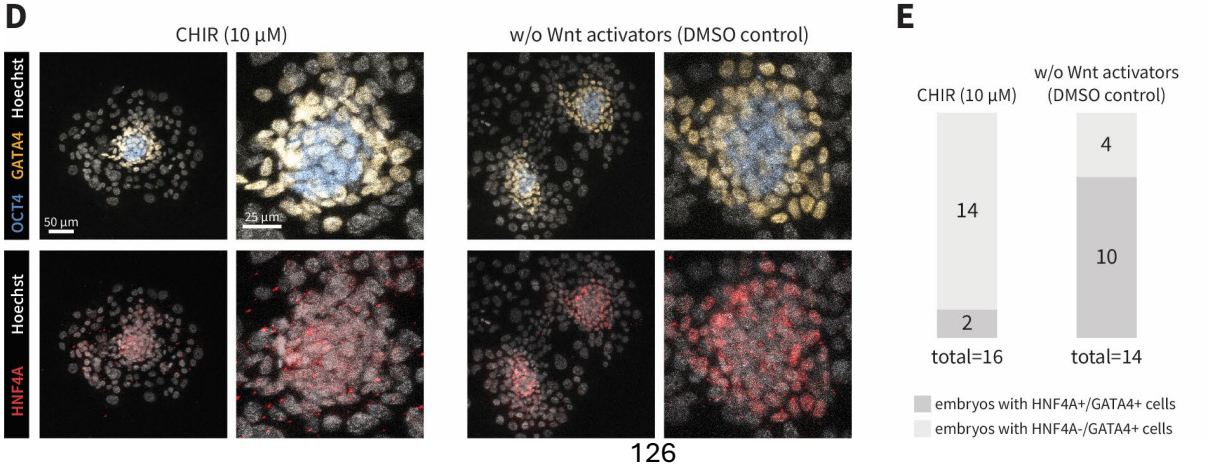
D
CHIR (10 µM)
w/o Wnt activators (DMSO control)
Hoechst
OCT4
GATA4
HNF4A
50 µm
25 µm
E
CHIR (10 µM)
w/o Wnt activators
(DMSO control)
14
2
4
10
total=16
total=14
embryos with HNF4A+/GATA4+ cells
embryos with HNF4A-/GATA4+ cells

Figure 4. Release from Wnt signalling induces visceral endoderm differentiation.

(**A**) mRNA expression levels of VE markers (*Afp*, *Apob*, *Dab2*, *Hnf4a*) and PrE marker (*Pdgfra*) of PrESCs cultured for 72 hours in PrESC medium without CHIR99021 (CHIR), supplemented with Wnt activators or inhibitors as indicated. PrESCs cultured with 10 µM CHIR were used as a control. 2% FBS was chosen as a control for Wnt3a conditioned medium (CM) which contains 10% FBS. Rspo1 CM alone should not induce Wnt signalling and was included as a control for WntS-Fc+Rspo1 CM. Data shown are from at least three independent experiments; mean is indicated by red bar. (**B**) Gene set enrichment analyses testing for the enrichment of VE specific genes among DEGs between PrESCs cultured without Wnt activators or with CHIR (left), between PrESCs cultured without Wnt activators or Wnt S-Fc (middle), or between PrESCs cultured with Wnt S-Fc or CHIR (right). DEGs were determined from bulk mRNA sequencing data of PrESCs cultured under the respective conditions for 72 hours. The VE gene set consists of genes that are upregulated in VE cells of embryos at E5.5 compared to PrE cells of embryos at E4.5 (Nowotschin *et al*, 2019). (**C**) Immunofluorescence stainings for pluripotency marker OCT4, VE marker HNF4A, and PrE marker GATA6 of PrESCs cultured for 72 hours in PrESC medium without CHIR, with IWP2 (2.5 µM), and supplemented with Wnt activators or inhibitors as indicated. (**D**) Immunofluorescence stainings of blastocysts that were isolated at E3.7 and initially cultured for 12 hours *in vitro* before post-implantation culture in IVC1 medium ± CHIR from E4.2-E5.5. This experiment was performed by Jolien Jacobs at Erasmus MC, Rotterdam, the Netherlands. (**E**) Number of embryos showing $HNF4A^{+}/GATA4^{+}$ double positive cells for the experiment shown in (D).

Figure 5

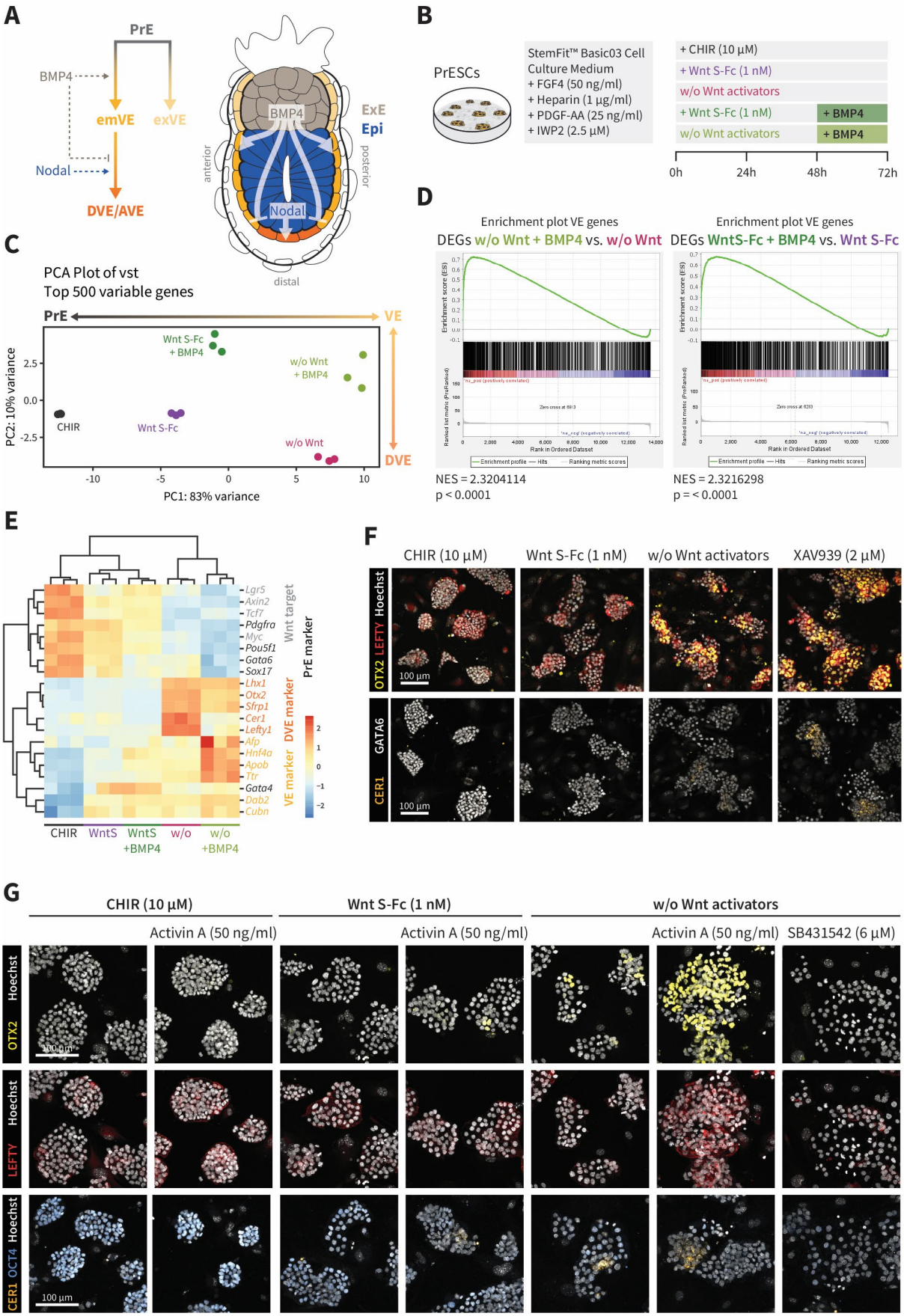
A
PrE
BMP4
emVE
exVE
Nodal
DVE/AVE
BMP4
Nodal
ExE
Epi
anterior
posterior
distal
B
PrESCs
StemFit™ Basic03 Cell Culture Medium
+ FGF4 (50 ng/ml)
+ Heparin (1 µg/ml)
+ PDGF-AA (25 ng/ml)
+ IWP2 (2.5 µM)
+ CHIR (10 µM)
+ Wnt S-Fc (1 nM)
w/o Wnt activators
+ Wnt S-Fc (1 nM)
+ BMP4
w/o Wnt activators
+ BMP4
0h
24h
48h
72h
C
PCA Plot of vst
Top 500 variable genes
PrE
VE
DVE
Wnt S-Fc + BMP4
w/o Wnt + BMP4
CHIR
Wnt S-Fc
w/o Wnt
PC2: 10% variance
PC1: 83% variance
D
Enrichment plot VE genes
DEGs w/o Wnt + BMP4 vs. w/o Wnt
NES = 2.3204114
p < 0.0001
Enrichment plot VE genes
DEGs WntS-Fc + BMP4 vs. Wnt S-Fc
NES = 2.3216298
p = < 0.0001
E
Lgr5
Axin2
Tcf7
Pdgfra
Myc
Pou5f1
Gata6
Sox17
Lhx1
Otx2
Sfrp1
Cer1
Lefty1
Afp
Hnf4a
Apob
Ttr
Gata4
Dab2
Cubn
Wnt target
PrE marker
DVE marker
VE marker
CHIR
WntS
WntS +BMP4
w/o
w/o +BMP4
F
CHIR (10 µM)
Wnt S-Fc (1 nM)
w/o Wnt activators
XAV939 (2 µM)
OTX2 LEFTY Hoechst
GATA6
CER1
100 µm
G
CHIR (10 µM)
Wnt S-Fc (1 nM)
w/o Wnt activators
Activin A (50 ng/ml)
Activin A (50 ng/ml)
Activin A (50 ng/ml)
SB431542 (6 µM)
Hoechst
OTX2
LEFTY
CER1 OCT4 Hoechst
100 µm

Figure 5. Wnt activity influences cellular response to differentiation signals BMP4 and Activin A.

(**A**) Schematic representation of known signalling pathways leading to specialisation of the distal visceral endoderm (DVE) in the post-implantation embryo. Nodal from the epiblast (Epi) specifies DVE fate, while BMP4 from the extra-embryonic ectoderm (ExE) counteracts DVE differentiation and restricts it only to the distal region of the embryonic VE (emVE). BMP4 is also necessary to specify emVE identity, which is distinct from extra-embryonic VE (exVE). Later, cells sharing similar markers with the DVE form the anterior VE (AVE) at the anterior side of the embryo at the interface between emVE and exVE (not shown). (**B**) PrESCs were cultured for 72 hours in PrESC medium without CHIR, with IWP2 (2.5 µM), and supplemented with either CHIR or Wnt S-Fc. For the last 24 hours of culture BMP4 (50 ng/ml) was added to the medium before harvesting the cells for bulk mRNA sequencing analysis at 72 hours. (**C**) PCA clustering of bulk mRNA sequencing replicates (n=3) of PrESCs of the respective experimental conditions as shown in (B). (**D**) Gene set enrichment analyses testing for the enrichment of VE specific genes among DEGs between PrESCs cultured without Wnt activators ± BMP4 (left), or between PrESCs cultured with Wnt S-Fc ± BMP4 (right). DEGs were determined from bulk mRNA sequencing data of PrESCs cultured under the experimental conditions as shown in (B). The VE gene set consists of genes that are upregulated in VE cells of embryos at E5.5 compared to PrE cells of embryos at E4.5 (Nowotschin *et al*, 2019). (**E**) Scaled gene expression heatmap of indicated PrE, Wnt target, VE, and DVE markers of PrESCs cultured under the experimental conditions as shown in (B). (**F**) Immunofluorescence stainings for DVE/AVE markers OTX2, LEFTY1, and CER1 of PrESCs cultured for 72 hours in PrESC medium without CHIR99021 (CHIR), with IWP2 (2.5 µM), and supplemented with Wnt activators or inhibitors as indicated. (**G**) Immunofluorescence stainings for DVE/AVE markers OTX2, LEFTY1, and CER1 of PrESCs cultured for 72 hours in PrESC medium without CHIR, with IWP2 (2.5 µM), and supplemented with CHIR, Wnt S-Fc, and Activin A as indicated. Treatment with the TGFβ inhibitor SB431542 was included as a negative control.

Figure 6

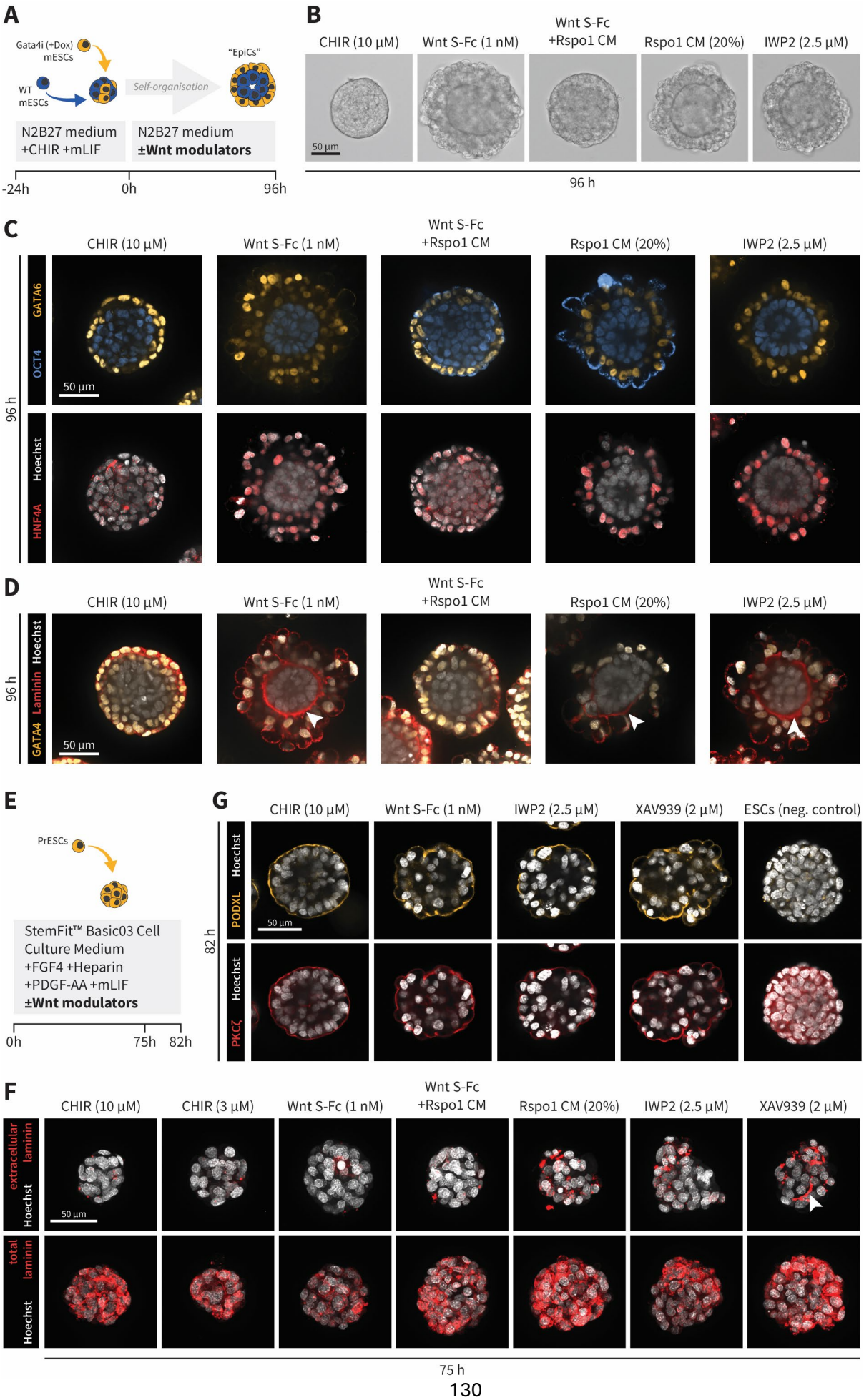
A
Gata4i (+Dox) mESCs
WT mESCs
Self-organisation
"EpiCs"
N2B27 medium +CHIR +mLIF
N2B27 medium ±Wnt modulators
-24h
0h
96h
B
CHIR (10 µM)
Wnt S-Fc (1 nM)
Wnt S-Fc +Rspo1 CM
Rspo1 CM (20%)
IWP2 (2.5 µM)
50 µm
96 h
C
CHIR (10 µM)
Wnt S-Fc (1 nM)
Wnt S-Fc +Rspo1 CM
Rspo1 CM (20%)
IWP2 (2.5 µM)
96 h
GATA6
OCT4
Hoechst
HNF4A
50 µm
D
CHIR (10 µM)
Wnt S-Fc (1 nM)
Wnt S-Fc +Rspo1 CM
Rspo1 CM (20%)
IWP2 (2.5 µM)
96 h
Hoechst
Laminin
GATA4
50 µm
E
PrESCs
StemFit™ Basic03 Cell Culture Medium +FGF4 +Heparin +PDGF-AA +mLIF ±Wnt modulators
0h
75h
82h
G
CHIR (10 µM)
Wnt S-Fc (1 nM)
IWP2 (2.5 µM)
XAV939 (2 µM)
ESCs (neg. control)
82 h
Hoechst
PODXL
PKCζ
50 µm
F
CHIR (10 µM)
CHIR (3 µM)
Wnt S-Fc (1 nM)
Wnt S-Fc +Rspo1 CM
Rspo1 CM (20%)
IWP2 (2.5 µM)
XAV939 (2 µM)
extracellular laminin
Hoechst
total laminin
50 µm
75 h

Figure 6. Wnt signalling prevents PrE differentiation and basement membrane formation in a 3D model of epiblast/PrE peri-implantation development.

(**A**) Gata4i mESCs were treated with Doxycycline for 5 hours before aggregating them with WT mESCs in N2B27 medium supplemented with CHIR99021 (CHIR, 3 μM) and mLIF (20 ng/ml). After 24 hours the aggregates were maintained in N2B27 supplemented with Wnt activators or inhibitors for 96 hours during which cells self-organised to form post-implantation like structures, termed "EpiCs". (**B**) Brightfield images of Gata4i-EpiCs after 96 hours of culture with Wnt activators and inhibitors as indicated. (**C**) Immunofluorescence stainings for PrE marker GATA6, pluripotency/epiblast marker OCT4, and VE marker HNF4A of Gata4i-EpiCs shown in (B). (**D**) Immunofluorescence stainings for PrE marker GATA4 and laminin of Gata4i-EpiCs shown in (B). White arrows point at the basement membrane deposited between Gata4i cells and ESCs. (**E**) PrESCs were aggregated in PrESC medium without CHIR, with mLIF (20 ng/ml), and supplemented with Wnt activators or inhibitors for either 75 or 82 hours. (**F**) Maximum intensity Z-projections of immunofluorescence stainings for extracellular or total cellular laminin of PrESC aggregates. Staining procedures were identical after fixation of the aggregates, however, cells were not permeabilised to detect extracellular laminin only. White arrow indicates laminin sheet deposited between cells. See also Figure S6G. (**G**) Immunofluorescence stainings for apical markers PODXL and PKCζ of PrESC aggregates. Unpolarised ESC aggregates were used as a negative control. See also Figure S6H.

Figure S2

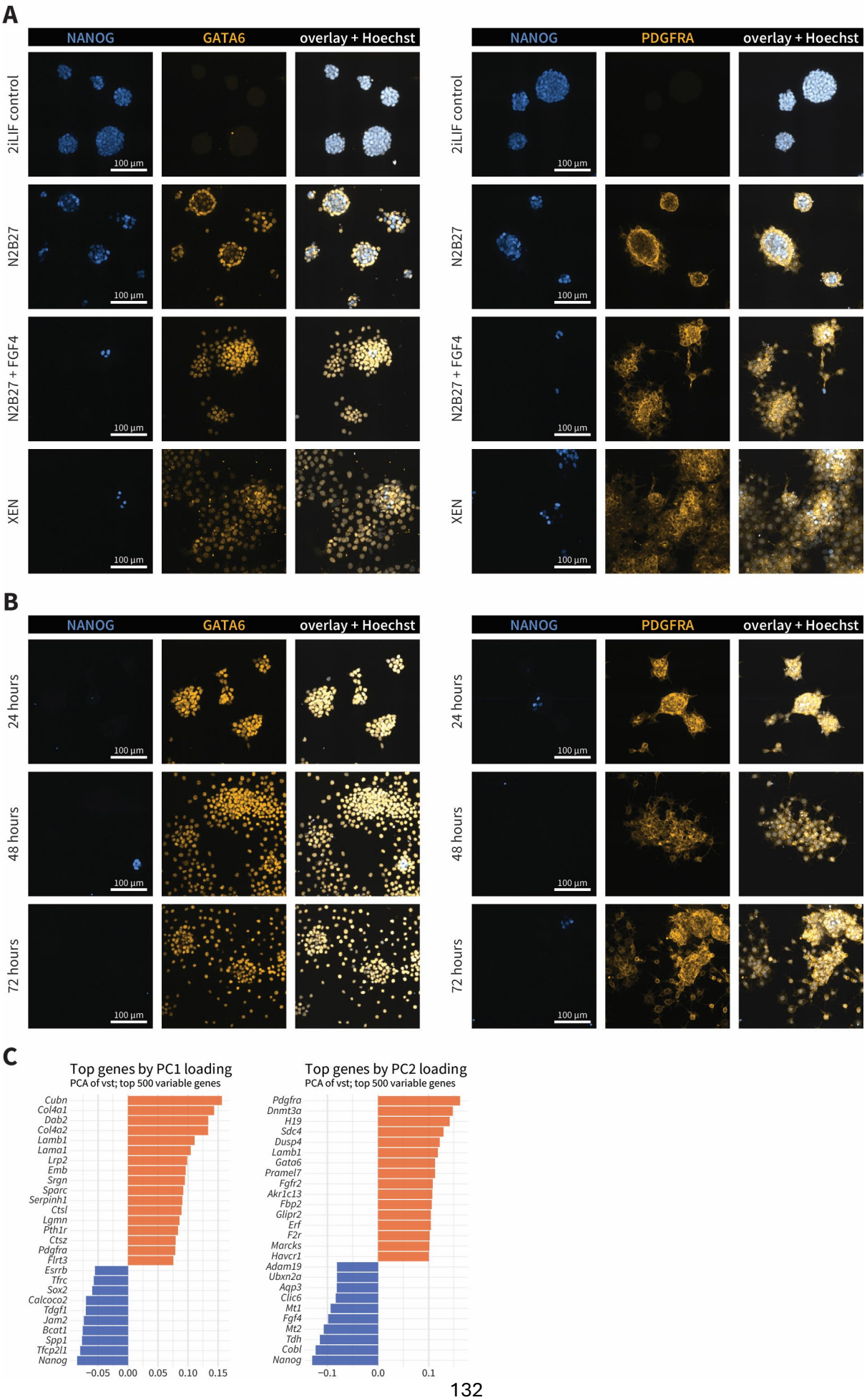
A
NANOG
GATA6
overlay + Hoechst
NANOG
PDGFRA
overlay + Hoechst
2iLIF control
N2B27
N2B27 + FGF4
XEN
100 µm
B
24 hours
48 hours
72 hours
C
Top genes by PC1 loading
PCA of vst; top 500 variable genes
Cubn
Col4a1
Dab2
Col4a2
Lamb1
Lama1
Lrp2
Emb
Srgn
Sparc
Serpinh1
Ctsl
Lgmn
Pth1r
Ctsz
Pdgfra
Flrt3
Esrrb
Tfrc
Sox2
Calcoco2
Tdgf1
Jam2
Bcat1
Spp1
Tfcp2l1
Nanog
−0.05
0.00
0.05
0.10
0.15
Top genes by PC2 loading
PCA of vst; top 500 variable genes
Pdgfra
Dnmt3a
H19
Sdc4
Dusp4
Lamb1
Gata6
Pramel7
Fgfr2
Akr1c13
Fbp2
Glipr2
Erf
F2r
Marcks
Havcr1
Adam19
Ubxn2a
Aqp3
Clic6
Mt1
Fgf4
Mt2
Tdh
Cobl
Nanog
−0.1
0.0
0.1

Figure S2

(**A**) To test which medium allows for efficient, homogenous differentiation of Gata4i mESCs we performed immunofluorescence stainings for PrE markers GATA6 and PDGFRA and epiblast marker NANOG after doxycycline (Dox) induction and culture for 48 hours in the indicated media. (**B**) Immunofluorescence stainings for PrE markers GATA6 and PDGFRA and epiblast marker NANOG after Dox induction and culture in N2B27 + FGF4 (20 ng/ml) + Heparin (1 µg/ml) for 24, 48, or 72 hours. (**C**) Principal component loadings associated with the top genes for the PCA shown in Figure 2D.

Figure S3

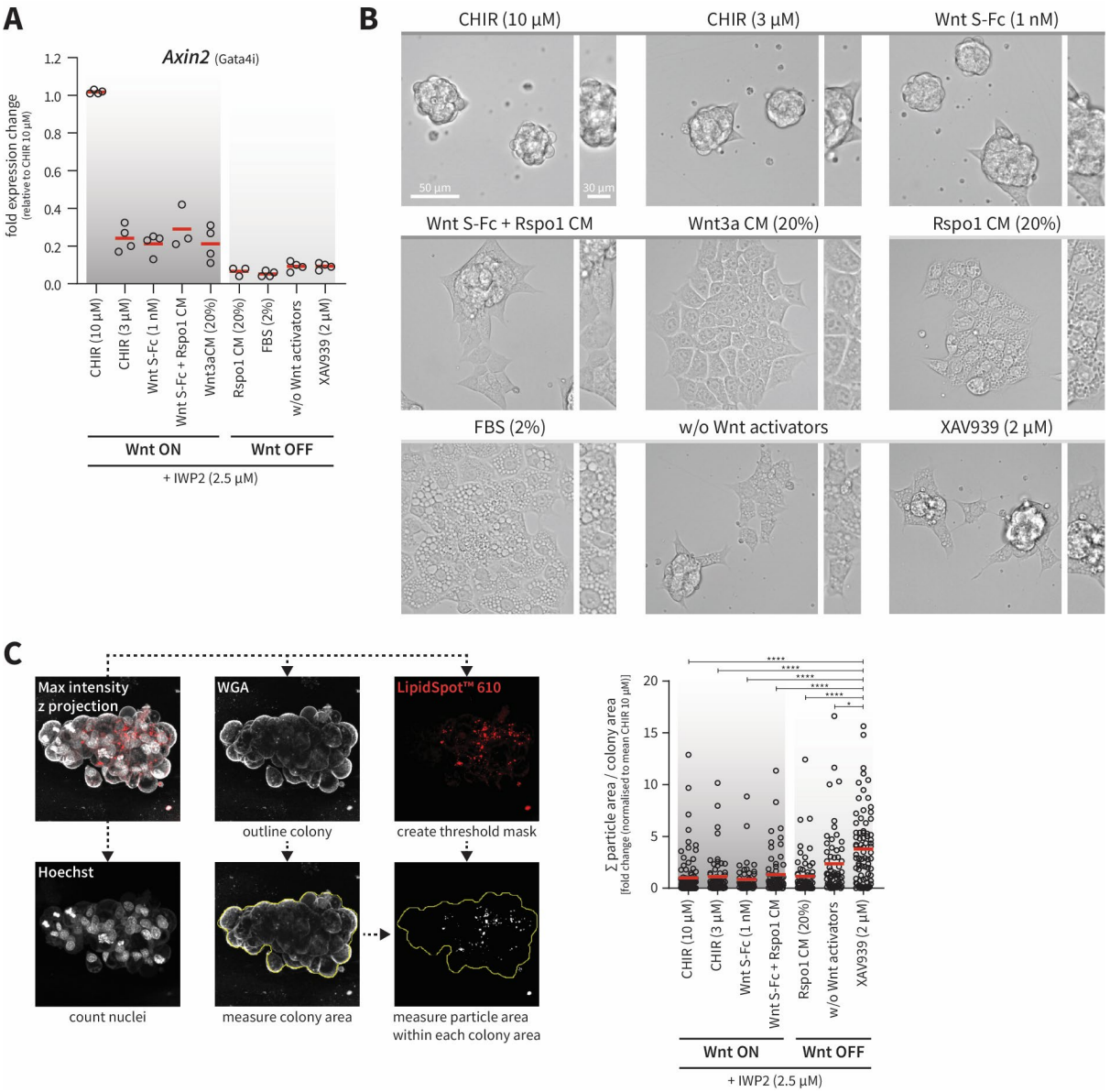
A
Axin2 (Gata4i)
fold expression change
(relative to CHIR 10 µM)
1.2
1.0
0.8
0.6
0.4
0.2
0.0
CHIR (10 µM)
CHIR (3 µM)
Wnt S-Fc (1 nM)
Wnt S-Fc + Rspo1 CM
Wnt3aCM (20%)
Rspo1 CM (20%)
FBS (2%)
w/o Wnt activators
XAV939 (2 µM)
Wnt ON
Wnt OFF
+ IWP2 (2.5 µM)
B
CHIR (10 µM)
CHIR (3 µM)
Wnt S-Fc (1 nM)
50 µm
30 µm
Wnt S-Fc + Rspo1 CM
Wnt3a CM (20%)
Rspo1 CM (20%)
FBS (2%)
w/o Wnt activators
XAV939 (2 µM)
C
Max intensity
z projection
WGA
LipidSpot™ 610
outline colony
create threshold mask
Hoechst
count nuclei
measure colony area
measure particle area
within each colony area
∑ particle area / colony area
[fold change (normalised to mean CHIR 10 µM)]
20
15
10
5
0
****
****
****
****
****
*
CHIR (10 µM)
CHIR (3 µM)
Wnt S-Fc (1 nM)
Wnt S-Fc + Rspo1 CM
Rspo1 CM (20%)
w/o Wnt activators
XAV939 (2 µM)
Wnt ON
Wnt OFF
+ IWP2 (2.5 µM)

Figure S3

(**A**) *Axin2* mRNA expression levels of Gata4i mESCs after Dox induction and culture for 72 hours in N2B27 medium with FGF4 (20 ng/ml) and Heparin (1 µg/ml), supplemented with Wnt activators or inhibitors as indicated. 2% FBS was chosen as a control for Wnt3a conditioned medium (CM) which contains 10% FBS. Rspo1 CM alone should not induce Wnt signalling and was included as a control for WntS-Fc+Rspo1 CM. Data shown are from at least three independent experiments; mean is indicated by red bar. (**B**) Brightfield images of Gata4i mESCs used for the analysis in (A). (**C**) Left: Workflow for image analysis of PrESCs stained with WGA, Hoechst, and LipidSpot™ 610. Right: Fraction of colony area filled with lipid droplets, plotted as fold change compared to the mean value of the CHIR 10 µM condition of each experiment. Data shown are from four independent experiments; mean is indicated by red bar. The data was analysed for statistically significant differences using a one-way ANOVA, followed by a Tukey's multiple comparisons test. $p<0.0001$ (****); $p<0.05$ (*)

Figure S4

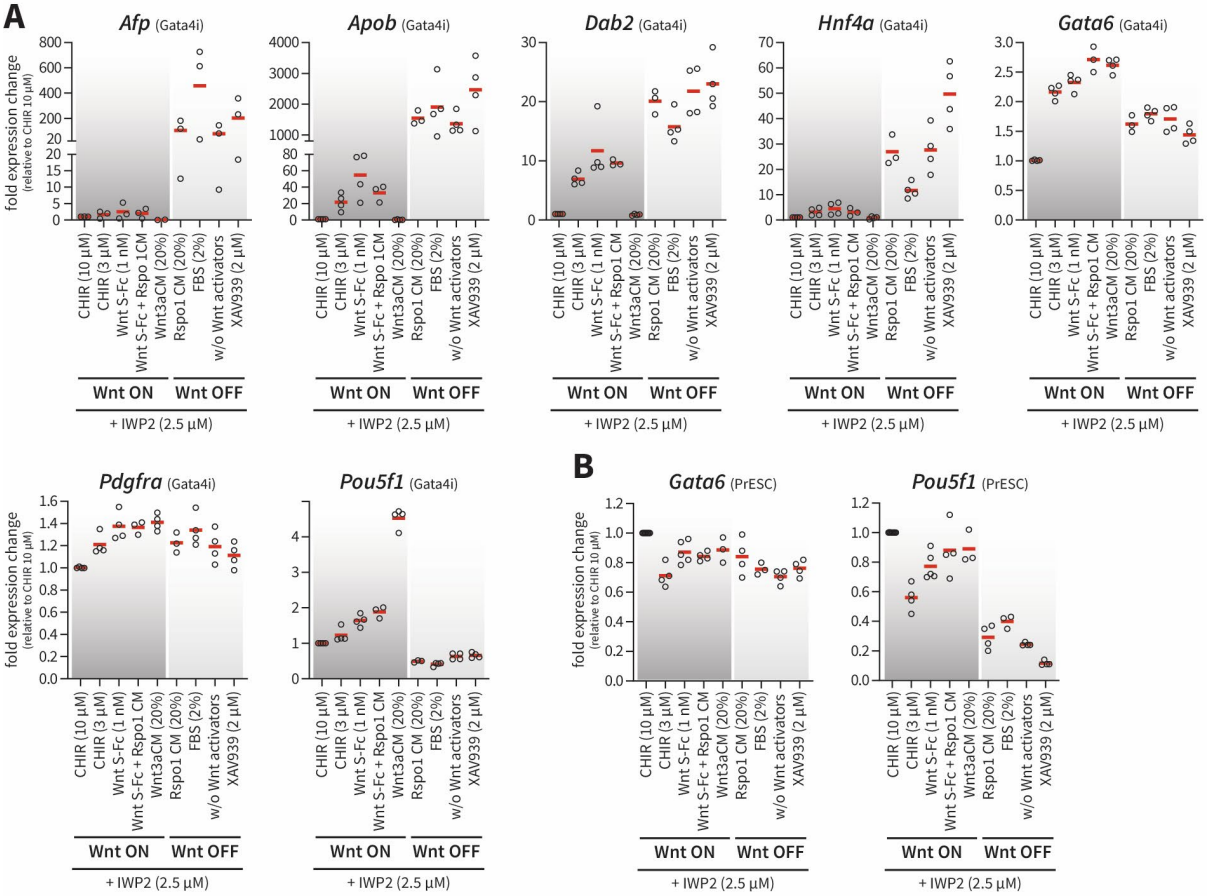

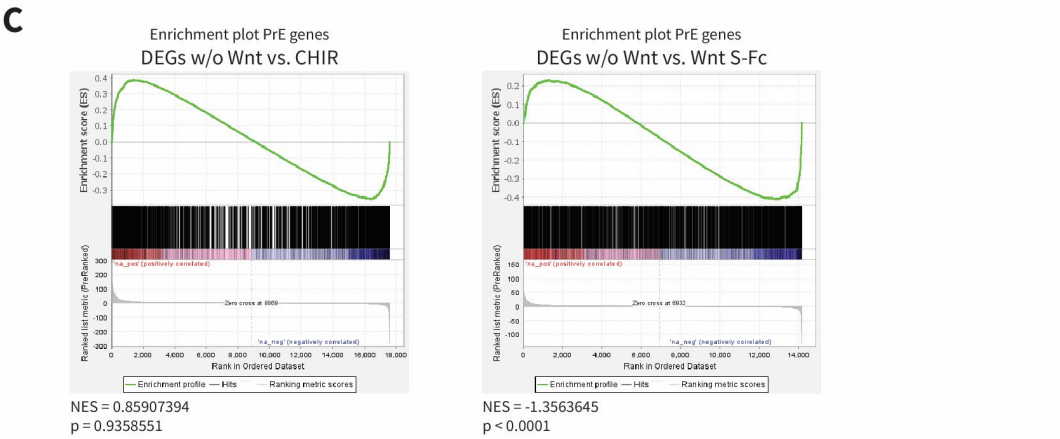

NES = 0.85907394
p = 0.9358551

NES = -1.3563645
p < 0.0001

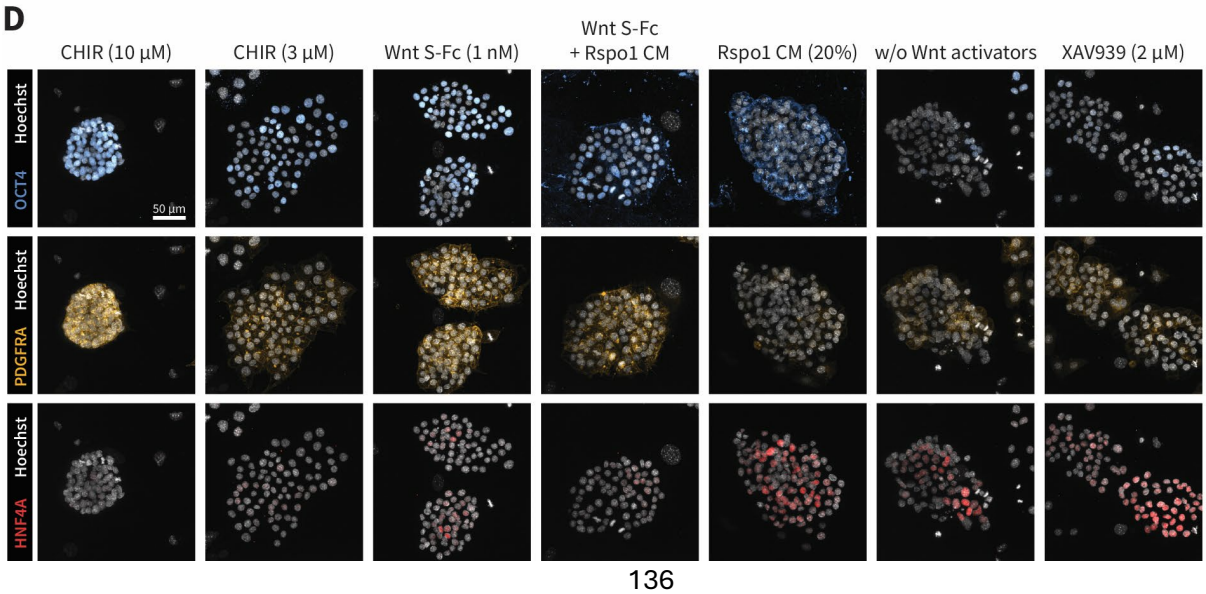

Figure S4

(**A**) mRNA expression levels of VE markers (*Afp*, *Apob*, *Dab2*, *Hnf4a*), PrE markers (*Gata6*, *Pdgfra*), and pluripotency marker (*Pou5f1*) of Gata4i mESCs after Dox induction and culture for 72 hours in N2B27 medium with FGF4 (20 ng/ml) and Heparin (1 µg/ml) supplemented with Wnt activators or inhibitors as indicated. 2% FBS was chosen as a control for Wnt3a conditioned medium (CM) which contains 10% FBS. Rspo1 CM alone should not induce Wnt signalling and was included as a control for WntS-Fc+Rspo1 CM. Data shown are from at least three independent experiments; mean is indicated by red bar. (**B**) mRNA expression levels PrE marker (*Gata6*) and pluripotency marker (*Pou5f1*) of PrESCs cultured for 72 hours in PrESC medium without CHIR99021 (CHIR), supplemented with Wnt activators or inhibitors as indicated. PrESCs cultured with 10 µM CHIR were used as a control. 2% FBS was chosen as a control for Wnt3a conditioned medium (CM) which contains 10% FBS. Rspo1 CM alone should not induce Wnt signalling and was included as a control for WntS-Fc+Rspo1 CM. Data shown are from at least three independent experiments; mean is indicated by red bar. (**C**) Gene set enrichment analyses testing for the enrichment of PrE specific genes among DEGs between PrESCs cultured without Wnt activators or with CHIR (left), or between PrESCs cultured without Wnt activators or Wnt S-Fc (right). DEGs were determined from bulk mRNA sequencing data of PrESCs cultured under the respective conditions for 72 hours. The PrE gene set consists of genes that are upregulated in PrE cells of embryos at E4.5 compared to VE cells of embryos at E5.5 (Nowotschin *et al*, 2019). (**D**) Immunofluorescence stainings for pluripotency marker OCT4, PrE marker PDGFRA, and VE marker HNF4A, of PrESCs cultured for 72 hours in PrESC medium without CHIR, with IWP2 (2.5 µM), and supplemented with Wnt activators and inhibitors as indicated.

Figure S5

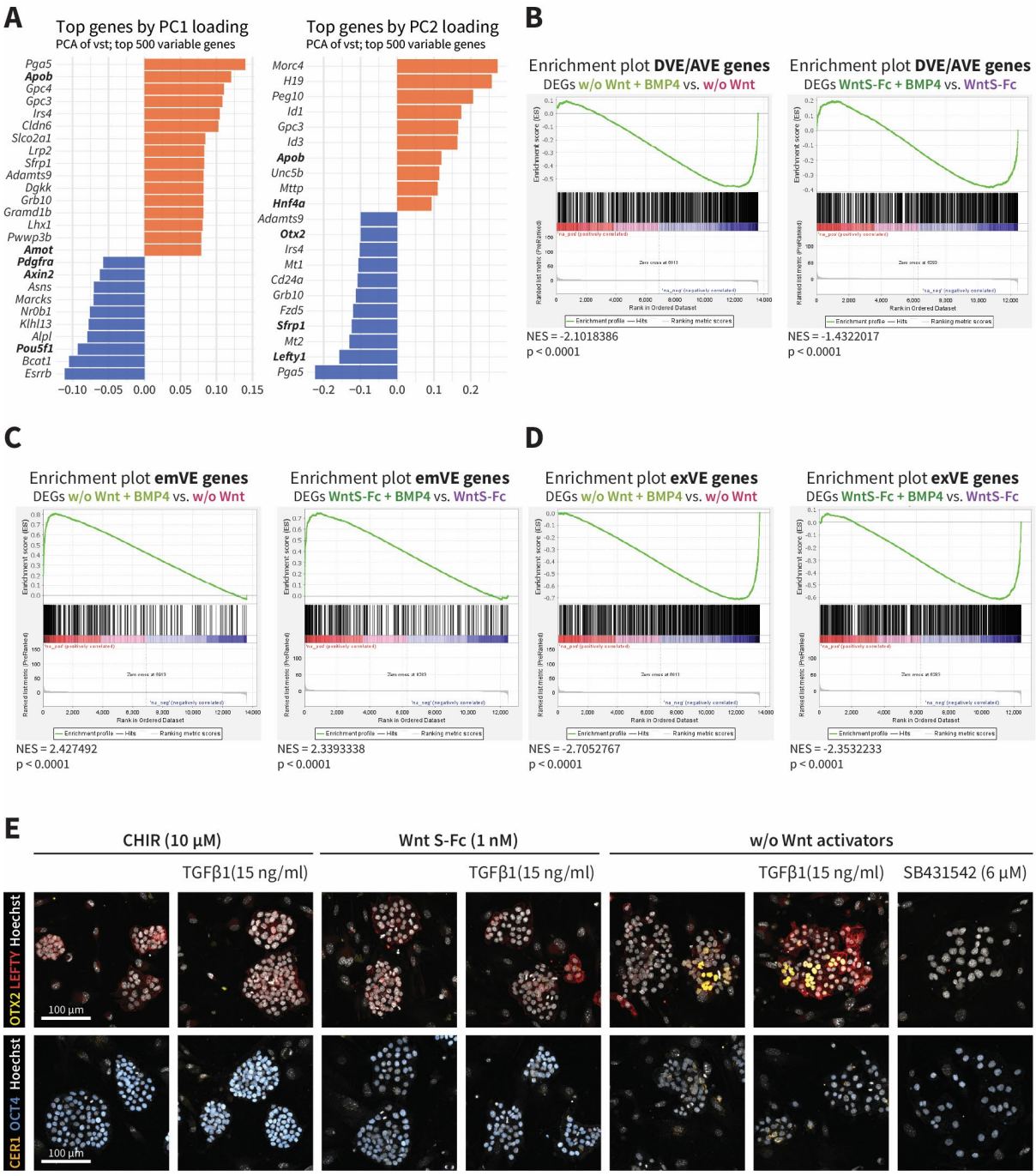
A
Top genes by PC1 loading
PCA of vst; top 500 variable genes
Pga5
Apob
Gpc4
Gpc3
Irs4
Cldn6
Slco2a1
Lrp2
Sfrp1
Adamts9
Dgkk
Grb10
Gramd1b
Lhx1
Pwwp3b
Amot
Pdgfra
Axin2
Asns
Marcks
Nr0b1
Klhl13
Alpl
Pou5f1
Bcat1
Esrrb
−0.10 −0.05 0.00 0.05 0.10 0.15
Top genes by PC2 loading
PCA of vst; top 500 variable genes
Morc4
H19
Peg10
Id1
Gpc3
Id3
Apob
Unc5b
Mttp
Hnf4a
Adamts9
Otx2
Irs4
Mt1
Cd24a
Grb10
Fzd5
Sfrp1
Mt2
Lefty1
Pga5
−0.2 −0.1 0.0 0.1 0.2
B
Enrichment plot DVE/AVE genes
DEGs w/o Wnt + BMP4 vs. w/o Wnt
NES = -2.1018386
p < 0.0001
Enrichment plot DVE/AVE genes
DEGs WntS-Fc + BMP4 vs. WntS-Fc
NES = -1.4322017
p < 0.0001
C
Enrichment plot emVE genes
DEGs w/o Wnt + BMP4 vs. w/o Wnt
NES = 2.427492
p < 0.0001
Enrichment plot emVE genes
DEGs WntS-Fc + BMP4 vs. WntS-Fc
NES = 2.3393338
p < 0.0001
D
Enrichment plot exVE genes
DEGs w/o Wnt + BMP4 vs. w/o Wnt
NES = -2.7052767
p < 0.0001
Enrichment plot exVE genes
DEGs WntS-Fc + BMP4 vs. WntS-Fc
NES = -2.3532233
p < 0.0001
E
CHIR (10 μM)
Wnt S-Fc (1 nM)
w/o Wnt activators
TGFβ1(15 ng/ml)
TGFβ1(15 ng/ml)
TGFβ1(15 ng/ml)
SB431542 (6 μM)
OTX2 LEFTY Hoechst
CER1 OCT4 Hoechst
100 μm
100 μm

Figure S5

(**A**) Principal component loadings associated with the top genes for the PCA shown in Figure 5C. (**B**)-(**D**) Gene set enrichment analyses testing for the enrichment of (**B**) distal/anterior VE (DVE/AVE)-, (**C**) embryonic VE (emVE)-, and (**D**) extra-embryonic (exVE)-specific genes among DEGs between PrESCs cultured without Wnt activators ± BMP4, or between PrESCs cultured with Wnt S-Fc ± BMP4. DEGs were determined from bulk mRNA sequencing data of PrESCs cultured under the respective conditions as shown in Figure 5B. The DVE/AVE, emVE, and exVE gene sets consist of DVE/AVE, emVE-, or exVE-specific genes between E5.25-E6.5, which have been published previously (Zhu *et al*, 2023). (**E**) Immunofluorescence stainings for DVE/AVE markers OTX2, LEFTY1, and CER1 of PrESCs cultured for 72 hours in PrESC medium without CHIR99021 (CHIR), with IWP2 (2.5 μM), and supplemented with CHIR, Wnt S-Fc, and TGFβ1 as indicated. Treatment with the TGFβ inhibitor SB431542 was included as a negative control. TGFβ1 was only added to the culture medium during the last 24 hours before fixation.

Figure S6

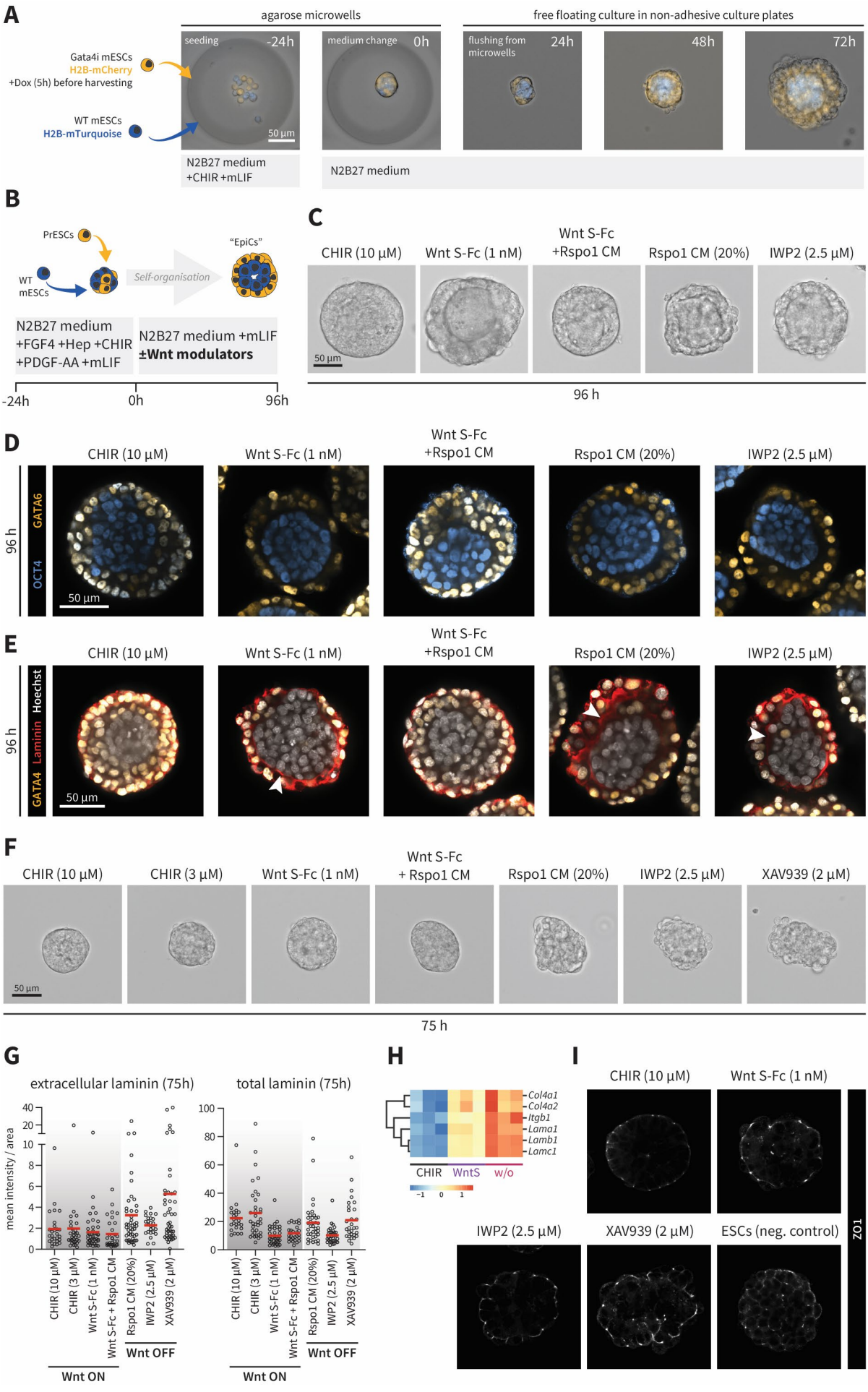
A
agarose microwells
free floating culture in non-adhesive culture plates
Gata4i mESCs
H2B-mCherry
+Dox (5h) before harvesting
WT mESCs
H2B-mTurquoise
seeding
-24h
medium change
0h
flushing from microwells
24h
48h
72h
50 µm
N2B27 medium +CHIR +mLIF
N2B27 medium
B
PrESCs
WT mESCs
Self-organisation
"EpiCs"
N2B27 medium +FGF4 +Hep +CHIR +PDGF-AA +mLIF
N2B27 medium +mLIF ±Wnt modulators
-24h
0h
96h
C
CHIR (10 µM)
Wnt S-Fc (1 nM)
Wnt S-Fc +Rspo1 CM
Rspo1 CM (20%)
IWP2 (2.5 µM)
50 µm
96 h
D
CHIR (10 µM)
Wnt S-Fc (1 nM)
Wnt S-Fc +Rspo1 CM
Rspo1 CM (20%)
IWP2 (2.5 µM)
96 h
GATA6
OCT4
50 µm
E
CHIR (10 µM)
Wnt S-Fc (1 nM)
Wnt S-Fc +Rspo1 CM
Rspo1 CM (20%)
IWP2 (2.5 µM)
96 h
Hoechst
Laminin
GATA4
50 µm
F
CHIR (10 µM)
CHIR (3 µM)
Wnt S-Fc (1 nM)
Wnt S-Fc + Rspo1 CM
Rspo1 CM (20%)
IWP2 (2.5 µM)
XAV939 (2 µM)
50 µm
75 h
G
extracellular laminin (75h)
total laminin (75h)
mean intensity / area
CHIR (10 µM)
CHIR (3 µM)
Wnt S-Fc (1 nM)
Wnt S-Fc + Rspo1 CM
Rspo1 CM (20%)
IWP2 (2.5 µM)
XAV939 (2 µM)
Wnt ON
Wnt OFF
H
Col4a1
Col4a2
Itgb1
Lama1
Lamb1
Lamc1
CHIR
WntS
w/o
I
CHIR (10 µM)
Wnt S-Fc (1 nM)
IWP2 (2.5 µM)
XAV939 (2 µM)
ESCs (neg. control)
ZO1

Figure S6

(**A**) Time course of Gata4i-EpiC formation. Gata4i mESCs and wild type (WT) mESCs were labelled with H2B-mCherry or H2B-mTurquoise to track the location of the respective lineage within EpiCs. (**B**) PrESCs were aggregated together with WT mESCs in N2B27 medium supplemented with FGF4 (50 ng/ml), Heparin (1 µg/ml), CHIR99021 (CHIR, 10 µM), PDGF-AA (25 ng/ml), and mLIF (20 ng/ml). After 24 hours the aggregates were further maintained in N2B27 supplemented with mLIF (20 ng/ml) and Wnt activators or inhibitors for 96 hours during which cells self-organised to form post-implantation like structures, termed "EpiCs". (**C**) Brightfield images of PrESC-EpiCs after 96 hours of culture in Wnt activators or inhibitors as indicated. (**D**) Immunofluorescence stainings for PrE marker GATA6 and pluripotency/epiblast marker OCT4 of PrESC-EpiCs shown in (C). (**E**) Immunofluorescence stainings for PrE marker GATA4 and laminin of PrESC-EpiCs shown in (C). White arrows point at the basement membrane deposited between PrESCs and ESCs. (**F**) Brightfield images of PrESC aggregates cultured in PrESC medium without CHIR, with mLIF (20 ng/ml), and supplemented with Wnt activators or inhibitors as indicated for 75 hours. (**G**) Mean fluorescence intensity of laminin signal of PrESC aggregates, normalised to the aggregate area, measured using sum-Z-projections. (**H**) Scaled gene expression heatmap of basement membrane components and integrin β1 of PrESCs cultured under the experimental conditions as shown in Figure 5B. (**I**) Immunofluorescence stainings of PrESC aggregates stained for ZO1, a scaffold protein at tight junctions of well-polarized epithelial cells. Unpolarised ESC aggregates were used as a negative control.

4.7. Methods

4.7.1. Stem cells and culture conditions

Gata4i mESCs (clone 5) were obtained from Christian Schröter's lab at the Max Planck Institute of Molecular Physiology, Dortmund, Germany (Raina *et al*, 2021). Cells were maintained on 0.1% gelatin coated tissue culture plates in 2iLIF medium, that is N2B27 basal medium (*i.e*. 1:1 DMEM/F-12 (in-house Media Lab) and Neurobasal medium (in-house Media Lab) supplemented with 1X N-2 supplement (Gibco, 17502048), 1X B-27 supplement (Gibco, 17504044), 1X GlutaMAX (Gibco, 35050038), 10 mM HEPES (in-house Media Lab), 100 µM β-mercaptoethanol (Gibco, 31350010), and 1X Penicillin-Streptomycin (Gibco, 15140122)) which was supplemented with 20 ng/ml mLIF (in-house Molecular Biology Services), 1 µM PD0325901 (MedChemExpress, HY-10254), and 3 µM CHIR99021 (MedChemExpress, HY-10182). Culture medium was changed daily, and cells were routinely passaged every three days using Accutase (Biozym Scientific, B423201) for cell detachment. For differentiation, cells were plated on 0.1% gelatin coated tissue culture plates and Doxycycline (MedChemExpress, HY-N0565B) was added the next day to the medium at a final concentration of 100 ng/ml. After five hours, the medium was removed and replaced with N2B27 basal medium supplemented with 20 ng/ml FGF4 (Qkine, Qk004) and 1 µg/ml Heparin (Sigma, H3149). XEN medium, which was used as a differentiation medium in one experiment (Figure S2A), was RPMI 1640 (in-house Media Lab) supplemented with 15% Foetal Bovine Serum (FBS, Sigma-Aldrich, F7524), 100 µM β-mercaptoethanol, 1X Penicillin-Streptomycin, and 1 mM Sodium Pyruvate (Gibco, 11360070).

One GFP-labelled (11-7 M) and one wild type (12-1 M) PrESCs line were obtained from Haruhiko Koseki's lab at the RIKEN Center for Integrative Medical Sciences, Wako, Japan (Yasuhide *et al*, 2022). Cells were maintained on feeders in PrESC medium, that is StemFit™ Basic03 Cell Culture Medium (Amsbio, SFB-503) supplemented with 10 µM CHIR99021, 50 ng/ml FGF4, 1 µg/ml Heparin, 25 ng/ml PDGF-AA (Qkine, Qk043), and 1X Penicillin-Streptomycin. Culture medium was changed daily, and cells were routinely passaged every three days using Accutase for cell detachment.

Depending on the experiment, 2.5 µM IWP2 (Tocris, 3533), 2 µM XAV939 (MedChemExpress, HY-15147), 1 nM WNT Surrogate-Fc Fusion Protein (ImmunoPrecise Antibodies, N001, Lot 3660), 20% Wnt3a conditioned medium, 20% Rspo1 conditioned medium, or 2% FBS were added to the medium as indicated. In most experiments, IWP2 was added to both Wnt ON and Wnt OFF conditions to prevent the secretion of any endogenous WNT ligands by the cells. For experiments related to DVE differentiation 15 ng/ml recombinant TGF (Qkine, Qk010), 50 ng/ml recombinant BMP4 (PeproTech, 315-27), or 6 µM SB431542 (MedChemExpress, HY-10431) were added to the medium as indicated.

G4 mouse ESCs were obtained from Andras Nagy's lab at the Lunenfeld Tanenbaum Research Institute, Toronto, Canada (George *et al*, 2007) and were cultured in 2iLIF medium as described above. Culture medium was changed daily, and cells were routinely passaged every three days using Accutase for cell detachment.

All cell lines were cultured under standard cell culture conditions at 37°C in a humidified atmosphere containing 5% CO_2 and 20% O_2.

4.7.2. Preparation of conditioned medium

L Wnt-3A cells were maintained in DMEM high glucose (in-house Media Lab) supplemented with 10% FBS, 10 mM HEPES, 1X GlutaMAX, 1X Penicillin-Streptomycin, and 125 µg/ml Zeocin™ Selection Reagent (Gibco, R25001). To prepare Wnt3a conditioned medium, cells were cultured in the same medium without Zeocin for 5-7 days before the medium was collected, centrifuged, and filter sterilised. Medium was stored at 4°C.

HA-R-Spondin1-Fc 293T cells were maintained in DMEM high glucose supplemented with 10% FBS, 10 mM HEPES, 1X GlutaMAX, 1 mM Sodium Pyruvate, 1X Penicillin-Streptomycin, and 300 µg/ml Zeocin™ Selection Reagent. To prepare Rspo1 conditioned medium, cells were cultured in Advanced DMEM/F-12 (Gibco, 12634010) supplemented with 10 mM HEPES, 1X GlutaMAX, and 1X Penicillin-Streptomycin for 7-10 days before the medium was collected, centrifuged, and filter sterilised. Medium was stored at -20°C.

4.7.3. EpiC formation

Agarose microwells (⌀ 200 µm) were fabricated as described previously (Vrij *et al*, 2016), and incubated with serum containing medium (*i.e.* DMEM high glucose supplemented with 10% FBS, 10 mM HEPES, 1X GlutaMAX, 1X MEM Non-Essential Amino Acids (Gibco, 11140035), and 50 µM β-mercaptoethanol) for at least 24 hours. Doxycycline (100 ng/ml) was added to the medium of Gata4i cells for 5 hours prior to harvesting to induce differentiation. Gata4i cells were then combined with G4 mESCs at a ratio of 3:2 in a single-cell suspension in N2B27 basal medium supplemented with 20 ng/ml mLIF and 3 µM CHIR99021. The suspension was seeded onto microwells aiming for 16 cells per microwell. After incubating for 24 hours, the medium was replaced with N2B27 basal medium supplemented with Wnt pathway modulators, as specified for each experiment. 48 hours after seeding, the aggregates were flushed from the microwells by gently pipetting up and down, and then transferred into non tissue culture treated 6-well plates (Falcon, 351146). Fresh medium was added each day and EpiCs were collected, washed in PBS, and fixed at the indicated time points after seeding.

For PrESC-EpiCs, PrESCs were harvested, plated on a 0.1% gelatin-coated plate, and incubated for 45 minutes to exclude feeder cells. PrESCs were then combined with G4 mESCs at a ratio of 3:2 in a single-cell suspension in N2B27 basal medium supplemented with 20 ng/ml mLIF, 10 µM CHIR99021, 50 ng/ml FGF4, 1 µg/ml Heparin, and 25 ng/ml PDGF-AA. The suspension was seeded onto microwells aiming for 16 cells per microwell. After incubating for 24 hours, the medium was replaced with N2B27 basal medium supplemented with 20 ng/ml mLIF and Wnt pathway modulators, as specified for each experiment. 48 hours after seeding,

the aggregates were flushed from the microwells by gently pipetting up and down, and then transferred into non tissue culture treated 6-well plates. Fresh medium was added each day and EpiCs were collected, washed in PBS, and fixed at the indicated time points after seeding.

4.7.4. PrESC aggregate formation

Agarose microwells were prepared as described for EpiC formation. PrESCs were harvested, plated on a 0.1% gelatin-coated plate, and incubated for 45 minutes to exclude feeder cells. PrESCs were then seeded onto microwells aiming for 16 cells per microwell in Basic03 Cell Culture Medium supplemented with 20 ng/ml mLIF, 50 ng/ml FGF4, 1 µg/ml Heparin, and 25 ng/ml PDGF-AA. Wnt pathway modulators were added as specified for each experiment. 48 hours after seeding, the aggregates were flushed from the microwells by gently pipetting up and down, and then transferred into non tissue culture treated 6-well plates. PrESC aggregates were collected, washed in PBS, and fixed at the indicated time points after seeding.

4.7.5. Embryo culture

The presented embryo experiment was conducted by Jolien Jacobs at Erasmus MC, Rotterdam, the Netherlands, and approved by the Centrale Commissie Dierproeven (the Hague, the Netherlands) and by the Erasmus MC Animal Ethical Committee. Embryos were obtained from crosses between FVB/N mice. For superovulation, female mice were injected intraperitoneally with Folligonan (5-7.5 IU in 100-150 µl) followed by another intraperitoneal injection of Chorulon (5-7.5 IU in 100-150 µl) 24 hours later. The superovulated females were then housed together with males for mating overnight. Males were removed the next day and females were checked for copulation plugs. Embryos were collected from the uteri at embryonic day E3.7 and kept in IVC1 medium (*i.e.* Advanced DMEM/F-12 supplemented with 20% FBS, 1X GlutaMAX, 1X Penicillin-Streptomycin, 1X ITS-X (Gibco, 51500056), 0.22% Sodium Lactate (Sigma-Aldrich, L7900), 1 mM Sodium Pyruvate, and 25 µM N-acetyl-L-Cysteine (Sigma-Aldrich, A7250) at 37°C, 5% O2, and 5% CO2. At embryonic day E4.2, embryos were transferred into imaging dishes (Ibidi, 80826) coated with 1:200 Cultrex Basement Membrane Extract (Bio-Techne, 3533-010-02), and incubated in IVC1 medium ± 10 µM CHIR99021 until embryonic day E5.5 when they were fixed.

4.7.6. Live cell images

Brightfield images of live 2D and 3D samples were taken using an EVOS™ M7000 Imaging System (Thermo Fisher Scientific). This system also allowed for the detection of GFP, H2B-mCherry, and H2B-mTurquoise in live cells.

4.7.7. Immunofluorescence

For stainings of cells cultured in 2D, cells were grown on 8-well chamber slides (Ibidi, 80826), washed with PBS, and fixed using 4% Formaldehyde (Invitrogen, 28908) in PBS for 15-20 minutes at room temperature (RT). 3D samples were washed once with PBS before fixation using 4% Formaldehyde in PBS for 30-40 minutes at RT.

Samples were permeabilised with 0.3% Triton-X100 in PBS (PBS-T) for one hour at RT followed by one hour of blocking at RT using 2% bovine serum albumin and 2% donkey serum (Biowest, S2170) in 0.1% PBS-T. When staining for extracellular laminin, the permeabilization step was omitted, and samples were directly placed into blocking solution. All samples were then incubated at 4°C overnight with primary antibodies diluted in blocking solution. The following day, samples were washed three times with 0.1% PBS-T and then incubated with the secondary antibodies in blocking solution for one hour at RT. Hoechst 33342 (Invitrogen, H3570) was used to counterstain the nuclei. Samples were washed another three times with 0.1% PBS-T and imaged in PBS on either a ZEISS Axio Observer inverted microscope equipped with a Yokogawa CSU X1 spinning disk and a Hamamatsu EM-CCD Camera C9100-13 or on an Olympus IX83 inverted microscope equipped with a Yokogawa W1 spinning disk and a Hamamatsu ORCA-Fusion Digital CMOS camera C14440-20UP. Images were analysed using ImageJ (Version 1.53c). A list of all antibodies used in this study is provided in Table S3.

4.7.8. LipidSpot™ staining

PrESCs were seeded into 8-well chamber slides on feeders in PrESC medium without CHIR99021, with IWP2 (2.5 µM), and supplemented with Wnt activators or inhibitors, as specified. Medium was changed daily. After three days 1X LipidSpot™ 610 dye (Biotium, 70069) was added to the medium and cells were incubated at 37°C for another hour. Cells were then washed once with PBS and fixed using 4% Formaldehyde for 15 min at RT. The samples were washed again with PBS, and a staining solution containing 1 µg/ml Wheat germ agglutinin (WGA, Invitrogen, W11261) and 2 µg/ml Hoechst 33342 in PBS were added for 30 minutes at RT. Samples were washed three times with PBS before imaging them on an Olympus IX83 inverted microscope equipped with a Yokogawa W1 spinning disk and a Hamamatsu ORCA-Fusion Digital CMOS camera C14440-20UP.

4.7.9. Image analysis and quantification

All images were analysed using Fiji (Schindelin *et al*, 2012). For the analysis of LipidSpot™ stainings, first, the “Freehand selections” tool was used to outline colonies on maximum intensity Z-projections of the WGA channel. The area of each selection (*i.e*. colony area) was recorded. Maximum intensity Z-projections of the LipidSpot™ channel were converted into threshold masks and the “Analyze Particles” tool was used to determine the number of particles

and their area within each selected colony area. The number of cells per colony was assessed by counting the number of nuclei in each selected colony area on maximum intensity Z-projections of the Hoechst 33342 channel. See also Figure S3C.

To quantify the expression levels of extracellular and total laminin of PrESC aggregates, first, the aggregates were outlined on sum intensity Z-projections of the Hoechst 33342 channel using the "Freehand selections" tool. The area of each selection was recorded, and the mean fluorescence intensity was measured within the selection area on sum intensity Z-projections of the laminin channel.

4.7.10. Endocytosis assay

This experiment was performed by Jolien Jacobs at Erasmus MC, Rotterdam, the Netherlands. PrESCs were cultured on feeders in 8-well chamber slides (Ibidi, 80826) for 72 hours in PrESC medium without CHIR99021, supplemented with 2 µM IWP2 and DMSO or 10 µM CHIR99021. As a control, 2 µM Latrunculin A (Cayman Chemical, 10010630) was added to the cells cultured with IWP2 five hours prior to performing the endocytosis assay. For the endocytosis assay, samples were incubated with 1 mg/ml TRITC-Dextran (Sigma-Aldrich, T1162) for 30 minutes. Cells were then washed three times with PBS and incubated for another 30 minutes in the respective culture medium supplemented with 1 µg/ml Hoechst 33342 before imaging.

4.7.11. RT-qPCR

RNA was extracted using the RNeasy Mini Kit (Quiagen, 74104) according to the manufacturer's instructions. Gata4i cells were washed once with PBS before adding lysis buffer directly to the culture dish. GFP-labelled PrESCs were harvested and sorted by FACS to remove non-fluorescent feeder cells before lysis. For cDNA synthesis RNA was incubated with 2.5 mM Oligo d(T)18 mRNA Primer (New England Biolabs, S1316S) and 0.5 mM dNTPs (in-house, Molecular Biology Services) at 65°C for five minutes. Reverse transcription was then performed using the SuperScript™ III Reverse Transcriptase (Invitrogen, 18080044) together with RNaseOUT™ Recombinant Ribonuclease Inhibitor (Invitrogen, 10777019) according to the protocol provided by the manufacturer. For the qPCR reactions GoTaq qPCR Master Mix (Promega, A6001) was used and 10 ng cDNA was provided as template per reaction. All qPCRs were performed using a Bio-Rad CFX Connect Real-Time PCR System. Relative expression levels of target genes were calculated with the ΔΔCt method using *Tbp* as an endogenous reference gene for internal normalisation. Sequence information for all primers can be found in Table S4.

4.7.12. Flow cytometry and FACS

Cells were harvested and resuspended as a single-cell suspension in PBS + 1% FBS. Gata4i cells were analysed for mCherry expression on a BD LSRFortessa™ Cell Analyzer and the data were analysed using FlowJo™. GFP-labelled PrESCs were sorted on a BD FACSAria™ III Cell Sorter to remove GFP negative feeder cells prior to bulk RNA extractions.

4.7.13. CellphoneDB analysis

CellphoneDB v4.0.0 (Garcia-Alonso *et al*, 2022) with database cellphonedb-data v4.1.0 was used to predict signalling interactions between blastocyst lineages from published single-cell RNA sequencing data sets of E3.5 and E4.5 embryos (Nowotschin *et al*, 2019). Two independent sequencing data sets for each embryonic timepoint were available (GSM3494334, GSM3494335, GSM3494336, and GSM3494337), but since integration of datasets introduces dependencies between data points, violating the assumptions of the statistical tests performed by CellphoneDB, data sets were analysed separately. We performed total count normalisation and then ran CellphoneDB with the default settings, using the cell annotation provided by the authors (available at https://endoderm-explorer.com/). This ensured that only cells meeting the original quality control criteria set by the authors were included in our analysis. All significant interactions predicted by the analysis for cells at E3.5 and E4.5 are listed in Table S1 and Table S2, respectively.

4.7.14. Bulk mRNA sequencing library preparation and sequencing

RNA was extracted using the RNeasy Mini Kit according to the manufacturer's instructions including a DNase digestion step during RNA purification. Gata4i cells were washed once with PBS before adding lysis buffer directly to the culture dish. GFP-labelled PrESCs were harvested and sorted by FACS to remove non-fluorescent feeder cells before lysis. Poly-A mRNA was isolated with the NEBNext® Poly(A) mRNA Magnetic Isolation Module (New England Biolabs, E7490) from 500 ng of total RNA. Enriched poly-A mRNA sequencing libraries were prepared using the NEBNext® Ultra™ II Directional RNA Library Prep Kit for Illumina (New England Biolabs, E7760). The fragment size of the libraries was assessed using the NGS HS analysis kit and a fragment analyser system (Agilent). The library concentrations were quantified with a KAPA Kit (Roche). The generated libraries were sequenced on an Illlumina NextSeq2000 (Illumina) with 50-bp paired end mode. For each sample, approximately 10 million reads were obtained.

4.7.15. Bulk mRNA sequencing data analysis

RNA-seq reads were first trimmed using trimgalore v0.5.0 and reads mapping to abundant sequences included in the iGenomes UCSC GRCm38 bundle (mouse rDNA, mouse

mitochondrial chromosome, phiX174 genome, adapter) were removed using bowtie2 v2.3.4.1 alignment. Remaining reads were analysed using genome and gene annotation for the GRCm38/mm10 assembly obtained from Mus musculus Ensembl release 102. Reads were aligned to the ii.GRCm38 genome using star v2.6.0c and reads in genes were counted with featureCounts (subread v1.6.2) and parameter -s 2. Differential gene expression analysis on raw counts, and principal component analysis on variance-stabilised, transformed (vst) count data were performed using DESeq2 v1.18.1. Heatmaps of vst count data were generated using pheatmap v1.0.12.

4.7.16. Gene set enrichment analysis

Gene set enrichment analyses (GSEA 4.2.3)(Subramanian *et al*, 2005) were run on pre-ranked gene lists with 10,000 permutations. To generate gene sets differentiating VE from PrE, sequencing data sets of E4.5 and E5.5 embryos (GSM3494336, GSM3494337, GSM3494338, and GSM3494339)(Nowotschin *et al*, 2019) were merged using Seurat 4.3.0 (Hao *et al*, 2021). Adopting the cell annotation provided by the authors (available at https://endoderm-explorer.com/), Seurat was used to identify differentially expressed features between PrE cells at E4.5 and all VE cells (*i.e.* cells annotated exVE, emVE, or VE) at E5.5. Gene sets specific to exVE, emVE, or DVE/AVE were obtained from Table S1 in Zhu *et al*, 2023. Pre-ranked gene lists were based on lists of DEGs between the specified conditions, excluding all genes for which an adjusted p value (padj) could not be calculated. A rank metric for each gene was calculated by multiplying the sign of its log2 fold change with the negative base-10 logarithm of its p-value.

4.7.17. Statistics and reproducibility

Sample sizes were not pre-determined using statistical methods. The number of replicas and any statistical tests used are indicated in the figure legends. Statistics were calculated using Graphpad Prism version 8.1.1.

4.8. Supplementary information

Table S1. Comprehensive CellphoneDB interactions list at E3.5

Table S2. Comprehensive CellphoneDB interactions list at E4.5

Table S3. Antibodies used in this study

Target	Manufacturer	Catalogue No	Dilution
Primary antibodies			
anti-CER1	R&D Systems	MAB1986	1:100
anti-GATA4	Invitrogen	14-9980-82	1:400
anti-GATA6	R&D Systems	AF1700	1:200
anti-HNF4α	Santa Cruz Biotechnology	sc-8987 (discont.)	1:300
anti-Laminin	Abcam	ab11575	1:500
anti-LEFTY	Abcam	ab22569	1:300
anti-NANOG	Abcam	ab80892	1:300
anti-OCT3/4	Santa Cruz Biotechnology	sc-5279	1:200
anti-OTX2	R&D Systems	AF1979	1:500
anti-PDGFRα	R&D Systems	AF1062	1:200
anti-PKCζ	Santa Cruz Biotechnology	sc-216	1:200
anti-Podocalyxin	R&D Systems	AF1556	1:300
anti-ZO1	Invitrogen	33-9100	1:100
Secondary antibodies			
anti-goat IgG Alexa Fluor™ 405	abcam	ab175665	1:500
anti-goat IgG Alexa Fluor™ Plus 488	Invitrogen	A32814	1:500
anti-goat IgG Alexa Fluor™ 647	Invitrogen	A21447	1:500
anti-mouse IgG Alexa Fluor™ 488	Invitrogen	A21202	1:500
anti-mouse IgG Alexa Fluor™ 568	Invitrogen	A10037	1:500
anti-mouse IgG Alexa Fluor™ 647	Invitrogen	A31571	1:500
anti-rabbit IgG Alexa Fluor™ 488	Invitrogen	A21206	1:500
anti-rabbit IgG Alexa Fluor™ 568	Invitrogen	A10042	1:500
anti-rabbit IgG Alexa Fluor™ 647	Invitrogen	A31573	1:500
anti-rat IgG Alexa Fluor™ 488	Invitrogen	A21208	1:500

anti-rat IgG Alexa Fluor™ 568	Invitrogen	A78946	1:500
anti-rat IgG Alexa Fluor™ 647	Invitrogen	A48272	1:500

Table S4. Primers used in this study

Target	Forward primer (5'-3')	Reverse primer (5'-3')
Afp	TGCGCTCTCTACCAGACCTT	ATCTTCCCGGTGAGGTCGAT
Apob	AGATGACCAGAGTGTGGAGC	TCACCATCAGACTCCTTGTACC
Axin2	TGACTCTCCTTCCAGATCCCA	TGCCCACACTAGGCTGACA
Dab2	GCGGCTATTTAAGTGGCGTT	GATACCAGCCAATCCCCGAC
Gata4 (3'UTR)	AGAGCTGTAGCCAACTGTGG	CTGCTACGGCCAGTAAGGTT
Gata6	ACCTCAGGGGTAGGGGCATC	TGTAGAGGCCGTCTTGACCT
Hnf4a	GGATATGGCCGACTACAGCG	AGATGGGGACGTGTCATTGC
mCherry	GCGCCTACAACGTCAACATC	GCGTTCGTACTGTTCCACGA
Pdgfra	GATCGGCCAGCCTCCTACAA	CAGCAAAGTCAGACCCTCGG
Pou5f1	CACTCACATCGCCAATCAGC	TGATCTTTTGCCCTTCTGGC
Tbp	GAAGAACAATCCAGACTAGCAGCA	CCTTATAGGGAACTTCACATCACAG

CHAPTER 5:
Discussion

Differentiation and morphogenesis during development strongly depends on the signalling interactions between developing tissues. At the time of implantation this involves interactions between the embryonic epiblast as well as the extra-embryonic PrE and trophectoderm. Embryonic and extra-embryonic lineages can be captured *in vitro* using defined combinations of signalling molecules. Moreover, their co-development around the time of implantation can be recapitulated in integrated stem cell-based models, providing valuable tools to learn about the interactions between embryonic and extra-embryonic lineages. Concurrently, understanding the signalling interactions between these lineages can inform on the signalling factors required for accurately mimicking embryonic and extra-embryonic lineages in stem cell cultures. Enhancing the fidelity with which stem cells mimic their *in vivo* counterparts will be necessary to improve current embryoid models, thus ensuring greater reliability in the results derived from them.

In the following chapter, I intend to (1) summarise the stem cell-based embryo models presented in this thesis and discuss their relevance for studying the interactions between embryonic and extra-embryonic lineages at the time of implantation and (2) describe how the studies presented here contribute to our understanding of the culture requirements of extra-embryonic stem cells.

5.1. Modelling embryonic and extra-embryonic lineage interactions at the time of implantation *in vitro*

5.1.1. Modelling epiblast and extra-embryonic endoderm co-development

In this thesis I presented two partial embryo models of epiblast and PrE co-development. These models take different approaches to generate aggregates of PrE- and epiblast-like cells, which have the capacity to self-organise to resemble post-implantation stages.

Recapitulating epiblast and extra-embryonic endoderm co-development from lineage sorting to pro-amniotic cavity formation

Previous studies have described the spontaneous differentiation of ESCs into extra-embryonic endoderm-like cells. However, these protocols traditionally relied on the use of foetal bovine serum, and the efficiency in specifying extra-embryonic endoderm fate was generally low (Shen & Leder, 1992; Murray & Edgar, 2001; Hamazaki *et al*, 2004). In contrast, our work (see Chapter 3) describes a serum-free, chemically defined medium which allows to efficiently generate extra-embryonic endoderm-like cells in ESC aggregates. PDGFRA+ cells specified in ESC aggregates in a salt-and-pepper manner, similar to the inner cells of the early blastocyst.

When transferred to minimal medium, PDGFRA+ cells efficiently sorted to the outside of the aggregates and deposited a basement membrane. This induced inner ESCs to polarise and eventually form a lumen, reminiscent of the pro-amniotic cavity. Alongside these morphological changes, we observed that prolonged co-culture of extra-embryonic endoderm-like cells with ESCs in EpiCs directed their fate towards a VE phenotype. Moreover, ESCs recovered from late EpiCs exhibited distinct transcriptomic signatures specific to germ layers. Conversely, aggregates containing only ESCs, without prior extra-embryonic endoderm induction, failed to even sustain proliferation in minimal medium. Thus, interactions between embryonic and extra-embryonic lineages support mutual maintenance and developmental progression in our model.

As EpiCs matured, both epiblast- and extra-embryonic endoderm-like cells upregulated *Nodal*, similar to their *in vivo* counterparts. Nodal$^{-/-}$ EpiCs recapitulated the phenotype seen in Nodal$^{-/-}$ embryos, characterised by the detachment of the VE from the epiblast and a thickening of the VE layer (Mesnard *et al*, 2006). In the embryo, Nodal plays a crucial role in signalling between epiblast and VE, especially for generating emVE and subsequently the DVE (Brennan *et al*, 2001; Mesnard *et al*, 2006; Kumar *et al*, 2015). Accordingly, cells with a DVE/AVE-like gene expression profile emerged in the extra-embryonic endoderm of mature EpiCs. However, additional stainings for DVE/AVE-specific markers would be necessary to confirm the establishment of a confined DVE/AVE-like domain. Nonetheless, constrained Brachyury+ domains were observed in the underlying ESCs, and some ESCs recovered from late EpiCs showed gene expression signatures of an anterior identity. This expression profile was absent in epithelialized ESCs cultured without an extra-embryonic endoderm layer, indicating that an AVE-like domain in EpiCs could indeed have been established. Overall, these findings suggest that, similar to the embryo, Nodal signalling between the embryonic and extra-embryonic endoderm compartment of EpiCs drives mutual co-development of both lineages, possibly by allowing for the specification of an AVE-like domain.

Consistent with the role of basement membrane formation in inducing epiblast polarisation and lumenogenesis (Bedzhov & Zernicka-Goetz, 2014), our model replicated the formation of a pro-amniotic-like cavity following lineage sorting and basement membrane deposition. Interestingly, while sorting and laminin deposition by outer PrE-like cells were also observed in previously published ICM organoids, the inner epiblast-like cells of ICM organoids failed to form a lumen (Mathew *et al*, 2019). Our study offers a potential explanation for this discrepancy, as we demonstrate that LIF inhibits lumenogenesis; however, LIF is included in the medium of ICM organoids. With this, our model confirms previous observations wherein LIF prevented pro-amniotic cavity formation (Shahbazi *et al*, 2017). Initially it was proposed that LIF prevents the production of negatively charged sialomucins, thus interfering with initiation of lumen formation (Shahbazi *et al*, 2017; Dumortier & Maître, 2017). However, a more recent study suggests that while these proteins may facilitate membrane separation through negative charge repulsion, they are ultimately dispensable for lumen formation (Kim *et al*, 2021). In this context, EpiCs could provide a useful platform for further investigating the mechanism by which LIF blocks lumenogenesis.

The role of Wnt signalling for PrE and epiblast differentiation and morphogenesis

The second EpiC protocol outlined in this thesis (see Chapter 4) also relied on the ability of aggregates of epiblast- and PrE-like cells to self-organise into post-implantation like structures in minimal medium. However, the approach differed in that I combined ESCs with cells resembling the PrE, achieved through either transient *Gata4* overexpression in ESCs or the use of PrESCs. Like with the preceding protocol, extra-embryonic endoderm-like cells sorted to the outside of the aggregates and deposited a basement membrane, followed by inner ESC polarisation and lumen formation. To distinguish between the two protocols in this chapter, the second stem cell-based model will be referred to as combined EpiCs (cEpiCs). Notably, a similar approach to the generation of cEpiCs has recently been published to form human embryoids of hypoblast/epiblast co-development (Okubo et al, 2024).

I utilised the cEpiC protocol to test the effect of Wnt agonists and inhibitors on the co-development of the epiblast and PrE during implantation stages. Our findings revealed that although Wnt does not prevent sorting, it clearly affects the morphology of the outer extra-embryonic endoderm-like cells of cEpiCs. When formed in the presence of Wnt agonists, these cells tightly overlayed the ESCs and did not express the VE marker HNF4A. This observation is consistent with our results demonstrating that active Wnt signalling prevents VE differentiation and alters cell morphology in 2D.

Besides the differences in cell morphology, I noticed a defect in basement membrane formation by the outer extra-embryonic endoderm-like cells. While this immediately affects epithelialization and consequent morphogenesis of the inner ESCs, the underlying cause remains undetermined. The potential role of Wnt in mechanistically regulating basement membrane formation has been explored in section 4.4. Although further validation of the observed phenotype must be conducted in embryos, cEpiCs will provide a valuable system to further dissect the mechanism by which Wnt activity regulates basement membrane deposition. Since cEpiCs are formed by combining PrE- and epiblast-like cells, they allow for individual manipulation of each lineage before aggregation, facilitating targeted experimental interventions. Such investigations could lead to significant discoveries, revealing how morphogenesis of one tissue is linked to the differentiation of another.

EpiCs in relation to other partial models of epiblast and extra-embryonic endoderm

With the presented EpiC models we have generated systems which mimic the co-development of epiblast and PrE from sorting to laminin deposition, akin to ICM organoids (Mathew *et al*, 2019). However, unlike ICM organoids, EpiCs progress to also form a pro-amniotic-like cavity and model the interactions between the epiblast and the VE at post-implantation stages. Thereby our models bridge the gap between late pre-implantation models (Mathew *et al*, 2019) and early post-implantation models of epiblast and VE (Schumacher *et al*, 2023). Nonetheless, the reliability of EpiCs to faithfully recapitulate AVE formation and anterior-posterior patterning events, as demonstrated previously (Schumacher *et al*, 2023), requires further validation.

With the establishment of a chemically defined medium, our protocol now offers an alternative approach to *Gata4* or *Gata6* overexpression for specifying extra-embryonic endoderm-like cells from ESCs. Furthermore, unlike other protocols published for mouse, cEpiCs offer the ability to manipulate PrE- and epiblast-like lineages individually before aggregation, such as through pre-treatments or genetic engineering.

5.1.2. Modifying the original blastoid protocol to extend blastoid development

ETiX embryoids, which resemble the early post-implantation conceptus around E5.5, have recently been shown to progress to post-gastrulation stages (Amadei *et al*, 2022). On the contrary, the efficient transition of blastoids towards E5.5.-like stages remains elusive (Rivron *et al*, 2018; Sozen *et al*, 2019; Li *et al*, 2019). This highlights our limited understanding of the factors dictating the developmental shift from pre-implantation blastocyst to post-implantation stages. By refining current protocols to efficiently support developmental progression of blastoids, we may gain valuable insights into the pivotal factors driving the pre- to post-implantation transition.

Enhancing the formation of PrE-like cells in blastoids

Given the limited capacity of ESCs to differentiate into extra-embryonic lineages, blastoids formed by combining TSCs with ESC aggregates mostly lack the formation of PrE-like cells (Rivron *et al*, 2018). However, a functional PrE is essential for developmental progression, particularly to form the basement membrane as a mechanical cue driving epiblast cup formation (Wallingford *et al*, 2013; Bedzhov & Zernicka-Goetz, 2014). Further evidence emphasising the importance of the PrE-lineage for developmental progression comes from studies on *Gata6*$^{-/-}$ embryos. Knocking out the PrE-specific transcription factor *Gata6* results in embryonic lethality immediately after implantation, attributed to insufficient growth and morphogenesis of the epiblast in the absence of a functional PrE (Morrisey *et al*, 1998; Koutsourakis *et al*, 1999). Conversely, using EPSCs to generate a higher number of PrE-like cells in blastoids enhanced their ability to progress into post-implantation like structures (Sozen *et al*, 2019). Thus, incorporating the PrE lineage in blastoids is indispensable if we aim to create integrated stem cell models of the full conceptus capable of transitioning into post-implantation-like stages.

While EPSCs demonstrate a propensity to generate more PrE-like cells, recent findings suggest that EPSCs more closely resemble the post-implantation epiblast at E5.5 (Posfai *et al*, 2021). Hence, EPSCs may not be the optimal choice for emulating the inner cells of a pre-implantation blastocyst-like structure. Leveraging our chemically defined medium, PrE-like cells can be obtained from ESC aggregates which better resemble the pre-implantation stage (Ying *et al*, 2008; Nichols & Smith, 2009). Combining chemically induced ESC aggregates with TSCs significantly enhanced the formation of PrE-like cells in blastoids. As expected, the increased number of extra-embryonic endoderm-like cells in blastoids extended their

developmental capacity. Specifically we observed the emergence of post-implantation-like structures when culturing these blastoids *in vitro* using protocols designed for the culture of mouse blastocysts beyond implantation stages. (Bedzhov *et al*, 2014b). However, whether these blastoids also have an extended developmental potential *in utero* remains to be determined.

Finally, building on the approach for generating cEpiCs, an alternative strategy to increase the number of PrE-like cells in blastoids could involve combining ESCs with PrE-like cells before seeding TSCs. In this way, each blastoid lineage would originate from a different stem cell line, allowing for individual manipulation of the starting cell line of each lineage prior to blastoid formation.

Recapitulating axis formation in blastoids

While the robust inclusion of PrE-like cells in blastoids is necessary to enhance their developmental potential, the adequate progression of blastoid trophectoderm towards post-implantation stages will be equally pivotal. The ability of blastoids to elicit a uterine implantation response (decidualisation)(Rivron *et al*, 2018; Sozen *et al*, 2019; Li *et al*, 2019) implies that trophoblast cells exhibit mural-like characteristics essential for uterine attachment and invasion. However, the post-implantation ExE is derived from the polar trophectoderm and is crucial for further embryo patterning (Rodriguez *et al*, 2005; Mesnard *et al*, 2006; Arnold & Robertson, 2009; Christodoulou *et al*, 2019). Therefore, it can be assumed that establishing a polar-mural axis with functional polar trophectoderm is vital for generating an ExE-like structure from blastoids.

Axis formation in blastoids has been reported based on the regionalised expression of CDX2 at the polar, and Keratin 8 (KRT8) on the mural side (Sozen *et al*, 2019). Moreover trophoblast cells recovered from blastoids exhibited distinct transcriptional profiles reflecting either a polar or mural phenotype (Sozen *et al*, 2019). However, the efficiency at which axis formation occurs was not stated by the authors. Upon replicating their protocol (see Chapter 2), we observed that axis formation occurred at a similar percentage compared to blastoids generated with ESCs and trophectoderm stem cells (TESCs).

The removal of FGF4 and TGFβ1 from the medium during blastoid formation significantly improved the establishment of a polar-mural axis. This finding aligns with the concept of "epiblast inducers" presented in Chapter 2, where molecules secreted by the epiblast (*i.e*. inducers) act on the directly adjacent polar trophectoderm. The spatial separation of the mural trophectoderm from inducers results in trophectoderm patterning. Similarly, previous studies have postulated a role of FGF4, originating from the epiblast, in maintaining polar trophectoderm undifferentiated while the mural trophectoderm differentiates (Tanaka *et al*, 1998). Consequently, the presence of FGF4 and TGFβ1 in the medium during blastoid formation exposes all cells to these signals, hindering trophectoderm regionalisation into polar and mural domains. Moving towards a more minimal culture medium could mitigate this issue by allowing

less disrupted signalling between the lineages during blastoid formation. This might promote the establishment of a polar-mural axis and allow for the reliable establishment of a polar trophectoderm that can form a functional ExE after implantation.

5.2. Considering inter-lineage signalling to refine culture conditions of extra-embryonic stem cells

Considerable efforts have been made to identify the signalling effectors capable of capturing ESCs as homogeneous cultures, matching the embryonic epiblast at precise developmental stages (refer to section 1.3.2.). In contrast, stem cell cultures derived from extra-embryonic lineages tend to be more heterogeneous, with cells resembling different developmental stages in the same dish. Understanding the signals that extra-embryonic lineages receive at distinct developmental time points, particularly those related to differentiation, could help in refining their culture conditions.

5.2.1. Refining TSC culture conditions by considering epiblast-derived signals

Generating homogenous pre-implantation-like TSC cultures

Culture conditions for TSCs typically involve the use of FGF ligands (primarily FGF4) along with either of the SMAD2/3 activators Activin or TGFβ1 (refer to section 1.3.2.). These protocols likely leverage the signalling interactions mediated by FGF4 and Nodal between the epiblast and the trophectoderm/ExE, which maintain proliferative, undifferentiated trophoblast cells *in vivo* (Tanaka *et al*, 1998; Guzman-Ayala *et al*, 2004). While TSCs can be maintained as self-renewing stem cell lines, they are notoriously heterogenous in their expression of important TSC markers like CDX2 or EOMES (Kubaczka *et al*, 2014; Kuales *et al*, 2015; Motomura *et al*, 2016). Our data (Chapter 2) confirmed this, showing that even chemically defined culture conditions (Kubaczka *et al*, 2014) permit heterogenous CDX2 expression. Moreover, we observed the co-existence of cells expressing transcriptional signatures of pre-implantation trophectoderm or post-implantation ExE within these cultures. Therefore, while the conventionally used FGF and Nodal-like signals effectively sustain proliferation and maintain cells undifferentiated, they are insufficient to define a pre- or post-implantation-like trophoblast state *in vitro*.

In the work presented here (Chapter 2), we investigated the signalling pathways that are active in the pre-implantation trophectoderm, and the expression of corresponding signalling molecules in the epiblast. Based on this, we incorporated BMP7, cAMP, IL11, and LPA alongside commonly used FGF4, TGFβ1, and Activin to formulate a novel TSC culture medium, referred to as TXV. Cells cultured under these conditions (TESCs) more closely resemble a pre-implantation trophectoderm state, show less variability in CDX2 levels, and overall higher CDX2 expression.

Reversibility of post-implantation trophoblast cells to pre-implantation stages *in vitro*
TSC lines can be derived from both E3.5 and E6.5 embryos using the same culture conditions. This may imply that cells reach a common state *in vitro* (Rayon *et al*, 2016), or it could be attributed to the permissiveness of commonly used culture conditions allowing for the co-existence of cells at various developmental stages. However, using TXV medium, which confines cells to a pre-implantation-like state, we could also derive TESCs from E6.5 embryos. This indicates that post-implantation cells can revert to pre-implantation like stages which is further supported by our data, demonstrating that cells fluctuate between CDX2 high and CDX2 low states. Cultures containing both pre- and post-implantation states are heterogenous for CDX2 expression, and this heterogeneity will be re-instated after sorting cells into distinct population based on their CDX2 expression levels. Overall, this suggests that pre- and post-implantation stages in trophoblast cells are interconvertible, unlike states of embryonic pluripotency, where post-implantation primed EpiSCs cannot revert into a pre-implantation naïve state (Guo *et al*, 2009).

Improving blastoids by restricting TSCs to a pre-implantation-like state
Consistent with the understanding that the developmental stages of TSCs are reversible, TSCs from heterogenous cultures can effectively mimic the pre-implantation trophectoderm in blastoids. Consistently, it has been shown that TSCs can reactivate trophectoderm-specific regulation of *Cdx2* expression when injected into blastocysts (Rayon *et al*, 2016). Thus, placing TSCs into the appropriate cellular context helps them acquire pre-implantation-like states. However, it is arguably preferable to start from a homogenous population resembling the pre-implantation trophectoderm when assembling a model of the pre-implantation conceptus. Indeed, when generating blastoids from TESCs, they formed more efficiently and implanted at higher numbers. This emphasises the importance of ensuring that the cells already in culture correspond to the correct developmental stage intended to be modelled in the embryoid. Nonetheless, also blastoids formed from TESCs did not support the formation of well-organised post-implantation ExE-like structures. It remains unclear whether this is due to remaining shortcomings in the TSC culture conditions or if this reflects deficiencies in interactions with the other lineages, such as with a post-implantation exVE.

5.2.2. Deciphering the signalling requirements of distinct extra-embryonic endoderm lineages *in vitro*

While protocols supporting the culture of ESCs and TSCs were already established before the turn of the millennium (Evans & Kaufman, 1981; Martin, 1981; Tanaka *et al*, 1998), the derivation of extra-embryonic endoderm cells from blastocysts was achieved only years later (Kunath *et al*, 2005). Culturing XEN cells requires the use of feeder cells and serum, resulting in a heterogeneous cell population representing various developmental stages (Kunath *et al*, 2005; Brown *et al*, 2010). Attempts to replicate a pre-implantation-like state of extra-embryonic endoderm led to modifications of the original XEN protocol and alternative approaches for

generating PrE-like cells from ESCs (Mulvey *et al*, 2015; Wamaitha *et al*, 2015; Anderson *et al*, 2017; Zhong *et al*, 2018). Nevertheless, deriving a homogeneous culture of PrE-like cells directly from embryos proved elusive. Recently, however, PrESCs were introduced – cell lines derived directly from blastocysts, considered the *in vitro* equivalent of the E4.5 PrE (Yasuhide *et al*, 2022). Although the culture of PrESCs still relies on feeder cells, the medium is chemically defined and includes the signalling molecules FGF4, PDGFA, and the GSK3 inhibitor (*i.e*. Wnt activator) CHIR99021.

The role of FGF4, PDGF, and Wnt for the maintenance of PrE-like cells *in vitro*

Given the pivotal roles of the epiblast-produced ligands FGF4 and PDGF for PrE lineage commitment and survival (refer to section 1.3.1.), it is apprehensible that these molecules have been utilised in the culture of extra-embryonic endoderm cells. PDGF has been instrumental in establishing pXEN lines, which exhibit characteristics of a developmentally earlier stage than conventional XEN cells (Zhong *et al*, 2018). Besides that, FGF4 was initially used in deriving XEN cells, yet it is neither necessary for their derivation nor maintenance (Kunath *et al*, 2005). However, FGF4 significantly influences the efficiency of ESC differentiation into PrE-like cells via induced *Gata4* overexpression. In fact, the addition of FGF4 following *Gata4* induction markedly increases the yield of PrE-like cells (Raina et al, 2021). This was also replicated in my experiments (Chapter 4). Consistently, our work also demonstrated that FGF4 significantly enhanced the yield of extra-embryonic endoderm cells in ESC aggregates (Chapter 3).

Notably, stable cell lines with PrE-like signatures, such as PrESCs or nEnd cells, employ either CHIR99021 or WNT3A, respectively (Anderson *et al*, 2017; Yasuhide *et al*, 2022). Although Wnt activity has been implicated in PrE fate commitment (Athanasouli *et al*, 2023), the role of Wnt for the PrE lineage after specification has not been further investigated. The data presented in Chapter 4 now underscores the significance of high cellular Wnt activity in maintaining PrE-like cells in an undifferentiated state, thereby retaining them as a homogenous pre-implantation like population. Wnt signalling thus seems to play a crucial role in sustaining the stemness of PrESCs, akin to its function in ESCs (Ying *et al*, 2008; ten Berge *et al*, 2011). Whether this exploits a biological phenomenon such as diapause or signifies the existence of a regulatory mechanism whereby Wnt activity prevents differentiation of blastocyst lineages to synchronise their development (discussed in section 4.4) remains to be seen.

Using BMP4 and Activin A to recapitulate extra-embryonic endoderm subtypes

BMP4 from the ExE, as well as Nodal from the epiblast, are the key signalling molecules to specify VE subtypes *in vivo* (refer to section 1.3.1.). Mirroring the role of these signalling molecules in the embryo, my data shows that BMP4 represses DVE/AVE-specific genes and promotes the transcriptional signature of emVE in PrESCs. Conversely, Activin A increases the expression of DVE/AVE-specific genes in the absence of Wnt agonists. This reinforces that Wnt maintains PrESCs in an undifferentiated state, making them unresponsive to differentiation signal like Activin A. Additionally, it prompts speculation on the potential use of BMP4 and

Activin A in generating homogeneous cultures of desired VE subtypes once cells are released from Wnt signalling.

BMP4 has previously been employed to differentiate XEN cells towards a VE-like identity (Julio *et al*, 2011; Artus *et al*, 2012). Therefore, in the absence of Wnt agonists and in combination with a Nodal inhibitor, BMP4 could be utilised to induce an emVE phenotype from PrESCs in culture. Conversely, by using a BMP inhibitor along with Activin A in the absence of Wnt activation, it should be possible to generate a homogenous population of DVE/AVE-like cells. A system like this could be highly beneficial for conducting in-depth studies on this essential cell type for anterior patterning. However, the use of FGF4 and PDGF in conjunction with BMP4 or Activin A, as conducted in my experiments, should be reassessed. Considering that especially PDGF is mostly important during pre-implantation development, its use might be redundant for the culture of post-implantation extra-embryonic endoderm cells. Nonetheless, these approaches could collectively capitalise on the signalling molecules used by the embryo to recreate distinct extra-embryonic lineages *in vitro*, enhancing our toolkit for investigating questions pertaining to specific subtypes of the extra-embryonic endoderm lineages.

5.3. Conclusion and outlook

In this thesis I presented three projects, each addressing separate biological questions concerning the developmental progression of embryonic and extra-embryonic lineages during implantation. Despite their individual focuses, these projects collectively offered insights into the signalling requirements for the culture of extra-embryonic stem cells. Moreover, they resulted in the development of new, and refinement of existing integrated embryoid models.

Embryoids represent a promising advancement in developmental biology, providing an alternative to the study of *in vivo* embryos, which is constrained by technical limitations and ethical considerations. Embryoids have the potential to significantly deepen our understanding of embryogenesis, revealing it as a process of guided self-organisation, directed also by the signalling interactions between emerging tissues (Morales *et al*, 2021). Integrated stem cell models will be particularly useful to elucidate the signalling dynamics between embryonic and extra-embryonic lineages that instruct self-organisation. With the models presented in this thesis we could underscore the pivotal role of the epiblast in patterning the trophectoderm, leading to the generation of polar and mural regions with distinct functions upon implantation (Chapter 2). Furthermore, through the creation of EpiCs, we elucidated the reciprocal interactions driving epiblast and PrE co-development during the pre- to post-implantation transition (Chapter 3). Lastly, using EpiCs, we found that Wnt signalling not only prevents the differentiation of PrE-like cells but also prevents them from establishing a basal membrane – a crucial morphogenetic cue for developmental progression of the epiblast *in viv*o (Chapter 4).

While embryoids have facilitated new discoveries, considerable efforts have also been devoted to benchmarking them to confirm that they accurately replicate developmental processes. Accordingly, a primary focus has been on validating the preservation of known interactions between embryonic and extra-embryonic tissues within embryoids. Similarly, in EpiCs we validated the recapitulation of previously documented interactions, such as basement membrane deposition and Nodal signalling between the epiblast and PrE (Chapter 3). These validations are crucial to ensure the reliability of future discoveries in embryoids regarding unknown signalling interactions.

Although the characterisation of embryoids is essential, the properties of their starting material is equally important. As exemplified in Chapter 2, refining the culture conditions of stem cells used for generating blastoids enhances blastoid quality. Significant progress has been made with chemically defined stem cell media, however, the scope of improvement extends beyond media formulation. We require a yet more comprehensive understanding of how individual components of the media influence cell state and behaviour. This meticulous understanding will yield valuable biological insights in itself but also lay the groundwork for enhanced integrated embryoid models. In conclusion, ongoing advancements in stem cell culture and embryoids will offer detailed insights into the processes of differentiation and morphogenesis, likely surpassing what could be achieved through *in vivo* studies alone.

References

Akhtar N & Streuli CH (2013) An integrin–ILK–microtubule network orients cell polarity and lumen formation in glandular epithelium. *Nat Cell Biol* 15: 17–27

Amack JD & Manning ML (2012) Knowing the Boundaries: Extending the Differential Adhesion Hypothesis in Embryonic Cell Sorting. *Science (80-)* 338: 212–215

Amadei G, Handford CE, Qiu C, De Jonghe J, Greenfeld H, Tran M, Martin BK, Chen D-Y, Aguilera-Castrejon A, Hanna JH, *et al* (2022) Embryo model completes gastrulation to neurulation and organogenesis. *Nature* 610: 143–153

Amadei G, Lau KYC, De Jonghe J, Gantner CW, Sozen B, Chan C, Zhu M, Kyprianou C, Hollfelder F & Zernicka-Goetz M (2020) Inducible Stem-Cell-Derived Embryos Capture Mouse Morphogenetic Events In Vitro. *Dev Cell*

Anderson KG V, Hamilton WB, Roske F V, Azad A, Knudsen TE, Canham MA, Forrester LM & Brickman JM (2017) Insulin fine-tunes self-renewal pathways governing naive pluripotency and extra-embryonic endoderm. *Nat Cell Biol* 19: 1164–1177

Arman E, Haffner-Krausz R, Chen Y, Heath JK & Lonai P (1998) Targeted disruption of fibroblast growth factor (FGF) receptor 2 suggests a role for FGF signaling in pregastrulation mammalian development. *Proc Natl Acad Sci* 95: 5082–5087

Arnold SJ & Robertson EJ (2009) Making a commitment: cell lineage allocation and axis patterning in the early mouse embryo. *Nat Rev Mol Cell Biol* 10: 91–103

Artus J, Douvaras P, Piliszek A, Isern J, Baron MH & Hadjantonakis A-K (2012) BMP4 signaling directs primitive endoderm-derived XEN cells to an extraembryonic visceral endoderm identity. *Dev Biol* 361: 245–262

Artus J & Hadjantonakis A-K (2012) Troika of the mouse blastocyst: lineage segregation and stem cells. *Curr Stem Cell Res Ther* 7: 78–91

Artus J, Kang M, Cohen-Tannoudji M & Hadjantonakis A-K (2013) PDGF signaling is required for primitive endoderm cell survival in the inner cell mass of the mouse blastocyst. *Stem Cells* 31: 1932–1941

Artus J, Panthier J-J & Hadjantonakis A-K (2010) A role for PDGF signaling in expansion of the extra-embryonic endoderm lineage of the mouse blastocyst. *Development* 137: 3361–3372

Athanasouli P, Balli M, De Jaime-Soguero A, Boel A, Papanikolaou S, van der Veer BK, Janiszewski A, Vanhessche T, Francis A, El Laithy Y, *et al* (2023) The Wnt/TCF7L1 transcriptional repressor axis drives primitive endoderm formation by antagonizing naive and formative pluripotency. *Nat Commun* 14: 1210

Aumailley M, Pesch M, Tunggal L, Gaill F & Fässler R (2000) Altered synthesis of laminin 1 and absence of basement membrane component deposition in β1 integrin-deficient embryoid bodies. *J Cell Sci* 113: 259–268

Barcroft LC, Offenberg H, Thomsen P & Watson AJ (2003) Aquaporin proteins in murine trophectoderm mediate transepithelial water movements during cavitation. *Dev Biol* 256: 342–354

Bassalert C, Valverde-Estrella L & Chazaud C (2018) Primitive Endoderm Differentiation: From Specification to Epithelialization. *Curr Top Dev Biol* 128: 81–104

Beck S, Le Good JA, Guzman M, Haim N Ben, Roy K, Beermann F & Constam DB (2002) Extraembryonic proteases regulate Nodal signalling during gastrulation. *Nat Cell Biol* 4: 981–985

Bedzhov I, Graham SJL, Leung CY & Zernicka-Goetz M (2014a) Developmental plasticity, cell fate specification and morphogenesis in the early mouse embryo. *Philos Trans R Soc B Biol Sci* 369: 20130538

Bedzhov I, Leung CY, Bialecka M & Zernicka-Goetz M (2014b) In vitro culture of mouse blastocysts beyond the implantation stages. *Nat Protoc* 9: 2732–2739

Bedzhov I & Zernicka-Goetz M (2014) Self-organizing properties of mouse pluripotent cells initiate morphogenesis upon implantation. *Cell* 156: 1032–1044

Belo JA, Bouwmeester T, Leyns L, Kertesz N, Gallo M, Follettie M & De Robertis EM (1997) Cerberus-like is a secreted factor with neuralizing activity expressed in the anterior primitive endoderm of the mouse gastrula. *Mech Dev* 68: 45–57

ten Berge D, Kurek D, Blauwkamp T, Koole W, Maas A, Eroglu E, Siu RK & Nusse R (2011) Embryonic stem cells require Wnt proteins to prevent differentiation to epiblast stem cells. *Nat Cell Biol* 13: 1070–1075

Bessonnard S, De Mot L, Gonze D, Barriol M, Dennis C, Goldbeter A, Dupont G & Chazaud C (2014) Gata6, Nanog and Erk signaling control cell fate in the inner cell mass through a tristable regulatory network. *Development* 141: 3637–3648

Bessonnard S, Vandormael-Pournin S, Coqueran S, Cohen-Tannoudji M & Artus J (2019) PDGF Signaling in Primitive Endoderm Cell Survival Is Mediated by PI3K-mTOR Through p53-Independent Mechanism. *Stem Cells* 37: 888–898

Biechele S, Cockburn K, Lanner F, Cox BJ & Rossant J (2013) Porcn-dependent Wnt signaling is not required prior to mouse gastrulation. *Development* 140: 2961–2971

Bielinska M, Narita N & Wilson DB (1999) Distinct roles for visceral endoderm during embryonic mouse development. *Int J Dev Biol* 43: 183–205

Boroviak T, Loos R, Bertone P, Smith A & Nichols J (2014) The ability of inner-cell-mass cells to self-renew as embryonic stem cells is acquired following epiblast specification. *Nat Cell Biol* 16: 516–528

Boroviak T, Loos R, Lombard P, Okahara J, Behr R, Sasaki E, Nichols J, Smith A & Bertone P (2015) Lineage-Specific Profiling Delineates the Emergence and Progression of Naive Pluripotency in Mammalian Embryogenesis. *Dev Cell* 35: 366–382

Bradley A, Evans M, Kaufman MH & Robertson E (1984) Formation of germ-line chimaeras from embryo-derived teratocarcinoma cell lines. *Nature* 309: 255–256

Brennan J, Lu CC, Norris DP, Rodriguez TA, Beddington RSP & Robertson EJ (2001) Nodal signalling in the epiblast patterns the early mouse embryo. *Nature* 411: 965–969

Brons IGM, Smithers LE, Trotter MWB, Rugg-Gunn P, Sun B, Chuva de Sousa Lopes SM, Howlett SK, Clarkson A, Ahrlund-Richter L, Pedersen RA, *et al* (2007) Derivation of pluripotent epiblast stem cells from mammalian embryos. *Nature* 448: 191–195

Brown K, Legros S, Artus J, Doss MX, Khanin R, Hadjantonakis A-K & Foley A (2010) A comparative analysis of extra-embryonic endoderm cell lines. *PLoS One* 5: e12016

Chan CJ, Costanzo M, Ruiz-Herrero T, Mönke G, Petrie RJ, Bergert M, Diz-Muñoz A, Mahadevan L

& Hiiragi T (2019) Hydraulic control of mammalian embryo size and cell fate. *Nature* 571: 112–116

Chazaud C, Yamanaka Y, Pawson T & Rossant J (2006) Early Lineage Segregation between Epiblast and Primitive Endoderm in Mouse Blastocysts through the Grb2-MAPK Pathway. *Dev Cell* 10: 615–624

Cheng AM, Saxton TM, Sakai R, Kulkarni S, Mbamalu G, Vogel W, Tortorice CG, Cardiff RD, Cross JC, Muller WJ, *et al* (1998) Mammalian Grb2 Regulates Multiple Steps in Embryonic Development and Malignant Transformation. *Cell* 95: 793–803

Chickarmane V & Peterson C (2008) A computational model for understanding stem cell, trophectoderm and endoderm lineage determination. *PLoS One* 3: e3478

Christodoulou N, Weberling A, Strathdee D, Anderson KI, Timpson P & Zernicka-Goetz M (2019) Morphogenesis of extra-embryonic tissues directs the remodelling of the mouse embryo at implantation. *Nat Commun* 10: 3557

Ciruna BG & Rossant J (1999) Expression of the T-box gene Eomesodermin during early mouse development. *Mech Dev* 81: 199–203

Cockburn K, Biechele S, Garner J & Rossant J (2013) The Hippo Pathway Member Nf2 Is Required for Inner Cell Mass Specification. *Curr Biol* 23: 1195–1201

Copp AJ (1978) Interaction between inner cell mass and trophectoderm of the mouse blastocyst. I. A study of cellular proliferation. *J Embryol Exp Morphol* 48: 109–125

Coucouvanis E & Martin GR (1995) Signals for death and survival: a two-step mechanism for cavitation in the vertebrate embryo. *Cell* 83: 279–287

Coucouvanis E & Martin GR (1999) BMP signaling plays a role in visceral endoderm differentiation and cavitation in the early mouse embryo. *Development* 126: 535–546

Cross JC (2000) Genetic insights into trophoblast differentiation and placental morphogenesis. *Semin Cell Dev Biol* 11: 105–113

Donnison M, Beaton A, Davey HW, Broadhurst R, L'Huillier P & Pfeffer PL (2005) Loss of the extraembryonic ectoderm in Elf5 mutants leads to defects in embryonic patterning. *Development* 132: 2299–2308

Dumortier JG & Maître J-L (2017) Early embryos kept in check. *Nature* 552: 178–179

Dumortier JG, Le Verge-Serandour M, Tortorelli AF, Mielke A, de Plater L, Turlier H & Maître J-L (2019) Hydraulic fracturing and active coarsening position the lumen of the mouse blastocyst. *Science (80-)* 365: 465–468

Duncan SA, Nagy A & Chan W (1997) Murine gastrulation requires HNF-4 regulated gene expression in the visceral endoderm: tetraploid rescue of Hnf-4−/− embryos. *Development* 124: 279–287

Enders AC, Given RL & Schlafke S (1978) Differentiation and migration of endoderm in the rat and mouse at implantation. *Anat Rec* 190: 65–77

Erlebacher A, Price KA & Glimcher LH (2004) Maintenance of mouse trophoblast stem cell proliferation by TGF-β/activin. *Dev Biol* 275: 158–169

Evans MJ & Kaufman MH (1981) Establishment in culture of pluripotential cells from mouse embryos. *Nature* 292: 154–156

Fan R, Kim YS, Wu J, Chen R, Zeuschner D, Mildner K, Adachi K, Wu G, Galatidou S, Li J, *et al* (2020) Wnt/Beta-catenin/Esrrb signalling controls the tissue-scale reorganization and maintenance of the pluripotent lineage during murine embryonic diapause. *Nat Commun* 11: 5499

Fan Y, Min Z, Alsolami S, Ma Z, Zhang E, Chen W, Zhong K, Pei W, Kang X, Zhang P, *et al* (2021) Generation of human blastocyst-like structures from pluripotent stem cells. *Cell Discov* 7: 81

Farese RVJ, Cases S, Ruland SL, Kayden HJ, Wong JS, Young SG & Hamilton RL (1996) A novel function for apolipoprotein B: lipoprotein synthesis in the yolk sac is critical for maternal-fetal lipid transport in mice. *J Lipid Res* 37: 347–360

Fässler R & Meyer M (1995) Consequences of lack of beta 1 integrin gene expression in mice. *Genes Dev* 9: 1896–1908

Feldman B, Poueymirou W, Papaioannou VE, DeChiara TM & Goldfarb M (1995) Requirement of FGF-4 for Postimplantation Mouse Development. *Science (80-)* 267: 246–249

Filimonow K & de la Fuente R (2022) Specification and role of extraembryonic endoderm lineages in the periimplantation mouse embryo. *Theriogenology* 180: 189–206

Filimonow K, Saiz N, Suwińska A, Wyszomirski T, Grabarek JB, Ferretti E, Piliszek A, Plusa B & Maleszewski M (2019) No evidence of involvement of E-cadherin in cell fate specification or the segregation of Epi and PrE in mouse blastocysts. *PLoS One* 14: e0212109

Foty RA & Steinberg MS (2004) Cadherin-mediated cell-cell adhesion and tissue segregation in relation to malignancy. *Int J Dev Biol* 48: 397–409

Frankenberg S, Gerbe F, Bessonnard S, Belville C, Pouchin P, Bardot O & Chazaud C (2011) Primitive Endoderm Differentiates via a Three-Step Mechanism Involving Nanog and RTK Signaling. *Dev Cell* 21: 1005–1013

Frum T, Murphy TM & Ralston A (2018) HIPPO signaling resolves embryonic cell fate conflicts during establishment of pluripotency in vivo. *Elife* 7: e42298

Garcia-Alonso L, Lorenzi V, Mazzeo CI, Alves-Lopes JP, Roberts K, Sancho-Serra C, Engelbert J, Marečková M, Gruhn WH, Botting RA, *et al* (2022) Single-cell roadmap of human gonadal development. *Nature* 607: 540–547

Gardner RL (2000) Flow of cells from polar to mural trophectoderm is polarized in the mouse blastocyst. *Hum Reprod* 15: 694–701

George SHL, Gertsenstein M, Vintersten K, Korets-Smith E, Murphy J, Stevens ME, Haigh JJ & Nagy A (2007) Developmental and adult phenotyping directly from mutant embryonic stem cells. *Proc Natl Acad Sci* 104: 4455–4460

Gerbe F, Cox B, Rossant J & Chazaud C (2008) Dynamic expression of Lrp2 pathway members reveals progressive epithelial differentiation of primitive endoderm in mouse blastocyst. *Dev Biol* 313: 594–602

Girgin MU, Broguiere N, Hoehnel S, Brandenberg N, Mercier B, Arias AM & Lutolf MP (2021) Bioengineered embryoids mimic post-implantation development in vitro. *Nat Commun* 12: 5140

Goissis MD, Bradshaw B, Posfai E & Rossant J (2023) Influence of FGF4 and BMP4 on FGFR2 dynamics during the segregation of epiblast and primitive endoderm cells in the pre-implantation mouse embryo. *PLoS One* 18: e0279515

Goldin SN & Papaioannou VE (2003) Paracrine action of FGF4 during periimplantation development maintains trophectoderm and primitive endoderm. *Genesis* 36: 40–47 doi:10.1002/gene.10192 [PREPRINT]

Gotoh N, Manova K, Tanaka S, Murohashi M, Hadari Y, Lee A, Hamada Y, Hiroe T, Ito M, Kurihara T, *et al* (2005) The Docking Protein FRS2α Is an Essential Component of Multiple Fibroblast Growth Factor Responses during Early Mouse Development. *Mol Cell Biol* 25: 4105–4116

Guo G, Huss M, Tong GQ, Wang C, Li Sun L, Clarke ND & Robson P (2010) Resolution of Cell Fate Decisions Revealed by Single-Cell Gene Expression Analysis from Zygote to Blastocyst. *Dev Cell* 18: 675–685

Guo G, Yang J, Nichols J, Hall JS, Eyres I, Mansfield W & Smith A (2009) Klf4 reverts developmentally programmed restriction of ground state pluripotency. *Development* 136: 1063–1069

Guzman-Ayala M, Ben-Haim N, Beck S & Constam DB (2004) Nodal protein processing and fibroblast growth factor 4 synergize to maintain a trophoblast stem cell microenvironment. *Proc Natl Acad Sci* 101: 15656–15660

Haffner-Krausz R, Gorivodsky M, Chen Y & Lonai P (1999) Expression of Fgfr2 in the early mouse embryo indicates its involvement in preimplantation development. *Mech Dev* 85: 167–172

Hamazaki T, Oka M, Yamanaka S & Terada N (2004) Aggregation of embryonic stem cells induces Nanog repression and primitive endoderm differentiation. *J Cell Sci* 117: 5681–5686

Hao Y, Hao S, Andersen-Nissen E, Mauck WM, Zheng S, Butler A, Lee MJ, Wilk AJ, Darby C, Zager M, *et al* (2021) Integrated analysis of multimodal single-cell data. *Cell* 184: 3573-3587.e29

Harrison SE, Sozen B, Christodoulou N, Kyprianou C & Zernicka-Goetz M (2017) Assembly of embryonic and extraembryonic stem cells to mimic embryogenesis in vitro. *Science (80-)* 356: eaal1810

He X, Liu J, Qi Y, Brakebusch C, Chrostek-Grashoff A, Edgar D, Yurchenco PD, Corbett SA, Lowry SF, Graham AM, *et al* (2010) Rac1 Is Essential for Basement Membrane-Dependent Epiblast Survival. *Mol Cell Biol* 30: 3569–3581

Henry MD & Campbell KP (1998) A Role for Dystroglycan in Basement Membrane Assembly. *Cell* 95: 859–870

Henry MD, Satz JS, Brakebusch C, Costell M, Gustafsson E, Fässler R & Campbell KP (2001) Distinct roles for dystroglycan, β1 integrin and perlecan in cell surface laminin organization. *J Cell Sci* 114: 1137–1144

Hirate Y, Hirahara S, Inoue K, Suzuki A, Alarcon VB, Akimoto K, Hirai T, Hara T, Adachi M, Chida K, *et al* (2013) Polarity-Dependent Distribution of Angiomotin Localizes Hippo Signaling in Preimplantation Embryos. *Curr Biol* 23: 1181–1194

Hogan BLM, Cooper AR & Kurkinen M (1980) Incorporation into Reichert's membrane of laminin-like extracellular proteins synthesized by parietal endoderm cells of the mouse embryo. *Dev Biol* 80: 289–300

Hohenester E & Yurchenco PD (2013) Laminins in basement membrane assembly. *Cell Adh Migr* 7: 56–63

Hoshino H, Shioi G & Aizawa S (2015) AVE protein expression and visceral endoderm cell behavior during anterior–posterior axis formation in mouse embryos: Asymmetry in OTX2

and DKK1 expression. *Dev Biol* 402: 175–191

Huang Y, Osorno R, Tsakiridis A & Wilson V (2012) In Vivo Differentiation Potential of Epiblast Stem Cells Revealed by Chimeric Embryo Formation. *Cell Rep* 2: 1571–1578

Johnson MH & Ziomek CA (1983) Cell interactions influence the fate of mouse blastomeres undergoing the transition from the 16- to the 32-cell stage. *Dev Biol* 95: 211–218

Julio MK, Alvarez MJ, Galli A, Chu J, Price SM, Califano A & Shen MM (2011) Regulation of extra-embryonic endoderm stem cell differentiation by Nodal and Cripto signaling. *Development* 138: 3885–3895

Kadokawa Y, Kato Y & Eguchi G (1987) Cell lineage analysis of the primitive and visceral endoderm of mouse embryos cultured in vitro. *Cell Differ* 21: 69–76

Kagawa H, Javali A, Khoei HH, Sommer TM, Sestini G, Novatchkova M, Scholte op Reimer Y, Castel G, Bruneau A, Maenhoudt N, *et al* (2022) Human blastoids model blastocyst development and implantation. *Nature* 601: 600–605

Kang M, Garg V & Hadjantonakis A-K (2017) Lineage Establishment and Progression within the Inner Cell Mass of the Mouse Blastocyst Requires FGFR1 and FGFR2. *Dev Cell* 41: 496-510.e5

Kang M, Piliszek A, Artus J & Hadjantonakis A-K (2013) FGF4 is required for lineage restriction and salt-and-pepper distribution of primitive endoderm factors but not their initial expression in the mouse. *Development* 140: 267–279

Kemp C, Willems E, Abdo S, Lambiv L & Leyns L (2005) Expression of all Wnt genes and their secreted antagonists during mouse blastocyst and postimplantation development. *Dev Dyn* 233: 1064–1075

Kim EJY, Sorokin L & Hiiragi T (2022a) ECM-integrin signalling instructs cellular position sensing to pattern the early mouse embryo. *Development* 149: dev200140

Kim K-A, Wagle M, Tran K, Zhan X, Dixon MA, Liu S, Gros D, Korver W, Yonkovich S, Tomasevic N, *et al* (2008) R-Spondin family members regulate the Wnt pathway by a common mechanism. *Mol Biol Cell* 19: 2588–2596

Kim YS, Fan R, Kremer L, Kuempel-Rink N, Mildner K, Zeuschner D, Hekking L, Stehling M & Bedzhov I (2021) Deciphering epiblast lumenogenesis reveals proamniotic cavity control of embryo growth and patterning. *Sci Adv* 7

Kim YS, Fan R, Lith SC, Dicke A-K, Drexler HCA, Kremer L, Kuempel-Rink N, Hekking L, Stehling M & Bedzhov I (2022b) Rap1 controls epiblast morphogenesis in sync with the pluripotency states transition. *Dev Cell* 57: 1937-1956.e8

Kime C, Kiyonari H, Ohtsuka S, Kohbayashi E, Asahi M, Yamanaka S, Takahashi M & Tomoda K (2019) Induced 2C Expression and Implantation-Competent Blastocyst-like Cysts from Primed Pluripotent Stem Cells. *Stem Cell Reports* 13: 485–498

Kinoshita M, Barber M, Mansfield W, Cui Y, Spindlow D, Stirparo GG, Dietmann S, Nichols J & Smith A (2021) Capture of Mouse and Human Stem Cells with Features of Formative Pluripotency. *Cell Stem Cell* 28: 453-471.e8

Koutsourakis M, Langeveld A, Patient R, Beddington R & Grosveld F (1999) The transcription factor GATA6 is essential for early extraembryonic development. *Development* 126: 723–732

Krawchuk D, Honma-Yamanaka N, Anani S & Yamanaka Y (2013) FGF4 is a limiting factor controlling the proportions of primitive endoderm and epiblast in the ICM of the mouse blastocyst. *Dev Biol* 384: 65–71

Kuales G, Weiss M, Sedelmeier O, Pfeifer D & Arnold SJ (2015) A Resource for the Transcriptional Signature of Bona Fide Trophoblast Stem Cells and Analysis of Their Embryonic Persistence. *Stem Cells Int* 2015: 218518

Kubaczka C, Senner C, Araúzo-Bravo MJ, Sharma N, Kuckenberg P, Becker A, Zimmer A, Brüstle O, Peitz M, Hemberger M, *et al* (2014) Derivation and maintenance of murine trophoblast stem cells under defined conditions. *Stem cell reports* 2: 232–242

Kumar A, Lualdi M, Lyozin GT, Sharma P, Loncarek J, Fu X-Y & Kuehn MR (2015) Nodal signaling from the visceral endoderm is required to maintain Nodal gene expression in the epiblast and drive DVE/AVE migration. *Dev Biol* 400: 1–9

Kunath T, Arnaud D, Uy GD, Okamoto I, Chureau C, Yamanaka Y, Heard E, Gardner RL, Avner P & Rossant J (2005) Imprinted X-inactivation in extra-embryonic endoderm cell lines from mouse blastocysts. *Development* 132: 1649–1661

Kunath T, Strumpf D & Rossant J (2004) Early Trophoblast Determination and Stem Cell Maintenance in the Mouse—A Review. *Placenta* 25: S32–S38

Langkabel J, Horne A, Bonaguro L, Holsten L, Hesse T, Knaus A, Riedel Y, Becker M, Händler K, Elmzzahi T, *et al* (2021) Induction of Rosette-to-Lumen stage embryoids using reprogramming paradigms in ESCs. *Nat Commun* 12: 7322

Lanner F & Rossant J (2010) The role of FGF/Erk signaling in pluripotent cells. *Development* 137: 3351–3360

Lau KYC, Rubinstein H, Gantner CW, Hadas R, Amadei G, Stelzer Y & Zernicka-Goetz M (2022) Mouse embryo model derived exclusively from embryonic stem cells undergoes neurulation and heart development. *Cell Stem Cell* 29: 1445-1458.e8

Lecuit T & Lenne P-F (2007) Cell surface mechanics and the control of cell shape, tissue patterns and morphogenesis. *Nat Rev Mol Cell Biol* 8: 633–644

Leivo I, Vaheri A, Timpl R & Wartiovaara J (1980) Appearance and distribution of collagens and laminin in the early mouse embryo. *Dev Biol* 76: 100–114

Li R, Zhong C, Yu Y, Liu H, Sakurai M, Yu L, Min Z, Shi L, Wei Y, Takahashi Y, *et al* (2019) Generation of Blastocyst-like Structures from Mouse Embryonic and Adult Cell Cultures. *Cell* 179: 687-702.e18

Linneberg-Agerholm M, Sell AC, Redo-Riveiro A, Proks M, Knudsen TE, Perera M & Brickman JM (2023) Enhancer status in the primitive endoderm supports unrestricted lineage plasticity in regulative development. *bioRxiv*: 2023.05.20.540779

Liu X, Tan JP, Schröder J, Aberkane A, Ouyang JF, Mohenska M, Lim SM, Sun YBY, Chen J, Sun G, *et al* (2021) Modelling human blastocysts by reprogramming fibroblasts into iBlastoids. *Nature* 591: 627–632

Loh Y-H, Wu Q, Chew J-L, Vega VB, Zhang W, Chen X, Bourque G, George J, Leong B, Liu J, *et al* (2006) The Oct4 and Nanog transcription network regulates pluripotency in mouse embryonic stem cells. *Nat Genet* 38: 431–440

Maître J-L, Berthoumieux H, Krens SFG, Salbreux G, Jülicher F, Paluch E & Heisenberg C-P (2012) Adhesion Functions in Cell Sorting by Mechanically Coupling the Cortices of

Adhering Cells. *Science (80-)* 338: 253–256

Malik V & Wang J (2022) Pursuing totipotency: authentic totipotent stem cells in culture. *Trends Genet* 38: 632–636

Manejwala FM, Cragoe EJ & Schultz RM (1989) Blastocoel expansion in the preimplantation mouse embryo: Role of extracellular sodium and chloride and possible apical routes of their entry. *Dev Biol* 133: 210–220

Mantalenakis SJ & Ketchel MM (1966) Frequency and extent of delayed implantation in lactating rats and mice. *Reproduction* 12: 391–394

Marks H, Kalkan T, Menafra R, Denissov S, Jones K, Hofemeister H, Nichols J, Kranz A, Francis Stewart A, Smith A, *et al* (2012) The Transcriptional and Epigenomic Foundations of Ground State Pluripotency. *Cell* 149: 590–604

Martin GR (1981) Isolation of a pluripotent cell line from early mouse embryos cultured in medium conditioned by teratocarcinoma stem cells. *Proc Natl Acad Sci U S A* 78: 7634–7638

Mathew B, Muñoz-Descalzo S, Corujo-Simon E, Schröter C, Stelzer EHK & Fischer SC (2019) Mouse ICM Organoids Reveal Three-Dimensional Cell Fate Clustering. *Biophys J* 116: 127–141

Matthews KRW, Wagner DS & Warmflash A (2021) Stem cell-based models of embryos: The need for improved naming conventions. *Stem Cell Reports* 16: 1014–1020

Mead RA (1993) Embryonic diapause in vertebrates. *J Exp Zool* 266: 629–641

Meder D, Shevchenko A, Simons K & Füllekrug J (2005) Gp135/podocalyxin and NHERF-2 participate in the formation of a preapical domain during polarization of MDCK cells. *J Cell Biol* 168: 303–313

Mesnard D, Guzman-Ayala M & Constam DB (2006) Nodal specifies embryonic visceral endoderm and sustains pluripotent cells in the epiblast before overt axial patterning. *Development* 133: 2497–2505

Mobley RJ, Raghu D, Duke LD, Abell-Hart K, Zawistowski JS, Lutz K, Gomez SM, Roy S, Homayouni R, Johnson GL, *et al* (2017) MAP3K4 Controls the Chromatin Modifier HDAC6 during Trophoblast Stem Cell Epithelial-to-Mesenchymal Transition. *Cell Rep* 18: 2387–2400

Moghe P, Belousov R, Ichikawa T, Iwatani C, Tsukiyama T, Graner F, Erzberger A & Hiiragi T (2023) Apical-driven cell sorting optimised for tissue geometry ensures robust patterning. *bioRxiv*: 2023.05.16.540918

Molè MA, Weberling A, Fässler R, Campbell A, Fishel S & Zernicka-Goetz M (2021) Integrin β1 coordinates survival and morphogenesis of the embryonic lineage upon implantation and pluripotency transition. *Cell Rep* 34: 108834

Molè MA, Weberling A & Zernicka-Goetz M (2020) Chapter Four - Comparative analysis of human and mouse development: From zygote to pre-gastrulation. In *Gastrulation: From Embryonic Pattern to Form*, Solnica-Krezel LBT-CT in DB (ed) pp 113–138. Academic Press

Molotkov A, Mazot P, Brewer JR, Cinalli RM & Soriano P (2017) Distinct Requirements for FGFR1 and FGFR2 in Primitive Endoderm Development and Exit from Pluripotency. *Dev Cell* 41: 511-526.e4

Molotkov A & Soriano P (2018) Distinct mechanisms for PDGF and FGF signaling in primitive endoderm development. *Dev Biol* 442: 155–161

Moore R, Tao W, Smith ER & Xu X-X (2014) The primitive endoderm segregates from the epiblast in β1 integrin-deficient early mouse embryos. *Mol Cell Biol* 34: 560–572

Morales JS, Raspopovic J & Marcon L (2021) From embryos to embryoids: How external signals and self-organization drive embryonic development. *Stem Cell Reports* 16: 1039–1050

Morgani S, Nichols J & Hadjantonakis A-K (2017) The many faces of Pluripotency: in vitro adaptations of a continuum of in vivo states. *BMC Dev Biol* 17: 7

Morrisey E, Tang Z, Sigrist K, Lu MM, Jiang F, Ip H & Parmacek M (1998) GATA6 regulates HNF4 and is required for differentiation of visceral endoderm in the mouse embryo. *Genes Dev* 12: 3579–3590

Motomura K, Oikawa M, Hirose M, Honda A, Togayachi S, Miyoshi H, Ohinata Y, Sugimoto M, Abe K, Inoue K, *et al* (2016) Cellular Dynamics of Mouse Trophoblast Stem Cells: Identification of a Persistent Stem Cell Type1. *Biol Reprod* 94: 1-14,122

Mulvey CM, Schröter C, Gatto L, Dikicioglu D, Fidaner IB, Christoforou A, Deery MJ, Cho LTY, Niakan KK, Martinez-Arias A, *et al* (2015) Dynamic Proteomic Profiling of Extra-Embryonic Endoderm Differentiation in Mouse Embryonic Stem Cells. *Stem Cells* 33: 2712–2725

Murohashi M, Nakamura T, Tanaka S, Ichise T, Yoshida N, Yamamoto T, Shibuya M, Schlessinger J & Gotoh N (2010) An FGF4-FRS2alpha-Cdx2 axis in trophoblast stem cells induces Bmp4 to regulate proper growth of early mouse embryos. *Stem Cells* 28: 113–121

Murray P & Edgar D (2001) The regulation of embryonic stem cell differentiation by leukaemia inhibitory factor (LIF). *Differentiation* 68: 227–234

Nagy A, Rossant J, Nagy R, Abramow-Newerly W & Roder JC (1993) Derivation of completely cell culture-derived mice from early-passage embryonic stem cells. *Proc Natl Acad Sci U S A* 90: 8424–8428

Neagu A, van Genderen E, Escudero I, Verwegen L, Kurek D, Lehmann J, Stel J, Dirks RAM, van Mierlo G, Maas A, *et al* (2020) In vitro capture and characterization of embryonic rosette-stage pluripotency between naive and primed states. *Nat Cell Biol* 22: 534–545

Nichols J, Silva J, Roode M & Smith A (2009) Suppression of Erk signalling promotes ground state pluripotency in the mouse embryo. *Development* 136: 3215–3222

Nichols J & Smith A (2009) Naive and primed pluripotent states. *Cell Stem Cell* 4: 487–492

Nishioka N, Inoue K, Adachi K, Kiyonari H, Ota M, Ralston A, Yabuta N, Hirahara S, Stephenson RO, Ogonuki N, *et al* (2009) The Hippo Signaling Pathway Components Lats and Yap Pattern Tead4 Activity to Distinguish Mouse Trophectoderm from Inner Cell Mass. *Dev Cell* 16: 398–410

Nishioka N, Yamamoto S, Kiyonari H, Sato H, Sawada A, Ota M, Nakao K & Sasaki H (2008) Tead4 is required for specification of trophectoderm in pre-implantation mouse embryos. *Mech Dev* 125: 270–283

Nowotschin S, Setty M, Kuo Y-Y, Liu V, Garg V, Sharma R, Simon CS, Saiz N, Gardner R, Boutet SC, *et al* (2019) The emergent landscape of the mouse gut endoderm at single-cell resolution. *Nature* 569: 361–367

O'Brien LE, Jou T-S, Pollack AL, Zhang Q, Hansen SH, Yurchenco P & Mostov KE (2001) Rac1

orientates epithelial apical polarity through effects on basolateral laminin assembly. *Nat Cell Biol* 3: 831–838

Ohinata Y & Tsukiyama T (2014) Establishment of trophoblast stem cells under defined culture conditions in mice. *PLoS One* 9: e107308

Ohnishi Y, Huber W, Tsumura A, Kang M, Xenopoulos P, Kurimoto K, Oleś AK, Araúzo-Bravo MJ, Saitou M, Hadjantonakis A-K, *et al* (2014) Cell-to-cell expression variability followed by signal reinforcement progressively segregates early mouse lineages. *Nat Cell Biol* 16: 27–37

Okubo T, Rivron N, Kabata M, Masaki H, Kishimoto K, Semi K, Nakajima-Koyama M, Kunitomi H, Kaswandy B, Sato H, *et al* (2024) Hypoblast from human pluripotent stem cells regulates epiblast development. *Nature* 626: 357–366

Orlando RA, Takeda T, Zak B, Schmieder S, Benoit VM, McQuistan T, Furthmayr H & Farquhar MG (2001) The glomerular epithelial cell anti-adhesin podocalyxin associates with the actin cytoskeleton through interactions with ezrin. *J Am Soc Nephrol* 12: 1589–1598

Perea-Gomez A, Cases O, Lelièvre V, Pulina M V, Collignon J, Hadjantonakis A-K & Kozyraki R (2019) Loss of Cubilin, the intrinsic factor-vitamin B12 receptor, impairs visceral endoderm endocytosis and endodermal patterning in the mouse. *Sci Rep* 9: 10168

Perea-Gomez A, Meilhac SM, Piotrowska-Nitsche K, Gray D, Collignon J & Zernicka-Goetz M (2007) Regionalisation of the mouse visceral endoderm as the blastocyst transforms into the egg cylinder. *BMC Dev Biol* 7: 96

Perea-Gómez A, Shawlot W, Sasaki H, Behringer RR & Ang S-L (1999) HNF3β and Lim1 interact in the visceral endoderm to regulate primitive streak formation and anterior-posterior polarity in the mouse embryo. *Development* 126: 4499–4511

Perea-Gomez A, Vella FDJ, Shawlot W, Oulad-Abdelghani M, Chazaud C, Meno C, Pfister V, Chen L, Robertson E, Hamada H, *et al* (2002) Nodal Antagonists in the Anterior Visceral Endoderm Prevent the Formation of Multiple Primitive Streaks. *Dev Cell* 3: 745–756

Perona RM & Wassarman PM (1986) Mouse blastocysts hatch in vitro by using a trypsin-like proteinase associated with cells of mural trophectoderm. *Dev Biol* 114: 42–52

Plusa B, Frankenberg S, Chalmers A, Hadjantonakis A-K, Moore CA, Papalopulu N, Papaioannou VE, Glover DM & Zernicka-Goetz M (2005) Downregulation of Par3 and aPKC function directs cells towards the ICM in the preimplantation mouse embryo. *J Cell Sci* 118: 505–515

Posfai E, Schell JP, Janiszewski A, Rovic I, Murray A, Bradshaw B, Yamakawa T, Pardon T, El Bakkali M, Talon I, *et al* (2021) Evaluating totipotency using criteria of increasing stringency. *Nat Cell Biol* 23: 49–60

Raina D, Bahadori A, Stanoev A, Protzek M, Koseska A & Schröter C (2021) Cell-cell communication through FGF4 generates and maintains robust proportions of differentiated cell types in embryonic stem cells. *Development* 148: dev199926

Ralston A, Cox BJ, Nishioka N, Sasaki H, Chea E, Rugg-Gunn P, Guo G, Robson P, Draper JS & Rossant J (2010) Gata3 regulates trophoblast development downstream of Tead4 and in parallel to Cdx2. *Development* 137: 395–403

Ralston A & Rossant J (2008) Cdx2 acts downstream of cell polarization to cell-autonomously promote trophectoderm fate in the early mouse embryo. *Dev Biol* 313: 614–629

Rayon T, Menchero S, Rollán I, Ors I, Helness A, Crespo M, Nieto A, Azuara V, Rossant J & Manzanares M (2016) Distinct mechanisms regulate Cdx2 expression in the blastocyst and in trophoblast stem cells. *Sci Rep* 6: 27139

Renfree MB & Shaw G (2000) Diapause. *Annu Rev Physiol* 62: 353–375

Rivera-Pérez JA, Mager J & Magnuson T (2003) Dynamic morphogenetic events characterize the mouse visceral endoderm. *Dev Biol* 261: 470–487

Rivron NC, Frias-Aldeguer J, Vrij EJ, Boisset J-C, Korving J, Vivié J, Truckenmüller RK, van Oudenaarden A, van Blitterswijk CA & Geijsen N (2018) Blastocyst-like structures generated solely from stem cells. *Nature* 557: 106–111

Robertson EJ (2014) Dose-dependent Nodal/Smad signals pattern the early mouse embryo. *Semin Cell Dev Biol* 32: 73–79

Rodriguez TA, Srinivas S, Clements MP, Smith JC & Beddington RSP (2005) Induction and migration of the anterior visceral endoderm is regulated by the extra-embryonic ectoderm. *Development* 132: 2513–2520

Rossant J (1987) Development of extraembryonic cell lineages in the mouse embryo. In *Experimental Approaches to Mammalian Embryonic Development*, Rossant J & Pedersen RA (eds) pp 97–120. Cambridge: Cambridge University Press

Rossant J (2018) Genetic Control of Early Cell Lineages in the Mammalian Embryo. *Annu Rev Genet* 52: 185–201

Rossant J & Tam PPL (2009) Blastocyst lineage formation, early embryonic asymmetries and axis patterning in the mouse. *Development* 136: 701 LP – 713

Rossant J & Tam PPL (2021) Opportunities and challenges with stem cell-based embryo models. *Stem cell reports* 16: 1031–1038

Ryan AQ, Chan CJ, Graner F & Hiiragi T (2019) Lumen Expansion Facilitates Epiblast-Primitive Endoderm Fate Specification during Mouse Blastocyst Formation. *Dev Cell* 51: 684-697.e4

Saiz N, Grabarek JB, Sabherwal N, Papalopulu N & Plusa B (2013) Atypical protein kinase C couples cell sorting with primitive endoderm maturation in the mouse blastocyst. *Development* 140: 4311–4322

Schindelin J, Arganda-Carreras I, Frise E, Kaynig V, Longair M, Pietzsch T, Preibisch S, Rueden C, Saalfeld S, Schmid B, *et al* (2012) Fiji: an open-source platform for biological-image analysis. *Nat Methods* 9: 676–682

Schröter C, Rué P, Mackenzie JP & Martinez Arias A (2015) FGF/MAPK signaling sets the switching threshold of a bistable circuit controlling cell fate decisions in embryonic stem cells. *Development* 142: 4205–4216

Schumacher S, Fernkorn M, Marten M, Kim YS, Bedzhov I & Schröter C (2023) Tissue-intrinsic Wnt signals antagonize Nodal-driven AVE differentiation. *bioRxiv*: 2023.05.19.541432

Seong J, Frias-Aldeguer J, Holzmann V, Kagawa H, Sestini G, Heidari Khoei H, Scholte Op Reimer Y, Kip M, Pradhan SJ, Verwegen L, *et al* (2022) Epiblast inducers capture mouse trophectoderm stem cells in vitro and pattern blastoids for implantation in utero. *Cell Stem Cell* 29: 1102-1118.e8

Shahbazi MN, Scialdone A, Skorupska N, Weberling A, Recher G, Zhu M, Jedrusik A, Devito LG, Noli L, Macaulay IC, *et al* (2017) Pluripotent state transitions coordinate morphogenesis in

mouse and human embryos. *Nature* 552: 239–243

Shen MM & Leder P (1992) Leukemia inhibitory factor is expressed by the preimplantation uterus and selectively blocks primitive ectoderm formation in vitro. *Proc Natl Acad Sci U S A* 89: 8240–8244

Simmons DG & Cross JC (2005) Determinants of trophoblast lineage and cell subtype specification in the mouse placenta. *Dev Biol* 284: 12–24

Singh AM, Hamazaki T, Hankowski KE & Terada N (2007) A Heterogeneous Expression Pattern for Nanog in Embryonic Stem Cells. *Stem Cells* 25: 2534–2542

Smith A (2017) Formative pluripotency: the executive phase in a developmental continuum. *Development* 144: 365–373

Smith KK & Strickland S (1981) Structural components and characteristics of Reichert's membrane, an extra-embryonic basement membrane. *J Biol Chem* 256: 4654–4661

Smyth N, Vatansever HS, Murray P, Meyer M, Frie C, Paulsson M & Edgar D (1999) Absence of basement membranes after targeting the LAMC1 gene results in embryonic lethality due to failure of endoderm differentiation. *J Cell Biol* 144: 151–160

Sozen B, Amadei G, Cox A, Wang R, Na E, Czukiewska S, Chappell L, Voet T, Michel G, Jing N, *et al* (2018) Self-assembly of embryonic and two extra-embryonic stem cell types into gastrulating embryo-like structures. *Nat Cell Biol* 20: 979–989

Sozen B, Cox AL, De Jonghe J, Bao M, Hollfelder F, Glover DM & Zernicka-Goetz M (2019) Self-Organization of Mouse Stem Cells into an Extended Potential Blastoid. *Dev Cell* 51: 698-712.e8

Srinivas S, Rodriguez T, Clements M, Smith JC & Beddington RSP (2004) Active cell migration drives the unilateral movements of the anterior visceral endoderm. *Development* 131: 1157–1164

Stephens LE, Sutherland AE, Klimanskaya I V, Andrieux A, Meneses J, Pedersen RA & Damsky CH (1995) Deletion of beta 1 integrins in mice results in inner cell mass failure and peri-implantation lethality. *Genes Dev* 9: 1883–1895

Stower MJ & Srinivas S (2018) Chapter Fourteen - The Head's Tale: Anterior-Posterior Axis Formation in the Mouse Embryo. In *Cell Fate in Mammalian Development*, Plusa B & Hadjantonakis A-KBT-CT in DB (eds) pp 365–390. Academic Press

Strumpf D, Mao C-A, Yamanaka Y, Ralston A, Chawengsaksophak K, Beck F & Rossant J (2005) Cdx2 is required for correct cell fate specification and differentiation of trophectoderm in the mouse blastocyst. *Development* 132: 2093–2102

Subramanian A, Tamayo P, Mootha VK, Mukherjee S, Ebert BL, Gillette MA, Paulovich A, Pomeroy SL, Golub TR, Lander ES, *et al* (2005) Gene set enrichment analysis: A knowledge-based approach for interpreting genome-wide expression profiles. *Proc Natl Acad Sci* 102: 15545–15550

Sutherland A (2003) Mechanisms of implantation in the mouse: differentiation and functional importance of trophoblast giant cell behavior. *Dev Biol* 258: 241–251

Suzuki D, Okura K, Nagakura S & Ogawa H (2022a) CDX2 downregulation in mouse mural trophectoderm during peri-implantation is heteronomous, dependent on the YAP-TEAD pathway and controlled by estrogen-induced factors. *Reprod Med Biol* 21: e12446

Suzuki D, Sasaki K, Kumamoto S, Tanaka K & Ogawa H (2022b) Dynamic Changes of Gene Expression in Mouse Mural Trophectoderm Regulated by Cdx2 During Implantation. *Front Cell Dev Biol* 10 (https://www.frontiersin.org/articles/10.3389/fcell.2022.945241) [PREPRINT]

Takaoka K & Hamada H (2012) Cell fate decisions and axis determination in the early mouse embryo. *Development* 139: 3–14

Takaoka K, Yamamoto M & Hamada H (2011) Origin and role of distal visceral endoderm, a group of cells that determines anterior–posterior polarity of the mouse embryo. *Nat Cell Biol* 13: 743–752

Takaoka K, Yamamoto M, Shiratori H, Meno C, Rossant J, Saijoh Y & Hamada H (2006) The Mouse Embryo Autonomously Acquires Anterior-Posterior Polarity at Implantation. *Dev Cell* 10: 451–459

Tanaka S, Kunath T, Hadjantonakis AK, Nagy A & Rossant J (1998) Promotion of trophoblast stem cell proliferation by FGF4. *Science* 282: 2072–2075

Tarazi S, Aguilera-Castrejon A, Joubran C, Ghanem N, Ashouokhi S, Roncato F, Wildschutz E, Haddad M, Oldak B, Gomez-Cesar E, *et al* (2022) Post-gastrulation synthetic embryos generated ex utero from mouse naive ESCs. *Cell* 185: 3290-3306.e25

Tesar PJ, Chenoweth JG, Brook FA, Davies TJ, Evans EP, Mack DL, Gardner RL & McKay RDG (2007) New cell lines from mouse epiblast share defining features with human embryonic stem cells. *Nature* 448: 196–199

Thomas P & Beddington R (1996) Anterior primitive endoderm may be responsible for patterning the anterior neural plate in the mouse embryo. *Curr Biol* 6: 1487–1496

Thomas PQ, Brown A & Beddington RSP (1998) Hex: a homeobox gene revealing peri-implantation asymmetry in the mouse embryo and an early transient marker of endothelial cell precursors. *Development* 125: 85–94

Torres-Padilla M-E, Richardson L, Kolasinska P, Meilhac SM, Luetke-Eversloh MV & Zernicka-Goetz M (2007) The anterior visceral endoderm of the mouse embryo is established from both preimplantation precursor cells and by de novo gene expression after implantation. *Dev Biol* 309: 97–112

Veltmaat JM, Orelio CC, Ward-Van Oostwaard D, Van Rooijen MA, Mummery CL & Defize LH (2000) Snail is an immediate early target gene of parathyroid hormone related peptide signaling in parietal endoderm formation. *Int J Dev Biol* 44: 297–307

Vinot S, Le T, Ohno S, Pawson T, Maro B & Louvet-Vallée S (2005) Asymmetric distribution of PAR proteins in the mouse embryo begins at the 8-cell stage during compaction. *Dev Biol* 282: 307–319

Vrij E, Rouwkema J, LaPointe V, van Blitterswijk C, Truckenmüller R & Rivron N (2016) Directed Assembly and Development of Material-Free Tissues with Complex Architectures. *Adv Mater* 28: 4032–4039

Vrij EJ, Scholte op Reimer YS, Fuentes LR, Guerreiro IM, Holzmann V, Aldeguer JF, Sestini G, Koo B-K, Kind J, van Blitterswijk CA, *et al* (2022) A pendulum of induction between the epiblast and extra-embryonic endoderm supports post-implantation progression. *Development* 149: dev192310

Waldrip WR, Bikoff EK, Hoodless PA, Wrana JL & Robertson EJ (1998) Smad2 Signaling in

Extraembryonic Tissues Determines Anterior-Posterior Polarity of the Early Mouse Embryo. *Cell* 92: 797–808

Wallingford MC, Angelo JR & Mager J (2013) Morphogenetic analysis of peri-implantation development. *Dev Dyn* 242: 1110–1120

Wamaitha SE, del Valle I, Cho LTY, Wei Y, Fogarty NME, Blakeley P, Sherwood RI, Ji H & Niakan KK (2015) Gata6 potently initiates reprograming of pluripotent and differentiated cells to extraembryonic endoderm stem cells. *Genes Dev* 29: 1239–1255

Wang X & Wu Q (2022) The Divergent Pluripotent States in Mouse and Human Cells. *Genes (Basel)* 13

Wassarman PM, Jovine L & Litscher ES (2004) Mouse zona pellucida genes and glycoproteins. *Cytogenet Genome Res* 105: 228–234

Watanabe T, Thayil A, Jesacher A, Grieve K, Debarre D, Wilson T, Booth M & Srinivas S (2010) Characterisation of the dynamic behaviour of lipid droplets in the early mouse embryo using adaptive harmonic generation microscopy. *BMC Cell Biol* 11: 38

Weberling A & Zernicka-Goetz M (2021) Trophectoderm mechanics direct epiblast shape upon embryo implantation. *Cell Rep* 34

Williams RL, Hilton DJ, Pease S, Willson TA, Stewart CL, Gearing DP, Wagner EF, Metcalf D, Nicola NA & Gough NM (1988) Myeloid leukaemia inhibitory factor maintains the developmental potential of embryonic stem cells. *Nature* 336: 684–687

Williamson RA, Henry MD, Daniels KJ, Hrstka RF, Lee JC, Sunada Y, Ibraghimov-Beskrovnaya O & Campbell KP (1997) Dystroglycan Is Essential for Early Embryonic Development: Disruption of Reichert's Membrane in Dag1-Null Mice. *Hum Mol Genet* 6: 831–841

Wray J, Kalkan T, Gomez-Lopez S, Eckardt D, Cook A, Kemler R & Smith A (2011) Inhibition of glycogen synthase kinase-3 alleviates Tcf3 repression of the pluripotency network and increases embryonic stem cell resistance to differentiation. *Nat Cell Biol* 13: 838–845

Xu Y, Zhao J, Ren Y, Wang X, Lyu Y, Xie B, Sun Y, Yuan X, Liu H, Yang W, *et al* (2022) Derivation of totipotent-like stem cells with blastocyst-like structure forming potential. *Cell Res* 32: 513–529

Yamamoto M, Beppu H, Takaoka K, Meno C, Li E, Miyazono K & Hamada H (2009) Antagonism between Smad1 and Smad2 signaling determines the site of distal visceral endoderm formation in the mouse embryo. *J Cell Biol* 184: 323–334

Yamamoto M, Saijoh Y, Perea-Gomez A, Shawlot W, Behringer RR, Ang S-L, Hamada H & Meno C (2004) Nodal antagonists regulate formation of the anteroposterior axis of the mouse embryo. *Nature* 428: 387–392

Yamanaka Y, Lanner F & Rossant J (2010) FGF signal-dependent segregation of primitive endoderm and epiblast in the mouse blastocyst. *Development* 137: 715 LP – 724

Yanagida A, Corujo-Simon E, Revell CK, Sahu P, Stirparo GG, Aspalter IM, Winkel AK, Peters R, De Belly H, Cassani DAD, *et al* (2022) Cell surface fluctuations regulate early embryonic lineage sorting. *Cell* 185: 777-793.e20

Yanagida A, Spindlow D, Nichols J, Dattani A, Smith A & Guo G (2021) Naive stem cell blastocyst model captures human embryo lineage segregation. *Cell Stem Cell* 28: 1016-1022.e4

Yang J, Ryan DJ, Wang W, Tsang JC-H, Lan G, Masaki H, Gao X, Antunes L, Yu Y, Zhu Z, *et al*

(2017a) Establishment of mouse expanded potential stem cells. *Nature* 550: 393–397

Yang Y, Liu B, Xu J, Wang J, Wu J, Shi C, Xu Y, Dong J, Wang C, Lai W, *et al* (2017b) Derivation of Pluripotent Stem Cells with In Vivo Embryonic and Extraembryonic Potency. *Cell* 169: 243-257.e25

Yasuhide O, A. ET, Hiroki S, Takashi W, Yusuke I, Yurie K, Atsunori S, Mami K, Yoko K, Takashi K, *et al* (2022) Establishment of mouse stem cells that can recapitulate the developmental potential of primitive endoderm. *Science (80-)* 375: 574–578

Ying Q-L, Wray J, Nichols J, Batlle-Morera L, Doble B, Woodgett J, Cohen P & Smith A (2008) The ground state of embryonic stem cell self-renewal. *Nature* 453: 519–523

Yu L, Wei Y, Duan J, Schmitz DA, Sakurai M, Wang L, Wang K, Zhao S, Hon GC & Wu J (2021) Blastocyst-like structures generated from human pluripotent stem cells. *Nature* 591: 620–626

Yu W, Datta A, Leroy P, O'Brien LE, Mak G, Jou T-S, Matlin KS, Mostov KE & Zegers MMP (2004) β1-Integrin Orients Epithelial Polarity via Rac1 and Laminin. *Mol Biol Cell* 16: 433–445

Zhang P, Zhai X, Huang B, Sun S, Wang W & Zhang M (2023) Highly efficient generation of blastocyst-like structures from spliceosomes-repressed mouse totipotent blastomere-like cells. *Sci China Life Sci* 66: 423–435

Zhang S, Chen T, Chen N, Gao D, Shi B, Kong S, West RC, Yuan Y, Zhi M, Wei Q, *et al* (2019) Implantation initiation of self-assembled embryo-like structures generated using three types of mouse blastocyst-derived stem cells. *Nat Commun* 10: 496

Zhong Y, Choi T, Kim M, Jung KH, Chai YG & Binas B (2018) Isolation of primitive mouse extraembryonic endoderm (pXEN) stem cell lines. *Stem Cell Res* 30: 100–112

Zhu Q, Ge J, Liu Y, Xu J-W, Yan S & Zhou F (2023) Decoding anterior-posterior axis emergence among mouse, monkey, and human embryos. *Dev Cell* 58: 63-79.e4